Centennial-Scale Elemental and Isotopic Variability in the Tropical and Subtropical North Atlantic Ocean

by

Matthew K. Reuer

Bachelor of Arts, Geology
Carleton College, 1995

Submitted in partial fulfillment of the requirements for the degree of

Doctor of Philosophy

at the

MASSACHUSETTS INSTITUTE OF TECHNOLOGY

and the

WOODS HOLE OCEANOGRAPHIC INSTITUTION

February 2002
[JUNE 2002]

Author .....
Joint Program in Oceanography/Applied Ocean Science and Engineering
Massachusetts Institute of Technology and Woods Hole Oceanographic Institution
February 15th, 2002

Certified by.....
Edward A. Boyle
Professor of Oceanography
Thesis Supervisor

Accepted by .....
Margaret K. Tivey
Chair, Joint Committee for Chemical Oceanography

Centennial-Scale Elemental and Isotopic Variability in the Tropical and Subtropical North Atlantic Ocean

by

Matthew K. Reuer

Submitted to the WHOI/MIT Joint Program in Oceanography
on February 15th, 2002, in partial fulfillment of the
requirements for the degree of
Doctor of Philosophy

Abstract

The marine geochemistry of the North Atlantic Ocean varies on decadal to centennial time scales, a consequence of natural and anthropogenic forcing. Surface corals provide a useful geochemical archive to quantify past mixed layer variability, and this study presents elemental and isotopic records from the tropical and subtropical North Atlantic. A consistent method for stable lead isotope analysis via multiple collector ICP-MS is first presented. This method is then applied to western North Atlantic surface corals and seawater, constraining historical elemental and isotopic lead variability. Six stable lead isotope profiles are developed from the western and eastern North Atlantic, demonstrating consistent mixed layer, thermocline, and deep water variability. Finally, coralline trace element records, including cadmium, barium, and lead, are presented from the Cariaco Basin.

First, a reliable method is developed for stable lead isotope analysis by multiple collector ICP-MS. This study presents new observations of the large (0.7% amu^{-1}), time-dependent mass fractionation determined by thallium normalization, including preferential light ion transmission induced by the acceleration potential and nebulizer conditions. These experiments show equivalent results for three empirical correction laws, and the previously proposed β_{Pb}/β_{Tl} correction does not improve isotope ratio accuracy under these conditions. External secondary normalization to SRM-981 provides one simple alternative, and a rationale is provided for this correction. With current intensities less than $1.5x10^{-12}$ A, external isotope ratio precision less than 200 ppm is observed (2σ). Matrix effects are significant with concomitant calcium in SRM-981 (-280 ppm at 257 μM [Ca]). With the appropriate corrections and minimal concomitants, MC-ICP-MS can reliably determine $^{206}Pb/^{207}Pb$ and $^{208}Pb/^{207}Pb$ ratios of marine carbonates and seawater.

Anthropogenic lead represents a promising transient oceanographic tracer, and its historical isotopic and elemental North Atlantic variability have been documented by proxy reconstructions and seawater observations. Two high-resolution surface coral and seawater time series from the western North Atlantic are presented, demonstrating past variability consistent with upper ocean observations. The elemental reconstruction suggests the primary lead transient was advected to the western North Atlantic from 1955 to 1968, with an inferred maximum lead concentration of 205 pmol kg^{-1} in 1971. The mean 1999 North Atlantic seawater concentration (38 pmol kg^{-1}) is equivalent to 1905, several decades prior to the initial consumption of leaded gasoline in the United States. A $^{206}Pb/^{207}Pb$ transient

from 1968 to 1990 is also observed, lagging the elemental transient by ten years. The provenance of this isotopic record is distinct from Arctic and European ice core observations and supports a 40% reduction in North American fluxes to this site from 1979-1983 to 1994-1998. Historical isotopic variability agrees with seawater observations, including an isotopic reduction in the western North Atlantic upper thermocline, a consistent $^{206}Pb/^{207}Pb$ thermocline maximum in the eastern North Atlantic, and deeper penetration of the elemental lead maximum.

The isotopic composition of anthropogenic lead provides important constraints regarding its time-dependent North Atlantic evolution. The 1998-2001 mixed layer isotopic distribution agrees with zonal atmospheric fluxes between radiogenic westerly and non-radiogenic northeasterly trade wind sources. A non-radiogenic $^{206}Pb/^{207}Pb$ (1.176) signature in the 1998 western subtropics suggests boundary current advection of equatorial lead, a possible consequence of reduced North American lead fluxes. Isotopic maxima are observed in the mid-latitude thermocline (σ_θ=27) of the eastern and western North Atlantic. This $^{206}Pb/^{207}Pb$ maximum is diminished in both the subpolar and equatorial regions due to the prevailing aerosol fluxes, current direction, thermocline ventilation, and lead scavenging. The admixture of Mediterranean Outflow Water reduces the isotopic maximum in the eastern North Atlantic, separable by $^{206}Pb/^{207}Pb$ and $^{208}Pb/^{207}Pb$ ratios. Finally, the deep water variability supports an anthropogenic signature relative to the North Atlantic natural background estimates, with an isotopic range smaller than previously observed. The deep water isotopic composition agrees with the western North Atlantic proxy record and provides a novel chronometric technique: lead ventilation ages of approximately 40 years are observed. Based on its time history, the utility of this tracer is demonstrated by comparing CFC-12 concentrations and $^{206}Pb/^{207}Pb$ ratios in the eastern North Atlantic, including a deep water isotopic boundary between 22 and 31°N.

Finally, the Cariaco Basin is an important archive of past climate variability given its response to inter- and extra-tropical climate forcing and the rapid accumulation of annually-laminated sediments. This study presents annually-resolved surface coral trace element records from Isla Tortuga, Venezuela, located within the upwelling center of this region. The dominant feature of the trace element records is a two-fold Cd/Ca reduction from 1945 to 1955 with no corresponding shift in Ba/Ca, in agreement with the expected hydrographic response to upwelling. Kinetic control of trace element ratios is inferred from Cd/Ca and Ba/Ca results between the coral species *S. siderea* and *M. annularis*, consistent with the established Sr/Ca kinetic artifact. Significant anthropogenic variability is also observed by Pb/Ca analysis, observing two maxima since 1920. These potential artifacts cannot completely account for the Cd/Ca transition, supporting a mid-century reduction in upwelling intensity. The trace element records better agree with historical climate records relative to sedimentary faunal abundance records, suggesting a linear response to North Atlantic extratropical forcing cannot account for the observed variability in this region.

Thesis Supervisor: Edward A. Boyle
Title: Professor of Oceanography

Acknowledgments

This thesis work greatly benefitted from the generosity, kindness, and diligence of many individuals at the Massachusetts Institute of Technology (MIT), Woods Hole Oceanographic Institution (WHOI), and elsewhere. Without the following people this work would have been impossible, and their efforts will be remembered beyond my limited years in graduate school.

First, several faculty members at MIT and WHOI greatly improved my graduate education. Lloyd Keigwin supported my initial years in the Joint Program, allowing me to study oceanography and pursue my academic interests. Both Lloyd Keigwin and Tim Eglinton provided encouragement, support, and patience during my first two years at Woods Hole. Several professors also inspired me to pursue geochemistry, notably Bill Jenkins, John Hayes, and Sam Bowring. Finally, John Edmond gave me a world-class introduction to science in general, and his recent passing was a great loss.

An essential aspect of this work was my experience in E34. Rick Kayser provided terrific laboratory and field support, maintaining order in a chaotic lab, finding misplaced tools, and carefully measuring seawater samples. Alla Skorokhod was a great confidant during my five years in E34, and I appreciated her humor, intelligence, and pragmatism. Processing trace element samples is not exactly a typical summer in the United States, and Emmanuelle Puceat provided expert help for the Tortuga record. Finally, Barry Grant was a master teacher of mass spectrometry, computers, machinery, and most technical matters beyond my limited abilities. Whenever disaster struck, the stock answer always was 'Ask Barry'.

Coral samples for this project were generously donated by Julie Cole and Ellen Druffel. Julie fostered my first steps in surface coral research, teaching me many sampling and diving techniques in Venezuela. Her surface coral samples from the Cariaco Basin and the western Pacific allowed development of several useful records and the opportunity to re-established trace element proxies in corals. Ellen Druffel and Sheila Griffin also donated surface coral cores from North Rock, Bermuda, invaluable samples collected nearly two decades ago.

Ed Boyle has provided first-rate scientific resources for this thesis project. Ed's scientific abilities, perseverance, and humor represent the best possible model for a graduate student.

His high personal and scientific standards were inspiring, and I was very fortunate to be his graduate student.

My family and friends have been highly supportive of this academic endeavor. My parents, brother, and sister-in-law have been excellent personal role models, and this thesis greatly reflects their support and advice. My friends and fellow students have also kept my sanity intact, with special thanks to Greg Hoke, Kate Jesdale, Juan Botella, Mark Schmitz, Karen Viskupic, and Yu-Han Chen. The students and post-docs of E34 are also thanked for their friendship, help, and advice, including Jess Adkins, Dominik Weiss, Bridget Bergquist, and Jingfeng Wu. Finally, Kalsoum Abbasi provided most of the encouragement and friendship needed to finish this project and still laugh at the end of the day.

Biographical Note

Matthew Reuer was born on December 12, 1972 in Rochester, Minnesota. He was raised in Rochester and graduated from John Marshall High School in 1991. In 1995 he received a Bachelor of Arts degree in geology from Carleton College. Upon graduating, the author was employed by the Colorado College from 1995 to 1996, working as a teaching assistant in the Department of Geology. In September 1996, he entered the MIT-WHOI Joint Program in Oceanography as a doctoral candidate, specializing in Chemical Oceanography under Edward Boyle. The author is a member of the American Geophysical Union and the Geochemical Society, and is the recipient of a NSF Graduate Research Fellowship, a MIT Presidential Fellowship, and a MIT Graduate Teaching award. Upon graduating from MIT in 2002, he will pursue a post-doctoral fellowship at Princeton University.

Contents

List of Figures

List of Tables

Chapter 1

Introduction

The trace element geochemistry of the world oceans is directly associated with multiple global-scale phenomena, including the global carbon cycle, the land-air-sea mass balance, and anthropogenic heavy metal emissions. Despite their established importance, limited time series observations presently exist, with most seawater observations spanning the past two decades from a few locations (Wu and Boyle, 1997a). To address this issue, surface corals offer an important archive to constrain past geochemical variations in the tropical and subtropical surface ocean at seasonal resolution. This thesis project utilizes this approach to (1) examine past tropical upwelling variability in the Cariaco Basin, Venezuela; (2) quantify the flux and provenance of anthropogenic lead in the western North Atlantic; and (3) compare the reconstructed lead variability with recent hydrographic observations from the eastern and western North Atlantic. These centennial-scale records demonstrate the non-steady state, time-dependent distribution of multiple trace elements in the tropical and subtropical surface ocean, resulting from both natural and anthropogenic forcing.

The utility of carbonate geochemical proxies has three prerequisites: a quantitative understanding of modern elemental distributions, a carbonate host faithfully recording seawater chemistry, and an isolatable signal of adequate magnitude. Marine trace element variability has been well-established (*e.g.*, Boyle *et al.*, 1976; Chan *et al.*, 1977; Boyle *et al.*, 1981; Bruland and Franks, 1983; Schaule and Patterson, 1983; Johnson *et al.*, 1997), quantifying the relative importance of biological cycling, atmospheric deposition, and ocean circulation on trace element geochemistry. Trace element proxies in marine carbonates

was first systematically established for Cd/Ca ratios in benthic foraminifera, including synchronous glacial–interglacial Cd/Ca and $\delta^{13}C$ variability linked to a glacial reduction in North Atlantic Deep Water formation (Boyle and Keigwin, 1982, 1987; Boyle, 1988). Finally, adequate surface ocean trace element variability is expected given a six-fold difference in cadmium concentrations across the equatorial Pacific (Boyle and Huested, 1983) and a two-hundred fold difference in anthropogenic lead fluxes observed in Arctic ice cores (Murozumi *et al.*, 1969; Boutron *et al.*, 1991; Candelone *et al.*, 1995).

Surface corals offer a promising, seasonally-resolved trace element archive, demonstrated by several previous studies (*e.g.*, Shen *et al.*, 1987; Lea *et al.*, 1989; Shen *et al.*, 1992a). Trace elements and their isotopes provide independent evidence for past variations in upwelling intensity, fluvial influxes, nutrient status, and anthropogenic fluxes in the tropical and subtropical surface ocean. These results provide new geochemical observations and test the underlying assumptions of the established coral proxies, including minor element ratios (Sr/Ca, Mg/Ca), stable isotopes ($\delta^{18}O$, $\delta^{13}C$), and radiogenic isotopes ($\Delta^{14}C$, ^{210}Pb, see reviews by Dunbar and Cole, 1993; Druffel, 1997; Gagan *et al.*, 2000). Trace element measurements can incorporate several elemental and isotopic proxies from an individual sample (*e.g.*, Cd, Ba, Pb, Zn, V, and Fe), although most of these systems are largely unexplored. The annual density couplets and rapid extension rates of surface corals, coupled with radiometric age-dating techniques (Edwards *et al.*, 1987), provide a continuous, independent, and high-resolution chronology.

1.1 Cadmium, Barium, and Lead Marine Geochemistry

The first consideration for trace element proxies is their modern hydrographic distribution. Given their low seawater concentrations relative to the major cations (*e.g.*, 49.7 pmol kg^{-1} for North Atlantic mean 1996 total lead concentration, Wu and Boyle, 1997a), trace element analyses prior to 1976 were frequently compromised by sampling and analytical contamination. The difficulty of trace element analyses is both minimizing and quantifying the blank contribution for each step of the sampling and analytical protocol (see Tables 1 and 2 of Patterson and Settle, 1976), frequently testing methods, materials, and reagents. For

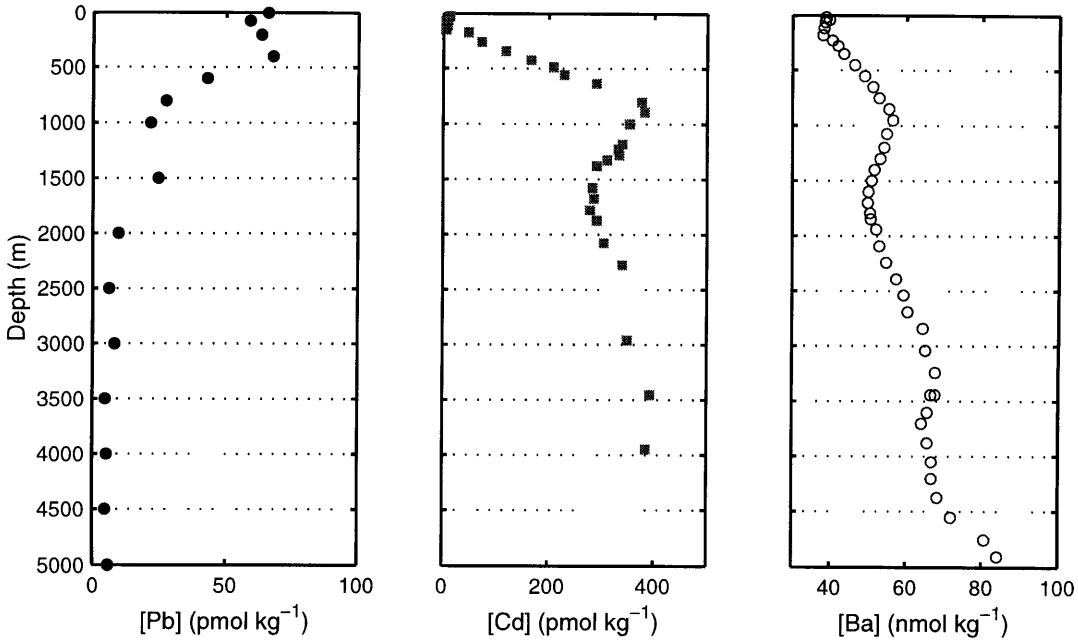

Figure 1-1: Water column profiles for cadmium, barium, and lead. The lead seawater profile, from Schaule and Patterson (1983, central northeast Pacific, 32°41'N, 145°00'W), exhibits clear particle-scavenging effects, with reduced concentrations from mixed layer to intermediate depths. The cadmium profile, from Wu and Boyle (1997b, eastern North Atlantic, 26°25'N, 33°40'W), shows a nutrient-like profile from biological uptake and remineralization. The barium profile demonstrates deeper barium regeneration from biogenic barite dissolution (Chan *et al.*, 1977). The secondary [Ba] maximum at 900 meters also reflects Antarctic Intermediate Water in the western North Atlantic.

seawater this challenge was addressed by several independent studies (Boyle and Edmond, 1976; Boyle *et al.*, 1976; Martin *et al.*, 1976; Bruland *et al.*, 1978; Schaule and Patterson, 1983), demonstrating consistent water column profiles among the major ocean basins (Figure 1-1). Here the generalized marine geochemistry of cadmium, barium, and lead is presented, demonstrating the relative importance of biological cycling, particle scavenging, and hydrography on their recent water column distribution.

Oceanic Cadmium Variability

The marine cadmium cycle is dominated by biological uptake and remineralization, resulting in a nutrient-type distribution similar to nitrate and phosphate. Boyle *et al.* (1976) first

demonstrated the correlation between seawater cadmium and phosphate concentrations in the Pacific, with water column Cd/P ratios (0.4 mmol/mol) consistent with plankton Cd/P ratios (0.4 to 0.7 mmol/mol). Water column profiles showed higher correlation with phosphate compared to silicate, suggesting cadmium regeneration from labile, organic-rich phytoplankton remains. Mechanistically, it has been suggested that part of the cadmium-phosphorus association results from carbonic anhydrase activity in marine phytoplankton (linked to zinc-carbonic anhydrase activity, Lee and Morel, 1995), and a distinct cadmium-carbonic anhydrase has been observed by Cullen *et al.* (1999). Direct correlation between cadmium, nitrate, and phosphate is complicated, however, by preferential trace element uptake relative to the major nutrients (see Figure 12 of Boyle *et al.*, 1981) and possible pCO_2 effects (Cullen *et al.*, 1999), resulting in multiple Cd/P relationships in the world oceans (Elderfield and Rickaby, 2000). Despite these complications, the nutrient-like distribution is demonstrated by cadmium accumulation within water masses; the North Atlantic deep water concentration (0.3 nmol kg^{-1}, Bruland and Franks, 1983) is approximately three-fold lower than the deep Pacific (1.0 nmol kg^{-1}, Bruland, 1980), consistent with diminished $\Delta^{14}C$ in the deep Pacific (see Figure 5-4 in Broecker and Peng, 1982). A large surface water cadmium concentration gradient (*ca.* 15 to 85 pmol kg^{-1}) across the eastern equatorial Pacific upwelling zone has also been observed by Boyle and Huested (1983), supporting its promise as an upwelling indicator. Thus cadmium geochemistry largely reflects major nutrient cycles and their hydrographic distribution.

The speciation of dissolved[1] cadmium in seawater is dominated by organic ligands and chloride complexes. As shown by Bruland (1992), 70% of dissolved cadmium in the central North Pacific mixed layer is bound to strong organic ligands, present at low concentrations ($K'_{cond} = 10^{12}$ M^{-1}, [L]<0.1 nM). This ligand was not observed below 175 meters, suggesting inorganic cadmium complexes are the primary species below the euphotic zone. Under standard conditions (pH 8.1, 25°C, 1 atm), cadmium chloride complexes are the principal species, including $CdCl_2^\circ$ (51%), $CdCl^+$ (39%), and $CdCl_3^-$ (6%, Zirino and Yamamoto, 1972). Free Cd^{2+} accounts for 2.5% of the dissolved inorganic fraction; other secondary

[1]Here 'dissolved' is operationally defined, reflecting all cadmium passing through a 0.45 μm filter and including colloidal and soluble phases.

species ($CdSO_4^\circ$, $CdOH^+$, $CdHCO_3^+$, and $CdCO_3^\circ$) are present below 1%.

The recent global cadmium cycle has been greatly altered by anthropogenic emissions. Background global cadmium emission estimates equal $1.3x10^9$ g yr^{-1} (Nriagu, 1989), whereas anthropogenic emissions reached $7.6x10^9$ g yr^{-1} in 1983, derived primarily from copper-nickel smelting, coal combustion, and steel manufacture (Nriagu and Pacyna, 1988). From surface coral Cd/Ca measurements from 1865 to 1982, Shen *et al.* (1987) inferred a five-fold increase in cadmium concentrations (0.26 to 1.37 nmol/mol) in the western North Atlantic surface ocean. The corresponding deep water response, however, should be minimal. For example, with an assumed area ($4.1x10^7$ km^2), depth (3800 meters), and cadmium concentration below 1000 meters (334 pM), the North Atlantic cadmium inventory equals $7.9x10^{12}$ g. If all the global cadmium emissions were deposited in the North Atlantic ($7.6x10^9$ g yr^{-1}) with no loss to particle scavenging, approximately one thousand years would be required to double the inventory. The biological uptake, regeneration, and advection of cadmium in the deep North Atlantic thus results in a heterogenous response to anthropogenic forcing.

Marine Barium Geochemistry

Barium geochemistry reflects the formation and regeneration of biogenic barite and the subsequent hydrographic distribution of dissolved barium, resulting in water column profiles similar to dissolved silica and alkalinity (Wolgemuth and Broecker, 1970; Chan *et al.*, 1977; Dehairs *et al.*, 1980; Collier and Edmond, 1984; Lea and Boyle, 1989). Upper ocean barium concentration gradients result from biogenic barite cycling, ranging from approximately 70 nmol kg^{-1} in the surface mixed layer to 100 nmol kg^{-1} at 2000 meters (Antarctic Circumpolar Current, Chan *et al.*, 1977). Bishop (1988) first observed the association among barite, opal, and organic carbon in marine particulate matter (>53 μm), noting high barium concentrations associated with siliceous diatom and dinoflagellate remains. The dissolution of these biogenic phases in marine sediments represents a significant barium source over high productivity regions: McManus *et al.* (1994) calculated a benthic barium flux of 25 to 50 nmol cm^{-2} yr^{-1} from the California continental margin. Second, hydrographic variability affects barium concentrations in the world oceans. For example, Chan *et al.* (1977) observed

barium concentration maxima in Antarctic Intermediate Water and Antarctic Bottom Water in the western North Atlantic, similar to the established silica distribution. Correlations among [Ba], [Si], and alkalinity should not be overstated, however, given their different sources in high-latitude regions (see Figure 16 of Chan *et al.*, 1977). Despite these complications, the marine barium cycle reflects barite formation in siliceous microenvironments, barium regeneration in seawater and marine sediments, and its subsequent hydrographic distribution.

In contrast to cadmium and lead, limited barium species are observed in seawater. Under standard conditions, Byrne *et al.* (1988) calculated 96% of dissolved barium exists as free Ba^{2+}, with only 4% present as $BaSO_4^\circ$. No association with organic ligands in seawater has been demonstrated.

Lead Geochemistry

The marine geochemistry of lead is dominated by aeolian deposition and scavenging, with no biological lead utilization. The importance of aeolian deposition was demonstrated by Schaule and Patterson (1981) for the central North Pacific, observing increased lead concentrations and ^{210}Pb activity from coastal western North America (Monterey Bay) to the subtropical North Pacific gyre (Hawaii), consistent with the spatial distribution of North Pacific ^{210}Pb (Nozaki *et al.*, 1976). The atmospheric transport pathway is also supported by vertical profiles in North Atlantic and Pacific, with low deep (26 pmol kg^{-1}, 2980 meters) and thermocline (77 pmol kg^{-1}, 1000 meters) lead concentrations in the Sargasso Sea relative to the surface mixed layer (160 pmol kg^{-1}, 0.5 meters). Scavenging and regeneration of aerosol-derived lead results in short residence times relative to cadmium and barium. From ^{226}Ra-^{210}Pb disequilibria (Craig *et al.*, 1973; Bacon *et al.*, 1976; Nozaki and Tsunogai, 1976), the lead residence time ranges from two years for the surface mixed layer to several decades for the upper thermocline. For example, Bacon *et al.* (1976) estimated integrated lead residence times of 20 to 93 years for six stations in the equatorial Atlantic over the depth range 451 to 5003 meters. Finally, mixed layer and upper thermocline lead also exhibits strong seasonality, demonstrated by Boyle *et al.* (1986) in the western North Atlantic. This seasonality reflects winter mixed layer depths reaching 200 meters, spring scavenging due to

elevated biological productivity, and summer accumulation within a stratified mixed layer. Thus the marine lead cycle reflects atmospheric inputs, seasonal upper-ocean variability, and particulate scavenging and regeneration.

The predominant atmospheric pathway warrants consideration. Recent atmospheric lead is associated with sub-micron, carbonaceous aerosols derived from high-temperature, anthropogenic sources (Rosman *et al.*, 1990), with a tropospheric residence time of 9.6±2.0 days (Francis *et al.*, 1970). As shown by the XRD analyses of Biggins and Harrison (1979), the composition of anthropogenic lead aerosols includes halogens derived from automobile exhaust (PbBrCl, PbBrCl·2NH_4Cl, and α-2PbBrCl·NH_4Cl) and sulfates ($PbSO_4$, $PbSO_4 \cdot (NH_4)_2SO_4$). Wet deposition dominates lead removal from the atmosphere, accounting for approximately 85% of the total deposition (see Duce *et al.*, 1991, and refs. therein). Solubility estimates of particulate-adsorbed lead are presently uncertain, ranging from 13 to 90% (Hodge *et al.*, 1978; Maring and Duce, 1990). Thus lead is effectively transported by and removed from the troposphere to the surface mixed layer.

Dissolved lead accounts for approximately 90% of the total lead concentration in oligotrophic gyres (Shen and Boyle, 1987), and a significant fraction of the dissolved phase might be complexed with organic ligands. For example, Capodaglio *et al.* (1990) observed 50 to 70% of dissolved lead is complexed with a strong organic ligand in the eastern North Pacific ($K'_{cond} = 10^{9.7}\ M^{-1}$); no North Atlantic measurements presently exist. The remaining dissolved phase is dominated by inorganic complexes: Whitfield and Turner (1980) calculated from equilibrium models that $PbCO_3^\circ$ accounts for 55% of the dissolved inorganic fraction, followed by $PbCl_2^\circ$ (11%), $Pb(CO_3,Cl_3)^-$ (10%), and $PbCl^+$ (7%). The remaining 17% includes chloride ($PbCl_3^-$, $PbCl_4^{2-}$), sulfate ($PbSO_4^\circ$), and hydroxide ($PbOH^+$) species, with free Pb^{2+} comprising less than 2% of total dissolved inorganic lead.

1.2 Anthropogenic Lead in Seawater

Of all heavy metals in the environment, global lead emissions have been most affected by human activities. The emission inventory method of Nriagu and Pacyna (1988) suggests 97% of modern lead fluxes are anthropogenic, and the global annual emissions for five met-

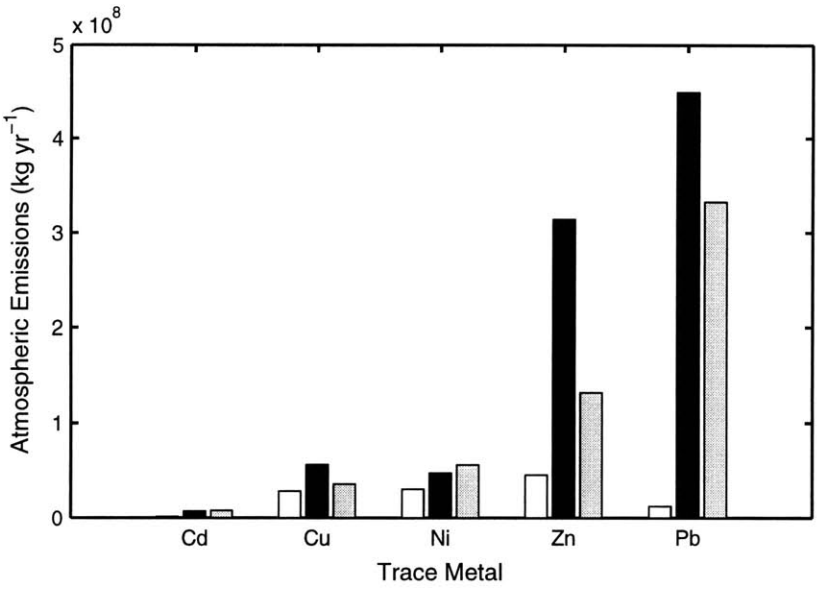

Figure 1-2: Global background and anthropogenic heavy metal emissions for cadmium, copper, nickel, zinc, and lead. The white bars reflect the background estimates of Nriagu (1989), the black bars denote the Nriagu (1979a) anthropogenic estimates for 1975, and the gray bars represent the Nriagu (1989) anthropogenic estimates for 1983. Note the predominance of zinc and lead relative to the other heavy metals, with the anthropogenic component from 56% for Cu to 97% for Pb in 1983.

als are shown in Figure 1-2. The median global lead emission for 1983 equals 3.3×10^{11} g yr^{-1}, thirty-fold higher than the natural background (1.2×10^{10} g yr^{-1} Nriagu, 1989). Natural lead sources include soil dusts (3.0×10^{9} g yr^{-1}), volcanic emissions (3.3×10^{9} g yr^{-1}), forest fires (1.9×10^{9} g yr^{-1}), seasalt aerosols (1.4×10^{9} g yr^{-1}), and continental particulate matter (1.3×10^{9} g yr^{-1}, Nriagu, 1989). As shown in Figure 1-3, adapted from Settle and Patterson (1980), anthropogenic lead production has occurred since approximately 5000 ^{14}C years before present, associated with the discovery of cupellation[2]. Modern anthropogenic emissions, however, are dominated by leaded gasoline consumption, accounting for approximately 75% of the total emissions in 1983. Historical variations in leaded gasoline consumption is shown in Figure 1-4, including consumption patterns in the United States and western Europe from 1930 to 1990. The smelting of non-ferrous metals (including pri-

[2]Cupellation is the separation of gold or silver from argentiferous lead, refining the ore in a porous furnace (a cupel). The impurity metals (*e.g.*, Pb, Cu, and Sn) are oxidized, vaporized, and partly adsorbed onto the porous cupel during blast heating. This fire assay and refining technique is considered the oldest quantitative chemical method; a thorough historical and technical review is given by Nriagu (1985).

mary lead, copper-nickel, and zinc-cadmium), accounts for the remaining 25%, although this contribution is currently increasing with the progressive phaseout of leaded gasoline from North America and western Europe (Wu and Boyle, 1997a).

Three properties of modern lead aerosols provide independent evidence of their primary anthropogenic origin. First, the elevated Pb/Ba ratio of pristine soils support its anthropogenic origin (Patterson and Settle, 1987). This technique normalizes lead concentrations with respect to barium, determining the natural Pb/Ba ratio from the High Sierra source quartz monzonite and a minor ($Ba_{seasalt}/Ba_{dust}$=0.07) seasalt correction to the aerosol Ba (Patterson and Settle, 1987). Using this method, Patterson and Settle (1987) estimated industrial lead accounted for 88% of total lead concentrations in High Sierra soil humus and litter. Measured aerosol lead concentrations are also approximately ten-fold smaller on air filters relative to precipitation at the same location, a consequence of high-temperature anthropogenic sources enriching the sub-micron, halogenated, and carbonaceous mode readily scavenged by wet deposition (Ng and Patterson, 1981; Patterson and Settle, 1981). Second, the aerosol lead fluxes across the central Pacific are greater in the Northern Hemisphere, ranging from 0.02 ng cm^{-2} yr^{-1} for the south polar cell to 50 ng cm^{-2} yr^{-1} in the North Pacific westerlies (Patterson and Settle, 1987, and refs. therein). An Atlantic-Pacific difference is also observed for the Northern Hemisphere, with 170 ng cm^{-2} yr^{-1} measured from the North Atlantic westerlies (*ibid.*). Finally, mass balance calculations support predominant anthropogenic fluxes. Assuming a two-year residence time in the upper 100 meters and a lead concentration of 160 pmol kg^{-1} (Schaule and Patterson, 1983), the resulting lead flux is 175 ng cm^{-2} yr^{-1}. This estimate is approximately six times greater than the maximum natural output flux of 30 ng cm^{-2} yr^{-1} calculated from the accumulation and lead concentration of pelagic sediments (Chow and Patterson, 1962). The difference between this anthropogenic to background ratio (5.8) and the Nriagu (1989) estimate shown in Figure 1-2 (27.7) most likely results from the spatial scales between global (Nriagu, 1989) and North Atlantic estimates; uncertainties in the lead residence time and possible seasonal aliasing of the Schaule and Patterson (1983) observation will also contribute to this difference.

The observed anthropogenic fluxes have corresponding seawater signatures. First, Wu and Boyle (1997b) observed a three fold reduction in seawater lead concentrations near

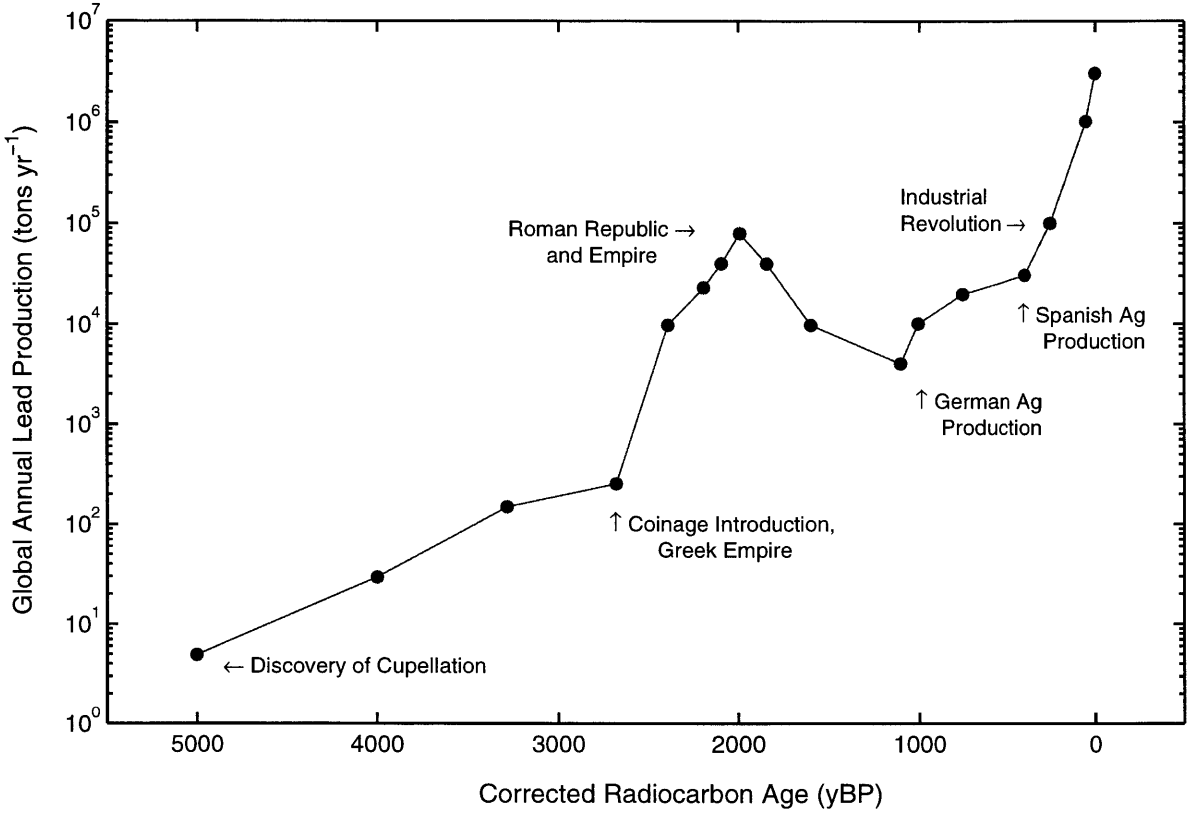

Figure 1-3: Historical global lead production since 5000 ^{14}C years before present, adapted from Settle and Patterson (1980). The derivation of this curve is based on the lead content of cerargyrite (AgCl), global silver production, and historical lead production data (see footnotes in Settle and Patterson, 1980). Note the ordinate is shown on a logarithmic scale.

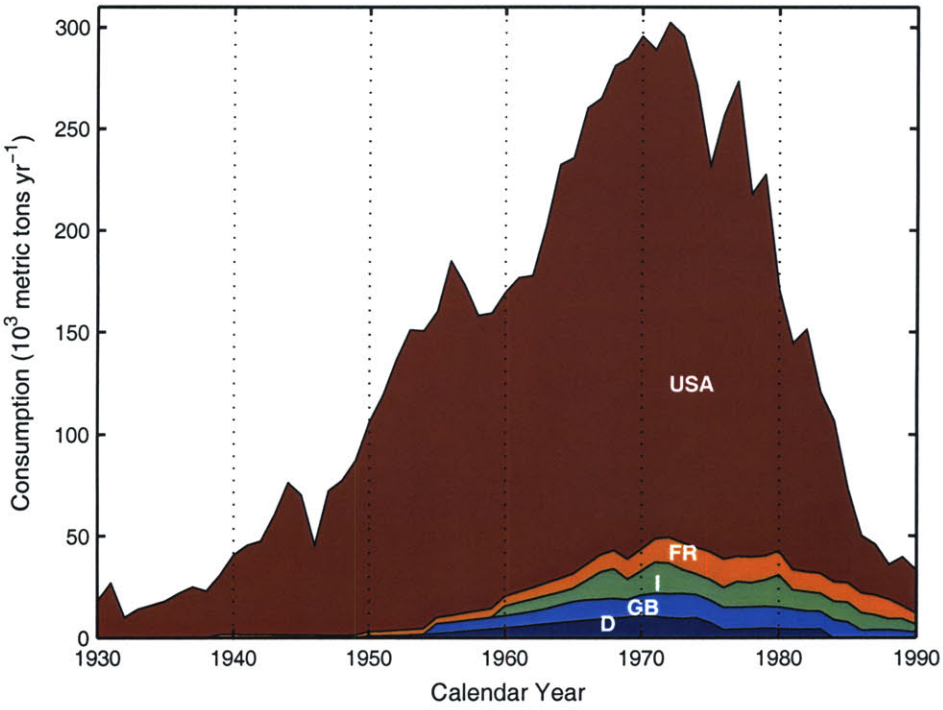

Figure 1-4: Historical leaded gasoline consumption, United States and western Europe. The figure and the associated data are taken from Wu and Boyle (1997a) and references therein. The nations shown include the United States (USA), France (FR), Italy (I), the United Kingdom (GB), and Germany (D). The maximum leaded gasoline consumption in the United States occurred in 1972, corresponding to 84% consumption with respect to the nations shown here.

Bermuda, from 160 pmol kg^{-1} (Schaule and Patterson, 1983) in 1979 to 49.7 pmol kg^{-1} in 1996 (Figure 1-5). This apparent reduction includes a large seasonal cycle due to the lead mixing–scavenging–accumulation cycle (see above and Boyle *et al.*, 1986). The three-fold reduction in seawater lead concentrations is concurrent with known reductions in leaded gasoline consumption in the United States from 1979 to 1993 ($190x10^3$ to $10x10^3$ metric tons yr^{-1}), providing a direct link between US lead emissions and seawater lead concentrations. Second, vertical lead concentration profiles provide additional evidence for reduced anthropogenic lead fluxes. Because the western North Atlantic upper thermocline is ventilated on decadal timescales (from ^3H–^3He measurements of Jenkins, 1980), a comparable reduction in thermocline lead concentrations should be observed. As shown in Figure 1-6, vertical profiles from 1979 (Schaule and Patterson, 1983) to 1998 (E. A. Boyle, unpublished results) exhibit a consistent reduction to approximately 1000 meters. The shape of the elemental

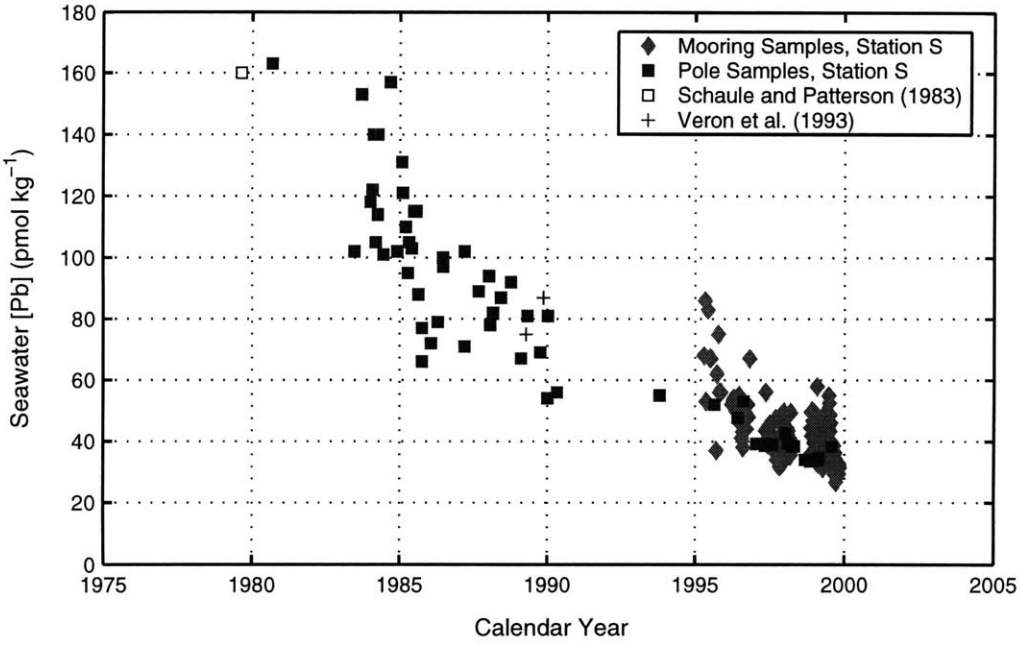

Figure 1-5: Bermuda seawater lead time series analysis, 1979-2000, adapted from Wu and Boyle (1997a). Surface mixed layer lead concentrations (in pmol kg^{-1}) from Station S are shown, including results from Schaule and Patterson (1983, □) and Véron *et al.* (1993, +). The closed squares were collected by the pole sampling method at Station S, and closed diamonds reflect MITESS mooring samples. See Wu and Boyle (1997a) for additional details.

profiles are clearly different, due to the declining mixed layer concentrations concurrent with reduced anthropogenic emissions, the increasing ventilation time scales with depth in the western North Atlantic (Jenkins, 1980), the seasonality of lead scavenging, regeneration, and accumulation within the upper 200 meters (Boyle *et al.*, 1986), and sampling or analytical artifacts. Both the western North Atlantic mixed layer and the thermocline lead concentrations have declined according to the anthropogenic lead transient.

Terrestrial and marine proxy data provide additional constraints regarding the anthropogenic transient. Measuring lead concentrations in ice near Camp Century, Greenland, Murozumi *et al.* (1969) first observed the Arctic anthropogenic transient, with lead concentrations increasing from less than 0.001 μg g^{-1} at 800 BC to greater than 0.200 μg g^{-1} in 1965. The greatest increase in lead concentration occurred after 1940, in agreement with Eurasian and North American leaded gasoline consumption patterns. A ten-fold concentra-

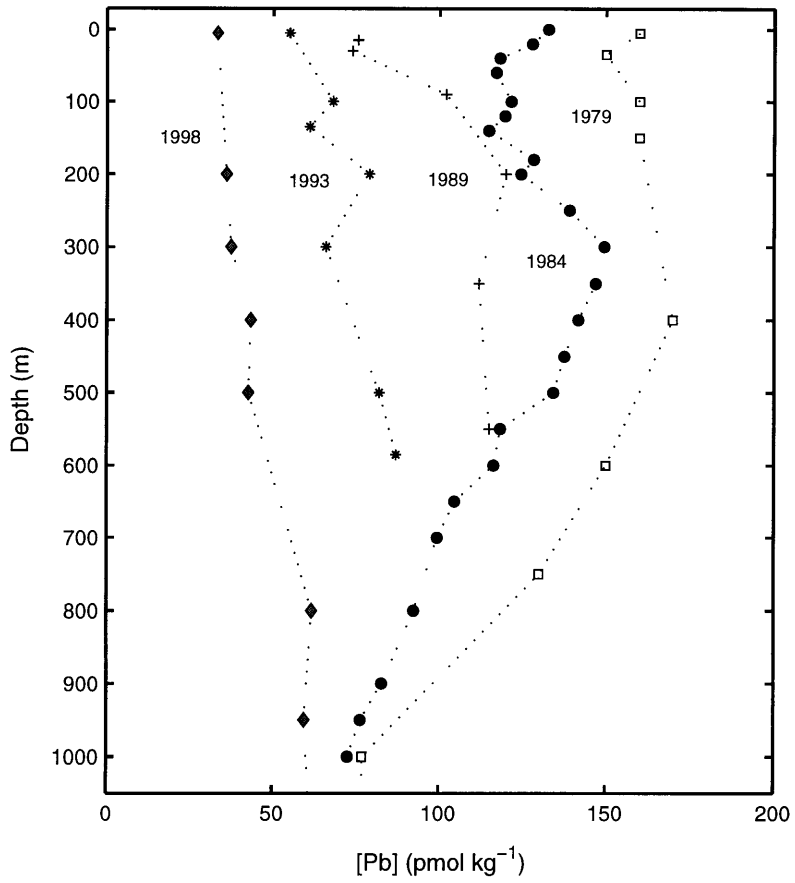

Figure 1-6: North Atlantic thermocline lead evolution: 1979 to 1998. Six profiles are shown from the western North Atlantic: Schaule and Patterson (1983, □, collected 1979), Boyle *et al.* (1986, •, collected 1984), Véron *et al.* (1993, +, collected 1989), Wu and Boyle (1997a, ∗, collected 1993), and unpublished results of E. A. Boyle [♦, collected 1998]. The 1984 profile represents the mean of three profiles taken in April, June, and September (Boyle *et al.*, 1986).

tion difference between 800 BC (<0.001 μg g^{-1}) and 1750 AD (0.011 μg g^{-1}) also suggests significant anthropogenic lead fluxes prior to the Industrial Revolution, in agreement with Figure 1-3. Other terrestrial records, including peat cores and lacustrine sediments, provide useful constraints on past anthropogenic variability (*e.g.*, Shirahata *et al.*, 1980; Ritson *et al.*, 1994; Graney *et al.*, 1995; Shotyk *et al.*, 1998; Weiss *et al.*, 1999). From a Jura Mountain peat core, Shotyk *et al.* (1998) observed a significant increase in Pb/Sc ratios at 3000 ^{14}C yr. BP, indicating the first European anthropogenic lead signatures associated with

Phoenician and Greek lead mining. The recent transient at the Jura Mountain site (15.7 mg m^{-2} yr^{-1}, 1979) was also 1570 times the natural background value (0.01 mg m^{-2} yr^{-1}), significantly higher than the Greenland natural to anthropogenic ratio. Finally, surface coral records (Shen and Boyle, 1987) and marine sediments (Ng and Patteron, 1982; Véron *et al.*, 1987) provide additional constraints on anthropogenic fluxes to the world oceans. Measuring the Pb/Ca ratio of surface corals from Bermuda and the Florida Straits, Shen and Boyle (1987) estimated an eleven-fold increase in anthropogenic lead fluxes to the western North Atlantic from 1884 (5.2 nmol/mol) to 1971 (56.7 nmol/mol). Proxy records provide independent evidence for global-scale, time-dependent anthropogenic lead fluxes to terrestrial and marine environments.

1.3 Lead Isotope Geochemistry

The isotopic composition of recent lead represents an established, independent atmospheric and oceanic tracer. Lead isotope fractionation is governed by the age and initial U-Th-Pb content of an ore body. Radiogenic ingrowth of ^{208}Pb from ^{232}Th, ^{207}Pb from ^{235}U, and ^{206}Pb from ^{238}U can be written as:

$$^{206}Pb = {}^{206}Pb_o + {}^{238}U \cdot \left[e^{\lambda_{238} t_o} - e^{\lambda_{238} t}\right] \quad (1.1)$$

$$^{207}Pb = {}^{207}Pb_o + {}^{235}U \cdot \left[e^{\lambda_{235} t_o} - e^{\lambda_{235} t}\right] \quad (1.2)$$

$$^{208}Pb = {}^{208}Pb_o + {}^{232}Th \cdot \left[e^{\lambda_{232} t_o} - e^{\lambda_{232} t}\right] \quad (1.3)$$

where the subscript [o] reflects the primeval isotopic abundance, t_o denotes the age of the Earth, t is the emplacement age, and λ_x represents the half lives for ^{238}U (1.55125x10^{-10} y^{-1}), ^{235}U (9.8485x10^{-10} y^{-1}), and ^{232}Th (4.9475x10^{-11} y^{-1}, Steiger and Jäger, 1977). The three equations for ^{206}Pb, ^{207}Pb, and ^{208}Pb result from two separate processes: (1) the radiogenic ingrowth of a daughter product within a closed system since the Earth's formation ($^{206}Pb = {}^{206}Pb_o + {}^{238}U \cdot \left[e^{\lambda_1 t_o} - 1\right]$); and (2) a correction for the emplacement age of the ore body, separating the daughter and parent isotopes ($^{206}Pb = {}^{206}Pb_o + {}^{238}U \cdot \left[e^{\lambda_1 t_o} - 1\right] - {}^{238}U \cdot \left[e^{\lambda_1 t} - 1\right]$). Normalizing these equations with respect to the non-radiogenic ^{204}Pb, the $^{206}Pb/^{204}Pb$ ratio can be determined from the initial $^{206}Pb/^{204}Pb$

ratio, the primeval $^{238}U/^{204}Pb$ ratio, and the age of the system. The consequence of radiogenic ingrowth and the different half lives is that older lead ores exhibit lower $^{206}Pb/^{207}Pb$ and $^{208}Pb/^{207}Pb$ ratios, resulting in large isotopic variability among modern lead ores of variable age and initial U-Th-Pb content (Figure 1-7). The isotopic composition of anthropogenic lead in a single reservoir will therefore reflect two time-dependent processes: (1) the isotopic composition of an individual anthropogenic source from a single region (e.g., leaded gasoline emissions from the United States); and (2) its weighted contribution to a single reservoir with respect to other sources and regions.

The utility of lead isotopes as an anthropogenic tracer was first suggested by Chow and Johnstone (1965), observing isotopic variability among the principal anthropogenic sources. Chow and Johnstone (1965) and Chow *et al.* (1975) demonstrated a large range in gasoline lead isotopes, a consequence of various ores utilized for tetraethyllead production. Comparing the $^{206}Pb/^{207}Pb$ results from these two studies, the isotopic differences are apparent within (1.115 to 1.160, n=10, San Diego) and between several regions in the United States (1.149: western US; 1.175: eastern US). The largest differences in leaded gasoline, however, are apparent among separate nations, with a 14% range observed between Bangkok, Thailand (1.072) and Santiago, Chile (1.238). Second, large isotopic variations have also been observed for coal samples from the United States, ranging from 1.126 for the Paleocene Northern Great Plains province to 1.252 for the Pennsylvanian Interior coal province (Chow and Earl, 1972). Direct experimental evidence exists for significant isotopic variability among multiple anthropogenic sources.

As expected from elemental lead analyses, the isotopic composition of aerosol lead is primarily anthropogenic. Chow and Earl (1970) demonstrated qualitative correlation between leaded gasoline and aerosol lead isotopes (n=5). Exact correlation should not be expected, due to atmospheric transport from different sources (*e.g.*, municipal incinerators or metal smelters) and the heterogeneous isotopic composition of individual sources. Chow and Johnstone (1965) also quantified the anthropogenic component by comparing the isotopic composition of leaded gasoline, recent aerosols, and background lead from abyssal Pacific sediments. With respect to the $^{206}Pb/^{207}Pb$ ratio, both Los Angeles aerosols (1.154) and Lassen Volcanic Park snow (1.144) were within analytical error of California leaded

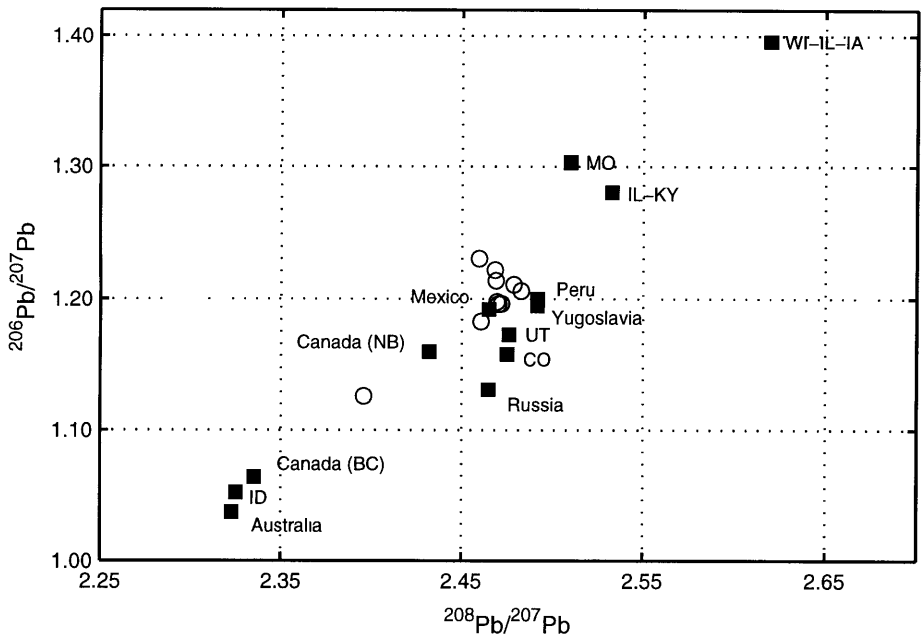

Figure 1-7: Lead-lead diagram for primary lead ores and coal, including the ore districts of the United States, Canada, Australia, Russia, Mexico, Peru, and Yugoslavia. US ores follow the common state abbreviations, and the Canadian ores include the New Brunswick (NB) and British Columbia (BC) districts. Lead ore isotope data are from Doe (1970) and Chow *et al.* (1975). Coal data from the United States are shown as open circles (Chow *et al.*, 1975).

gasoline (1.145) and were clearly different from abyssal Pacific sediments (1.197). These observations are confirmed by global-scale aerosol and precipitation analyses: aerosol lead generally reflects its anthropogenic source (Bollhöfer and Rosman, 2000; Simonetti *et al.*, 2000; Bollhöfer and Rosman, 2001).

With accurate, time-dependent isotopic source estimates, one can calculate their relative contributions. Three examples of this technique are given here. First, the relative lead contribution to tropospheric aerosols was quantified by Sturges and Barrie (1987), using the divergent median $^{206}Pb/^{207}Pb$ ratios from the United States (1.217±0.008, n=39) and Canada (1.151±0.007, n=37) to determine their contributions to central Ontario in 1984 (43% US) and 1986 (24% US). Second, the provenance of oceanic lead was determined by Hamelin *et al.* (1997), measuring the isotopic composition of seawater and aerosols in the western North Atlantic. For 1995, the authors estimated a 40 to 60% contribution

to the subtropical North Atlantic gyre from the United States. Finally, Rosman *et al.* (1993) measured the isotopic composition of Greenland snow to estimate anthropogenic lead sources since the late 1960s. The authors observed a $^{206}Pb/^{207}Pb$ increase from 1967 to 1977 (*ca.* 1.16 to 1.20), followed by a comparable reduction from 1978 to 1988. Thus isotopic variability in the atmosphere and ocean results from differences in both source composition and contribution, with an inferred reduction in US fluxes from 79% in 1972 to 8% in 1988.

1.4 Coral Biology and Calcification

Given the past elemental and isotopic variability, surface corals provide a useful reconstruction of its marine signature. Before addressing coral geochemistry, one must first consider its biological context. The corals utilized for this study include the colonial, reef-building scleractinian corals (subclass Zoantharia, class Anthozoa, subphylum Cnidaria, phylum Coelenterata). Following the nomenclature of Schuhmacher and Zibrowius (1985), the three Atlantic genera included here (*Diploria*, *Siderastrea*, and *Montastrea*) are zooxanthellate, constructional, and hermatypic corals. The difference between constructional and hermatypic should be noted: constructional reflects the formation of a durable carbonate structure (*e.g.*, bioherms or reefs), whereas hermatypic reflects contribution to a reef framework. A brief review of coral structure and calcification is provided; extensive discussion is given by Wells (1956) and Barnes and Chalker (1990).

The coral polyp represents the primary unit of scleractinian corals, comprised of a cylindrical column, terminated above by a horizontal oral disk and below by a basal disk (Figure 1-8). The oral disk includes several nematocyst-bearing tentacles and an esophagus-like stomodaeum leading to an internal gastrovacular cavity, or coelenteron (Wells, 1956). The internal cavity typically contains six to twenty-four mesenterial filaments attached to the stomodaeum, responsible for digestion, nutrient adsorption, and gonad production. The polyp walls consist of three tissue layers common to the Cnideria: the ectoderm, the mesoglea, and the endoderm. Ectodermal cells near basal disk are known as calcioblasts, responsible for aragonite precipitation. Photosynthetic symbiotic dinoflagellate algae, pre-

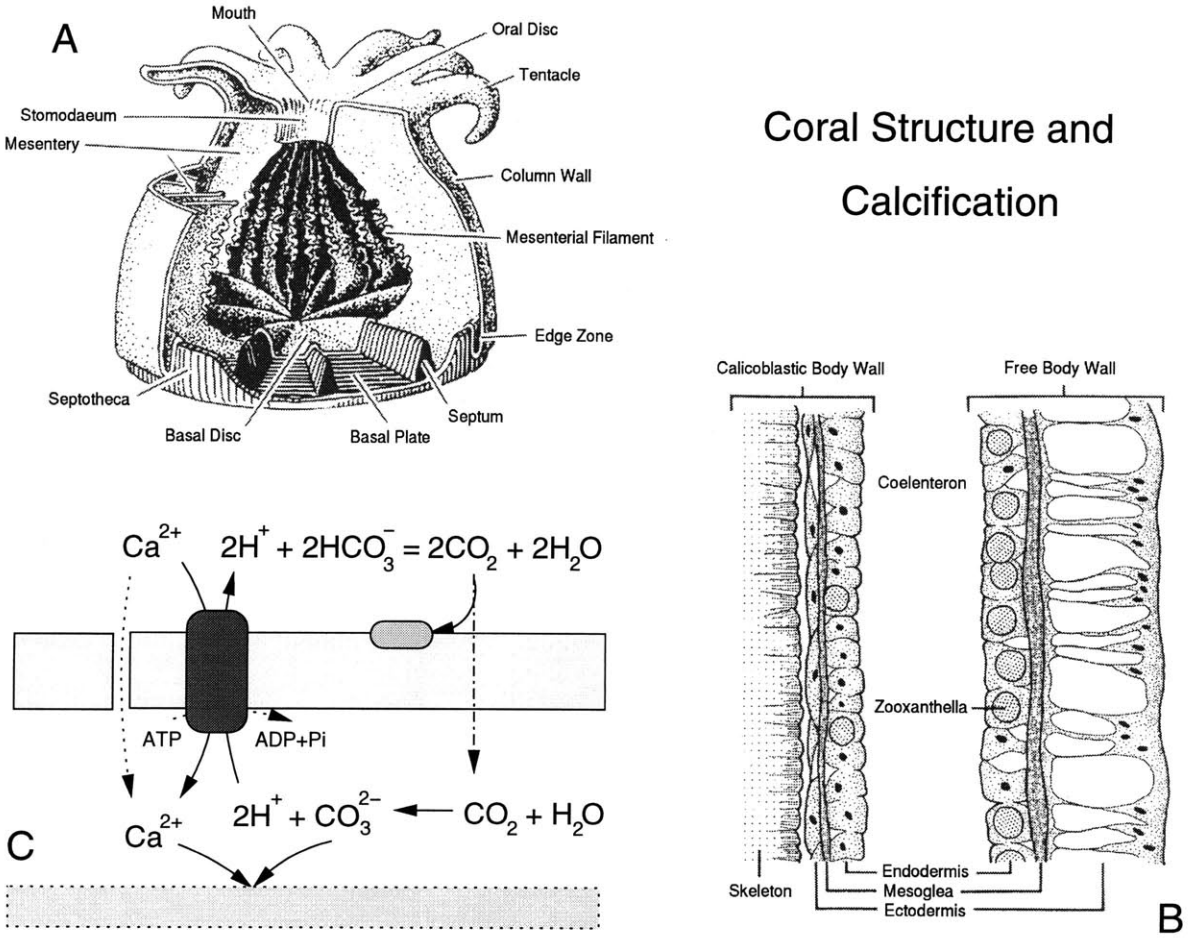

Figure 1-8: Surface coral structure and calcification. Figure A reflects the generalized polyp anatomy, including the oral disk, the polyp cylinder, and the basal disk (modified from Wells, 1956). Note the convoluted shape of the basal disk forming the aragonitic septa. Figure B shows the three tissue layers present throughout the polyp, including the ectodermis, the cell-free mesoglea, and the symbiont-bearing endodermis (modified from Barnes and Chalker, 1990). Figure C denotes the hypothetical McConnaughey *et al.* (1997) 'trans' calcification model. Ambient Ca^{2+} crosses the cell membrane either by active transport with Ca^{2+}-ATPase or passive ion channels. Protons generated from calcification are exchanged for Ca^{2+} at the expense of ATP. The resulting CO_2 is either utilized by chlorophyll for photosynthesis or diffuses across the cell membrane.

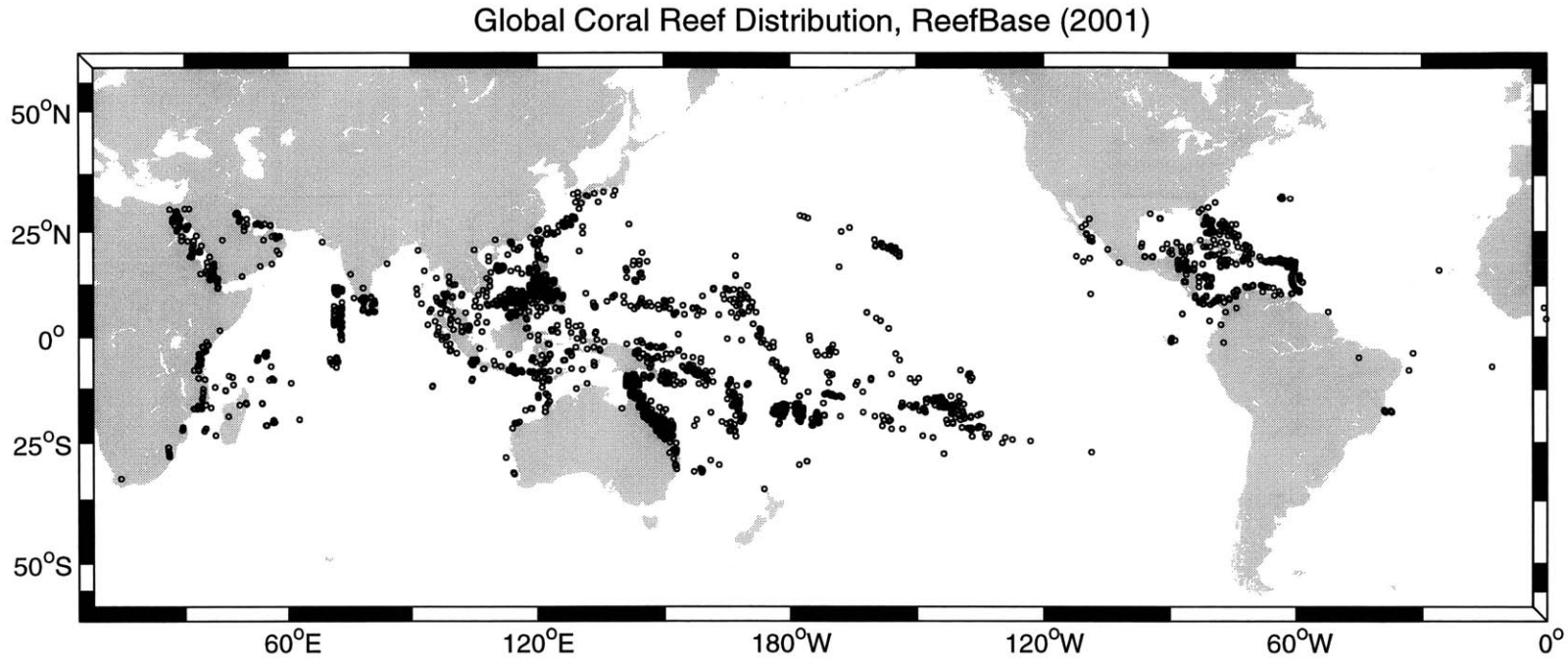

Figure 1-9: Global coral reef distribution, taken from the 2001 ReefBase unpublished data set. Note the latitudinal distribution of reefs in the Atlantic and Pacific and the limited available substrate in the eastern equatorial Pacific.

dominantly *Symbiodinium microadriacticum*, are also present throughout the polyp (Barnes and Chalker, 1990). Thus surface coral polyps include specialized, adaptive cell structures within a simple body plan.

The aragonite skeleton consists of two primary components: the corallum, the skeletal features deposited by the polyp colonies, and the coenosteum, the external skeletal structures supporting the intra-polyp region. Within the cylindrical corallum vertical, radiating partitions called septa are present, deposited from the basal disc. Horizontal structures deposited within and outside the polyp walls are known as dissepiments, tabular sheets formed by upward growth of the basal disc and coenosarc. The basic units of coral aragonite are known as sclerodermites, consisting of acicular, aragonite fibers 0.2 to 0.7 μm in diameter and 20 μm in length (Swart, 1981). The sclerodermites radiate from a center of calcification (Barnes, 1970), a consequence of non-syntaxial crystal growth under highly supersaturated conditions. Coral skeletons reflect specialized morphologies arising from a biological template, including the growth, distribution and morphology of coral polyps.

What are the biochemical mechanisms responsible for this complex architecture? One possible explanation for aragonite precipitation is provided by the 'trans' calcification model of McConnaughey *et al.* (1997), linking symbiont photosynthesis and calcification in corals (Figure 1-8). The trans calcification model couples proton generated by calcification with CO_2 consumed by photosynthesis:

$$Ca^{2+} + HCO_3^- = CaCO_3\ (s) + H^+ \quad (1.4)$$

$$H^+ + HCO_3^- = CH_2O + O_2 \quad (1.5)$$

The cross-membrane exchange of Ca^{2+} for $2H^+$ requires either Ca^{2+}–ATPase or passive ion channels, whereas CO_2 is either consumed by photosynthesis or diffuses across the membrane. Supporting evidence for this model includes analogous proton pumps observed in calcareous plants, observed Ca^{2+}–ATPase activity in asymbiotic and symbiotic corals, and higher calcification rates in zooxanthellate corals (see McConnaughey *et al.*, 1997; Goreau *et al.*, 1996, and refs. therein). Direct experimental evidence for the trans model, however, is still limited.

A consequence of the McConnaughey *et al.* (1997) model is the link between coral growth and the reef environment, and several previous studies have observed optimal coral growth rates under specific conditions, including light availability (Goreau and Goreau, 1959; Goreau, 1963; Wellington and Glynn, 1983, and refs. therein), sedimentation (Dodge *et al.*, 1974), temperature (16 to 30°C), and salinity (25 to 40‰). These limits restrict coral reef formation to the upper water column (1 to approximately 40 meters) in temperate and tropical latitudes (32°S to 35°N). Currently known global reef sites are shown in Figure 1-9, demonstrating the importance of substrate availability and sea surface temperature on the modern coral reef distribution.

The primary feature of the surface coral skeleton is the annual density couplet, first suggested by Ma (1934) to reflect seasonal growth rate variations. Density band formation results from three processes: (1) addition of new skeleton to the basal disk; (2) thickening of the existing skeleton through the depth of the tissue layer; and (3) periodic uplift of the tissue layer (Barnes and Lough, 1993). The principal cause of density band formation is debated, although seasonal variations in light intensity, sea surface temperature, and reproduction are key parameters (Wellington and Glynn, 1983).

The annual periodicity of density band formation is supported by several observations, including autoradiography, tissue staining at repeated intervals, and stratigraphic correlation. Knutson *et al.* (1972) correlated autoradiographs generated from ^{90}Sr decay to density band patterns, noting agreement between bomb test dates at Eniwetak Atoll, the density band number, and the coral collection date. Surface coral tissues repeatedly stained with alizarin-red also support the annual timing of density band formation, matching density bands with the known staining dates (Hudson *et al.*, 1976, A. Cohen, personal communication). Finally, stratigraphic correlation between density band width and meterological data supports their annual frequency: Hudson *et al.* (1976) observed perfect correlation between reduced band widths and winter air temperature minima in the Florida Straits. Density bands provide two important constraints for surface coral analyses: a continuous, measurable chronology from an established datum and stratigraphic tie points for inter-core comparisons.

Coral aragonite offers several advantages for geochemical and paleoclimate studies (see

recent reviews by Druffel, 1997; Gagan *et al.*, 2000). First, a continuous stratigraphy devoid of bioturbation provides new information regarding sub-annual to centennial-scale variability. Second, multiple geochemical proxies can be analyzed from a single sample, including stable isotopes, trace elements, radiogenic isotopes, and minor elements (see below). Third, long, continuous records can be generated from an individual colony, extending up to 400 years in some cases (Dunbar *et al.*, 1994). Finally, coral dating by the radiocarbon and U/Th techniques provides independent age estimates, providing accurate chronological constraints for discrete samples.

1.5 Surface Coral Trace Element Geochemistry

The trace element geochemistry of coral aragonite provides unique information regarding sea surface temperature, anthropogenic fluxes, and the circulation history of the tropical oceans. Presently several minor or trace elements have been identified as constituents in coral aragonite, and their relative abundance can reflect either seawater concentration (*e.g.*, Cd, Ba, Mn, and Pb, Shen and Boyle, 1988a; Lea *et al.*, 1989; Linn *et al.*, 1990; Shen *et al.*, 1992a; Delaney *et al.*, 1993) or sea surface temperature (*e.g.*, Sr, U, and Mg, Beck *et al.*, 1992; de Villiers *et al.*, 1995; Min *et al.*, 1995; Shen and Dunbar, 1995; Mitsuguchi *et al.*, 1996; Shen, 1996; Alibert and McCulloch, 1997). Elemental ratio analysis provides independent paleotemperature and paleochemical estimates in addition to established surface coral proxies, including oxygen-18 and carbon-13 (*e.g.*, Fairbanks and Matthews, 1978; Fairbanks and Dodge, 1979; Dunbar and Wellington, 1981; Cole *et al.*, 1993; Dunbar *et al.*, 1994). Here the basis of surface coral trace element geochemistry is presented, focusing on the successful application of cadmium, barium, and lead.

Carbonate trace element proxies rely on solid solution of a divalent cation for Ca^{2+} in aragonite or calcite. This substitution can be quantified by a non-thermodynamic partition coefficient (Henderson and Kracek, 1927), D_p, reflecting the relative uptake of a trace element from seawater:

$$D_p = \left[\frac{X^{2+}}{Ca^{2+}}\right]_{coral} / \left[\frac{X^{2+}}{Ca^{2+}}\right]_{seawater} \tag{1.6}$$

where X^{2+} denotes any divalent cation. The partition coefficient defined in Equation 1.6 is distinct from a thermodynamic distribution coefficient (K_d), which must include activity coefficients for the solid and solution phases (see review by Morse and Bender, 1990). Assuming a constant D_p and measured elemental ratios, one can then estimate past changes in surface ocean chemistry.

This inference, however, has several complications. First, it is unlikely that solid solution occurs at thermodynamic equilibrium given rapid, biologically-mediated aragonite precipitation. For example, Shen and Boyle (1987) measured inorganic Pb/Ca distribution coefficients of 20 to 35, one order of magnitude greater than D_p values observed for coral aragonite (2 to 3). This discrepancy agrees with observed reductions in K_d at elevated precipitation rates (for $D_p > 1$, Lorens, 1981). Second, lattice substitution might not account for all cations present in biogenic carbonates. Based on leaching experiments, Amiel *et al.* (1973) suggested minor elements in coral aragonite (Sr^{2+}, Mg^{2+}, Na^+, and K^+) are predominantly interstitial or adsorbed onto crystal surfaces, observing only 10% of coral strontium exists in the mineral lattice. This conclusion was supported by x-ray spectroscopy observations of Greegor *et al.* (1997), estimating at least 40% of coral strontium exists as strontianite ($SrCO_3$), not simply strontium-substituted aragonite ($[Sr,Ca]CO_3$). Similar observations for trace elements in aragonite presently do not exist. Finally, coral growth rates signficantly affect trace and minor element ratios. de Villiers *et al.* (1994, 1995) observed significant reductions in Sr/Ca ratios (0.1 to 0.2 mmol/mol) between corals with extension rates of 6 and 14 mm yr^{-1}, respectively. A similar growth-rate dependence has been observed for other systems, including the trace elements (Ba/Ca, Cd/Ca, and Mn/Ca, G. Shen, unpublished data) and stable isotopes (oxygen-18 and carbon-13, McConnaughey, 1989a,b).

Despite these complications, several independent observations support consistent elemental partitioning. Swart (1981) observed agreement between coralline and seawater Sr/Ca ratios in culture experiments, with no difference in strontium D_p among three coral species (4.6 to 96.0 mmol/mol, n=7). Historical climate and geochemical records also support consistent elemental uptake. For example, Shen and Boyle (1987) observed Pb/Ca

variability at North Rock, Bermuda and the Florida Straits associated with historical lead consumption, including the introduction and phaseout of leaded gasoline (Figure 1-10). Lea *et al.* (1989) and Shen *et al.* (1987) also documented qualitative correlation between El Niño-Southern Oscillation (ENSO) events and diminished Ba/Ca and Cd/Ca ratios in the Galápagos Islands, shown in Figure 1-11. The observed anticorrelation between the Ba/Ca ratio and SST results from upwelling of cool, high [Ba] upper thermocline waters during the La Niña phase of the ENSO cycle (see review by Webster and Palmer, 1997). Shen *et al.* (1992a) observed consistent down-core variability in Cd/Ca, Ba/Ca, $\delta^{13}C$, and $\delta^{18}O$, correlating Galápagos SST with Cd/Ca (r=-0.72) and Ba/Ca (r=-0.80) variability from 1965 to 1982. Finally, a positive correlation is observed (r=0.83) between surface coral Cd/Ca ratios and mean annual mixed layer [PO_4], including eight coral species from ten sites in the tropical Atlantic, Pacific, and Indian Oceans (Table 1.2). From these observations, the trace element geochemistry of corals will reflect past variations in seawater chemistry.

The observed range of surface coral trace elements should be emphasized. Surface coral multi-element analysis shown in Table 1.1 and Figure 1-12 demonstrates most elements exhibit partition coefficients close to unity. A shift in the partition coefficient due to changing coral growth rates might falsely estimate seawater elemental ratios. The large range of trace element ratios, however, diminishes the importance of the kinetic artifacts. For example, a ten-fold increase in Pb/Ca ratios was observed by Shen and Boyle (1987) from 1884 (5.2 nmol/mol) to 1971 (56.7 nmol/mol). Kinetic effects can introduce significant offsets for Sr/Ca paleothermometry (2 to 4°C), but the 2 to 3% difference in absolute Sr/Ca ratios (see Figure 1A of de Villiers *et al.*, 1995) will not affect the interpretation of trace element records.

1.6 Project Outline

This project offers several new perspectives regarding the trace element geochemistry of scleractinian corals. First, a reliable and precise method for stable lead isotope ratio analysis by multiple collector ICP-MS is presented in Chapter 2, addressing mass fractionation effects, isotope ratio precision and accuracy, and sample matrix effects in MC-ICP-MS.

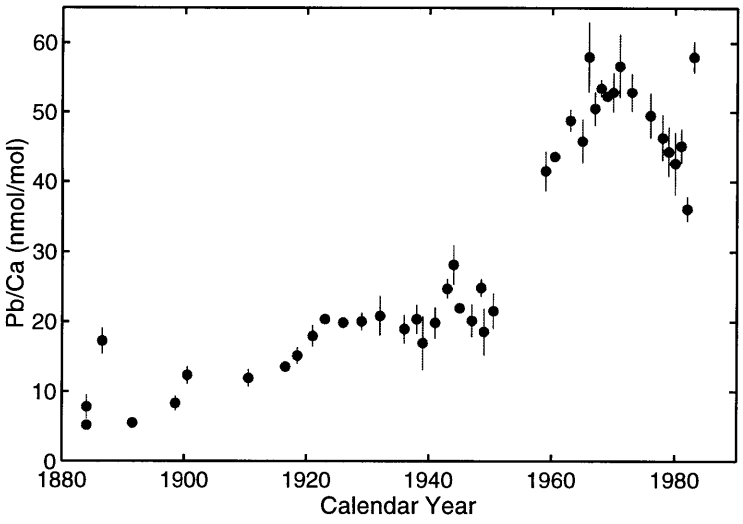

Figure 1-10: North Rock, Bermuda Pb/Ca record of Shen and Boyle (1987). This record exhibits three known features of North American lead production: (1) the gradual increase in lead emissions resulting from non-ferrous metal production; (2) an abrupt increase from 1951 to 1973 due to leaded gasoline emissions; and (3) a subsequent reduction in Pb/Ca ratios reflecting leaded gasoline phaseout.

Second, an elemental and isotopic anthropogenic lead reconstruction in the western North Atlantic is presented (Chapter 3), including surface coral and seawater observations from North Rock and Station S, Bermuda. This study extends the initial observations of Shen and Boyle (1987) and resolves several discrepancies among previous results. These records represent the first composite North Atlantic record from corals and modern seawater from 1885 to the present. The proxy record developed in Chapter 3 then supports the modern seawater observations in Chapter 4, linking past anthropogenic fluxes to its elemental and isotopic North Atlantic distribution. Finally, elemental analysis of surface corals from the Cariaco Basin, including Cd/Ca, Ba/Ca, and Pb/Ca ratios, provide new insights for past coastal upwelling in this region. The Cariaco Basin observations demonstrate a centennial-scale reduction in upwelling intensity linked to historical climate records and tropical climate variability. These surface coral results provide independent and quantitative estimates of past surface ocean chemistry and underscore the significance of centennial-scale, non-steady state chemical variability in the North Atlantic Ocean.

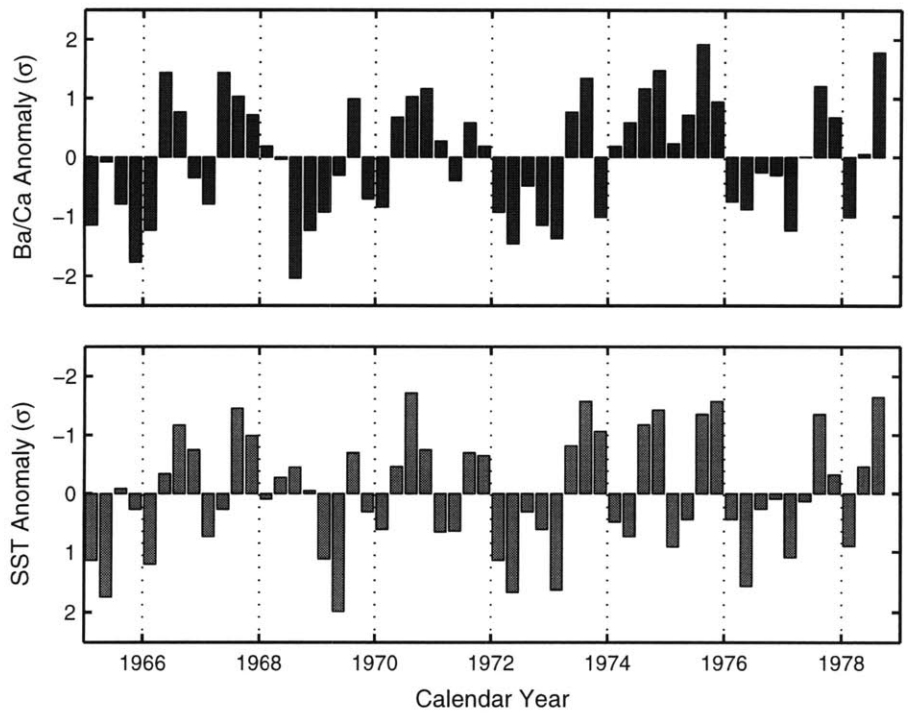

Figure 1-11: Galápagos Ba/Ca (Lea *et al.*, 1989) and local sea surface temperature comparison, 1σ standardized departures. The surface coral record reflects the Ba/Ca ratio of *Pavona clavus* (μmol/mol), taken from Punta Pitt, San Cristobal Island, Galápagos. The temperature record includes quartile SSTs from Academy Bay, Santa Cruz Island, Galápagos.

Element	Valence	Radius (Å)	$[X/Ca]_{coral}$	$[X/Ca]_{seawater}$	D_p	Reference
Cd	2	1.10	$3.69x10^{-9}$	$4.36x10^{-9}$	0.85	1, 2
Ba	2	1.42	$5.27x10^{-6}$	$4.52x10^{-6}$	1.16	3
Mn	2	0.96	$2.40x10^{-8}$	$2.23x10^{-7}$	0.11	4, 5
Pb	2	1.29	$3.00x10^{-8}$	$1.24x10^{-8}$	2.41	6
Zn	2	0.90	$7.80x10^{-9}$	$5.83x10^{-9}$	1.34	7, 5
V	4	0.72	$1.01x10^{-7}$	$3.79x10^{-6}$	0.03	7, 8
Mg	2	0.89	$4.40x10^{-3}$	$5.15x10^{0}$	0.01	9, 10
Sr	2	1.26	$9.18x10^{-3}$	$8.59x10^{-3}$	1.07	11
La	3	1.16	$1.76x10^{-9}$	$1.59x10^{-9}$	1.11	12, 13
Ce	3	1.14	$3.39x10^{-9}$	$1.54x10^{-9}$	2.21	12, 13
Nd	3	1.11	$2.48x10^{-9}$	$1.60x10^{-9}$	1.55	12, 13
Sm	3	1.08	$7.64x10^{-10}$	$3.58x10^{-10}$	2.14	12, 13
Eu	3	1.00	$1.39x10^{-10}$	$9.43x10^{-11}$	1.47	12, 13
Gd	3	1.05	$1.04x10^{-9}$	$5.24x10^{-10}$	1.98	12, 13
Dy	3	1.03	$9.40x10^{-10}$	$6.17x10^{-10}$	1.52	12, 13
Er	3	1.00	$7.84x10^{-10}$	$4.82x10^{-10}$	1.62	12, 13
Yb	3	0.99	$6.90x10^{-10}$	$4.17x10^{-10}$	1.66	12, 13
Lu	3	0.98	$1.01x10^{-10}$	$5.74x10^{-11}$	1.76	12, 13

Table 1.1: Surface coral cation compilation. References for coral and seawater elemental ratios include: 1. Shen *et al.* (1987); 2. Boyle and Huested (1983); 3. Lea *et al.* (1989); 4. Shen *et al.* (1991); 5. Bruland and Franks (1983); 6. Shen and Boyle (1987); 7. Shen (1986); 8. Huizenga and Kester (1982); 9. Mitsuguchi *et al.* (1996); 10. Broecker and Peng (1982); 11. de Villiers *et al.* (1994); 12. Sholkovitz and Shen (1995); and 13. Sholkovitz and Schneider (1991). The effective ionic radii (octahedral coordination) for all cations are taken from Shannon (1976).

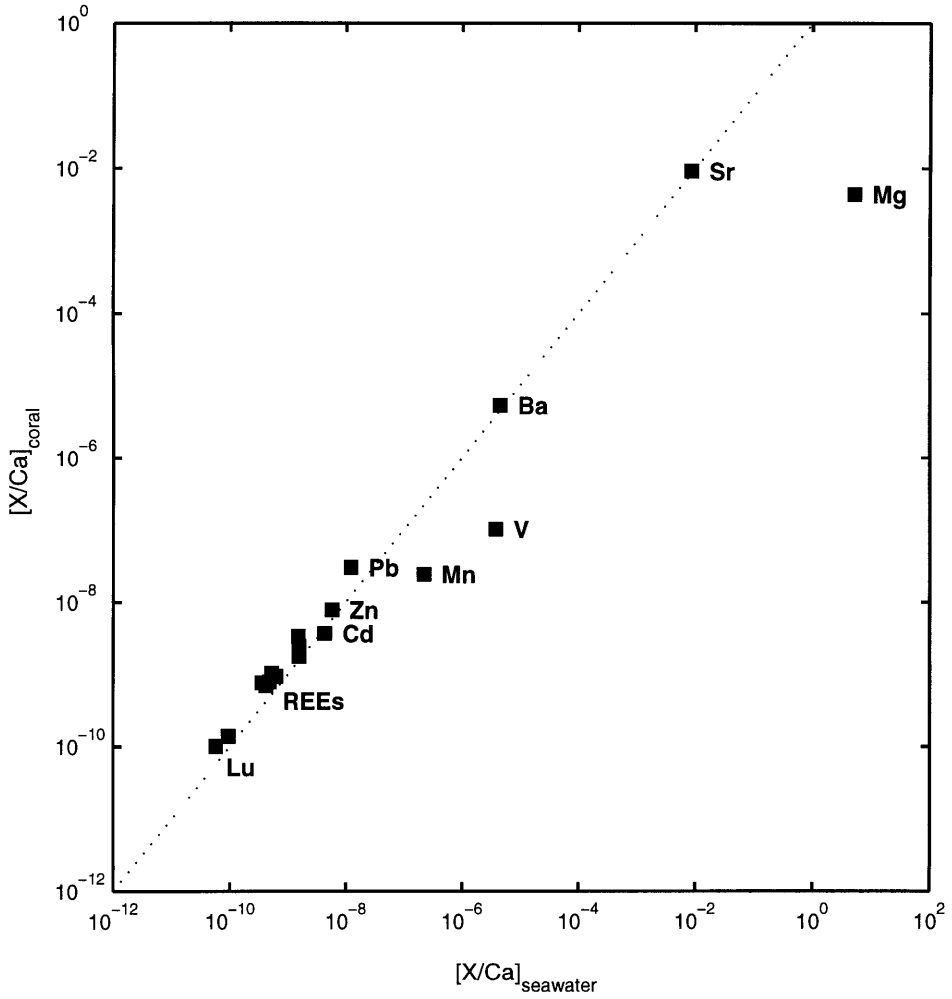

Figure 1-12: Element-calcium ratios for surface corals and seawater. All data and associated references are given in Table 1.1. The abscissa reflects element-calcium ratios for surface corals, the ordinate denotes the corresponding seawater ratios, and the dashed line reflects D_p=1. The left side thus corresponds to preferential uptake by surface corals, whereas the right side corresponds to exclusion. Note the observed exclusion of Mn^{2+}, V^{4+}, and Mg^{2+}, a possible consequence of steric (Mn, Mg) and charge (V) effects.

Reef Site	Latitude	Longitude	Coral Species	$[PO_4]$	Cd/Ca	Ref.
North Rock, Bermuda	32°29'N	64°48'W	*Diploria strigosa*	0.0884	0.44	1
Lisianski Island, Hawaii	26°0'N	174°0'W	*Porites lobata*	0.1173	1.52	1
Florida Straits	24°57'N	80°33'W	*Montastrea annularis*	0.1177	1.74	1
Mauritius	20°0'S	57°30'E	*Platygyra rustica*	0.1639	0.60	1
Eniwetak	11°20'N	162°20'E	*Favia speciosa*	0.2229	2.63	1
Taborio, Tarawa	1°0'N	173°0'E	*Hydnophora microconos*	0.2915	1.42	1
Los Roques, Venezuela	11°55'N	66°20'W	*Montastrea annularis*	0.2972	2.07	2
Isla Tortuga, Venezuela	10°54'N	65°20'W	*Montastrea annularis*	0.3214	2.32	2
Española, Galápagos	1°12'S	89°33'W	*Pavona clavus*	0.6080	3.06	3
San Cristobal, Galápagos	0°45'S	89°36'W	*Pavona clavus*	0.6080	5.30	4

Table 1.2: Mixed layer mean annual phosphate (μM) and surface coral Cd/Ca (nmol/mol) from the North Atlantic, Pacific, and Indian Oceans. References include: 1. Shen (1986); 2. M. Reuer, unpublished data; 3. Linn *et al.* (1990); and 4. Shen *et al.* (1992b). Mean annual phosphate results are taken from Conkright *et al.* (1994). The Cd/Ca results from North Rock, Bermuda (1867-1899) and the Florida Straits (1878-1931) were selected to minimize anthropogenic contributions.

Chapter 2

Lead Isotope Analysis of Marine Carbonates and Seawater by Multiple Collector ICP-MS

2.1 Introduction

Isotope ratio analysis by multiple collector ICP-MS (MC-ICP-MS) is a promising mass spectrometric technique, and its merits are well-established for geochemistry (see reviews by Walder, 1997; Halliday *et al.*, 2000). Previous studies have addressed lead isotope analysis of NIST standard reference materials and standard rock digests (*e.g.*, Walder and Freedman, 1992; Hirata, 1996; Belshaw *et al.*, 1998; Rehkämper and Halliday, 1998; White *et al.*, 2000; Thirlwall, 2001, and refs. therein), examining the importance of mass fractionation, normalization techniques, and matrix effects on isotope ratio precision and accuracy. Here several new observations are provided, focusing on marine carbonate and seawater $^{207}Pb/^{206}Pb$ and $^{208}Pb/^{206}Pb$ analysis. The described method accommodates moderate sample masses (3 to 6 ng), exhibits favorable precision (<200 ppm, 2σ), and provides a consistent and rapid technique for this environmental tracer.

First, the analytical context should be considered. The utility of lead isotopes as an anthropogenic tracer was first established by T. J. Chow and coworkers (Chow and John-

stone, 1965; Chow and Earl, 1970, 1972; Chow *et al.*, 1975). These studies demonstrated systematic, global-scale isotopic variability among leaded gasoline, coal, and aerosols samples. For example, a 14% range in leaded gasoline $^{206}Pb/^{207}Pb$ was observed between Bangkok, Thailand (1.072) and Santiago, Chile (1.238, Chow *et al.*, 1975). The unique isotopic composition of multiple anthropogenic sources provides new constraints on heavy metal provenance in the atmosphere and oceans (*e.g.*, Sturges and Barrie, 1987; Church *et al.*, 1990; Véron *et al.*, 1994; Hamelin *et al.*, 1997; Alleman *et al.*, 1999; Bollhöfer and Rosman, 2001). Proxy records, including ice cores (Rosman *et al.*, 1993, 2000), peat records (Shotyk *et al.*, 1998; Weiss *et al.*, 2000), and surface corals (Shen and Boyle, 1987) have also demonstrated significant time-dependent isotopic variability. Two common characteristics of anthropogenic lead analysis are thus low concentrations within complex natural matrices (*e.g.*, seawater or carbonates) and a large expected isotopic range.

A second consideration is the difference between MC-ICP-MS and established thermal ionization mass spectrometric (TIMS) techniques. The established advantages of MC-ICP-MS include the ionization of most elements within the high-temperature (4500 to 8000°K) inductively coupled plasma (*e.g.*, Fe and Hf) and the introduction of various sample types at atmospheric pressure (*e.g.*, solutions, ablated aerosols, or chromatography isolates). For stable lead isotopes, the principal advantage is greater sample throughput and fewer sample preparation steps. With a turreted thermal source (n=12), throughput is approximately one sample per hour (S. Bowring, personal communication), requiring sample loading and filament exchange. With conservative washouts and sample acquisition by MC-ICP-MS, approximately four to five samples can be analyzed per hour. This advantage, however, only applies to standard glassware configurations (see below); the use of membrane desolvating nebulizers reduces throughput to TIMS levels. For $^{206}Pb/^{207}Pb$ and $^{208}Pb/^{207}Pb$ analysis of environmental samples, the wide isotopic range and large sample quantity represent a promising application of MC-ICP-MS.

2.2 Methods

Sample preparation followed standard laboratory protocols for trace element analysis, including acid, reagent, and plasticware preparation under Class 100 conditions. A complete description of these techniques is provided in Shen and Boyle (1988a) and Appendix A. Here the specific protocols for lead isotope analysis of seawater and surface corals are briefly described.

2.2.1 Surface Coral and Seawater Sample Preparation

Surface coral samples were cleaned using a modified technique of Shen and Boyle (1988a) described in Appendix A, quantitatively removing contaminant organic or oxide phases from the coral skeleton. The isotopic composition of occluded contaminants does not equal the aragonite lead, creating significant, non-systematic, and positive biases. The efficacy of the cleaning technique was determined by replicate Pb/Ca analysis of homogenized splits, utilizing isotope dilution ICP-MS and AAS at MIT (VG Plasmaquad 2^+). The isotope dilution method included direct analysis of dissolved, diluted coral, adding a calibrated ^{204}Pb spike (Oak Ridge National Laboratory) to all samples. Where Pb/Ca replicates did not agree to 2 nmol/mol, samples were reprocessed and reanalyzed, only measuring the isotopic composition of adequately cleaned samples.

Second, moderate volume seawater samples were prepared by the $Mg(OH)_2$ coprecipitation method (Wu and Boyle, 1997b; Weiss *et al.*, 2000). Larger sample volumes were required (160 to 240 mL) relative to elemental analysis (1200 μL) given the necessary counting statistics, Faraday cup noise, and low seawater lead concentrations (50 pmol kg^{-1}, 1996 average, n=18, Wu and Boyle, 1997a). Surface samples were collected with established procedures, including underway sampling (Vink *et al.*, 2000), pole sampling with a polycarbonate bottle clamp, and vane sampling. Hydrocasts utilized the MITESS automated trace element sampler described in Dickey *et al.* (1998). Seawater lead was preconcentrated by excess $Mg(OH)_2$ coprecipitation, adding 400 μL of vapor-distilled ammonia to each 40 mL sub-sample, mixing the precipitate by shaking and inversion, and separating the $Mg(OH)_2$ (s) by centrifugation. Dissolved aragonite and seawater $Mg(OH)_2$ (s) concentrates were

Instrumental Parameter	Set Point	Unit
Nebulizer gas	0.905	L min^{-1}
Auxiliary gas	0.890	L min^{-1}
Cool gas	13.50	L min^{-1}
Forward power	1350	W
Reflected power	<3	W
Expansion Pirani	$3.0x10^{-1}$	mbar
Intermediate Pirani	$1.0x10^{-2}$	mbar
Analyzer Pirani	<0.01	mbar
Hexapole ion gauge	$3.2x10^{-4}$	mbar
Analyzer ion gauge	$1.1x10^{-8}$	mbar
Acquistion time	250	seconds
Uptake rate	100	μL min^{-1}
^{209}Bi sensitivity	2,100,000	cps ppb^{-1}

Table 2.1: IsoProbe MC-ICP-MS instrumental conditions. The hexapole ion gauge pressure includes a collision cell argon gas flow of 1.500 mL min^{-1}, and the analyzer pressure has varied from $1.1x10^{-8}$ to $2.2x10^{-8}$ mbar over seven months. The acquisition time reflects 25, 10 second integrations.

reduced to dryness in 3 mL Savillex PFTE beakers and redissolved in 400 μL 1.1N HBr (Seastar).

Lead separation from the sample matrix includes established anion exchange techniques described by Kraus and Moore (1953) and Strelow (1978). Teflon mini-columns (75 μL) were constructed from Teflon shrink tubing (4:1 shrink ratio, 9.53 mm, Texloc) and Teflon supports. Eichrom AG-1x8 (chloride form, 200-400 mesh) anion exchange resin was utilized, cleaned for seven days in triple-distilled 6.0N HCl with continuous agitation. Before use the resin was rinsed 20x in dH_2O and sized by gravitational settling, retaining the intermediate fraction. The loaded resin was then cleaned with 1000 μL 6.0N HCl and converted to the Br^- form with 400 μL 1.1N HBr. The major cations are eluted with 400 μL 1.1N HBr, complexing sample lead as $PbBr_4^{2-}$. The columns are converted to the Cl^- form with 200 μL 2.0N HCl, and the sample is eluted with 500 μL 6.0N HCl. Quantitative lead recoveries were observed from the column separation, equal to 99.98% (n=3) in the 6.0N HCl fraction.

2.2.2 MC-ICP-MS Configuration

Lead isotope analysis was completed on a Micromass IsoProbe ICP-MS at MIT, including the standard instrumental configuration under Class 100 conditions. A schematic of the MIT IsoProbe is shown in Figure 2-1, and general instrumental parameters are given in Table 2.1. The introduction system includes a Teflon microconcentric nebulizer (Microflow PFA-100, 100 μL min^{-1}, Elemental Scientific), a cyclonic spray chamber cooled to 4°C (Jacketed Twister, Glass Expansion), and a Fassel quartz torch (Glass Expansion). Experiments with multiple introduction methods showed improved signal stability and precision with the PFA nebulizer, peristaltic pumping, and small internal diameter pump tubing (0.19 mm ID, Ismatec). The water-cooled interface includes nickel sampling, skimmer, and collimator cones with an accelerating potential of -600V (at 40% extraction). The accelerated ion beam is axially-focused and thermalized within a 6 MHz, RF-only hexapole-collision cell, reducing the energy range of the incoming ions from 30V to approximately 1V. The theoretical limit for ^{208}Pb thermalization by ^{40}Ar equals 0.1V, however, a compromise between transmission and the ion energy distribution is required, increasing the average ion energy to approximately 1V (Turner *et al.*, 2000). The thermalized ions are then focused by five electrostatic lenses (extraction, Y-focus, Y-slit, Z-focus, Z-slit) with a final acceleration potential of -6000V. Following the lens stack, the ions are separated by a stigmatic-focusing, Cross geometry magnet reviewed by Turner *et al.* (2000). Finally, the separated ions are detected with a dynamic multiple collector array, consisting of seven Channeltron electron multipliers, nine Faraday collectors, and one axial Daly detector.

A quantitative estimate of the true analyte intensity (I_t) from the measured intensity (I_m requires several established corrections, including mass spectral backgrounds associated with the Faraday cup offsets (I_{ms}), the solvent blank (I_s), the instrumental blank (I_i), the procedural blank (I_p), isobaric interferences (I_{iso}), and tailing from adjacent masses ($\pm$3 amu, I_{tail}). This can be written simply as:

$$I_t = I_m - I_{ms} - I_s - I_i - I_p - I_{iso} - I_{tail} \tag{2.1}$$

The first three corrections (I_{ms}, I_s, and I_i) are determined by on-peak zero (OPZ) anal-

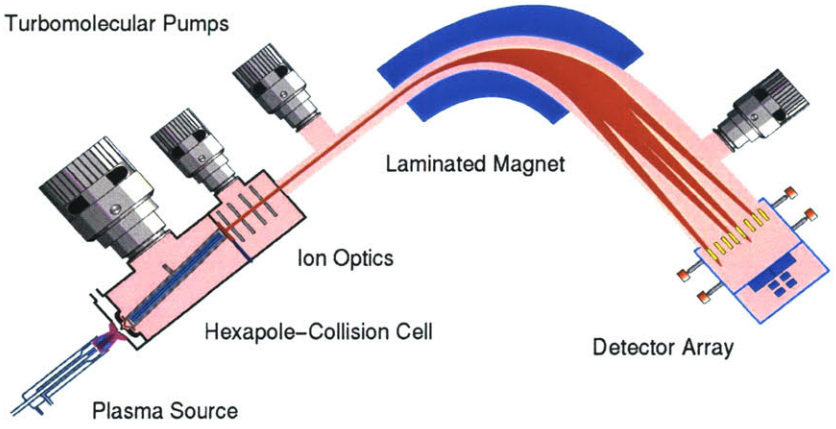

Figure 2-1: IsoProbe MC-ICP-MS schematic, including a standard ICP source, hexapole-collision cell interface, stigmatic-focusing magnet, and dynamic detector array. Image courtesy of Micromass UK Ltd. Please see the text for a detailed description of the components.

ysis for each measurement, continuously monitored to assess sample or standard memory effects. Prior to OPZ measurements, washout intervals of at least six minutes were used with 0.5N HNO_3 and 0.5N HCl, monitoring both signal intensity and the isotope ratios. Two procedural blanks were analyzed for every column series (n=14), and representative results are shown in Table 2.2. The isotopic composition of the procedural blank could not be determined by static Faraday collection given the low signal intensity (the $^{206}Pb/^{207}Pb$ range equals 0.832 to 1.033). The ^{204}Hg isobaric interference was determined via simultaneous ^{202}Hg analysis, correcting ^{204}Hg with an assumed abundance ratio of 0.2299 corrected for mass fractionation by thallium normalization (see Section 2.3.1). Finally, the tailing correction must include the abundance sensivity (AS) for each peak (i) three[1] mass units above and below the analyte mass, determined by daily analysis of the monoisotopic ^{209}Bi, following Thirlwall (2001). This is given simply as:

$$I_{tail} = \sum_{i=-3}^{3} I_i \cdot AS_i \tag{2.2}$$

where I_i reflects the on-peak intensity ± 3 amu and AS denotes the corresponding abun-

[1]The mass range is determined by tailing of the expected significant peaks. If ^{204}Pb is to be accurately determined, one must use a range of ± 4 amu to account for ^{208}Pb tailing.

Date	4/3/01	5/6/01	6/9/01	7/11/01	8/4/01	9/9/01
^{208}Pb (A)	$2.97\text{x}10^{-15}$	$6.52\text{x}10^{-16}$	$1.24\text{x}10^{-15}$	$1.65\text{x}10^{-15}$	$1.40\text{x}10^{-15}$	$1.02\text{x}10^{-15}$
Pb (ppt)	9.3	2.3	3.7	6.5	3.1	3.1
Pb (pg)	4.9	1.2	1.9	3.4	1.6	1.6

Table 2.2: Procedural blank analysis, MC-ICP-MS. Six representative procedural blanks over five months are shown, including the ^{208}Pb signal intensity (in amperes), the lead concentration (parts per trillion), and the total blank mass. The total procedural blanks are consistently less than 5 pg.

dance sensitivity. Static and scanning analyses of ^{209}Bi were completed weekly or following any pressure shift. With an analyzer pressure of $1.1\text{x}10^{-8}$ mbar, the average abundance sensitivities relative to ^{209}Bi are: 2.5 ppm (-3 amu), 4.4 ppm (-2 amu), 13.6 ppm (-1 amu), 6.1 ppm (+1 amu), 5.9 ppm (+2 amu), and 3.1 ppm (+3 amu). These values are stable to ± 2 ppm (2σ) under the same vacuum conditions. Comparable results to Thirlwall (2001) were observed at -1 amu (mass 208; 23.4 ppm: MIT; 21.0 ppm: Royal Holloway) at similar analyzer pressures ($2.2\text{x}10^{-8}$ mbar: MIT, $2.5\text{x}10^{-8}$ mbar: Royal Holloway). Systematic correction techniques presently exist to account for reagent, instrumental, and mass spectral contributions.

Finally, the small sample masses analyzed here preclude precise ^{206}Pb/^{204}Pb analysis. With moderate-volume North Atlantic seawater samples (0.160 kg, 38.1 pmol kg^{-1} for 1999) and the parameters given in Table 2.1, the counting statistic for the ^{206}Pb/^{204}Pb ratio is 489 ppm (2σ). The limit does not include Faraday cup noise and uncertainties associated with the ^{204}Hg correction. Low signal intensities limit accurate and precise ^{204}Pb ratio analysis; the focus of this study will be ^{207}Pb/^{206}Pb and ^{208}Pb/^{206}Pb determinations.

2.3 Results and Discussion

Several MC-ICP-MS analytical experiments are presented, including mass fractionation effects, isotope ratio precision, and matrix effects. These observations are not necessarily applicable to other instruments, isotopic systems, or interface configurations. These results provide, however, a simple and consistent framework for lead isotope ratio analysis by the IsoProbe MC-ICP-MS.

2.3.1 Mass Fractionation in MC-ICP-MS

Mass fractionation is well-known phenomenon in ICP-MS systems, resulting from space charge repulsion and ion beam defocusing effects (see review by Niu and Houk, 1996). Space charge effects in ICP-MS generally results in preferential heavy ion transmission: following charge separation between the sampling cone and skimmer, increased positive ion density behind the skimmer repels lighter ions, whereas heavy ions remain axially-focused (see Plate 1 in Montaser, 1998). Elemental fractionation has been demonstrated by simulation modeling, ion current observations, ion deposition experiments, and tandem quadrupole TOF observations (Gillson *et al.*, 1988; Chen and Houk, 1996; Allen *et al.*, 1997; Burgoyne *et al.*, 1997, and refs. therein). Comparable isotopic observations do not presently exist for MC-ICP-MS, requiring empirical corrections to quantify mass fractionation[2].

Mass corrections have been successfully addressed by double- and triple-spiking methods for TIMS and MC-ICP-MS (see Thirlwall, 2000, 2001, and refs. therein), quantifying mass fractionation and the true isotopic ratio by comparing spiked and unspiked samples. An alternative technique for MC-ICP-MS lead isotope analysis is thallium normalization (Longerich *et al.*, 1987). This method relies on concurrent analysis of a thallium isotopic standard, applying the calculated mass fractionation factor to the lead isotope ratios. Here the exponential empirical correction was assumed, and differences among these corrections will be addressed. For exponential fractionation, the true (t) $^{205}Tl/^{203}Tl$ ratio can be determined via the measured ratio (m), the mass ratio (M_{205}/M_{203}), and an exponential fractionation factor (β):

$$\left(\frac{^{205}Tl}{^{203}Tl}\right)_t = \left(\frac{^{205}Tl}{^{203}Tl}\right)_m \left(\frac{M_{205}}{M_{203}}\right)^{\beta} \tag{2.3}$$

Applying the thallium fractionation factor (β_{Tl}) to lead, one can simultaneously correct for instrumental mass fractionation.

To test these assumptions, a stock 32 nM SRM-981 standard was repeatedly analyzed. Mass fractionation was induced by the nebulizer gas flow rate and the extraction lens potential, motivated by the observations of Burgoyne *et al.* (1997, see their Figure 4).

[2]The empirical nature of these corrections should be emphasized, based on the complexity of an accelerating, densely-charged, high-temperature plasma through the ICP-MS interface.

Established blank and background corrections were completed for each analysis, and the results are shown in Figure 2-3. For optimized instrumental conditions (0.890 to 0.910 L min^{-1}, 30 to 40% extraction), the mass fractionation factor is approximately β =-1.2 (0.7% amu^{-1}), corresponding to the expected preferential heavy ion transmission. Increased nebulizer flow rates result in reduced sampling depths, diminished solvent loading (via reduced solvent to gas ratios with constant peristaltic pumping), and a defocused ion beam. At approximately 0.925 L min^{-1}, significant light ion transmission was observed. This effect is asymmetrical, with approximately constant fractionation despite a 35% increase in ^{208}Pb intensity from 0.870 to 0.900 L min^{-1}. Second, the extraction potential was reduced, decreasing the ion beam intensity and increasing the mass fractionation factor. These results follow the expected relationship between space charge effects and mass fractionation: as ion beam intensities drop, greater light ion transmission occurs. The magnitude of this effect, including *positive* mass fractionation factors, was unexpected, and a complete explanation requires ion trajectory modeling under comparable conditions.

2.3.2 Lead Isotope Ratio Accuracy

The mass fractionation results were then utilized to test the empirical corrections, following the method of Russell *et al.* (1978). As shown in Figure 2-3, the measured $^{207}Pb/^{206}Pb$ and $^{205}Tl/^{203}Tl$ ratios were normalized via the assumed true isotope ratios from Thirlwall (2000) and Dunstan *et al.* (1980), respectively. As shown in Table 2.5, best agreement among SRM-981 $^{207}Pb/^{206}Pb$ and $^{208}Pb/^{206}Pb$ ratios is observed for the Thirlwall (2000, ^{207}Pb-^{204}Pb double spike) and Galer and Abouchami (1998, ^{207}Pb-^{206}Pb-^{204}Pb triple spike) TIMS methods; the Thirlwall (2000) double spike results were selected as the reference ratios for this study. Exponential ($R_t = R_m \cdot (M_2/M_1)^{\beta}$), power ($R_t = R_m \cdot (1+\beta)^{M_2/M_1}$), and linear ($R_t = R_m \cdot [1 + \beta(M_2 - M_1)]$) corrections were then calculated for a given β range (-1 to 2). No difference is apparent between the linear and exponential models, whereas the power law better fits the $^{207}Pb/^{206}Pb$ extrema. For the $^{208}Pb/^{206}Pb$ ratio (not shown), the improved power law fit is not observed. The differences between the models shown in Figure 2-3 should not be overstated, as the residuals assume 'true' isotopic ratios and equivalent fractionation factors for thallium and lead. The large standard deviations (220

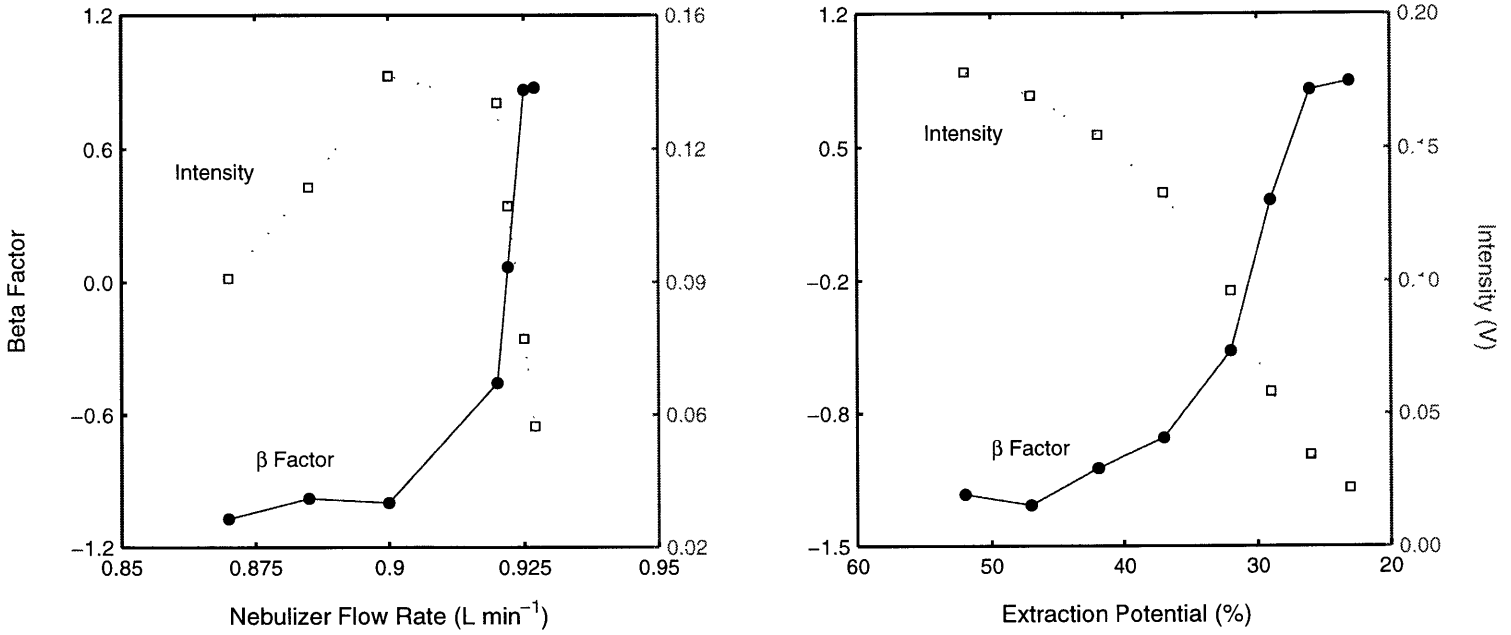

Figure 2-2: IsoProbe mass fractionation experiments. The open squares reflect the ^{208}Pb intensity for each experiment, and the closed circles denote the exponential fractionation factor (β). The left abscissae correspond to the exponential mass fractionation factor, and the right abscissae reflect ^{208}Pb intensities. Nebulizer flow rate (L min^{-1}) and extraction potential (%) are given on the left and right panels.

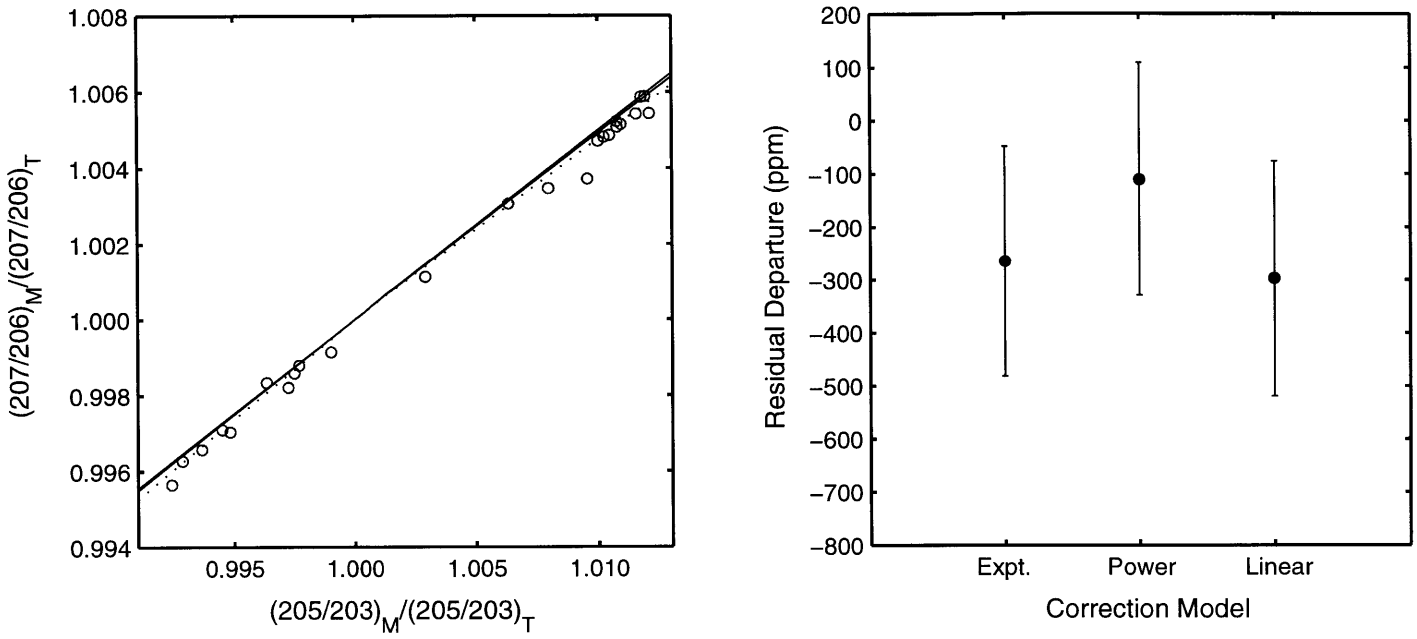

Figure 2-3: Empirical mass fractionation models for MC-ICP-MS. The left panel shows the normalized lead and thallium ratios and the corresponding mass fractionation models. The solid lines reflect the linear and exponential models, and the dashed line reflects the power law model. The right panel shows the mean and 2σ standard deviation for the model residuals. Differences among models are not significant at the 95% confidence interval.

ppm, 2σ) suggest these results represent a worst-case scenario, and the three models are generally comparable under these conditions.

A second consideration is the assumed equivalence of the mass fractionation factors, β_{Pb} and β_{Tl}. Hirata (1996) observed a linear dependence between mass fractionation and atomic mass (85 to 208 amu), and improved accuracy was observed with a $\beta_{\mathrm{Pb}}/\beta_{\mathrm{Tl}}$ correction. The Hirata (1996) correction was determined by measuring the slope of the mass fractionation trend versus atomic mass from ^{85}Rb to ^{208}Pb, then calculating $\beta_{\mathrm{Pb}}/\beta_{\mathrm{Tl}}$ from the slope and intermediate masses of Tl (204) and Pb (206.5). To test this method, the $\beta_{\mathrm{Pb}}/\beta_{\mathrm{Tl}}$ ratio was calculated according to Maréchal *et al.* (1999) and White *et al.* (2000), shown in Figure 2-4 and Table 2.3. Differences among the four beta ratios are not statistically significant at the 95% confidence interval, and all ratios are within error of unity. In contrast to Hirata (1996), the $\beta_{\mathrm{Pb}}/\beta_{\mathrm{Tl}}$ correction offers slight improvement over standard thallium normalization (Table 2.3), whereas correction of the 'true' ^{205}Tl/^{203}Tl ratio greatly improves isotope ratio accuracy Rehkämper and Halliday (see 1998). We suggest this difference results from secondary fractionation effects discussed by White *et al.* (2000), including Faraday cup efficiencies, amplifier gains, and ion optics (*e.g.*, misalignment of the image plane with respect to the detector array). A simple rationale for this effect is given in Appendix I. The β_{Pb}/β_{Tl} correction cannot be discounted for other instruments or configurations, given its successful application by Hirata (1996). For our experimental conditions, however, variations in the $\beta_{\mathrm{Pb}}/\beta_{\mathrm{Tl}}$ ratio alone cannot completely explain instrumental mass fractionation.

Secondary mass fractionation effects can be directly addressed by the MC-ICP-MS double-spiking technique Thirlwall (*e.g.*, 2000), accounting for the cumulative mass fractionation of a sample and known isotopic spike. An alternative solution is external normalization to SRM-981 following Tl normalization (modified from Belshaw *et al.*, 1998). The disadvantage of this method is it requires assumed true isotopic ratios, requiring possible re-normalization of disparate data sets. These corrections are also significant relative to the analytical precision (see below), ranging from -304 to 220 ppm (n=12) over six months. However, the secondary correction factors are stable on weekly to monthly time scales, are precisely determined by replicate analyses, and provide a simple solution to secondary mass fractionation effects.

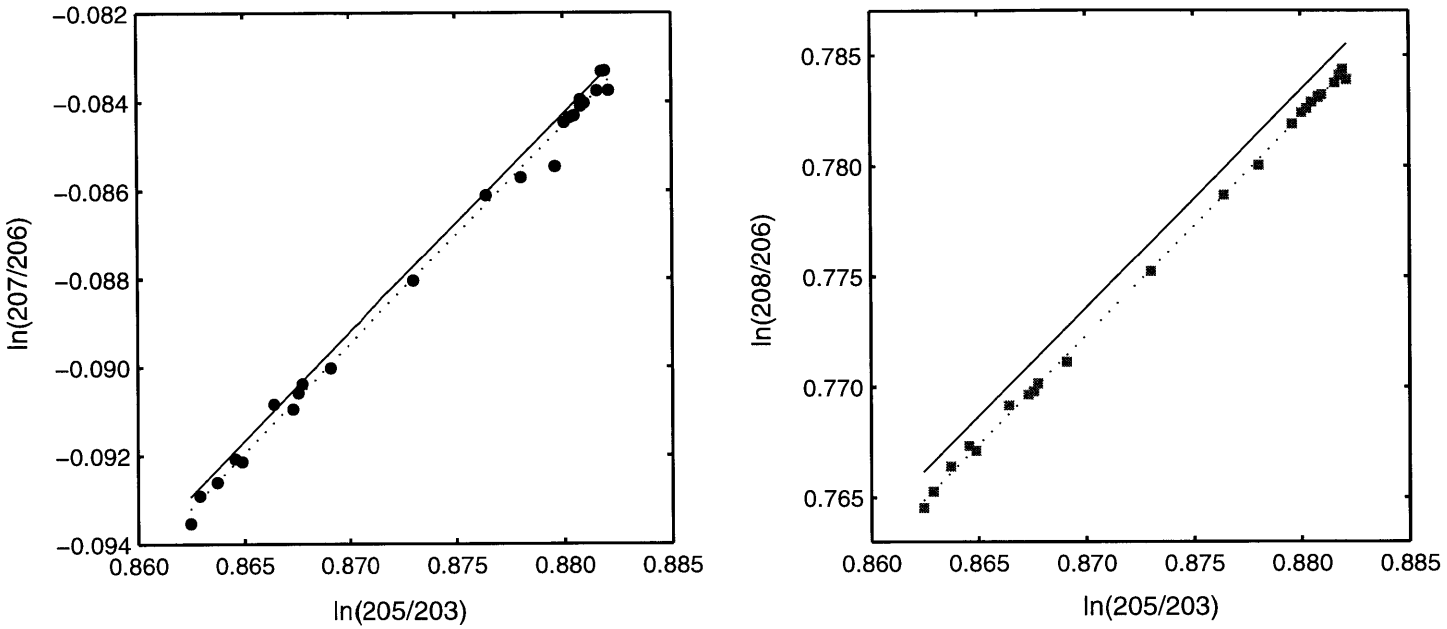

Figure 2-4: Log transforms of $^{207}Pb/^{206}Pb$, $^{208}Pb/^{206}Pb$, and $^{205}Tl/^{203}Tl$. The solid line corresponds to the theoretical slope and intercept calculated from the assumed true isotopic ratios (see text), whereas the dotted lines reflect type-II linear regressions (York, 1966). The resulting slopes, intercepts, and uncertainties are given in Table 2.3, and the differences between the observed and theoretical slopes are not significant at the 95% confidence interval.

Ratio	$(\text{Slope})_T$	$(\text{Slope})_M$	$(\beta_{Pb}/\beta_{Tl})_m$	$(\text{Inter.})_T$	$(\text{Inter.})_M$	$(\beta_{Pb}/\beta_{Tl})_b$
208/206	0.98555	0.99191	1.00645	-0.08384	-0.09063	1.00792
2σ	†	0.00908	0.00921	0.00020	0.00849	0.00927
207/206	0.49413	0.49517	1.00210	-0.51910	-0.52028	1.00273
2σ	†	0.00995	0.02014	0.00012	0.00930	0.02163

Table 2.3: SRM-981 mass fractionation experiment. The theoretical (T) slope and intercept for the regression are given, utilizing the isotopic ratios of Dunstan *et al.* (1980) and Thirlwall (2000) for the intercept. The measured (M) slope (m) and intercept (b) are taken from Figure 2-4. No uncertainty in the atomic masses is assumed (†), and the 2σ standard deviation for Columns 4, 5, and 7 are determined by error propagation.

Isotope Ratio	R_1	Δ_1	R_2	Δ_2	R_3	Δ_3
$^{208}Pb/^{206}Pb$	2.16507	-1213	2.16512	-1189	2.16774	17
$^{207}Pb/^{206}Pb$	0.91446	-256	0.91446	-252	0.91469	4

Table 2.4: SRM-981 accuracy experiment. Here R_x reflects three correction experiments, and Δ corresponds to the respective departures (in ppm) from Thirlwall (2000). Experiment 1 represents thallium normalization, experiment 2 reflects the β_{Pb}/β_{Tl} correction of Hirata (1996), and experiment 3 corresponds to the true $^{205}Tl/^{203}Tl$ correction of Rehkämper and Halliday (1998).

2.3.3 Lead Isotope Ratio Precision

Instrumental mass fractionation directly affects isotope ratio precision, and three separate experiments were completed for its assessment. First, short-term stability over fourteen days was tested, including multiple glassware, nebulizer, interface, and hexapole configurations. These experiments were consistently completed after 90 minutes of torch ignition, providing an estimate of worst-case, hourly-scale departures. Following thallium normalization, the first block of four (as 30, ten second integrations) was used to determine secondary normalization factors for the remaining three blocks (assuming true ratios from Thirlwall, 2000). The results are shown in Figure 2-5, and the 2σ relative standard deviations for the $^{207}Pb/^{206}Pb$ and $^{208}Pb/^{206}Pb$ ratios are 75 and 110 ppm, respectively. Second, SRM-981 was analyzed 22 times over sixteen hours to assess daily isotope ratio stability, calculating the secondary normalization factors with bracketing standards. No instrument parameters were altered during this experiment, and the resulting deviations are 142 ($^{207}Pb/^{206}Pb$) and

172 ($^{208}Pb/^{206}Pb$) ppm. Finally, a stock SRM-981 standard was analyzed every three samples for twelve analytical sessions. The resulting daily vector of n standard analyses was divided into alternating 'standards' [1:2:n] and 'samples' [2:2:n-1], determining the secondary normalization factors from the daily average. No significant trends in the isotopic ratios were observed for the twelve sessions, and the resulting 2σ deviations are 177 ($^{207}Pb/^{206}Pb$) and 240 ($^{208}Pb/^{206}Pb$) ppm. This final estimate is the most realistic, because it includes multiple analytical sessions (12 to 16 hours), variable sample and standard matrices, and possible memory effects. The respective counting statistics for the third experiment are 93 and 77 ppm; approximately one third to one half of the uncertainty can be ascribed to the limited signal intensity.

The external precision should be considered within the context of this application. Previous lead isotope analysis from western North Atlantic surface corals ranged from 1.184 to 1.215 with respect to $^{206}Pb/^{207}Pb$, or 25,500 ppm (Shen and Boyle, 1987). The isotopic range in the modern (1987 to 1989) North Atlantic mixed layer is comparable (1.166 to 1.197, 25,900 ppm, Véron *et al.*, 1993; Hamelin *et al.*, 1997; Weiss *et al.*, 2000). The highest external precision estimate given above (240 ppm) corresponds to a signal-to-noise ratio of 107. The MC-ICP-MS method shown here is thus adequate for both surface corals and seawater, quantitatively resolving modern isotopic variability.

2.3.4 Matrix Effects in MC-ICP-MS

Sample matrix effects represent an important consideration for MC-ICP-MS. Elevated concomitants generally increase space charge effects and heavy ion transmission in ICP-MS (see above), and the observed magnitude depends upon the analyte-concomitant mass difference, the concomitant concentration, and the nebulizer flow rate (see review by Horlick and Montaser, 1998). To evalulate this effect, four gravimetric calcium standards (0.260 to 257 μM) were spiked with SRM-981 and thallium, measuring each isotopic standard four times. Instrumental parameters (*e.g.*, nebulizer flow rate and torch position) were not adjusted throughout the analytical session. Calcium-free SRM-981 was analyzed before and after the experiment, and the results are shown in Figure 2-6. Significant departures were observed for both isotopic ratios, with the 0.260 μM calcium standard exhibiting a -44 ppm

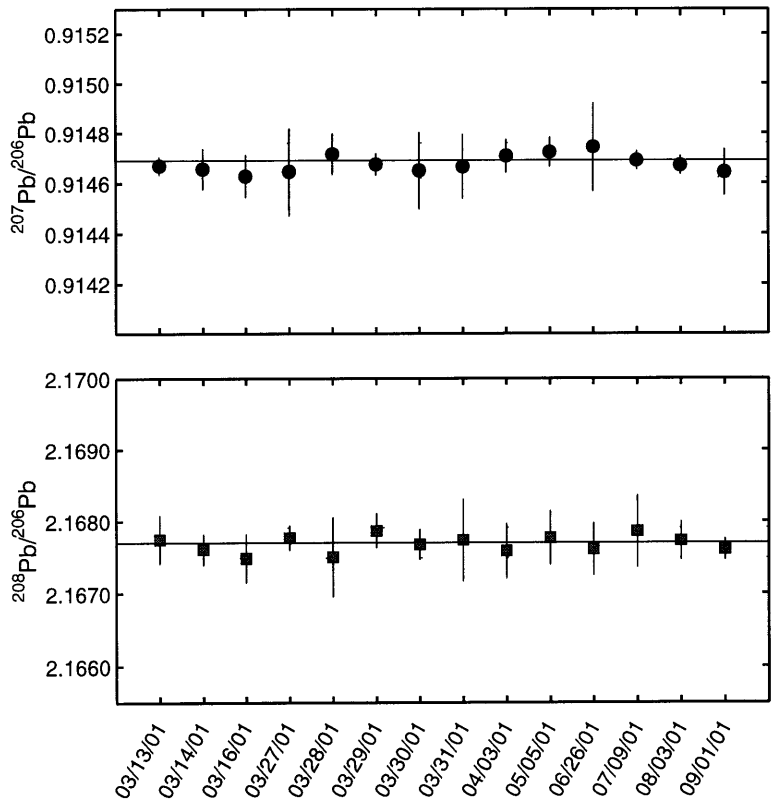

Figure 2-5: SRM-981 external precision experiments. The upper panel represents the mean and 2σ standard deviation for the $^{207}Pb/^{206}Pb$ ratio (75 ppm), and the lower panel reflects the $^{208}Pb/^{206}Pb$ ratio (110 ppm). The solid and dashed lines represent the mean and 2σ deviation of the Thirlwall (2000) TIMS double-spike analysis.

departure from Thirlwall (2000). Higher concentrations yielded greater offsets and external precision, reaching -280 ppm for 257 μM [Ca]. These results cannot be explained by space charge effects, supported by three observations. First, the trend is in the opposite direction from expectation, with increased concomitants favoring light ion transmission. Second, the final calcium-free SRM-981 departure is -354 ppm, well outside the analytical precision and in agreement with the previous matrix standard. Third, no mass bias effects have been observed for other isotopic systems, including 100 ppm Na and Al additions to U500 (Z. Palacz, personal communication). Memory effects cannot explain this trend given the repeated introduction of only the SRM-981 isotope standard and a lead-free calcium standard. These matrix effects, however, are consistent with Figure 2-3 and ion beam defocusing, governed

in this case by salt deposition on the micro-flow nebulizer, sampling cone, and skimmer. Visible calcium deposition was observed after these experiments, resulting from repeated analysis of high-[Ca] solutions over a four hour period. As the ion flux is reduced through a smaller sampling orifice, the space charge effect might diminish due to lower ion densities, favoring light ion transmission. This result might not be observed, however, if the concomitant does not accumulate on the interface or if inadequate salts are deposited. Thus matrix effects are significant for precise isotope ratio analysis; external normalization with matrix-matched standards, however, offers one possible solution. For seawater and coral analysis, elimination of the major cations by anion exchange chromatography and consistent matrix matching were adopted.

2.3.5 Method Assessment and Application

To assess this analytical technique, the SRM-981 accuracy and precision were compared to previous TIMS and MC-ICP-MS determinations. As a reference point, the double- and triple-spiking TIMS methods were first considered, and best agreement between the $^{207}Pb/^{206}Pb$ and $^{208}Pb/^{206}Pb$ ratios was observed for two studies (Galer and Abouchami, 1998; Thirlwall, 2000). The mean and 2σ standard deviation of the MC-ICP-MS analyses shown here agree with the TIMS result, although the overall external precision is reduced given secondary mass fractionation effects (see above). The results of this study are comparable to previous MC-ICP-MS SRM-981 measurements, with improved long-term external precision using secondary normalization. However, the signal intensities employed for this study ($1.5x10^{-12}A$) are at least one order of magnitude lower than previous observations, and reported MC-ICP-MS intensities are greater than $3x10^{-11}A$. Favorable $^{207}Pb/^{206}Pb$ and $^{208}Pb/^{206}Pb$ external precision is thus possible at considerably reduced signal intensities.

Evaluating this proposed method, surface coral and seawater samples from the North Atlantic were analyzed by MC-ICP-MS, shown in Figures 3-3 and 3-7. For the proxy record, the observed range equals a signal-to-noise ratio of 175 with respect to the $^{206}Pb/^{207}Pb$ external precision (177 ppm). Variations between adjacent samples also includes possible cleaning errors, not strictly the instrumental precision (see discussion in Shen and Boyle,

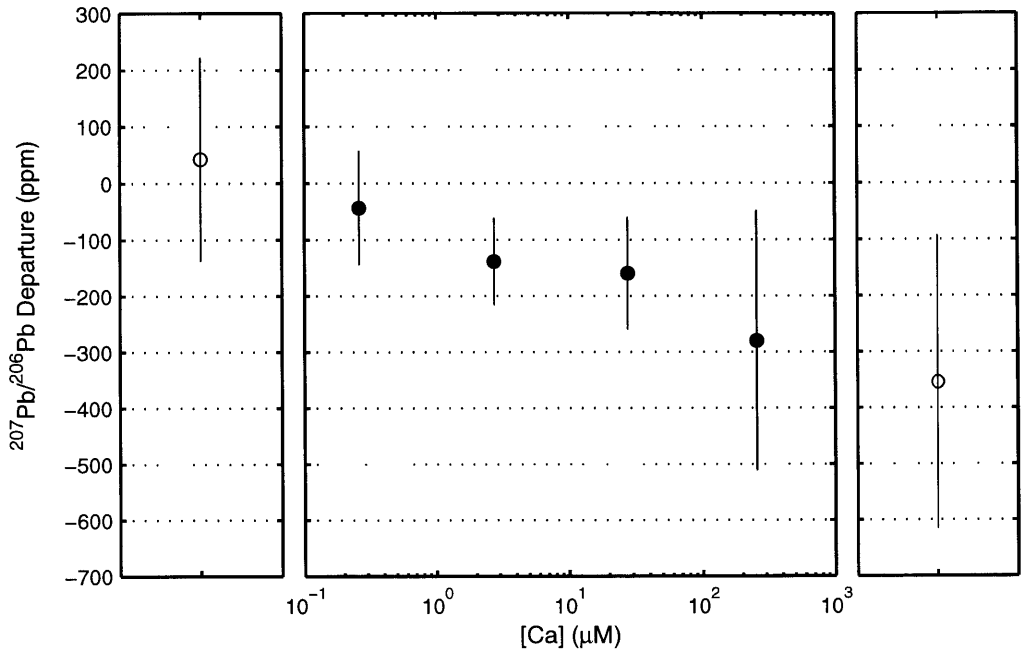

Figure 2-6: IsoProbe calcium matrix experiments, SRM-981. The open circles represent calcium-free SRM-981 standards analyzed before and after the experiment. The closed circles reflect lead-free calcium standards (0.26 to 257 μM) spiked with SRM-981 and thallium. Each result includes the mean and $\pm 2\sigma$ standard deviation of four analyses, and note the elevated light ion transmission with increasing calcium concentrations.

N.	$^{207}Pb/^{206}Pb$	2σ	$^{208}Pb/^{206}Pb$	2σ	n	Reference	Method
1	0.91469	0.00007	2.16770	0.00021	31	Thirlwall (2000)	^{207}Pb-^{204}Pb double spike
2	0.91475	0.00004	2.16771	0.00010	60	Galer and Abouchami (1998)	^{207}Pb-^{206}Pb-^{204}Pb triple spike
3	0.91459	0.00013	2.16701	0.00043	11	Todt *et al.* (1996)	^{205}Pb-^{202}Pb double spike
4	0.91468	0.00037	2.16733	0.00052	109	Woodhead *et al.* (1995)	^{207}Pb-^{204}Pb double spike
5	0.91472	0.00053	2.16747	0.00144	10	Hamelin *et al.* (1985)	^{207}Pb-^{204}Pb double spike
-	0.91472	0.00007	2.16771	0.00050	2	Mean TIMS: References 1 and 2	
6	0.91488	0.00008	2.16770	0.00024	36	Thirlwall (2000)	^{207}Pb-^{204}Pb double spike
7	0.91470	0.00016	2.16686	0.00068	25	Thirlwall (2000)	Tl, exp. corr., $^{205}Tl/^{203}Tl$=2.38890
8	0.91455	0.00007	2.16693	0.00020	8	Rehkämper and Mezger (2000)	Tl, exp. corr., $^{205}Tl/^{203}Tl$=2.38705
9	0.91450	0.00005	2.16589	0.00014	32	Rehkämper and Halliday (1998)	Tl, exp. corr., $^{205}Tl/^{203}Tl$=2.38710
10	0.91459	0.00005	2.16629	0.00014	32	Rehkämper and Halliday (1998)	Tl, exp. corr., $^{205}Tl/^{203}Tl$=2.38755
11	0.91433	0.00003	2.16469	0.00086	8	Hirata (1996)	Tl, power corr.
12	0.91462	0.00004	2.16636	0.00082	8	Hirata (1996)	Tl, power corr., β correction
-	0.91460	0.00018	2.16639	0.00304	7	Mean MC-ICP-MS: References 6 to 12	
-	0.91474	0.00042	2.16701	0.00084	12	This study	Tl, exp. corr.
-	0.91472	0.00016	2.16776	0.00052	12	This study	Tl, exp. corr., renormalized to [1]

Table 2.5: SRM-981 compilation, TIMS and MC-ICP-MS. Studies 1 to 5 reflect TIMS double- or triple-spike techniques, whereas the final seven studies utilize thallium normalization (exponential or power law correction) or double-spike techniques with MC-ICP-MS. Note the agreement between Thirlwall (2000) and Galer and Abouchami (1998) for both the $^{207}Pb/^{206}Pb$ and $^{208}Pb/^{206}Pb$ ratios. The MC-ICP-MS results exhibit greater uncertainty with respect to $^{208}Pb/^{206}Pb$, and our results are within error of the TIMS observations.

1988a). Despite this possible limitation, we have observed reasonable agreement (250 ppm) between 1981 coral and 1982 seawater samples, supporting their separate processing methods, lead concentrations, and sample matrices. The seawater results agree with previous thermal ionization results (Véron *et al.*, 1994; Hamelin *et al.*, 1997), analyzing comparable seawater samples in the western North Atlantic. Finally, North Atlantic lead isotope profiles are consistent with the upper thermocline ventilation time scale and the proxy record, and good agreement is observed within the surface mixed layer and homogeneous North Atlantic Deep Water. These North Atlantic seawater and surface coral results represent one possible application of the MC-ICP-MS method for anthropogenic lead analysis in terrestrial and marine environments.

2.4 Conclusions

This analytical method represents a promising technique for lead isotope analysis. With signal intensities less than 1.5×10^{-12}A, external precision for the $^{207}Pb/^{206}Pb$ and $^{208}Pb/^{206}Pb$ ratios are generally less than 200 ppm, ranging from 75 to 177 ppm for $^{207}Pb/^{206}Pb$ (2σ). Utilizing both thallium normalization and external correction to SRM-981, isotope ratio accuracy better than 200 ppm is routinely possible, and the correction factors are stable on weekly to monthly time scales. For a typical analytical session (12 to 16 hours), thirty samples and twelve standards can be analyzed. The MC-ICP-MS method provides a useful, rapid, and consistent method for $^{207}Pb/^{206}Pb$ and $^{208}Pb/^{206}Pb$ analysis of seawater and marine carbonates.

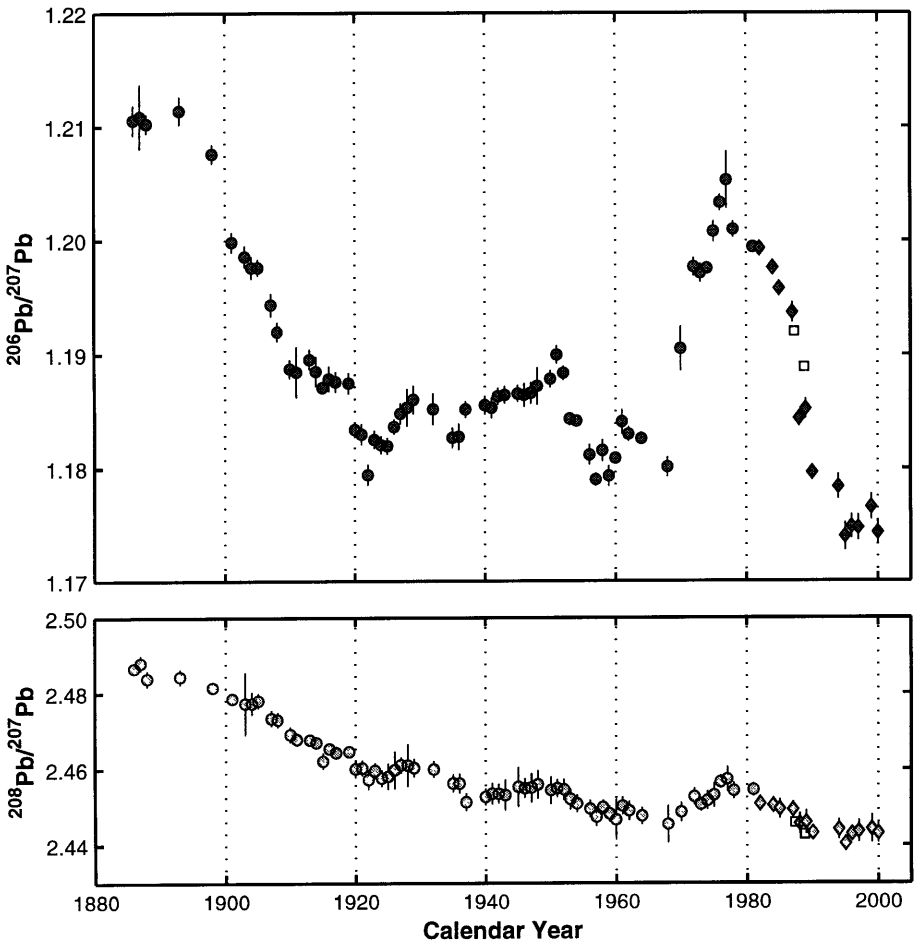

Figure 2-7: Western North Atlantic surface coral proxy record and seawater time series, analyzed by MC-ICP-MS. Upper panel: reconstructed $^{206}Pb/^{207}Pb$ ratio for Bermuda surface corals (closed circles) and western North Atlantic seawater (closed diamonds, Station S). The open squares reflect the TIMS seawater lead isotope analyses of Véron *et al.* (1994, sampled March, 1987) and Hamelin *et al.* (1997, sampled August, 1988). Lower panel: same as above for $^{208}Pb/^{207}Pb$. Note the agreement among adjacent samples within the record and the isotopic range observed.

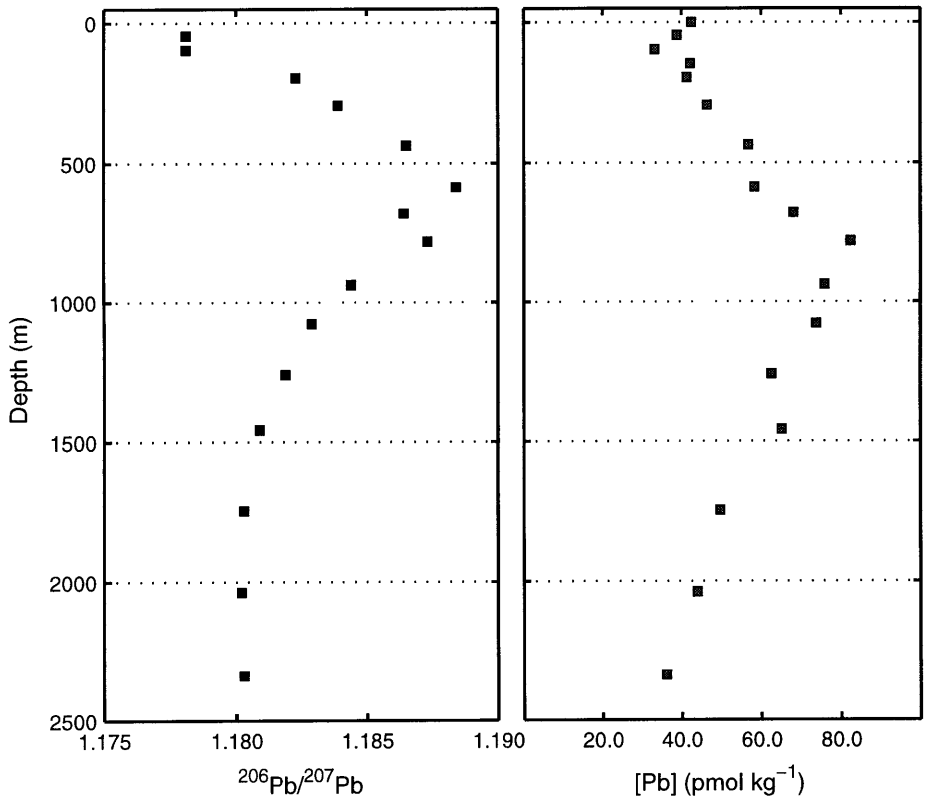

Figure 2-8: Eastern North Atlantic stable lead isotope (MC-ICP-MS) and lead concentration profiles (ID-ICP-MS): Endeavor-328, Station 7 (31°0'N, 31°0'W). The left panel reflects the $^{206}Pb/^{207}Pb$ ratio, and the right panel denotes total lead concentrations. Note the observed upper thermocline maximum in $^{206}Pb/^{207}Pb$ and the agreement among mixed layer and deep water isotopic ratios. The depth difference of the elemental and isotopic maxima results from an eleven-year phase lag between the elemental (1947-1989, not shown) and isotopic (1968-1990) North Atlantic lead transients. See Chapter 4 for additional details.

2.5 Appendix I

Mass fractionation in MC-ICP-MS has multiple potential sources, including the plasma interface, the ion optics, and the detector array. Here one rationale is presented for secondary fractionation effects, assuming the exponential mass fractionation law. This argument demonstates the relative importance of the slope and intercept terms shown in Figure 2-4. In the simplest case, variations in ion detection (*e.g.*, collector efficiencies, amplifier gains, or ion optics) introduce a secondary fractionation factor into Equation 2.3:

$$\left(\frac{^{205}\mathrm{Tl}}{^{203}\mathrm{Tl}}\right)_t = \left(\frac{^{205}\mathrm{Tl}}{^{203}\mathrm{Tl}}\right)_m \left(\frac{\mathrm{M}_{205}}{\mathrm{M}_{203}}\right)^{\beta} \cdot \alpha_1 \tag{2.4}$$

where α_1 corresponds to an arbitrary offset between two masses. Each isotope ratio will have a separate gain factor (α_1, α_2, α_3, etc.). Collector efficiencies and amplifier gains are generally corrected by repeated analysis of multiple isotopic standards and constant current gain calibrations, respectively. However, improper focusing of the optical plane (K. Collerson, personal communication) and other artifacts can introduce a secondary fractionation. For brevity, the atomic mass term (a constant) is assigned a new variable, τ:

$$\tau = \ln\left(\frac{\mathrm{M}_{205}}{\mathrm{M}_{203}}\right) \Big/ \ln\left(\frac{\mathrm{M}_{208}}{\mathrm{M}_{206}}\right) \tag{2.5}$$

Rewriting the Maréchal *et al.* (1999) derivation with the secondary fractionation factors for $^{205}\mathrm{Tl}/^{203}\mathrm{Tl}$ (α_1) and $^{208}\mathrm{Pb}/^{206}\mathrm{Pb}$ (α_2), one obtains

$$\begin{aligned} \ln\left(\frac{^{208}\mathrm{Pb}}{^{206}\mathrm{Pb}}\right)_m &= \left[\frac{1}{\tau} \cdot \frac{\beta_{\mathrm{Pb}}}{\beta_{\mathrm{Tl}}} \cdot \left(\frac{^{205}\mathrm{Tl}}{^{203}\mathrm{Tl}}\right)_m\right] \\ &+ \left[\ln\left(\frac{^{208}\mathrm{Pb}}{^{206}\mathrm{Pb}} - \ln(\alpha_2)\right)_t - \frac{1}{\tau} \cdot \frac{\beta_{\mathrm{Pb}}}{\beta_{\mathrm{Tl}}} \cdot \ln\left(\frac{^{205}\mathrm{Tl}}{^{203}\mathrm{Tl}} - \ln(\alpha_1)\right)_t\right] \end{aligned} \tag{2.6}$$

where α_1 and α_2 reflect the $^{205}\mathrm{Tl}/^{203}\mathrm{Tl}$ and $^{208}\mathrm{Pb}/^{206}\mathrm{Pb}$ secondary factors, respectively. As shown by Maréchal *et al.* (1999), this equation describes a line in the $\ln(^{205}\mathrm{Tl}/^{203}\mathrm{Tl})$ – $\ln(^{208}\mathrm{Pb}/^{206}\mathrm{Pb})$ domain, with the two arguments on the right corresponding to the slope and intercept, respectively. The primary result of Equation 2.6 is the secondary factors are present in the intercept term, graphically shown in Figure 2-9. This difference provides a

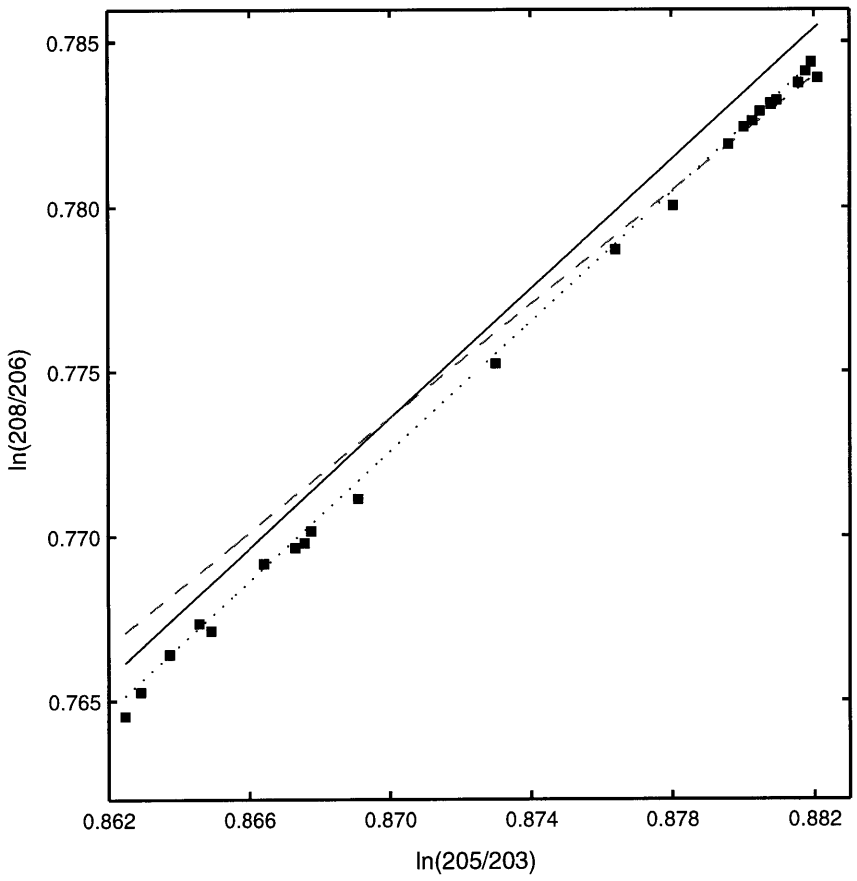

Figure 2-9: Secondary fractionation correction for MC-ICP-MS, following Figure 2-4. The solid line corresponds to the simplest case, where $\beta_{Tl} = \beta_{Pb}$, the dashed line includes a $\beta_{\mathrm{Pb}}/\beta_{\mathrm{Tl}}$ correction following Hirata (1996), and the dotted line reflects a secondary fractionation correction.

simple rationale for isotope ratio offsets observed in previous studies and the $^{205}\mathrm{Tl}/^{203}\mathrm{Tl}$ optimization technique of Rehkämper and Halliday (1998). Several indepedent techniques can account for this effect, including double-spiking techniques, $^{205}\mathrm{Tl}/^{203}\mathrm{Tl}$ optimization, and secondary SRM-981 normalization.

Chapter 3

Anthropogenic Lead in the North Atlantic Ocean: Historical Isotopic and Elemental Variability

3.1 Introduction

Anthropogenic lead represents an unique transient tracer in the world oceans, and its flux, residence time, and provenance have been determined via seawater concentration measurements (Schaule and Patterson, 1983; Boyle *et al.*, 1986; Wu and Boyle, 1997a), $^{226}Ra/^{210}Pb$ and $^{210}Po/^{210}Pb$ disequilibria (Craig *et al.*, 1973; Bacon *et al.*, 1976), and stable lead isotopic ratios (Flegal *et al.*, 1989; Véron *et al.*, 1994; Hamelin *et al.*, 1997; Alleman *et al.*, 1999). Quantitative understanding of lead's elemental and isotopic hydrography requires accurate historical boundary conditions. The purpose of this study is to present high-resolution surface coral and seawater time series from the western North Atlantic, demonstrating past elemental and isotopic variability consistent with modern water column profiles.

Marine elemental lead reconstructions have previously utilized surface coral Pb/Ca ratios in the western North Atlantic (Shen *et al.*, 1987; Shen and Boyle, 1987) and Caribbean (Dodge and Gilbert, 1984) regions, and the inferred concentration trends agree with historical emission estimates (Shen and Boyle, 1987) and terrestrial proxy records (Murozumi

et al., 1969; Boutron *et al.*, 1991; Candelone *et al.*, 1995; Shotyk *et al.*, 1998; Weiss *et al.*, 1999). Several unresolved issues with the North Atlantic Pb/Ca records currently exist. The time derivative of the coral records differs between 1950 and 1960: Shen and Boyle (1987) observed d[Pb/Ca]/dt of 2.4 nmol mol^{-1} yr^{-1} (1951 to 1959), whereas the Shen (1986) results equal 6.8 nmol mol^{-1} yr^{-1} (1951 to 1955). This difference was attributed to sample contamination despite agreement among sample replicates. Direct comparison between the Bermuda proxy data and a nearby seawater time series also does not exist (Wu and Boyle, 1997a). To address these issues, a high-resolution elemental record has been developed from North Rock, Bermuda, providing a new comparison between recent seawater observations and inferred lead concentrations since 1884.

The past isotopic variability of North Atlantic lead also reflects the contributions and composition of multiple anthropogenic sources. Previous surface coral $^{206}Pb/^{207}Pb$ analyses from the North Atlantic (Shen and Boyle, 1987) support a large isotopic range (1.184 to 1.215) and increased isotopic ratios from 1959 to 1974. The limited surface coral results (1887 to 1980) cannot explain the recent (1984 to 1998) upper thermocline isotopic reduction (Shen and Boyle, 1988b; Sherrell *et al.*, 1992; Véron *et al.*, 1993, 1998, this study). The $^{206}Pb/^{207}Pb$ minimum inferred from the coral record (1.184) is also significantly greater than recent North Atlantic Deep Water (NADW) observations from the western equatorial Atlantic (1.144, Alleman *et al.*, 1999), suggesting either surface corals do not reflect the past mixed layer composition, the inferred variability is of local significance, or the reported seawater measurements do not represent lead conservatively advected within NADW. A high-resolution surface coral isotopic record and multiple North Atlantic water column profiles were developed to address these issues, providing consistent observations between past isotopic variability and modern North Atlantic hydrography.

3.2 Methods

Two surface coral species, *Diploria strigosa* and *Diploria labyrinthiformis*, were collected in 1983 from North Rock, Bermuda by E. Druffel and coworkers. The colonies were cored at a water depth of 11 meters, and complete description of the coral sampling and radiocarbon

analysis is provided in (Druffel, 1989). The North Rock site, located 10 kilometers north of Bermuda, was chosen for its measured lead concentrations equal to the western North Atlantic (Shen and Boyle, 1987), its proximity to the North American westerlies, and the large integrated area within the subtropical North Atlantic gyre (see review by Schmitz and McCartney, 1993). Surface coral chronologies were based on the annual density band couplets of *Diploria* (Logan and Tomascik, 1991) and radiocarbon observations. These two cores provide a continuous, overlapping chronology, with age ranges of 1884 to 1955 (*D. strigosa*) and 1936 to 1983 (*D. labyrinthiformis*). No previous trace element analyses were completed on these cores, providing an independent assessment of the Shen and Boyle (1987) results.

Seawater samples were collected from the western (*Oceanus-326*, Station 1, 33°42'N, 57°40'W) and eastern (*Endeavor-328*, Station 7, 31°0'N, 31°0'W) North Atlantic in 1998 and 1999, respectively. Profile samples were collected with the MITESS trace element sampler (Dickey *et al.*, 1998). This system consists of twelve automated, programmable sampling units composed of ultra-high molecular weight polyethylene. The units open an acid-cleaned 500 mL HDPE bottle at a specified time, remain open for a rinse interval, then close. All samples were acidified to pH<2 with triple-distilled 6N HCl, adding 2 mL to 1 L of unfiltered seawater. Large volume (1-2 L) surface mixed layer samples were collected from Station S (32°29'N, 64°48'W) from 1983 to 1999, using the pole sampling technique. The corresponding elemental results are given in Wu and Boyle (1997a).

Surface coral and seawater sample preparation followed established methods for trace element analysis (Shen and Boyle, 1988a; Wu and Boyle, 1997b; Weiss *et al.*, 2000), and a complete description is provided in Chapter 2 and Appendix A. Pb/Ca ratios were determined by isotope dilution ICP-MS ([Pb], VG PlasmaQuad 2^+) and flame AAS ([Ca], Perkin-Elmer 403). The isotope dilution method utilized a ^{204}Pb spike (Oak Ridge National Laboratory) continuously calibrated with a gravimetric lead concentration standard (J. T. Baker). The mean standard deviation for Pb/Ca replicates is 5.2% (2σ), including analytical and cleaning uncertainties. Stable lead isotope ratios were determined by multiple collector ICP-MS (Micromass IsoProbe). The mean external isotope ratio precision was less than 200 ppm (2σ) for $1.5\text{x}10^{-12}$A ^{208}Pb signal intensities, using thallium and SRM-981

normalization. Agreement between the surface coral and seawater results supports these analytical methods, and a 250 ppm difference is observed between 1981 coral and 1982 seawater $^{206}Pb/^{207}Pb$. Previous thermal ionization analyses of western North Atlantic seawater (see Figure 3-3, Véron *et al.*, 1994; Hamelin *et al.*, 1997) support the accuracy of these methods.

Quantitative estimates of past seawater lead concentrations require assessment of partition coefficients (D_p). The non-thermodynamic definition of Henderson and Kracek (1927) is used to estimate seawater lead concentrations:

$$D_p = [Pb/Ca]_{coral} \,/\, [Pb/Ca]_{seawater} \quad (3.1)$$

$$[Pb]_{seawater} = [Pb/Ca]_{coral} \cdot [Ca]_{seawater} \,/\, D_p \quad (3.2)$$

where $[Ca]_{seawater}$ is an assumed constant, 10.3 mM. Shen and Boyle (1987) directly compared Bermuda seawater (n=7) and surface coral Pb/Ca (*D. strigosa*) from 1983 to 1984, calculating a partition coefficient of 2.3 (see Table 2 in Shen and Boyle, 1987), in agreement with a second *D. strigosa* D_p estimate from the Southern Reef Preserve, Bermuda (2.1). The limited temporal range of our Pb/Ca record precludes a direct seawater comparison, and the partition coefficient for the high-resolution record was determined by the resulting Shen and Boyle (1987) concentration record. An assessment of this method and its uncertainties are described in the following section.

3.3 Results and Discussion

3.3.1 Western North Atlantic Elemental Lead Records

The high-resolution surface coral Pb/Ca record, shown in Figure 3-1, generally agrees with the previous Shen and Boyle (1987) observations, including the gradual Pb/Ca rise from 1884 to 1947 followed by an abrupt increase from 1947 to 1955. This variability likely reflects two anthropogenic processes: (1) increased anthropogenic lead emissions from non-ferrous metal smelting (Pb, Cu, Ni, Zn, Cd), coal combustion, and steel manufacture throughout the Industrial Revolution; and (2) the consumption of leaded gasoline in the United States

and Europe, with maximum US consumption in 1972 (Wu and Boyle, 1997a). The relative magnitude of the Pb/Ca variability between the high-resolution record and Shen and Boyle (1987) are comparable despite different analytical methods and surface coral species. Both Pb/Ca records suggest a ten-fold increase in Pb/Ca throughout the twentieth century, ranging from 6 nmol/mol in 1884 to 60 nmol/mol in 1969. The high-resolution Pb/Ca record supports previous observations from North Rock, Bermuda.

The two coral records also contain several important differences. The two coral species shown here generally agree from 1938 to 1947, following a significant correction (7.7 nmol/mol, r=0.96) to the *D. labyrinthiformis* core. Although an abrupt Pb/Ca transition near 1950 is consistently observed, the initial timing of this transition differs between this study (1947) and Shen and Boyle (1987, 1951). This difference might be resolved by historical economic data: a known increase in US leaded gasoline consumption occurred from 1946 to 1956 (Wu and Boyle, 1997a), favoring the high-resolution record. Elevated Pb/Ca ratios are also observed from 1958 to 1965, despite agreement among sample replicates and adjacent samples. Finally, the most recent Pb/Ca reduction is not observed in the high-resolution record due to excessive tissue layer organic contaminants. The four observations from 1971 to 1974 are higher than the Shen and Boyle (1987) results; no reasonable basis exists, however, for their elimination.

To determine past seawater lead concentrations, the Shen and Boyle (1987) record was compared to the western North Atlantic seawater time series (Wu and Boyle, 1997a). The first partition coefficient utilized (D_p=2.3) was calculated from seven North Rock seawater measurements (128±26 pM) and *D. strigosa* Pb/Ca from 1983 to 1984 (30 nmol/mol). This result, shown in Figure 3-2, includes an offset between the inferred lead concentration and western North Atlantic lead measurements (1979 to 1983). To correct this offset, the 1979 Schaule and Patterson (1983) observation (160 pM) was compared with the coral record[1], and better agreement is observed (D_p=2.9). The high-resolution record was then calibrated with the inferred concentration record, calculating D_p from the 1884-1947 interval. The

[1]The 1979 estimate represents a single July analysis from Schaule and Patterson (1983), and the expected shallow mixed layer might introduce a positive bias to an annual mean (see Boyle *et al.*, 1986). The profile of Schaule and Patterson (1983), however, shows a diminished concentration gradient to 400 meters, suggesting the single observation is approximately equal to the mean annual concentration. This assumption was tested with the Boyle *et al.* (1986) profile time series, and the corresponding uncertainty does not exceed 6%.

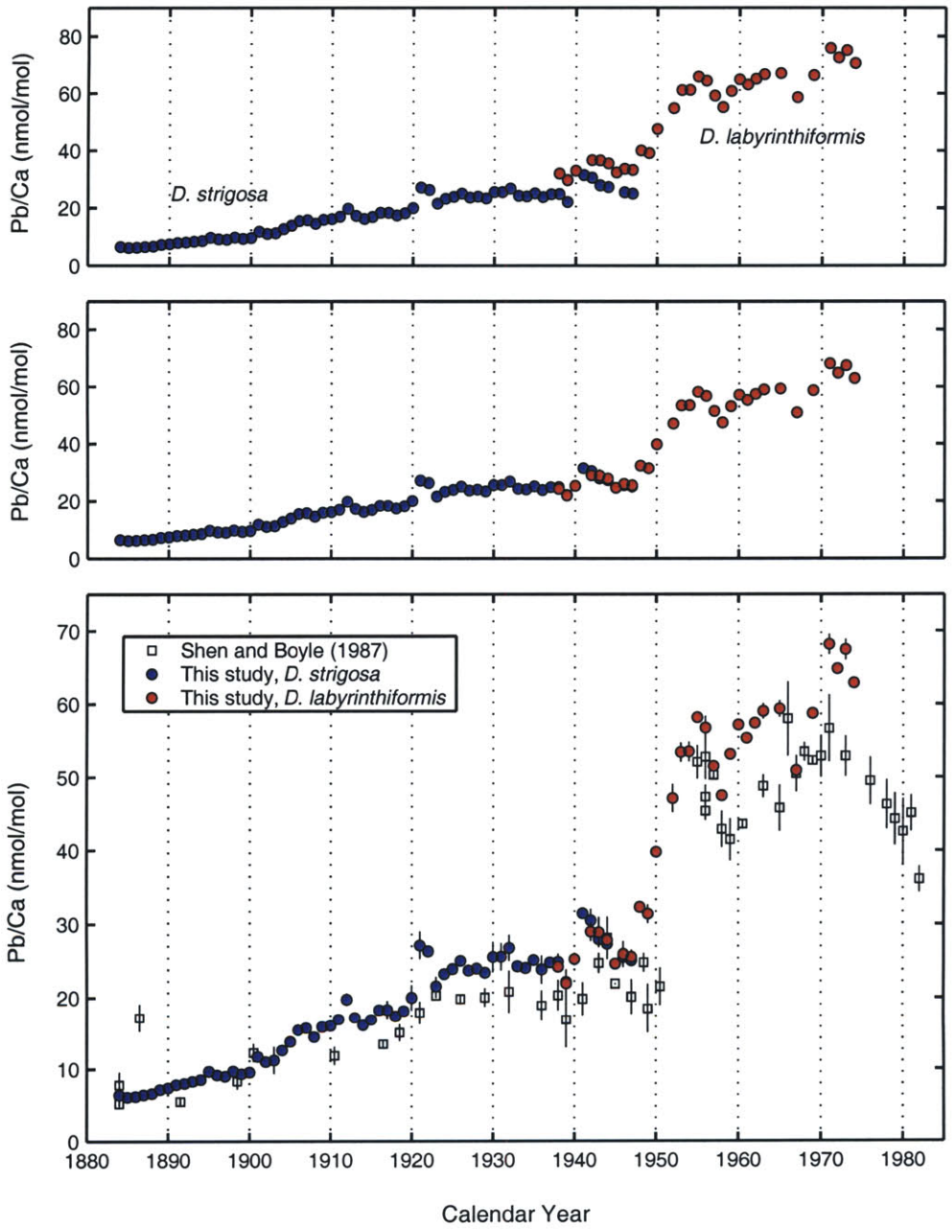

Figure 3-1: North Rock surface coral Pb/Ca records. The top panel reflects the raw Pb/Ca results (in nmol/mol) for the surface corals *D. strigosa* (blue) and *D. labyrinthiformis* (red). The middle panel shows the 7.7 nmol/mol correction applied to the *D. labyrinthiformis* record, calculated from the overlap. The bottom panel compares the composite record with the previous result of Shen and Boyle (1987). Error bars reflect $\pm 2\sigma$ of sample replicates.

resulting distribution coefficient was 3.6, approximately 25% higher than the corrected Shen and Boyle (1987) estimate (2.9). Significant offsets in trace element ratios are thus observed within and among coral species from the same location.

The observed Pb/Ca offsets between the two *Diploria* cores and the Shen and Boyle (1987) record suggests kinetic effects might account for some of the relative Pb/Ca variability. This hypothesis is supported by established kinetic controls on the isotopic (McConnaughey, 1989a,b), minor element (de Villiers *et al.*, 1994, 1995), and trace element (Cd/Ca and Ba/Ca, see Chapter 5) composition of coral aragonite. Reduction in coral growth rates might increase the Pb/Ca ratio with no associated change in seawater lead concentration, resulting from temperature, salinity, turbidity, or other changes in the reef environment. These significant offsets suggest individual trace element analyses from multiple coral colonies or species must be interpreted with caution. Several observations, however, suggest kinetic effects are not the principal determinants of the recent North Rock Pb/Ca variability. Annual coral extension rates across the 1947-1955 Pb/Ca transition are equal (0.33 ± 0.10 cm yr^{-1} for 1938-1947, 0.33 ± 0.07 cm yr^{-1} for 1955-1974), implying no reduction in coral growth correlated with the Pb/Ca transition. Agreement is also observed (r=0.96) between the *D. strigosa* and *D. labyrinthiformis* records despite the Pb/Ca offset. These observations support consistent elemental partitioning within individual coral colonies over the past century, requiring multi-year, colony-based calibrations. This consistency is supported by agreement between adjacent samples from 1884 to 1947: the kinetic 'noise' is smaller than the inferred change in seawater lead concentrations.

What are the implications of the Bermuda lead reconstruction? The lowest inferred lead concentration is approximately 20 pmol kg^{-1} in 1884, likely including a significant anthropogenic component given US lead ore production during this period ($3.4x10^5$ metric tons in 1900, USBM Minerals Yearbook). The seawater lead concentration associated with industrialization is 75 pmol kg^{-1}, followed by an abrupt increase to 200 pmol kg^{-1} in 1971. Relative to the 1884 coral estimate, a ten-fold increase in anthropogenic lead fluxes to the western North Atlantic resulted from leaded gasoline consumption, metal smelting, and other industrial emissions in the early 1970s. Comparing the seawater time series with the proxy record, the mean annual 1999 concentration is equivalent to 1904, several decades

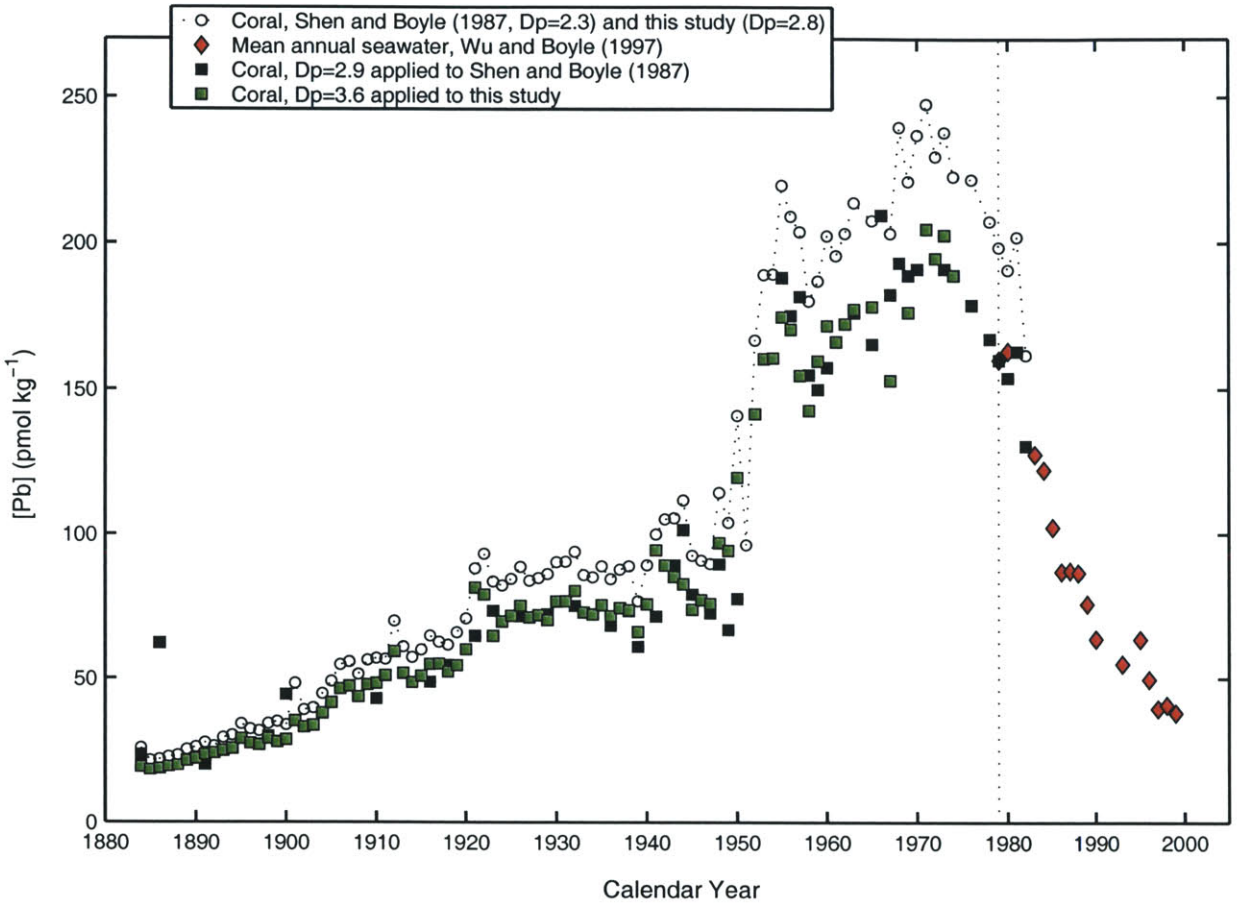

Figure 3-2: Western North Atlantic lead reconstruction. The open circles reflect mean annual lead concentrations calculated from surface coral Pb/Ca ratios, including the original Shen and Boyle (1987) calibration (D_p=2.3) and the high-resolution record (D_p=2.8). The blue and black squares reflect the two coral records calibrated with respect to the Schaule and Patterson (1983) 1979 observation. The red squares denote the mean annual seawater lead concentrations calculated from the Wu and Boyle (1997a) time series. Note the relative agreement between the two coral calibrations and the 1979-1983 seawater [Pb] measurements.

prior to the initial leaded gasoline consumption in the United States (1923).

3.3.2 Western North Atlantic Lead Isotope Records

Centennial-scale isotopic variability is observed in the proxy record, including a $^{206}Pb/^{207}Pb$ reduction from 1886 to 1922, diminished variability from 1922 to 1968, and an isotopic maximum from 1968 to 1990 (Figure 3-3). The first observed $^{206}Pb/^{207}Pb$ reduction likely reflects increased consumption of non-radiogenic US coal (Chow and Earl, 1972), smelting of non-radiogenic lead ores within North America, and other emissions throughout the Industrial Revolution (see Nriagu and Pacyna, 1988). Increased $^{206}Pb/^{207}Pb$ from 1968 to 1977 has been previously observed in San Diego aerosols (Chow *et al.*, 1975), Bermuda corals (Shen and Boyle, 1987), and High Sierra lake sediments (Shirahata *et al.*, 1980). This trend is best explained by lead ore production in the United States: the southeast Missouri district accounted for 40% of total US lead ore production in 1966, increasing to 93% in 1982 (USBM Minerals Yearbook, 1983)[2]. Given its radiogenic composition (1.303 for $^{206}Pb/^{207}Pb$, Brown, 1967) relative to other US districts (Colorado, Idaho, and Utah, Delevaux *et al.*, 1966; Stacey *et al.*, 1968; Zartman and Stacey, 1971) and imported ores (Canada, Mexico, and Peru, Chow *et al.*, 1975; Cumming *et al.*, 1979; Gunnesch *et al.*, 1990), a corresponding North American isotopic shift is expected. The United States was also the dominant leaded gasoline consumer at this time (80% in 1970, International Lead and Zinc Study Group, 1992); an ore production shift within the United States might therefore affect the western North Atlantic mixed layer.

The subsequent $^{206}Pb/^{207}Pb$ reduction is best explained by the relative lead contributions to the North Atlantic, not the isotopic composition of a single region. From 1982 to 1990 no comparable reduction occurred within US lead aerosols, supported by direct isotopic measurements (Sturges and Barrie, 1987; Church *et al.*, 1990; Bollhöfer and Rosman, 2001) and Chesapeake Bay sediments (F. Marcantonio, in press). Three observations support increased European lead contributions to the North Atlantic: (1) increased relative gasoline consumption from 1982 to 1990 (41% to 74%, International Lead and Zinc

[2]Tetraethyllead production records in the United States are proprietary, therefore no direct evidence for the use of southeast Missouri ores presently exists.

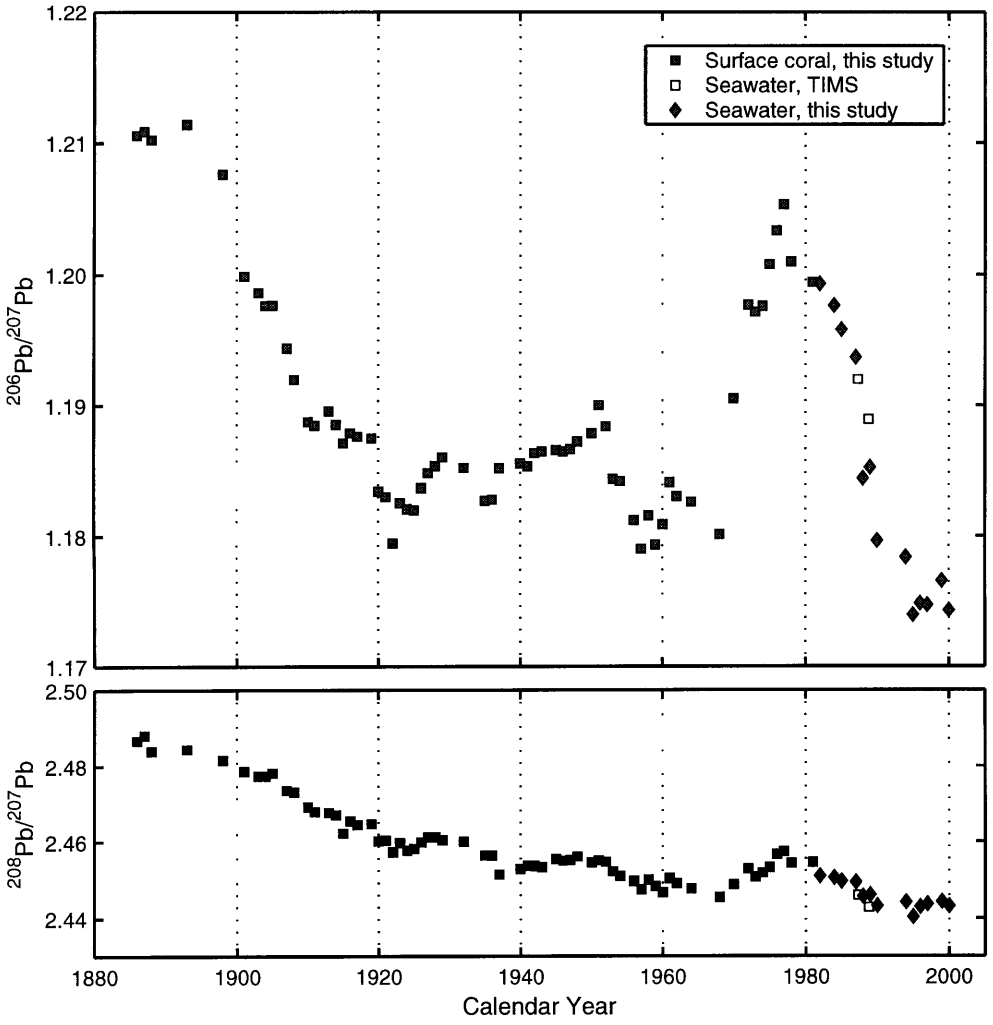

Figure 3-3: Western North Atlantic lead isotope reconstruction. The $^{206}Pb/^{207}Pb$ and $^{208}Pb/^{207}Pb$ ratios for Bermuda surface corals (closed squares) and Station S seawater (closed diamonds) are shown. Open squares reflect the seawater lead isotope analyses of Véron *et al.* (1994, sampled March, 1987) and Hamelin *et al.* (1997, sampled August, 1988). All results are tabulated in Appendix B.

Study Group, 1992); (2) the non-radiogenic composition of European lead aerosols relative to North America (Bollhöfer and Rosman, 2001); and (3) a concurrent isotopic maximum observed in the Summit, Greenland ice core record (Figure 3-4). A simple binary mixing calculation, shown in Table 3.1, provides additional evidence for this hypothesis. These qualitative estimates demonstrate North American sources dominated North Atlantic an-

Source	Interval	$^{206}Pb/^{207}Pb$	2σ	$^{208}Pb/^{207}Pb$	2σ	Percentage
North Atlantic	1994-1998	1.176	0.004	2.443	0.003	–
North America	1994-1998	1.206	0.005	2.453	0.007	48±2
Europe	1994-1998	1.135	0.001	2.410	0.002	52±2
North Atlantic	1979-1983	1.200	0.002	2.453	0.004	–
North America	1979-1983	1.206	0.027	2.453	0.027	90±23
Europe	1979-1983	1.115	0.032	2.391	0.035	10±23

Table 3.1: Lead provenance estimates for the western North Atlantic. A description of the relevant assumptions and uncertainties is provided in Appendix I.

thropogenic lead from 1979 to 1983, whereas North American and European contributions were approximately equal from 1994 to 1998.

To what extent does the North Atlantic isotopic record differ from previous annual-scale proxy observations? Ice core records from Summit, central Greenland (Rosman *et al.*, 1994) and Mont Blanc, France (Rosman *et al.*, 2000) provide a useful comparison (Figure 3-4). Despite separate chronologies, the three records exhibit distinct isotopic histories, reflecting the opposing isotopic composition of North American and European anthropogenic lead. The Mont Blanc record is consistently less radiogenic than the North Atlantic record and is dominated by an isotopic minima at 1978, attributed to the deliberate use of Australian lead ores in northern Italy (Facchetti and Giess, 1982). The Greenland record includes a seasonal isotopic cycle, a isotopic maxima concurrent with the Bermuda record, and an intermediate isotopic composition reflecting anthropogenic contributions from North America and Europe. Finally, the western North Atlantic record is consistently more radiogenic than the European and Greenland observations, reflecting predominant North American contributions to the western North Atlantic.

The relative importance of the anthropogenic sources is further shown by a $^{206}Pb/^{207}Pb$–$^{208}Pb/^{207}Pb$ diagram in Figure 3-5. From this comparison, the earliest coral sample (1886) is distinct from the eastern and western North Atlantic pelagic background estimates (Chow and Patterson, 1962), consistent with known US lead production at this time (see above). The North Atlantic results exhibit at least three mixing trends and follow a unique time trajectory from 1886 to 1913. The time trajectories from 1913 to the present are non-unique in $^{206}Pb/^{207}Pb$–$^{208}Pb/^{207}Pb$ space. This comparison supports the admixture of

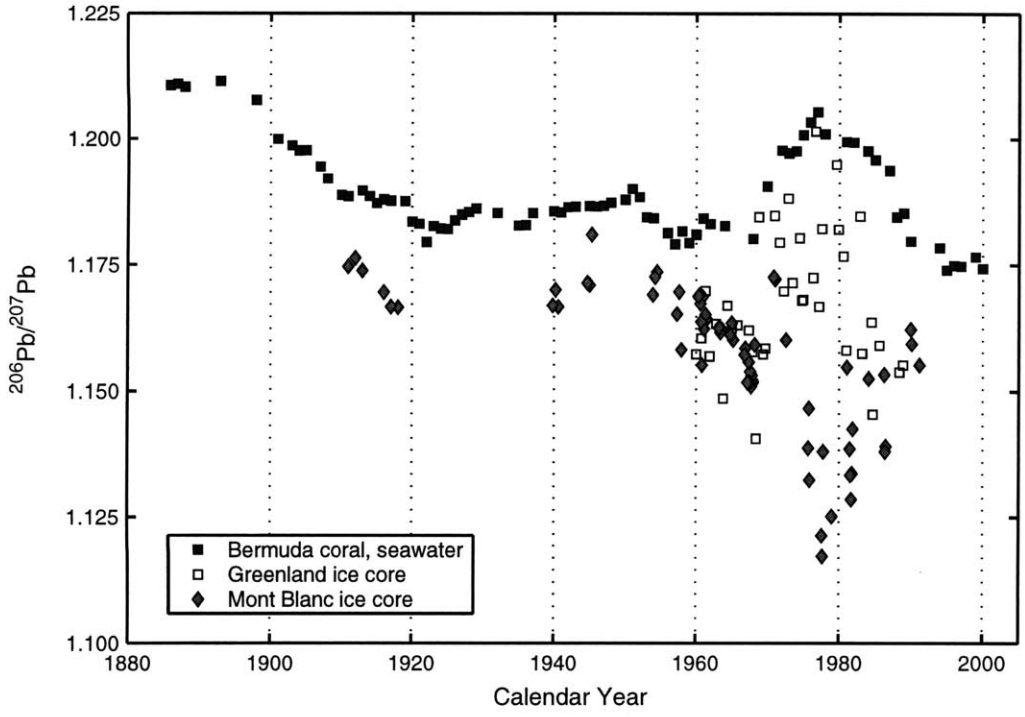

Figure 3-4: Lead isotope proxy comparison, $^{206}Pb/^{207}Pb$. Three annual-scale records are shown: the North Atlantic surface coral and seawater time series (this study), the Summit, Greenland ice core record of Rosman *et al.* (1994), and the Mont Blanc ice core results of Rosman *et al.* (2000). Note the isotopic maximum observed in both the North Atlantic and Greenland records.

North American and European lead in Arctic ice (Rosman *et al.*, 1993), and the greatest US contribution to the Summit site occurred in 1977. The least radiogenic isotopic ratios are present in the modern North Atlantic, following the Mont Blanc mixing line (Rosman *et al.*, 2000).

The reconstructed isotopic variability is consistent with water column observations, and all isotopic and elemental profile results are provided in Tables 4.2 and 4.3. A $^{206}Pb/^{207}Pb$ reduction has been directly observed in the western North Atlantic thermocline from 1984 to 1998, shown in Figure 4-9 (Shen and Boyle, 1988b; Sherrell *et al.*, 1992; Véron *et al.*, 1993, 1998, this study). As thermocline ventilation rates increase with depth in the western North Atlantic (from ^{3}H–^{3}He ages, Jenkins, 1980), a thermocline maximum in 1998 (800

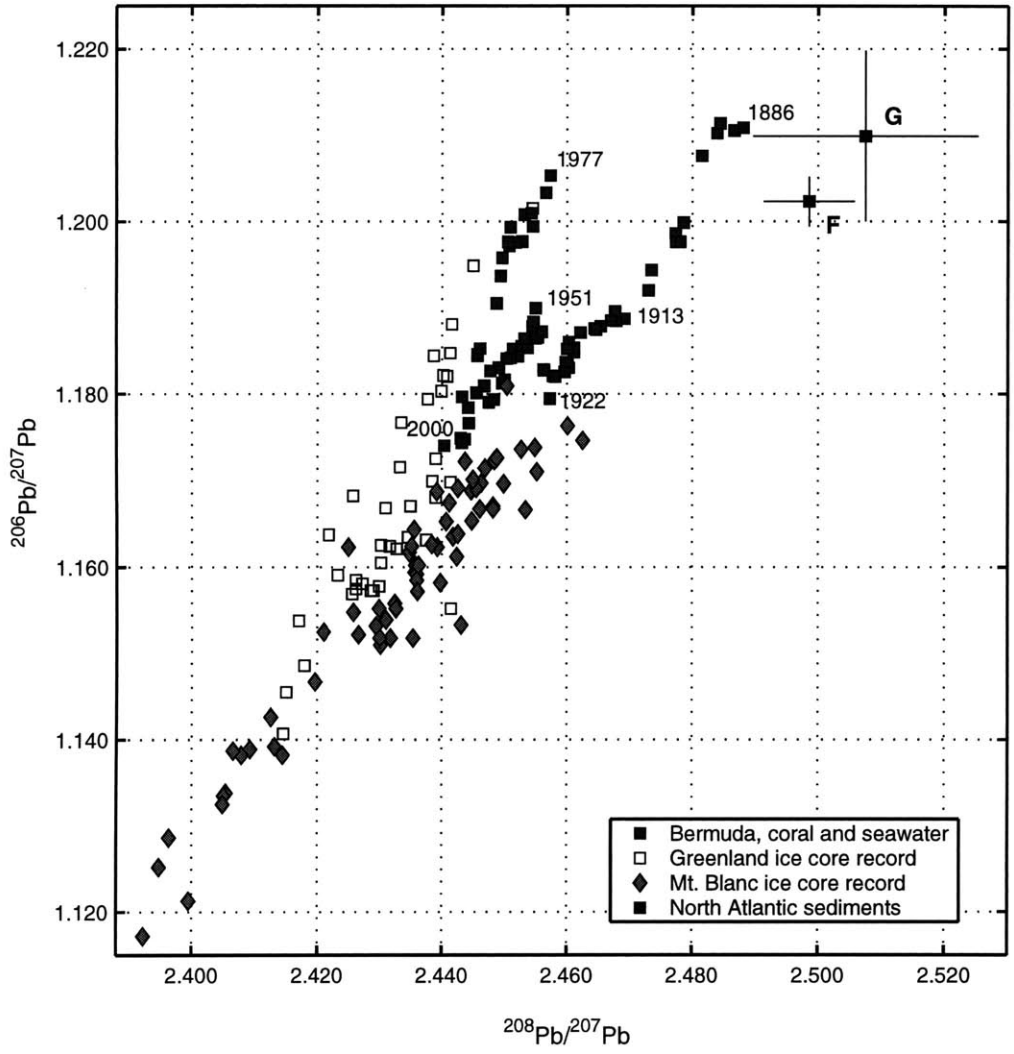

Figure 3-5: Triple isotope diagram for the North Atlantic, Greenland, and European proxy records. The records follow Figure 3-4, and selected years are shown for the coral and seawater measurements. The western (G, n=16) and eastern (F, n=5) North Atlantic pelagic background estimates are also shown for comparison (Chow and Patterson, 1962). One anomalous observation from Group G ($^{206}Pb/^{207}Pb$=1.1737) was eliminated prior to the calculation, and error bars represent $\pm 2\sigma$ of sample populations.

meters) results from the time-dependent mixed layer variability. Convergence of the isotope profiles below 600 meters generally agrees with the 17-year mean water mass residence time (Jenkins, 1980) and the 21-year time difference between the $^{206}Pb/^{207}Pb$ maximum

(1977) and the latest thermocline profile (1998). The $^{206}Pb/^{207}Pb$ reduction from 1977 to the present has not yet penetrated to the lower thermocline. The resulting isotopic maximum has been directly observed in the eastern and western North Atlantic, suggesting this variability is not confined to Bermuda. The elemental and isotopic maxima are offset by 200 meters, in agreement with the 11-year phase lag between the primary isotopic (1968 to 1990) and elemental (1947 to 1989) transients. The proxy and seawater observations thus provide consistent evidence for decoupled isotopic and elemental lead variability in the North Atlantic Ocean.

3.4 Conclusions

Elemental and isotopic surface coral and seawater records support the variable flux and provenance of anthropogenic lead. Coralline Pb/Ca ratios from the western North Atlantic provide useful constraints for the elemental transient, suggesting a ten-fold increase in seawater lead concentrations relative to 1884. Kinetic lead discrimination introduces significant uncertainties for absolute concentration estimates, requiring interpretative caution for Pb/Ca records. Past isotopic variability in this region results from the variable composition and contribution of North American and European sources, with a hypothesized two-fold reduction in North American fluxes from 1981 to 1996. Most importantly, these records have unique, consistent water column signatures throughout the North Atlantic, providing new model constraints for this transient anthropogenic tracer.

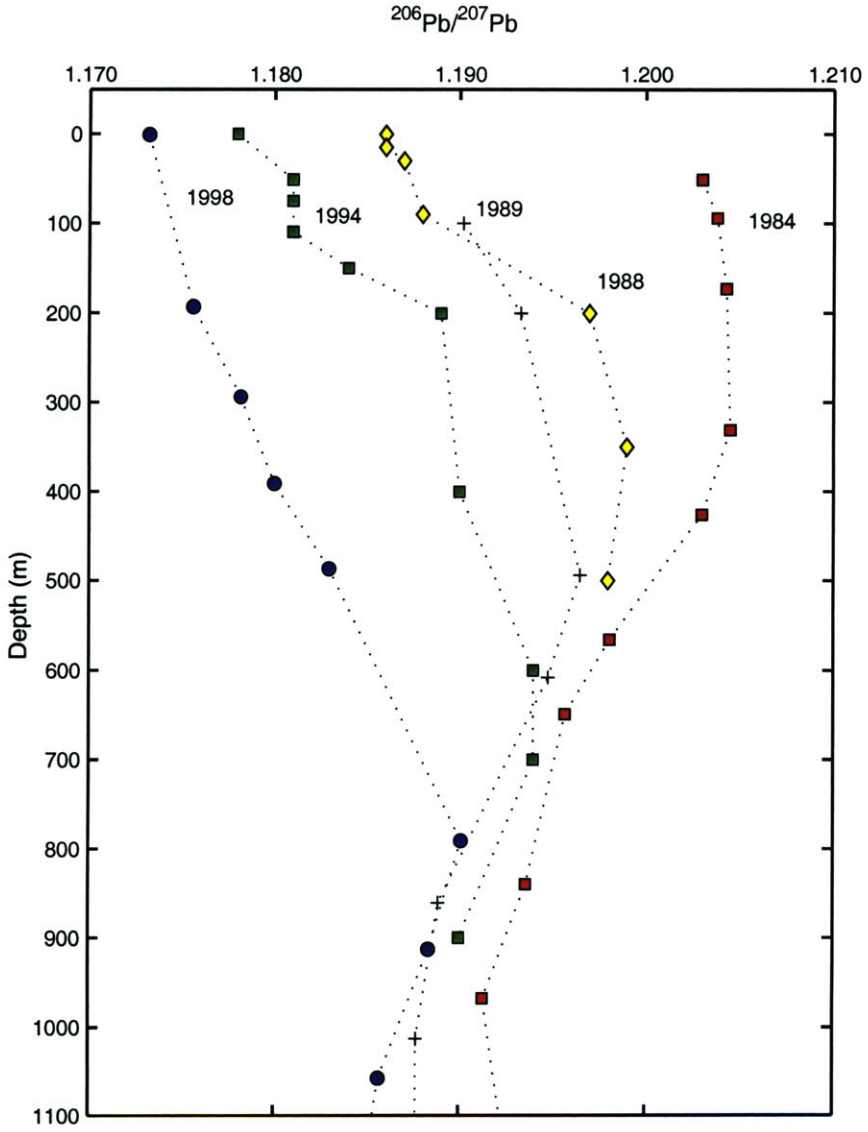

Figure 3-6: Western North Atlantic thermocline $^{206}Pb/^{207}Pb$ evolution, 1984 to 1998. The profile data are from Shen and Boyle (1988b, sampled in 1984 at Station S, 32°2'N, 64°30'W), Sherrell *et al.* (1992, sampled in 1988 near Station S, 32°0'N, 64°10'W), Véron *et al.* (1993, sampled in 1989 at BATS, 31°5'N, 64°1'W), Véron *et al.* (1998, sampled in 1994 at BATS), and this study (sampled in 1998 at 33°42'N, 57°40'W). Differences among site locations should be considered when interpreting these profiles. Note the consistent $^{206}Pb/^{207}Pb$ thermocline reduction and the isotopic maximum (800 meters) in the 1998 profile.

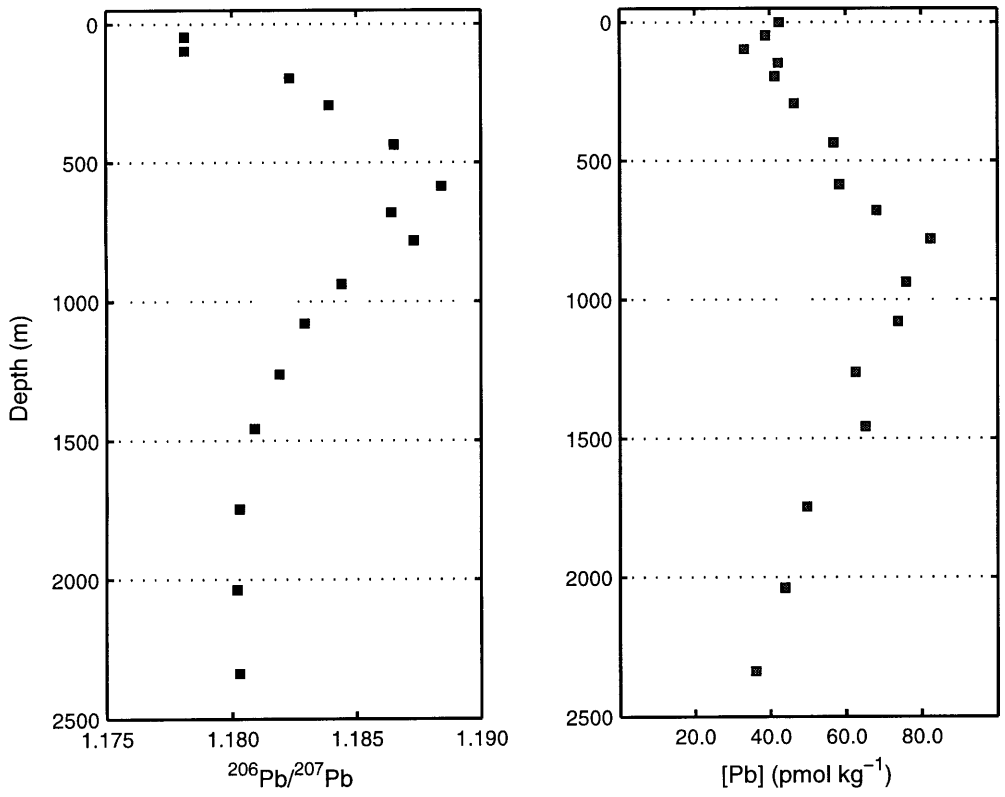

Figure 3-7: Eastern North Atlantic stable lead isotope and lead concentration profiles: *Endeavor-328*, Station 7 (31°0'N, 31°0'W). The left panel reflects the $^{206}Pb/^{207}Pb$ ratio, and the right panel denotes total lead concentrations. Note the offset between the elemental and isotopic maxima, resulting from an 11-year phase lag between the elemental (1947-1989) and isotopic (1968-1990) North Atlantic transients.

3.5 Appendix I

The binary mixing calculation includes several qualitative assumptions. Ideally, annual flux-weighted isotopic records would be available from each anthropogenic source, determining their respective contributions to the North Atlantic. For this calculation, the North Atlantic estimates reflect the mean and 2σ standard deviation of the Bermuda surface coral and seawater observations. The 1994 to 1998 North American and European estimates are taken from the aerosol observations of Bollhöfer and Rosman (2001), and the estimates shown are concentration-weighted for each continent. The 1979-1983 European ratios represent unweighted means from the Grousset *et al.* (1994) compilation, whereas the 1979-1983 North American estimates are assumed constant (1.206). The 1979-1983 source estimates contain the greatest uncertainty given 1981 aerosol (1.224, Patterson and Settle, 1987) and 1979-1981 Chesapeake Bay (1.198, F. Marcantonio, in press) observations. With these best available source estimates, the lead provenance of the western North Atlantic remains qualitative, but these uncertainties are less than the calculated differences.

Chapter 4

Stable Lead Isotopes in the Subtropical and Tropical North Atlantic Ocean

Anthropogenic lead represents a useful diagnostic of biogeochemical cycles in the North Atlantic Ocean. The utility of this tracer is based on its transient influx from anthropogenic emissions (Schaule and Patterson, 1983; Boyle *et al.*, 1986; Shen and Boyle, 1987; Véron *et al.*, 1993; Wu and Boyle, 1997a), its predominant atmospheric source (Jickells *et al.*, 1984; Patterson and Settle, 1987; Church *et al.*, 1990), and its constrained mixed layer and upper thermocline residence time (Craig *et al.*, 1973; Bacon *et al.*, 1976; Nozaki and Tsunogai, 1976). One promising aspect of marine lead geochemistry is its stable isotopic composition, and several previous studies have documented water column and surface ocean variability in the North Atlantic and North Pacific Oceans (Flegal *et al.*, 1986; Véron *et al.*, 1994; Hamelin *et al.*, 1997; Alleman *et al.*, 1999). Limited synoptic and time series observations, however, currently exist. This study presents six hydrographic profiles from the eastern and western North Atlantic, demonstrating surface ocean, thermocline, and deep water variability consistent with the heterogeneous, time-dependent distribution of this isotopic tracer.

4.1 Introduction

The direct response of the modern North Atlantic to anthropogenic lead influxes is well-established. Seawater time series analysis of the surface mixed layer and thermocline demonstrate reduced lead concentrations and $Pb/^{210}Pb$ ratios concurrent with leaded gasoline regulation in the United States and Europe (Wu and Boyle, 1997a; Véron *et al.*, 1998, and refs. therein). Additional evidence for lead's anthropogenic origin includes flux estimates from the modern and pre-anthropogenic North Atlantic (Schaule and Patterson, 1983), surface coral Pb/Ca analysis (Shen and Boyle, 1987), and interhemispheric seawater concentration gradients (Helmers and Rutgers van der Loeff, 1993). This direct response likely results from the magnitude of global atmospheric lead emissions ($3x10^8$ kg yr^{-1} in 1983, Nriagu and Pacyna, 1988), limited biological uptake relative to other bioactive trace elements (Boyle *et al.*, 1986), and its diminished deep ocean inventory.

The isotopic composition of seawater lead provides useful constraints regarding its anthropogenic sources and transport. Mixed layer results of Véron *et al.* (1994), Hamelin *et al.* (1997), and Weiss *et al.* (2000) exhibit a zonal distribution in the modern North Atlantic (1987-1989), shown in Figure 4-1[1]. This distribution is consistent with westerly radiogenic North American lead fluxes (Sturges and Barrie, 1987; Church *et al.*, 1990; Bollhöfer and Rosman, 2001), easterly non-radiogenic trade wind fluxes (Hamelin *et al.*, 1989; Grousset *et al.*, 1994; Bollhöfer and Rosman, 2001), and their subsequent advection within and removal from the subtropical gyre. The 25°N isotopic boundary also agrees with the 1990 lead concentration gradient observed by Helmers and Rutgers van der Loeff (1993) across the tropical-subtropical boundary (37±2.8 to 80±0.1 pmol kg^{-1} from 24°10.0'N to 28°58.6'N, ANT IX/1). The isotopic composition of contemporaneous seawater and aerosol lead are not necessarily equal (Véron *et al.*, 1993; Hamelin *et al.*, 1997). This inequality results from the different residence time of mixed layer (2 years, Bacon *et al.*, 1976) and atmospheric (9.6±2.0 days, Francis *et al.*, 1970) lead, rapid current velocities within the western boundary current and North Atlantic Drift (30 cm s^{-1}, Fratantoni, 2001), and the seasonally-variable anthro-

[1]This comparison is inexact given the observed isotopic reduction in the western North Atlantic (1987-1989, Chapter 3) and a seasonal sampling bias from March (Hamelin *et al.*, 1997) to September (Véron *et al.*, 1994). These complications, however, are secondary relative to the large isotopic range.

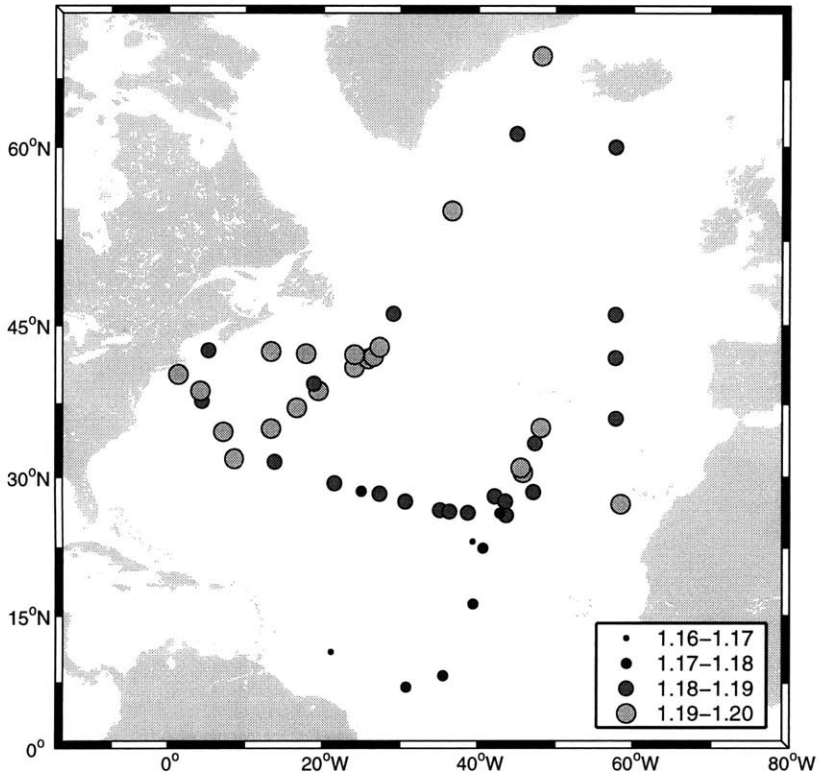

Figure 4-1: North Atlantic $^{206}Pb/^{207}Pb$ distribution, 1987 to 1989. The $^{206}Pb/^{207}Pb$ ratio is plotted with respect to four bins (1.16 to 1.20), compiled from Véron *et al.* (1994, collected 1988), Hamelin *et al.* (1997, collected 1987), and Weiss *et al.* (2000, collected 1989). Note the isotopic boundary at 25°N, reflecting northeasterly atmospheric transport of Eurasian lead (Hamelin *et al.*, 1989) to the tropical-subtropical boundary.

pogenic lead contributions from North America and Europe (*e.g.*, Shen and Boyle, 1988b; Wu and Boyle, 1997a). Isotopic variability has also been observed within the principal deep and intermediate North Atlantic water masses (Alleman *et al.*, 1999; Véron *et al.*, 1999), suggesting a deep water anthropogenic signature despite low seawater lead concentrations.

This study complements these observations via hydrographic profiles from the western and eastern North Atlantic. These results address the changing isotopic composition of the upper ocean, notably the relative contributions of recent European and North American lead. Second, the advection of the recent isotopic transient within the North Atlantic thermocline is discussed, with an isotopic maximum linked to atmospheric deposition and thermocline ventilation. Finally, the isotopic composition of North Atlantic Deep Water

is presented, providing new evidence for deep anthropogenic fluxes consistent with North Atlantic proxy observations.

4.2 Methods

A key consideration for lead isotopic analysis is proper sampling and analysis given contamination issues discussed by Patterson and Settle (1976). This study includes three recently-developed techniques: the MITESS automated trace element sampler (see Chapter 3 and Dickey *et al.*, 1998), the $Mg(OH)_2$ coprecipitation method (Wu and Boyle, 1997b; Weiss *et al.*, 2000), and multiple-collector ICP-MS (Walder and Freedman, 1992). This technique represents a reliable technique for seawater lead isotope analysis, and a brief synopsis is provided in Section 4.2.1.

Three separate cruises in the western and eastern North Atlantic are included here (1998 to 2001), and the hydrographic stations are shown in Figure 4-2 and Table 4.1. Surface ocean trace element samples were collected before and after each station with the 'towed fish' sampling method (Vink *et al.*, 2000), providing replicates for the hydrocast mixed layer samples. Continuous CTD measurements (Sea-Bird Electronics) were taken to determine θ-S properties at each station, and on-board silicate, phosphate, and salinity analyses were completed from discrete Niskin rosette samples. Trace element hydrocast samples were collected with the automated MITESS sampler, composed of ultra-high molecular weight polyethylene (Dickey *et al.*, 1998). The alkaline batteries should be modified for abyssal pressures exceeding 2800 psi, drilling into the two void spaces to prevent rupture at depth (R. Cortesi, unpublished data). The 500 mL hydrocast samples were acidified with 1 mL triple-distilled 6.0N HCl in a laminar flow bench immediately following collection, and the acid stock solutions were retained for process blank analysis.

4.2.1 Analytical Methodology

Seawater lead isotope analysis followed the method of Chapter 2. First, seawater lead was preconcentrated from 160 to 240 mL via $Mg(OH)_2$ (s) coprecipitation (Wu and Boyle, 1997b; Weiss *et al.*, 2000), scaling the sample volume to lead concentrations determined by isotope

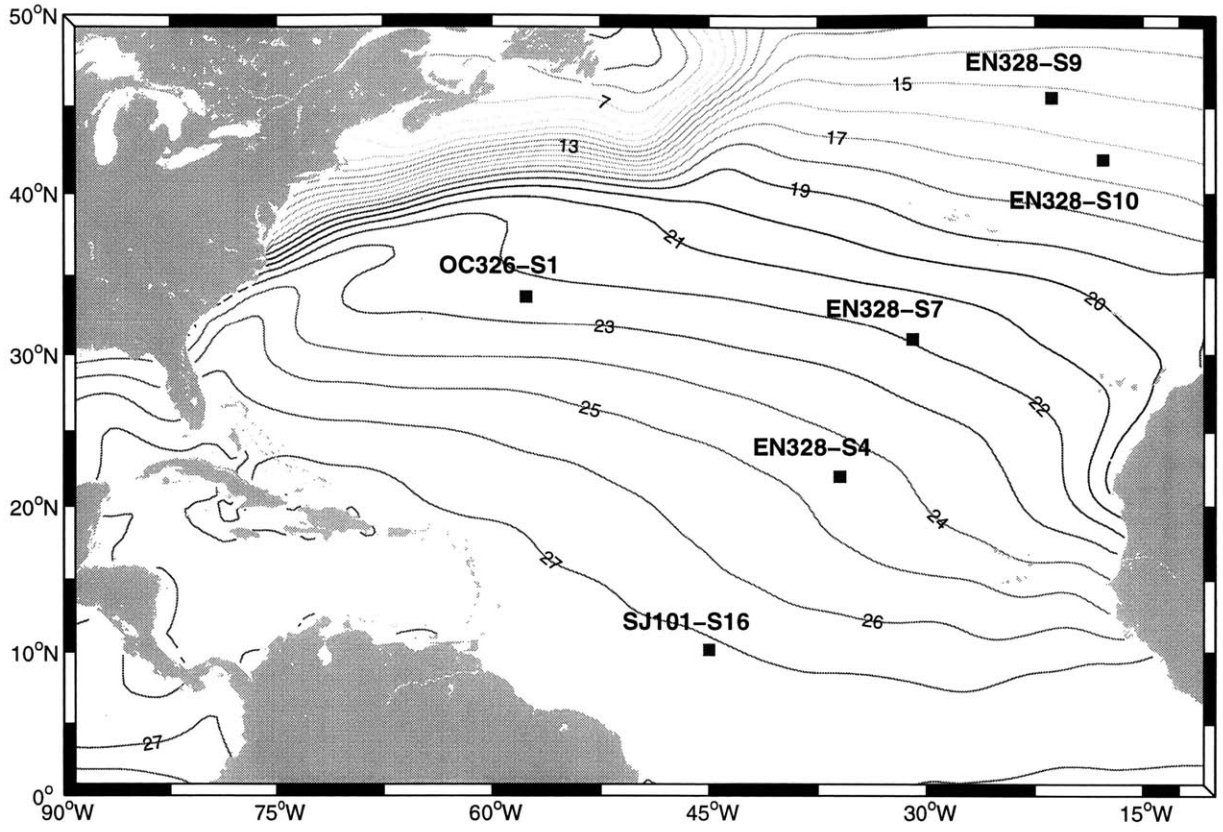

Figure 4-2: North Atlantic site location map, including hydrographic stations from Endeavor-328, Oceanus-326, and Seward Johnson-101. The mean annual sea surface temperature field is shown to delineate the Gulf Stream position (Da Silva *et al.*, 1994). These abbreviations will be adopted throughout this study.

Cruise	Stat.	Latitude	Longitude	Date	Temp.	Sal.	Z_{mix}	Z_{bath}
Endeavor-328	4	22°0'N	36°0'W	9/99	26.945	37.459	45	4910
Endeavor-328	7	31°0'N	31°0'W	9/99	26.410	37.075	57	4400
Endeavor-328	9	45°31'N	21°29'W	9/99	18.890	35.748	107	4001
Endeavor-328	10	42°0'N	17°45'W	9/99	20.483	35.911	67	5054
Oceanus-326	1	33°42'N	57°40'W	7/98	26.235	36.266	84	4538
Seward Johnson-101	16	10°10'N	45°0'W	1/01	25.985	36.237	29	4760

Table 4.1: Hydrographic stations, eastern and western North Atlantic. Temperature (°C) and salinity (psu) reflect discrete measurements, mixed layer depth (Z_{mix}, meters) denotes mean annual values from Levitus *et al.* (1994), and water column depths (Z_{bath}, meters) are taken from ETOPO5 (National Geophysical Data Center, 1988).

dilution ICP-MS (see Wu and Boyle, 1997b). Details regarding the lead isotope dilution method are provided in Chapter 3. The preconcentrated sample was separated from the major cation matrix via HBr-HCl anion exchange chromatography (*e.g.*, Kraus and Moore, 1953; Strelow, 1978), retaining $PbBr_4^{2-}$ onto AG-1x8 resin (Eichrom) and eluting the retentate as $PbCl_3^-$. The purified sample was analyzed by multiple collector ICP-MS (MC-ICP-MS, Micromass IsoProbe), correcting for mass fractionation by thallium normalization and repeated SRM-981 analysis (see Chapter 2). Abundance sensitivity was determined by daily ^{209}Bi analysis (Thirlwall, 2001), and instrumental blanks were subtracted by individual 'on-peak zeros'. Two process blanks were also analyzed for each column series. External precision with respect to dilute SRM-981 standards is less than 200 ppm (2σ) for both $^{208}Pb/^{206}Pb$ and $^{207}Pb/^{206}Pb$ ratios with ^{208}Pb signal intensities from $1.3x10^{-12}$ to $1.8x10^{-12}$ A ($R=10^{11}$ Ω, n=12). Triplicate analysis of mixed layer samples from EN328-S7 yields a mean external precision of 291 ppm (2σ), a realistic estimate given possible sample matrix effects, variable column blanks, and sample handling. Approximately 35 to 40 samples can be analyzed during a 16-hour IsoProbe session. Both the sampling and analytical methods provide a rapid and consistent technique for seawater $^{206}Pb/^{207}Pb$ and $^{208}Pb/^{207}Pb$ analysis.

4.2.2 Site Hydrography and Climatology

The hydrography and climatology of the six tropical and subtropical stations warrants consideration. Three features of the surface climatology are shown in Figure 4-3, taken from Levitus *et al.* (1994) and Da Silva *et al.* (1994). Seasonal and spatial variations in mixed layer depth, seawater density, and surface wind speed are shown, determining the respective thermocline ventilation, isopycnal distribution, and aerosol deposition patterns at each site. Winter mixed layer depths are greatest at Stations 9 and 10 (250 meters), ventilating the σ_θ=27 isopycnal between 45 and 50°N. The wind vectors suggest Station 1 will best reflect North American westerly atmospheric lead fluxes, whereas Stations 1 and 16 might exhibit European and North African lead sources.

The site hydrography includes several characteristic North Atlantic water masses (Figure 4-4). The linear θ-S reduction corresponds to the well-known North Atlantic Central Water (NACW), formed by winter water mass subduction near the subtropical-subpolar convergence (Iselin, 1936). The high salinity core at Station 10 reflects Mediterranean Outflow Water, observed from 950 to 1050 meters at this site. Antarctic Intermediate Water is best observed at Station 16, shown as the θ-S minimum below the NACW trend. North Atlantic Deep Water (NADW) dominates the deep hydrography relative to Antarctic Bottom Water (AABW), best shown by the θ-S maximum (5°C) at Station 16. The predominance of NADW is supported by binary mixing calculations: assuming end-member NADW–AABW silicate concentrations from the Broecker and Peng (1982) compilation, the relative NADW contribution ranges from 73% (Station 4) to 90% (Station 1).

4.3 Results and Discussion

The primary isotopic results of this study are shown in Figure 4-5 and Table 4.2, including six lead isotope profiles from the western and eastern North Atlantic. The elemental results from the same samples are shown in Figure 4-6 and Table 4.3. The $^{206}Pb/^{207}Pb$ and $^{208}Pb/^{207}Pb$ profiles are plotted with respect to latitude, including the eastern subtropical North Atlantic (Stations 9, 10, 7, and 4), western subtropical North Atlantic (Station 1), and the equatorial North Atlantic (Station 16). These profiles were collected over a two year

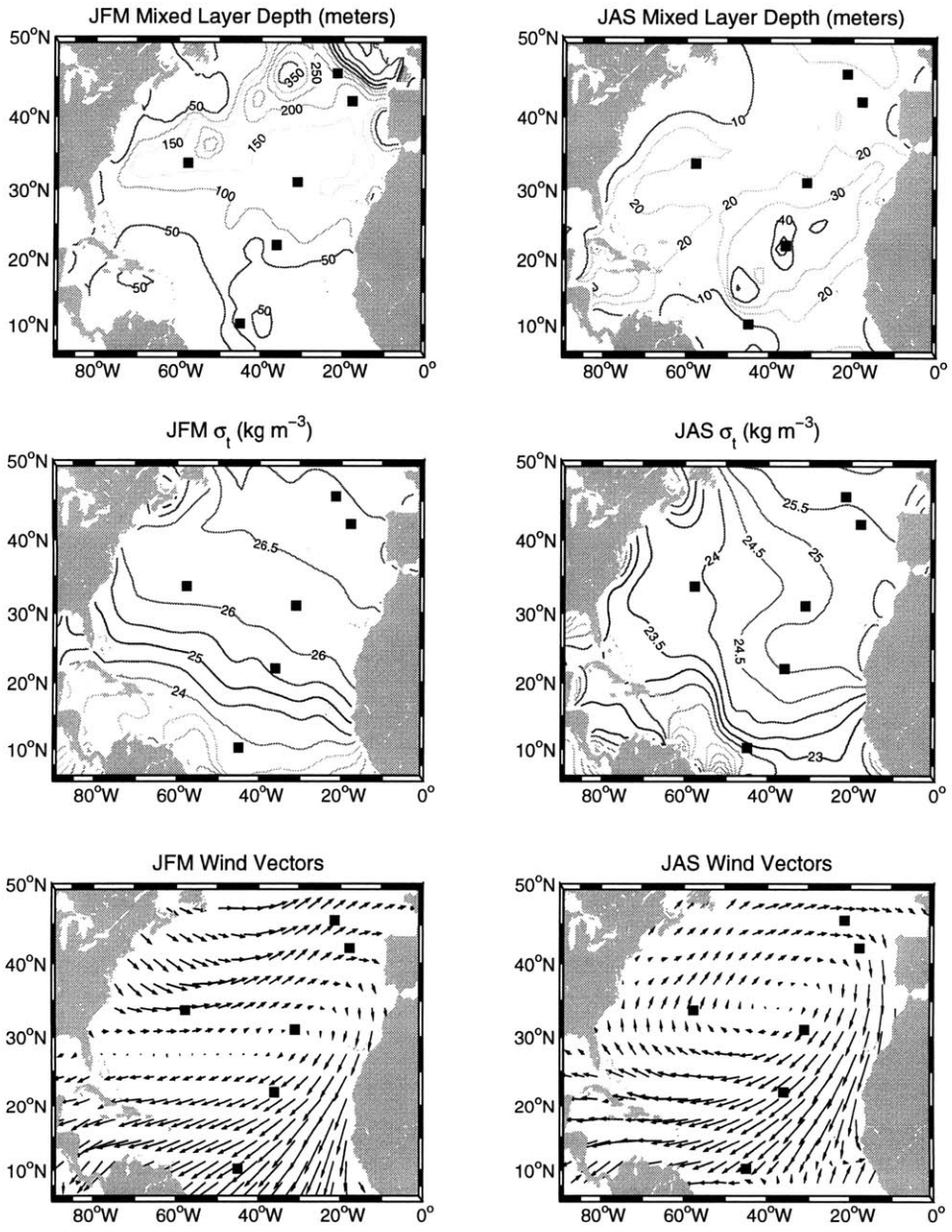

Figure 4-3: North Atlantic seasonal mixed layer depth, density, and wind speed vectors. The mean conditions for January-February-March (JFM) and July-August-September (JAS) are shown, including mixed layer depth (meters), σ_t seasonal isopleths (kg m^{-3}, Levitus *et al.*, 1994), and normalized wind speed (Da Silva *et al.*, 1994). The wind vectors were averaged from the original 0.5x0.5° to 3.0x3.0° for clarity. Note the deep (250 meter) winter mixed layer depths at Stations 9 and 10, the winter outcropping of thermocline isopycnals at the northern sites, and the predominant winter westerlies at Station 1.

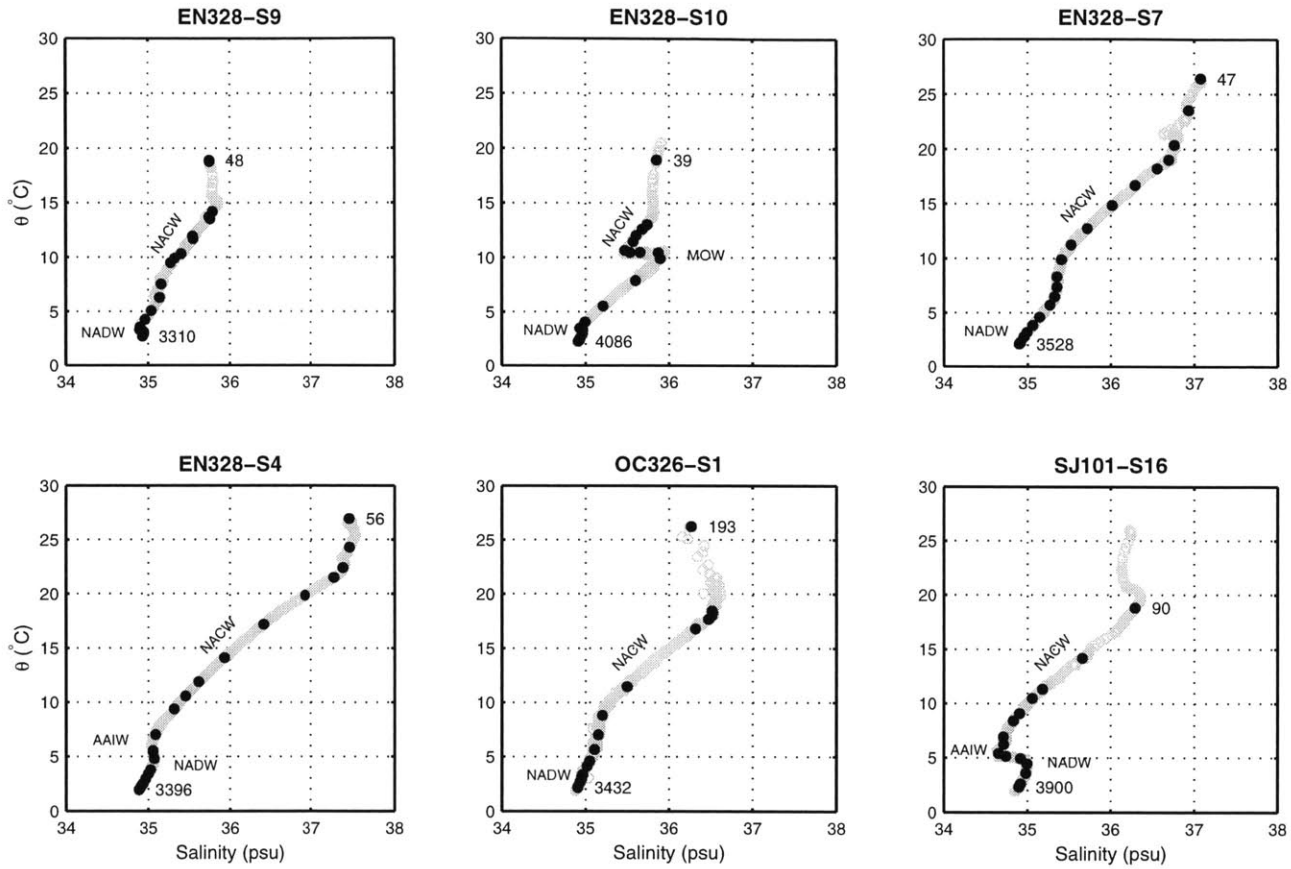

Figure 4-4: θ-S diagrams, including the continuous CTD results (gray) and the associated discrete MITESS samples (black). Minimum and maximum depths are also given for each station. Acronyms include Mediterranean Outflow Water (MOW), North Atlantic Central Water (NACW), Antarctic Intermediate Water (AAIW), and North Atlantic Deep Water (NADW). These results show the discrete MITESS samples adequately sample several key North Atlantic water masses.

interval, reflecting near-synoptic conditions within each deep water mass. For discussion the isotopic profiles are divided into three components: the surface layer (0 to 200 meters), the thermocline and intermediate water (200 to 2000 meters), and the deep water (2000 to 4000 meters) component.

Table 4.2: North Atlantic lead isotope results, 1998 to 2001. Here the results for each station are provided (see Table 4.1), including water column depth (meters), potential temperature (°C), salinity (psu), σ_θ (kg m^{-3}), and the two lead isotope ratios. Analytical standard deviation (2σ) represents the internal statistics for 30, ten second integrations.

St.	**Dep.**	θ	**Sal.**	σ_θ	**206/207**	2σ	**208/207**	2σ
1	1	26.235	36.266	23.943	1.1732	0.0010	2.4435	0.0030
1	193	18.300	36.523	26.399	1.1756	0.0010	2.4429	0.0032
1	294	18.021	36.516	26.468	1.1782	0.0016	2.4438	0.0041
1	391	17.676	36.472	26.523	1.1800	0.0023	2.4445	0.0059
1	487	16.814	36.317	26.616	1.1830	0.0016	2.4482	0.0039
1	791	11.472	35.500	27.122	1.1901	0.0021	2.4498	0.0052
1	913	8.803	35.203	27.351	1.1884	0.0016	2.4504	0.0043
1	1057	7.030	35.154	27.576	1.1857	0.0016	2.4500	0.0043
1	1236	5.659	35.106	27.719	1.1843	0.0015	2.4509	0.0040
1	1490	4.620	35.052	27.799	1.1844	0.0019	2.4509	0.0048
1	1741	4.147	35.016	27.824	1.1843	0.0011	2.4507	0.0032
1	2231	3.396	34.966	27.863	1.1831	0.0011	2.4507	0.0030
1	2461	3.192	34.958	27.877	1.1829	0.0013	2.4508	0.0038
1	2692	2.946	34.947	27.893	1.1836	0.0014	2.4518	0.0039
1	2964	2.627	34.931	27.910	1.1850	0.0014	2.4533	0.0037
1	3432	2.168	34.905	27.930	1.1867	0.0019	2.4549	0.0053
4	56	24.292	37.463	25.450	1.1793	0.0010	2.4469	0.0040
4	102	22.404	37.386	25.949	1.1795	0.0014	2.4478	0.0035
4	151	21.510	37.276	26.121	1.1784	0.0023	2.4456	0.0062
4	201	19.852	36.923	26.305	1.1812	0.0021	2.4461	0.0055
4	296	17.198	36.412	26.589	1.1847	0.0021	2.4460	0.0049
4	438	14.096	35.931	26.927	1.1881	0.0026	2.4484	0.0071
4	584	11.889	35.618	27.131	1.1880	0.0020	2.4481	0.0060
4	664	10.563	35.456	27.249	1.1872	0.0028	2.4478	0.0069
4	957	7.009	35.087	27.525	1.1847	0.0017	2.4485	0.0041
4	1222	5.556	35.057	27.693	1.1852	0.0011	2.4527	0.0032
4	1473	4.812	35.071	27.794	1.1872	0.0031	2.4582	0.0119
4	1886	3.774	35.027	27.872	1.1859	0.0029	2.4581	0.0078
4	2117	3.409	35.000	27.888	1.1873	0.0046	2.4614	0.0139
4	2442	2.929	34.965	27.907	1.1881	0.0054	2.4617	0.0139
4	2848	2.569	34.938	27.919	1.1899	0.0052	2.4599	0.0122

Data continued on next page

Table 4.2: *Data continued from previous page*

St.	Dep.	θ	Sal.	σ_θ	**206/207**	2σ	**208/207**	2σ
4	3396	2.241	34.911	27.928	1.1910	0.0077	2.4654	0.0177
7	47	23.523	36.932	25.276	1.1783	0.0019	2.4452	0.0029
7	98	20.337	36.763	26.048	1.1783	0.0024	2.4458	0.0035
7	98	20.337	36.763	26.048	1.1783	0.0023	2.4445	0.0034
7	197	18.186	36.558	26.454	1.1829	0.0030	2.4455	0.0026
7	295	16.676	36.294	26.623	1.1842	0.0023	2.4471	0.0034
7	436	14.879	36.018	26.825	1.1866	0.0023	2.4483	0.0036
7	586	12.734	35.716	27.043	1.1888	0.0018	2.4493	0.0033
7	680	11.259	35.520	27.175	1.1865	0.0019	2.4468	0.0036
7	782	9.903	35.405	27.326	1.1867	0.0014	2.4478	0.0028
7	937	8.310	35.351	27.543	1.1846	0.0015	2.4492	0.0028
7	1078	7.381	35.348	27.680	1.1831	0.0009	2.4500	0.0019
7	1261	6.498	35.322	27.784	1.1821	0.0008	2.4507	0.0014
7	1458	5.725	35.264	27.839	1.1812	0.0015	2.4505	0.0021
7	1745	4.606	35.142	27.875	1.1806	0.0012	2.4501	0.0017
7	2038	3.857	35.060	27.892	1.1803	0.0013	2.4506	0.0022
7	2337	3.198	34.990	27.901	1.1808	0.0017	2.4518	0.0024
7	3528	2.261	34.912	27.929	1.1812	0.0020	2.4532	0.0032
9	48	18.756	35.750	25.685	1.1825	0.0013	2.4481	0.0038
9	146	13.690	35.743	26.857	1.1834	0.0013	2.4469	0.0036
9	195	13.511	35.757	26.906	1.1839	0.0015	2.4465	0.0043
9	291	12.676	35.640	26.987	1.1871	0.0012	2.4485	0.0035
9	392	11.909	35.545	27.066	1.1870	0.0009	2.4482	0.0024
9	446	11.697	35.550	27.111	1.1863	0.0010	2.4482	0.0032
9	641	9.872	35.325	27.266	1.1843	0.0012	2.4484	0.0035
9	660	9.474	35.276	27.295	1.1842	0.0017	2.4482	0.0043
9	841	7.508	35.156	27.507	1.1861	0.0013	2.4506	0.0038
9	1005	6.281	35.140	27.665	1.1854	0.0014	2.4510	0.0042
9	1189	5.068	35.038	27.735	1.1851	0.0022	2.4514	0.0053
9	1353	4.264	34.961	27.764	1.1839	0.0014	2.4504	0.0041
9	1732	3.571	34.899	27.788	1.1834	0.0020	2.4489	0.0053
9	2061	3.333	34.896	27.812	1.1827	0.0014	2.4482	0.0039
9	2321	3.282	34.922	27.839	1.1822	0.0013	2.4490	0.0038
9	2840	2.944	34.943	27.891	1.1835	0.0012	2.4507	0.0036
9	3310	2.727	34.929	27.903	1.1831	0.0020	2.4520	0.0049
10	39	18.929	35.855	25.721	1.1797	0.0019	2.4438	0.0052
10	147	13.025	35.740	26.991	1.1794	0.0024	2.4438	0.0064
10	197	12.589	35.684	27.037	1.1808	0.0023	2.4443	0.0063
10	294	12.014	35.612	27.095	1.1830	0.0030	2.4468	0.0070
10	441	11.464	35.575	27.174	1.1811	0.0023	2.4458	0.0062
10	588	10.641	35.474	27.248	1.1830	0.0023	2.4466	0.0063
10	688	10.464	35.536	27.331	1.1814	0.0018	2.4458	0.0054
10	780	10.459	35.655	27.426	1.1821	0.0019	2.4462	0.0058
10	931	10.430	35.873	27.605	1.1804	0.0014	2.4483	0.0044
10	1078	9.901	35.898	27.719	1.1800	0.0015	2.4479	0.0045
10	1272	7.886	35.602	27.811	1.1814	0.0009	2.4487	0.0029

Data continued on next page

Table 4.2: *Data continued from previous page*

St.	Dep.	θ	Sal.	σ_θ	206/207	2σ	208/207	2σ
10	1440	5.519	35.211	27.822	1.1813	0.0008	2.4471	0.0023
10	1680	4.043	34.995	27.817	1.1814	0.0015	2.4465	0.0040
10	1906	3.494	34.935	27.826	1.1819	0.0012	2.4477	0.0032
10	2215	3.348	34.963	27.865	1.1796	0.0013	2.4467	0.0037
10	2518	2.983	34.961	27.899	1.1788	0.0017	2.4455	0.0045
10	3050	2.517	34.935	27.923	1.1792	0.0020	2.4467	0.0056
10	3350	2.355	34.922	27.928	1.1811	0.0057	2.4531	0.0165
10	3604	2.281	34.915	27.931	1.1811	0.0050	2.4508	0.0110
10	4086	2.176	34.905	27.934	1.1815	0.0053	2.4522	0.0127
16	90	18.823	36.295	26.087	1.1718	0.0028	2.4432	0.0075
16	130	14.177	35.659	26.689	1.1653	0.0024	2.4408	0.0059
16	165	11.330	35.182	26.886	1.1741	0.0016	2.4443	0.0046
16	200	10.484	35.055	26.941	1.1734	0.0053	2.4425	0.0147
16	375	9.087	34.903	27.060	1.1720	0.0051	2.4416	0.0136
16	450	8.402	34.833	27.114	1.1729	0.0030	2.4429	0.0076
16	625	6.929	34.713	27.236	1.1770	0.0029	2.4453	0.0082
16	725	6.230	34.714	27.331	1.1768	0.0020	2.4453	0.0055
16	850	5.404	34.653	27.386	1.1751	0.0024	2.4466	0.0066
16	1050	5.145	34.744	27.491	1.1766	0.0022	2.4485	0.0060
16	1250	4.937	34.915	27.653	1.1813	0.0034	2.4509	0.0083
16	1500	4.433	34.993	27.773	1.1828	0.0032	2.4512	0.0085
16	2000	3.571	34.977	27.853	1.1895	0.0023	2.4529	0.0063
16	3250	2.611	34.918	27.903	1.1842	0.0034	2.4544	0.0086
16	3900	2.314	34.896	27.915	1.1863	0.0030	2.4559	0.0075

Table 4.3: Lead concentration results, eastern and western North Atlantic. Lead concentrations (in pmol kg^{-1}), potential temperature (°C), and salinity (psu) for the four stations are included, with station numbers following Figure 4-2. The parenthetical depths (m) correspond to the shallowest CTD measurement at each station, assigning this approximation to z=0.

St.	Dep.	[Pb]	θ	Sal.	σ_θ	St.	Dep.	[Pb]	θ	Sal.	σ_θ
7	0 (3)	42.5	26.411	37.075	24.497	9	0 (4)	50.3	18.890	35.748	25.648
7	47	38.8	23.523	36.932	25.276	9	48	39.0	18.756	35.750	25.685
7	98	33.2	20.337	36.763	26.048	9	100	45.6	14.187	35.791	26.787
7	148	42.2	19.002	36.699	26.353	9	146	45.9	13.690	35.743	26.857
7	197	41.3	18.186	36.558	26.454	9	195	50.7	13.511	35.757	26.906
7	295	46.4	16.676	36.294	26.623	9	392	57.7	11.909	35.545	27.066
7	436	56.8	14.879	36.018	26.825	9	446	56.3	11.697	35.550	27.111

Data continued on next page

Table 4.3: *Data continued from previous page*

St.	Dep.	[Pb]	θ	Sal.	σ_θ	St.	Dep.	[Pb]	θ	Sal.	σ_θ
7	586	58.3	12.734	35.716	27.043	9	616	69.2	10.304	35.406	27.255
7	680	68.1	11.259	35.520	27.175	9	641	78.9	9.872	35.325	27.266
7	782	82.4	9.903	35.405	27.326	9	660	82.3	9.474	35.276	27.295
7	937	75.9	8.310	35.351	27.543	9	841	65.4	7.508	35.156	27.507
7	1078	73.8	7.381	35.348	27.680	9	1005	61.9	6.281	35.140	27.665
7	1261	62.6	6.498	35.322	27.784	9	1189	66.6	5.068	35.038	27.735
7	1458	65.1	5.725	35.264	27.839	9	1353	65.3	4.264	34.961	27.764
7	1745	49.7	4.606	35.142	27.875	9	1732	62.0	3.571	34.899	27.788
7	2038	43.9	3.856	35.060	27.892	9	2061	52.2	3.333	34.896	27.812
7	2337	36.1	3.198	34.990	27.901	9	2321	45.8	3.282	34.922	27.839
7	2681	15.9	2.797	34.956	27.913	9	2702	32.2	3.076	34.944	27.879
7	3528	27.6	2.261	34.912	27.929	9	2817	38.5	2.962	34.943	27.889
4	0 (3)	28.8	26.946	37.459	24.616	9	2840	25.6	2.944	34.943	27.891
4	56	35.0	24.292	37.463	25.450	9	3310	16.3	2.727	34.929	27.903
4	102	34.9	22.404	37.386	25.949	1	0 (7)	33.2	26.235	36.266	23.943
4	151	39.4	21.510	37.276	26.121	1	152	47.5	18.435	36.517	26.358
4	201	38.5	19.852	36.923	26.305	1	193	36.1	18.300	36.523	26.399
4	296	48.4	17.198	36.412	26.589	1	294	37.5	18.021	36.516	26.468
4	438	64.9	14.096	35.931	26.927	1	391	43.4	17.676	36.472	26.523
4	584	89.4	11.889	35.618	27.131	1	487	42.7	16.814	36.317	26.616
4	664	94.4	10.563	35.456	27.249	1	791	61.8	11.472	35.500	27.122
4	765	84.6	9.375	35.315	27.344	1	913	59.6	8.803	35.203	27.351
4	957	49.5	7.009	35.087	27.525	1	1057	61.6	7.030	35.154	27.576
4	1222	41.7	5.556	35.057	27.693	1	1236	73.7	5.659	35.106	27.719
4	1244	36.2	5.443	35.058	27.707	1	1490	57.3	4.620	35.052	27.799
4	1473	25.4	4.812	35.071	27.794	1	1741	64.3	4.147	35.016	27.824
4	1886	24.4	3.774	35.027	27.872	1	2231	57.7	3.396	34.966	27.863
4	2117	18.8	3.409	35.000	27.888	1	2461	40.3	3.192	34.958	27.877
4	2442	13.1	2.929	34.965	27.907	1	2692	35.5	2.946	34.947	27.893
4	2848	17.7	2.569	34.938	27.919	1	2964	32.6	2.627	34.931	27.910
4	3396	14.1	2.241	34.911	27.928	1	3432	25.7	2.168	34.905	27.930

4.3.1 Surface Ocean Variability

The isotopic composition of the North Atlantic surface ocean was first considered (Figure 4-7)[2]. As shown in Figure 4-1, significant $^{206}Pb/^{207}Pb$ variability (1.166 to 1.197) results from the distinct isotopic composition of North American and European anthropogenic sources, (*e.g.*, Chow and Earl, 1970; Chow *et al.*, 1975; Sturges and Barrie, 1987; Grousset *et al.*, 1994; Bollhöfer and Rosman, 2001), their atmospheric transport to the subtropical-tropical

[2]To maximize the number of observations, samples below the mean annual mixed layer depth were also included, calculating the 0 to 200 meter average for each station.

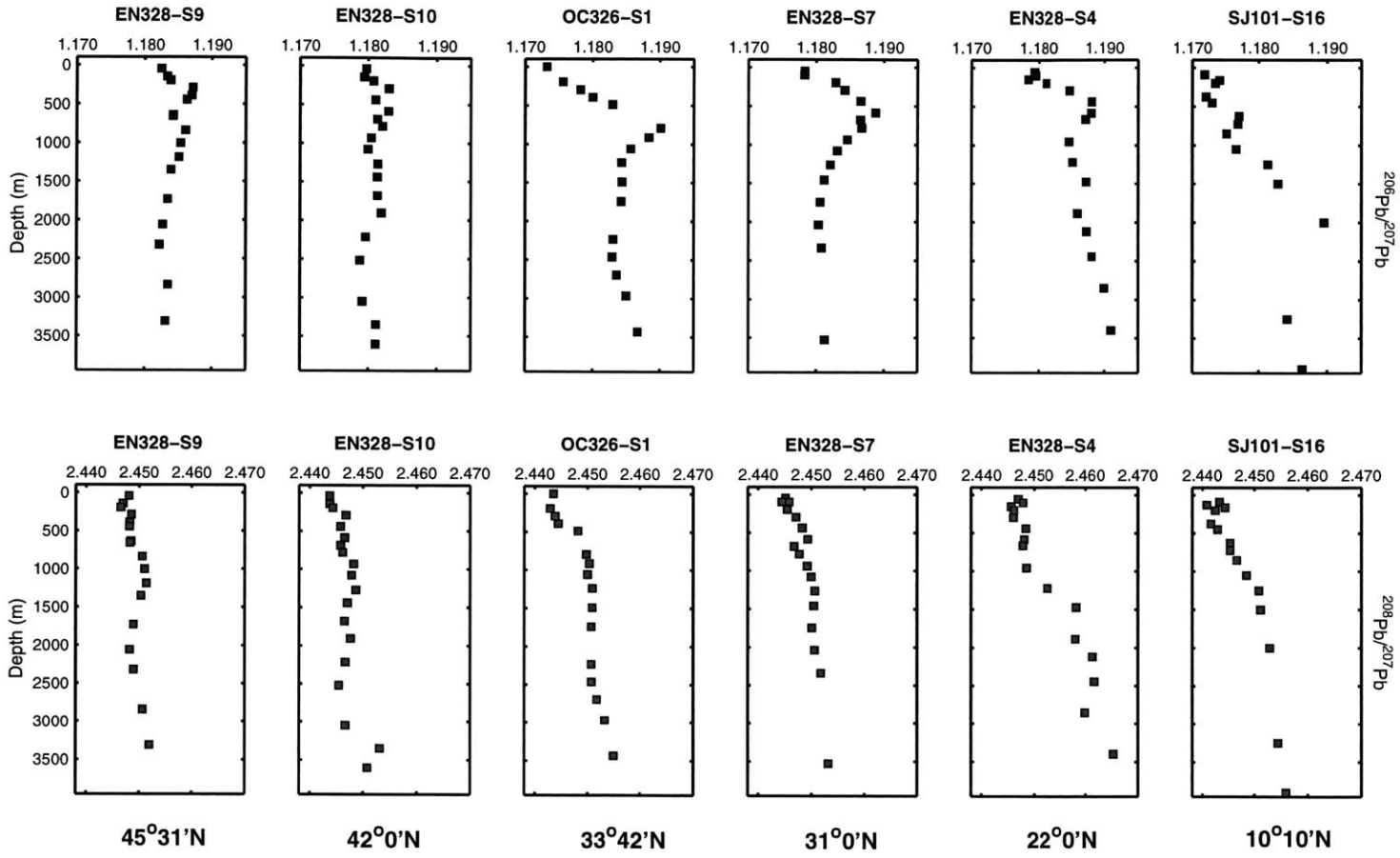

Figure 4-5: Lead isotope profiles for the eastern and western North Atlantic (1998 to 2001). The upper panels show the $^{206}Pb/^{207}Pb$ ratio versus depth, and the lower panels reflect the $^{208}Pb/^{207}Pb$ ratios. The panels are oriented with respect to latitude, ranging from 45°31'N (Station 9) to 10°10'N (Station 16).

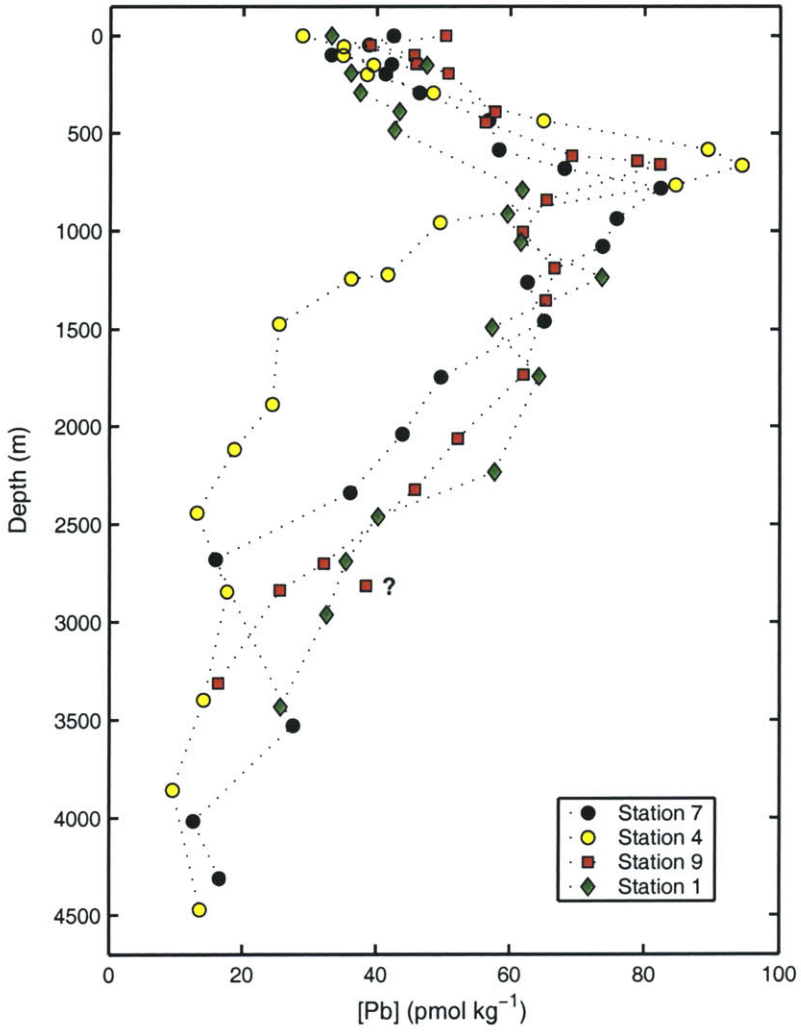

Figure 4-6: Lead concentration profiles for the eastern and western North Atlantic, 1998 to 2001. Four concentrations profiles are shown, including the western North Atlantic Station 1 and eastern North Atlantic Stations 4, 7, and 9. Note the reduced lead concentrations at Station 4 below 1000 meters.

gyres (Hamelin *et al.*, 1989; Church *et al.*, 1990; Véron *et al.*, 1993), and the short mixed layer residence time due to particle scavenging (*ca.* 2 years). These observations raise two questions. First, to what extent has the isotopic composition of the North Atlantic varied from 1987-1989 to 1998-2001? Second, how does the present isotopic variability reflect

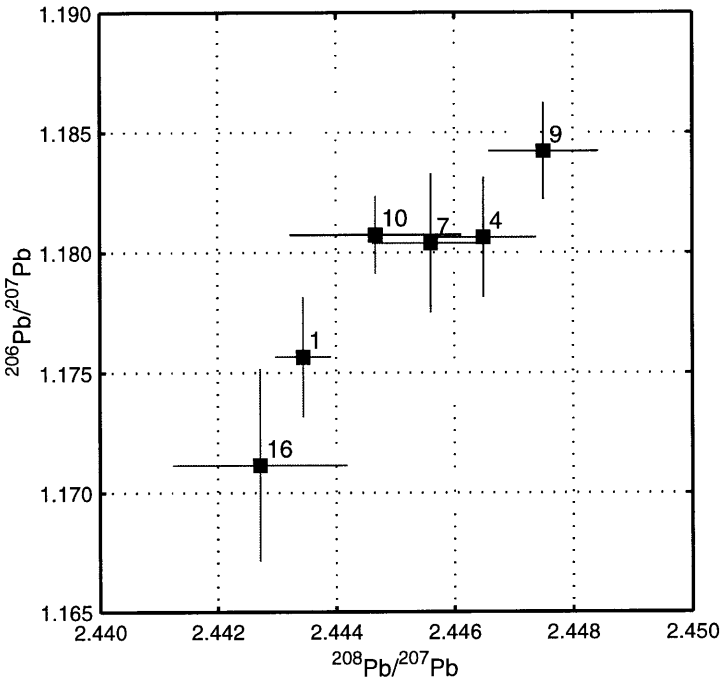

Figure 4-7: North Atlantic surface ocean lead isotope results. The $^{206}Pb/^{207}Pb$ and $^{208}Pb/^{207}Pb$ observations for each station are shown, including the upper 200 meters. The large apparent uncertainty might reflect the isotopic seasonality observed by Shen and Boyle (1988b) in the western North Atlantic. Error bars are $\pm 2\sigma$ of the sample populations, and please see Figure 4-2 for the corresponding station numbers.

atmospheric lead deposition or the subtropical gyre circulation?

The upper ocean results suggest an apparent shift in both the mean subtropical isotopic composition and its North Atlantic distribution. The mean $^{206}Pb/^{207}Pb$ ratio (1.181) is less than the 1987-1989 composite from 22 to 45°N (1.188), supporting a shift in lead provenance discussed in Chapter 3. The least radiogenic isotopic ratios are observed at the equatorial Station 16 (1.171±0.004) and western North Atlantic Station 1 (1.176±0.003). Eastern North Atlantic Stations 4, 10, and 7 are consistently more radiogenic, with a mean $^{206}Pb/^{207}Pb$ ratio of 1.181. The northern Station 9 contains the most radiogenic surface ocean composition (1.184±0.002). These observations do not agree with the general distribution shown in Figure 4-1, where the most radiogenic, North American signatures are

observed in the western North Atlantic. Instead, isotopic ratios characteristic of European-North African sources are now observed in this region.

What is the cause of this isotopic shift? North American sources do not provide an adequate explanation: Bollhöfer and Rosman (2001) observed a flux-weighted aerosol $^{206}Pb/^{207}Pb$ ratio of 1.206±0.005 from the United States and Canada (1994 to 1998, n=9), significantly above the western North Atlantic Station 1 observation (1.176±0.003). A possible explanation is the changing relative contributions of North American and European lead, best shown by the western North Atlantic reconstruction in Chapter 3. The 1998 Station 1 observation (1.176±0.003) equals the 1997-1999 Station S, Bermuda mean (1.176±0.003), suggesting these results are directly comparable. The time series and upper ocean observations are positively correlated (r=0.95, Figure 4-8), suggesting binary mixing between North America and European-North African sources explain the recent temporal and spatial variability in the eastern and western North Atlantic.

Two observations suggest binary mixing cannot explain all of the surface ocean observations. First, the slope and intercept of the North Atlantic observations do not agree with the best end-member estimates calculated in Chapter 3 (Bollhöfer and Rosman, 2001). This suggests either these estimates do not reflect recent European-North African contributions to the North Atlantic or a third anthropogenic source must be considered. Note that low $^{206}Pb/^{207}Pb$-high $^{208}Pb/^{207}Pb$ ratios were observed in eastern and western Europe by Bollhöfer and Rosman (2001), and the resulting European end-member was weighted by low $^{208}Pb/^{207}Pb$ observations in France. A European source cannot be strictly eliminated on this basis, favoring the former interpretation. Second, Véron *et al.* (1994) observed diminished $^{208}Pb/^{207}Pb$ near the European continental shelf relative to our mixed layer observations. This suggests other high-resolution features should be expected from multiple anthropogenic sources, similar to the isotopically-heterogeneous upwelling filaments observed by Flegal *et al.* (1989) within the California current system.

If binary mixing is assumed, why are non-radiogenic isotopic ratios observed in the subtropical western North Atlantic, closest to the radiogenic North American source (Figure 4-3)? Seasonal sampling bias cannot explain this result considering the equal Station S 1997-1999 mean and the Station 1 result (see above). Given the radiogenic composition

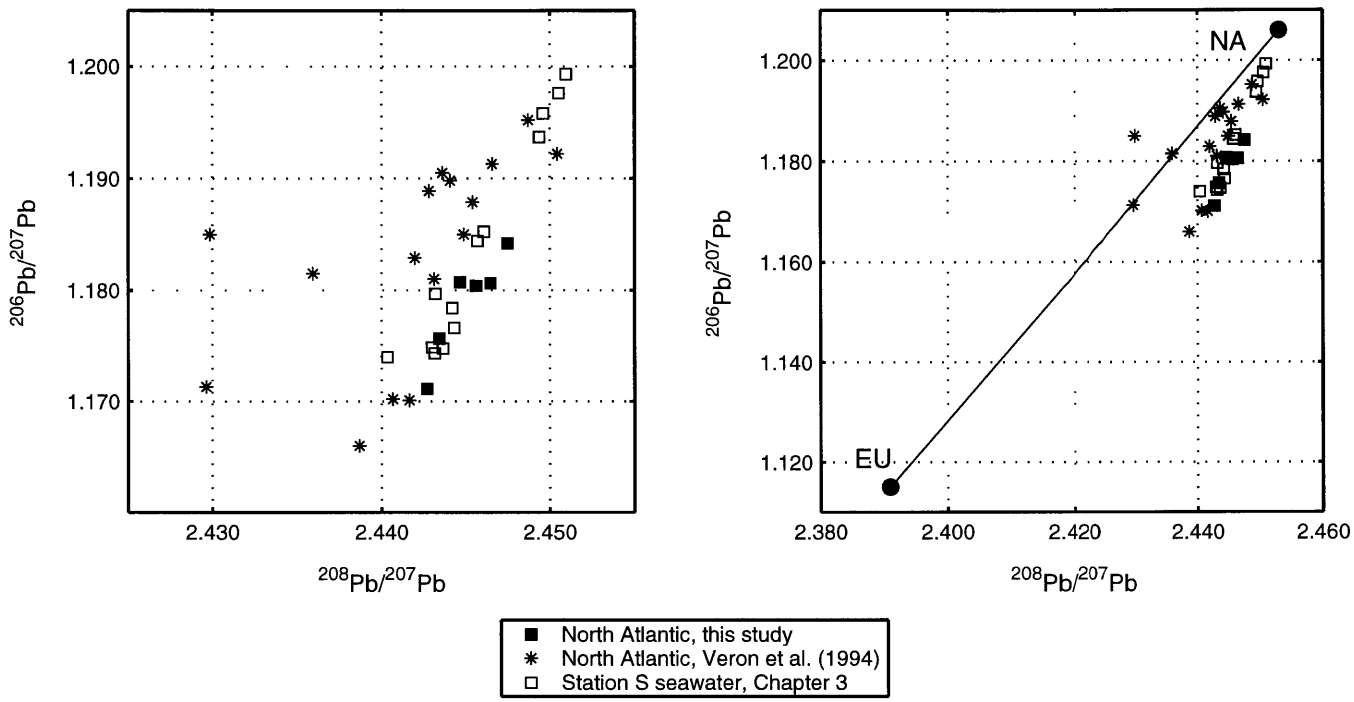

Figure 4-8: North Atlantic surface ocean lead isotope comparison. The left panel shows the results of Véron *et al.* (1994), a western North Atlantic seawater time series (Chapter 3), and this study. The right panel compares these results with the North American (NA) and European (EU) end-member estimates calculated from Bollhöfer and Rosman (2001). Note the offset to lower $^{208}Pb/^{207}Pb$ ratios along the mixing line relative to the observations.

of North American aerosols and the upper thermocline, this isotopic anomaly requires a southern source, either easterly trade wind fluxes or a Caribbean source advected to the subtropical gyre. The non-radiogenic signal is then replaced by westerly radiogenic lead deposited within the eastern subtropical gyre, an expected consequence of radiogenic North American precipitation and aerosols (*e.g.*, Simonetti *et al.*, 2000; Bollhöfer and Rosman, 2001).

This hypothesis requires basin-scale advection of an equatorial signal within the western boundary current. From a decadal (1990 to 1999) compilation of drogued satellite-tracked drifters, Fratantoni (2001) measured current speeds from 15 to >30 cm s^{-1} in the western boundary current. If one assumes a conservative mean current speed of 15 cm s^{-1} and the generalized path described in Appendix I (7500 km), 1.6 years is required to advect eastern Caribbean lead to the western North Atlantic, less than the estimated mixed layer residence time (*ca.* 2 yr.). This estimate will increase by including the current retroflections in the Colombian Basin and the Gulf of Mexico (2.7 yr.) or diminish by assuming a higher mean current speed. This approximation demonstrates, however, that advection of equatorial, non-radiogenic lead (see Hamelin *et al.*, 1989) might potentially affect the isotopic composition of the western North Atlantic.

4.3.2 Thermocline Variability

The isotopic composition of the North Atlantic thermocline reflects the time-dependent composition of the surface mixed layer (Shen and Boyle, 1987, 1988b; Sherrell *et al.*, 1992; Véron *et al.*, 1993, 1998), its lateral advection and mixing along isopycnal surfaces (Shen and Boyle, 1988b), and its heterogeneous atmospheric deposition (Hamelin *et al.*, 1989; Church *et al.*, 1990). As discussed in Chapter 3, the mixed layer isotopic transient from 1968 to 1990 and increasing thermocline ventilation rates with depth (Jenkins, 1980) result in a thermocline $^{206}Pb/^{207}Pb$ maximum in the western North Atlantic. The isotopic maximum is observed at the mid-latitude Stations 1, 4, and 7 in the western and eastern North Atlantic. At 45°N, the isotopic maximum is diminished due to possible advection of non-radiogenic lead, consistent with greater winter mixed layer depths, thermocline ventilation, and proximity to the European continent. The anthropogenic origin of the Station 9 isotopic profile

is corroborated by the concentration maximum shown in Figure 4-6; the vertical isotopic profile cannot be interpreted as a dilution effect. South of the tropical-subtropical boundary at Station 16, the thermocline transient is also absent, resulting from the prevailing southeasterly Guiana current receiving northeasterly anthropogenic lead fluxes.

To evalulate the mid-latitude transient, the elemental and isotopic data were compared via σ_θ diagrams, shown in Figures 4-9 and 4-10. These results demonstrate a consistent isotopic transient to approximately σ_θ=27. Eastern North Atlantic Stations 4 and 7 are well-correlated above the 27.5 isopycnal (r=0.98), suggesting similar atmospheric input and ventilation. Differences between the eastern (4,7) and western (1) basins likely reflect the separate isotopic boundary conditions. Below σ_θ=27, the Station 1 results are more radiogenic than Stations 4 and 7, consistent with the radiogenic North American fluxes to the western North Atlantic shown in Figure 4-1. Above σ_θ=27, the reduced $^{206}Pb/^{207}Pb$ ratios at Station 1 reflect the recent advection of equatorial lead to this site (see above). Comparison between the elemental and isotopic distribution in Figure 4-10 also shows consistently deeper penetration of the elemental signal at Stations 4 and 7, possibly resulting from the ten-year lag of the isotopic transient observed in the western North Atlantic proxy record (see Chapter 3). The isotopic and elemental boundary conditions are independent, resulting in distinct water column profiles.

Finally, Mediterranean Outflow Water (MOW) exhibits an unique isotopic signature, although its expected $^{206}Pb/^{207}Pb$ composition from aerosol observations (*e.g.*, 1.118 to 1.156, Maring *et al.*, 1987) is diminished by mixing with the radiogenic transient. To separate the two components, the $^{206}Pb/^{207}Pb$ and $^{208}Pb/^{207}Pb$ ratios from σ_θ=27.29 to 27.82 were compared between Stations 9 and 10. The mean ratios are significantly less radiogenic at Station 10 ($^{206}Pb/^{207}Pb$=1.181±0.002, $^{208}Pb/^{207}Pb$=2.447±0.002, n=6) relative to Station 9 ($^{206}Pb/^{207}Pb$=1.184±0.002, $^{208}Pb/^{207}Pb$=2.450±0.003, n=7), although the difference is slight. MOW does not exhibit a large non-radiogenic signal at this site despite the established anthropogenic lead inputs to this region.

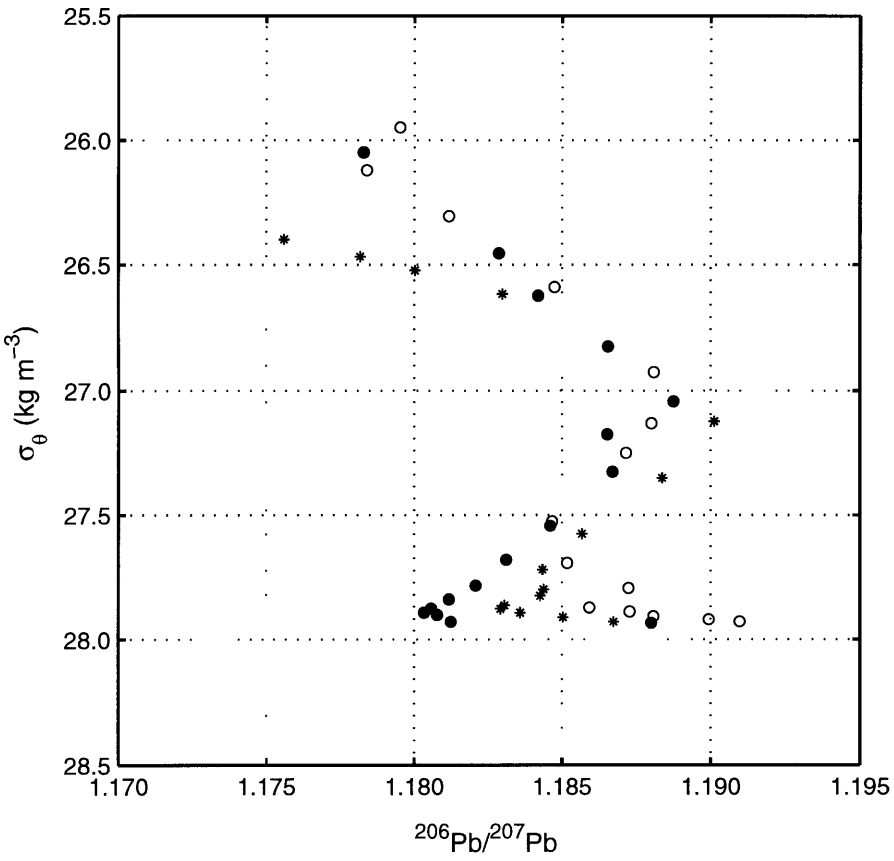

Figure 4-9: σ_θ–^{206}Pb/^{207}Pb plot, eastern and western subtropical North Atlantic. The mid-latitude stations are shown for comparison, including the western Station 1 ($*$) and the eastern Stations 4 ($\circ$), and 7 ($\bullet$). All σ_θ values were calculated according to Gill (1982, Appendix 3). Note the agreement between Stations 4 and 7 above σ_θ=27, whereas Station 1 exhibits distinct offsets from the eastern North Atlantic.

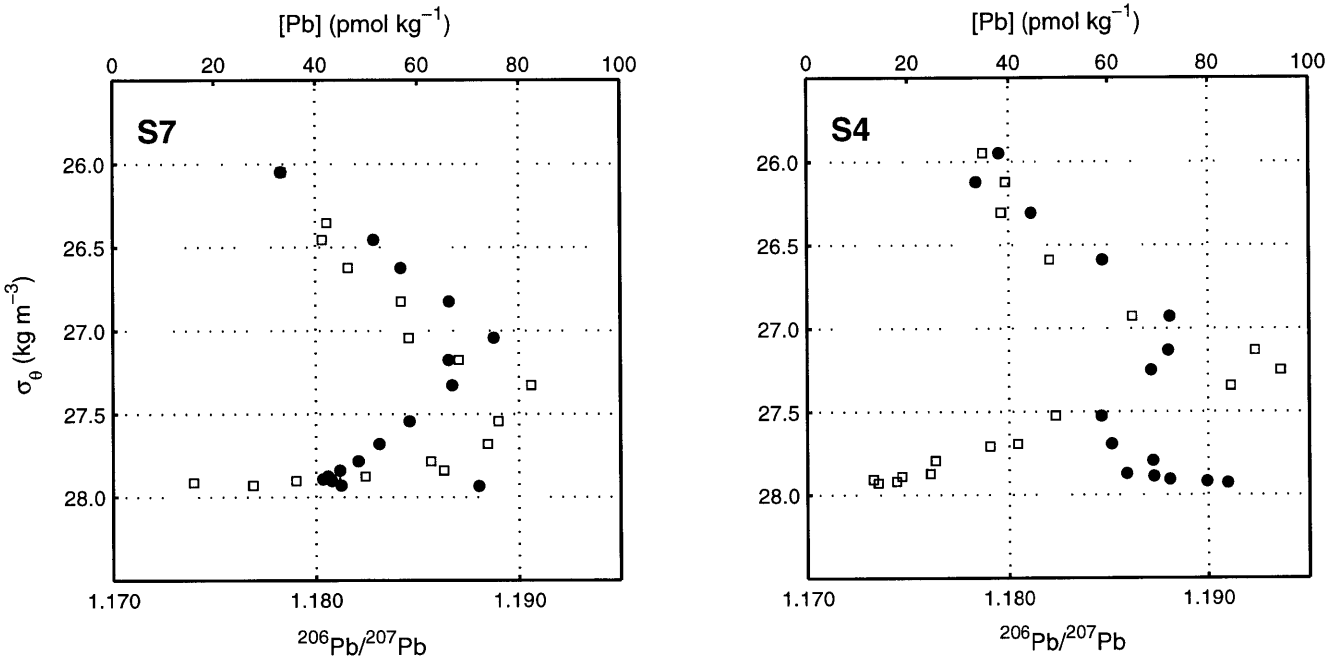

Figure 4-10: Thermocline elemental and stable isotope comparison, Stations 7 and 4. The two panels reflect the $^{206}Pb/^{207}Pb$ (•) and [Pb] (□) results versus σ_θ for Stations 7 (left) and 4 (right). Note the deeper elemental maxima at both stations and the contrasting density distribution between the two sites.

4.3.3 Deep Water Variability

Given significant Northern Hemisphere anthropogenic lead production for the past two millenia (*ca.* 10^8 kg yr^{-1} at 2000 ^{14}C yr. BP, Settle and Patterson, 1980, and refs. therein) and North Atlantic deep water ventilation ages from $\Delta^{14}C$ observations and models (105 to 490 years, Broecker *et al.*, 1988; England and Rahmstorf, 1999), a corresponding anthropogenic isotopic signal has been observed in the deep North Atlantic (Shen and Boyle, 1987; Alleman *et al.*, 1999; Véron *et al.*, 1999). To test these results, the hydrographic observations were averaged between 2000 and 4000 meters, maximizing the number of observations while excluding Antarctic Intermediate Water (see Bainbridge, 1987). Simple averaging introduces uncertainty due to hydrographic variability, but these uncertainties are less than the observed difference.

The deep water results, shown in Figure 4-11, were first compared to the 'natural background' isotopic estimates, the western North Atlantic surface coral record, and previous deep water observations. The expected departure from the Chow and Patterson (1962) North Atlantic pelagic background estimates was observed[3], supporting anthropogenic contributions to North Atlantic Deep Water suggested by Alleman *et al.* (1999). Quantifying the exact contribution is difficult given the variable, time-dependent composition of anthropogenic lead and the uncertain Holocene pre-anthropogenic estimate, but a significant deep water $^{208}Pb/^{207}Pb$ departure is evident.

Comparison between the western North Atlantic coral proxy record and seawater isotopic ratios represents a novel chronometric technique. The lead isotope chronology is based on the surface coral record, utilizing radiocarbon analysis and the annual coral density bands. A requirement of this method is general agreement between the proxy and seawater observations, and this consistency is shown in Figure 4-11. Best agreement with the deep water observations is observed from 1947 to 1968. This interpretation should not be overstated: a single site from the western subtropical gyre cannot account for all the expected deep isotopic variability. For example, the Station 4 deep water result falls between the two surface

[3]The Chow and Patterson (1962) estimate represents the mean of multiple pelagic sediment and manganese nodule analyses from the western and eastern North Atlantic. The exact chronology of these results is uncertain.

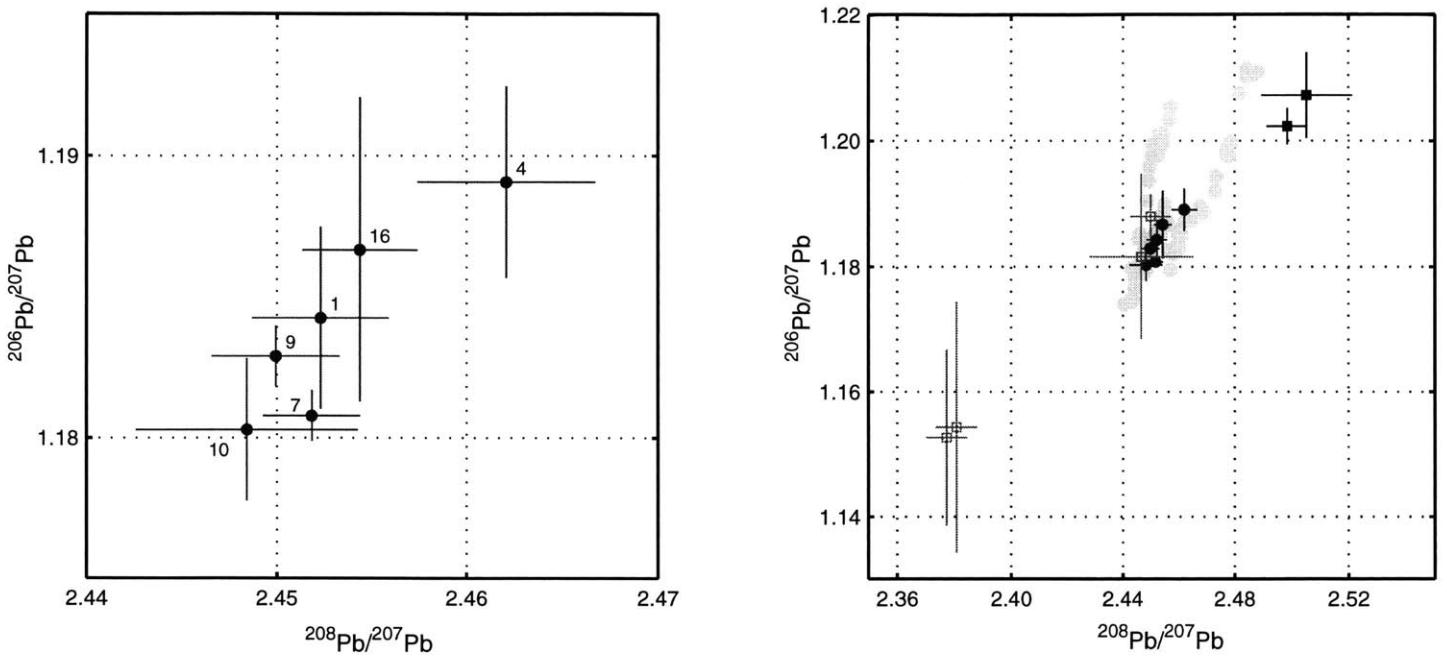

Figure 4-11: North Atlantic deep water isotopic variability. The left panel includes the 2000 to 4000 meter analyses for the six profiles, including the station numbers following Figure 4-2. The right panel includes the profile results (•), the North Atlantic pelagic background estimates from Chow and Patterson (1962, regions F and G, ■), and the Alleman *et al.* (1999) North Atlantic results from the same depth interval (□). The gray circles correspond to the western North Atlantic isotopic reconstruction described in Chapter 3, and error bars are $\pm 2\sigma$ of the sample populations.

coral mixing lines, implying either age or source mixing. The first $^{206}Pb/^{207}Pb$ reduction in 1898 suggests this technique might better constrain centennial-scale deep water variability relative to the other transient tracers.

The deep water results show the 1998 to 2001 $^{206}Pb/^{207}Pb$ ratios are constrained between 1.180 and 1.189 at these sites, a smaller range than previously observed. Direct comparison is possible between Station 16 (10°10'N 45°0'W, 1.187) and the IOC III-6 site (8°0'N 45°0'W, 1.154) of Alleman *et al.* (1999). This offset is significant, and this discrepancy cannot be reconciled with limited results from two laboratories. Three observations favor the higher number: (1) the isotopic range of the North Atlantic proxy record shown in Chapter 3, 1.174 to 1.211; (2) consistent isotopic ratios among deep water dominated by NADW, 1.180 to 1.189; and (3) the expected ventilation of low $^{206}Pb/^{207}Pb$ anthropogenic lead into a high $^{206}Pb/^{207}Pb$ deep water background inferred from the Chow and Patterson (1962) results. Laboratory intercalibrations and additional deep water observations will best resolve this discrepancy.

The linear deep water trend warrants consideration. An isotopic gradient is observed between the northern (7, 9, and 10) and southern (4, 16) stations, consistent with increasing ventilation ages to the south and east of the Deep Western Boundary Undercurrent (*e.g.*, Broecker *et al.*, 1988). The large isotopic difference between Stations 4 and 7 was unexpected, however, given comparable $\Delta^{14}C$ observations at the nearby TTO-TAS Stations 73 (-112±11‰) and 80 (-110±22‰, Östlund and Grall, 1987). Contamination artifacts cannot explain this observation given the convergence of multiple elemental profiles shown in Figure 4-6. This isotopic boundary, however, is supported by a corresponding concentration reduction, with diminished lead concentrations between Stations 7 (30.9 pmol kg^{-1}) and 4 (14.6 pmol kg^{-1}) from 2000 to 4000 meters[4]. Quasi-conservative advection of the anthropogenic lead transient provides one possible explanation for the deep elemental and isotopic boundary.

To what extent can the deep water isotopic variability be attributed to particulate

[4]The elemental and isotopic differences between these stations are not well-explained by **sampling** contamination. Contamination sources from a US vessel or laboratory ($^{206}Pb/^{207}Pb \approx 1.21$) would result in a positive bias for both the isotopic ratio and lead concentration; the opposite is observed between Stations 4 and 7.

scavenging and regeneration, the primary lead removal mechanism? Comparison between the mixed layer and deep water variability suggests the scavenging-regeneration cycle is not the dominant mechanism for North Atlantic deep water variability. In Figure 4-1, a mixed layer $^{206}Pb/^{207}Pb$ reduction is observed between 31 and 22°N, whereas deep water $^{206}Pb/^{207}Pb$ increases across the tropical-subtropical boundary. Conservative advection of the lead transient is supported by the 'continuum' box model results of Boyle *et al.* (1986), observing reasonable agreement between thermocline lead concentration profiles and purely advective model experiments. To test this assumption, isotopic mass balance observations between the particulate and dissolved phases are required within multiple isopycnal surfaces.

Finally, the deep isotopic boundary is compared to equivalent CFC-12 observations from the Doney and Bullister (1992) eastern North Atlantic section (Figure 4-12). The $^{206}Pb/^{207}Pb$ deep water isotopic boundary relative to [CFC-12] might reflect their respective historical inputs. From the western North Atlantic surface coral record (see Chapter 3), the first inferred $^{206}Pb/^{207}Pb$ reduction occurred in 1898, whereas the initial reconstructed increase in atmospheric [CFC-12] occurred in 1937 (Doney and Bullister, 1992). Southern displacement of the isotopic boundary relative to [CFC-12] might reflect the forty-year time difference between the anthropogenic transients. These initial results require additional targeted observations in this region, but they suggest an significant isotopic transition between 22 and 31°N within the eastern North Atlantic.

4.4 Conclusions

The lead isotopic composition of the North Atlantic surface ocean, thermocline, and deep water demonstrates the importance of atmospheric input and hydrography on its modern North Atlantic isotopic distribution. Three conclusions are obtained from these observations:

1. The 1998-2001 surface ocean differs from previous North Atlantic observations, resulting from the changing source contributions of anthropogenic lead. An isotopic gradient is observed between the western and eastern North Atlantic, possibly resulting from the advection of equatorial, non-radiogenic lead. The observed surface ocean

$^{206}Pb/^{207}Pb$ range for these six stations and time interval is 1%.

2. A persistent lead isotope transient is observed in the mid-latitude North Atlantic thermocline, centered on the σ_θ=27 isopycnal. To the north the advection and scavenging of recent, non-radiogenic lead and Mediterranean Outflow Water diminishes the thermocline isotopic transient. The equatorial station also exhibits no comparable thermocline signal due to the prevailing northeasterly trades and southeasterly Guiana Current.

3. The North Atlantic deep water exhibits a clear anthropogenic signature consistent with western North Atlantic proxy records. Significant isotopic and elemental gradients are observed between 22 and 31°N in the 1999 eastern North Atlantic, with a mean apparent deep water 'lead age' of 40 years. Finally, the deep water isotopic range among these six North Atlantic sites (1.180 to 1.189 for $^{206}Pb/^{207}Pb$) is much smaller than previously observed.

These observations represent an initial reconnaissance regarding the North Atlantic stable lead isotope distribution, and additional water column observations and non-steady state models are required to verify these hypotheses. Most importantly, these preliminary results support the potential utility of lead isotopes to quantify time-dependent elemental sources and pathways in the world oceans.

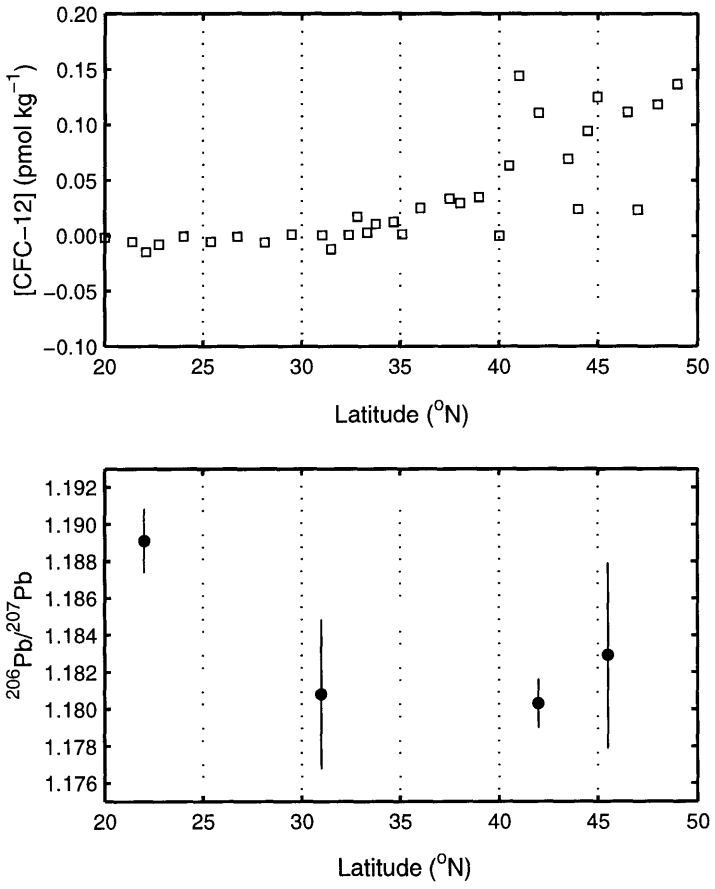

Figure 4-12: CFC-12 and lead isotope comparison, eastern North Atlantic. The CFC-12 concentrations (in pmol kg^{-1}) reflect the 2000 to 4000 meter average for an equivalent comparison, taken from the Doney and Bullister (1992) Oceanus-202 section. The $^{206}Pb/^{207}Pb$ results are from Stations 4, 7, 9, and 10, and error bars reflect $\pm 2\sigma$. Note the large isotopic gradient between the southern stations relative to the CFC-12 variability.

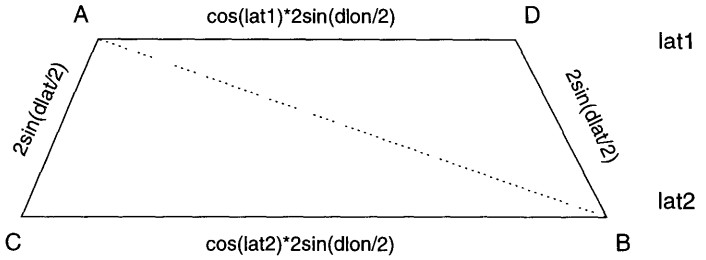

Figure 4-13: Spherical distances between two points on a planar trapezoid. The upper parallel reflects lat1, and the lower parallel equals lat2. The final result $\overline{AB}$ is simply determined by the Pythagorean theorem. Please see the text for discussion.

4.5 Appendix I

The haversine formula[5] is a simple method for calculating spherical distances, and it represent an approximation (valid to *ca.* 1%) given the equatorial bulge of the geoid. The radius of a spherical Earth, R, is generally assumed from the SI definition of 'nautical mile', equal to 1.852 km arc minute^{-1}. This definition results in R=6357 km. A brief derivation is provided, and more detailed description is provided by Sinnott (1984).

The first step is determining the chord length between two points on a sphere ($\overline{AB}$). The length $\overline{AB}$ within the unit circle equals $2sin(\theta/2)$, where θ denotes angle AOB from center O. Along the equator of a sphere, chord length can be simply calculated from the longitude difference ($dlon$), equal to $2sin(dlon/2)$. Similarly, the chord length between two points along a meridian can be determined from the latitude difference ($dlat$), equal to $2sin(dlat/2)$. With increasing latitude, the parallel chord length equals $2sin(dlon/2) \cdot cos(lat)$ (as $lat \rightarrow 90°, cos(lat) \rightarrow 0$). On a sphere, the distance between two points can be determined from a planar, isoceles trapezoid (Figure 4-13). Following the Pythagorean theorem, the chord distance $\overline{AB}$ can be calculated ($AB^2 = AC^2 + CB \cdot AD$), and the resulting straight-line distance simply equals:

$$AB^2 = 4 \cdot [sin^2(dlat/2) + cos(lat1) \cdot cos(lat2) \cdot sin^2(dlon/2)] \tag{4.1}$$

[5]This calculation was provided by R. Pawlowicz, checked and modified with the derivation shown here.

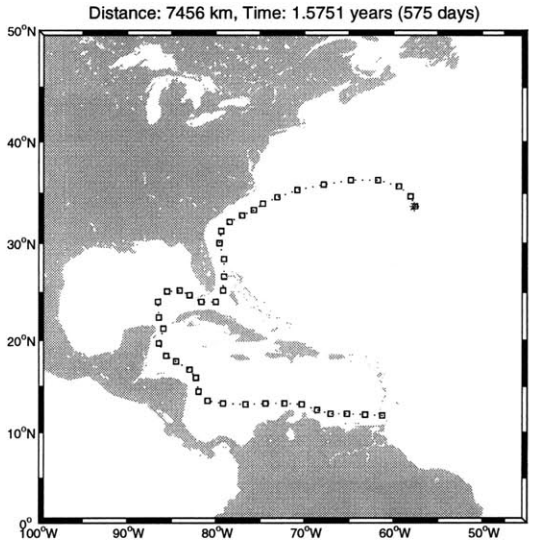

Figure 4-14: Particle trajectory approximation, western North Atlantic Station 1. The trajectory follows the western boundary current delineated by Fratantoni (2001). Station 1 is shown as the end point of the calculation.

This result provides the chord length between two points on the sphere.

The second step is determining the angle (θ) between points A, B, and the center of the sphere ($\theta = AOB$). To determine θ, the previous result is rewritten as the square of half $\overline{AB}$:

$$a = (AB/2)^2 = sin^2(dlat/2) + cos(lat1) \cdot cos(lat2) \cdot sin^2(dlon/2) \tag{4.2}$$

If half the chord length ($\overline{AB}$) is known within a unit circle, $tan(\theta/2) = (\sqrt{a}/\sqrt{1-a})$, and therefore $\theta = 2 \cdot arctan(\sqrt{a}/\sqrt{1-a})$. The great circle distance is then calculated by $d = R \cdot \theta$, where R reflects the assumed radius of a spherical Earth. This simple calculation was then used to graphically determine cumulative distances from a base map, and the trajectory used in this study is shown in Figure 4-14.

Chapter 5

Centennial-Scale Tropical Upwelling Variability Inferred from Coralline Trace Element Proxies

The tropical North Atlantic exhibits significant interdecadal climate variability as determined by historical climate records, paleoclimate proxy data, and coupled ocean-atmosphere general circulation models (*e.g.*, Folland *et al.*, 1986; Hastenrath, 1990; Servain, 1991; Peterson *et al.*, 1991; Chang *et al.*, 1997). The timing and magnitude of its Holocene variability have been addressed by multiple sedimentary proxies from the anoxic Cariaco Basin (Peterson *et al.*, 1991; Hughen *et al.*, 1996b; Black *et al.*, 1999; Haug *et al.*, 2001, and refs. therein). The inferred variability from the sedimentary records can be tested by high-resolution surface coral records, providing an annually-resolved, multi-decadal comparison. Despite several established geochemical proxies (see reviews by Dunbar and Cole, 1993; Druffel, 1997; Gagan *et al.*, 2000) and surveyed reef sites in this region, limited surface coral observations presently exist (Cole *et al.*, 1993). This study presents surface coral trace element records from the Cariaco Basin upwelling zone, demonstrating trace element variability consistent with historical climate records and providing possible evidence for a centennial-scale reduction in tropical upwelling.

5.1 Introduction

The Cariaco Basin is an important tropical paleoclimate archive based its response to regional climate forcing and the annual accumulation of sedimentary couplets. Coastal upwelling in this region is determined by the position of the Intertropical Convergence Zone (ITCZ) and the associated North Atlantic wind stress anomalies. The rapid accumulation (>100 cm kyr^{-1}) of laminated sediments within an anoxic water column creates a high-resolution, annual-scale sedimentary record (*e.g.*, Richards and Vaccaro, 1956; Peterson *et al.*, 1991; Hughen *et al.*, 1996a). Geochemical and micropaleontological proxies have been developed from this sedimentary record, including planktonic $\Delta^{14}C$ (Hughen *et al.*, 1998, 2000), sedimentary gray scale records (Hughen *et al.*, 1996b), faunal abundance records (Peterson *et al.*, 1991; Black *et al.*, 1999), planktonic $\delta^{18}O$ (Lin *et al.*, 1997), and major element chemistry (Haug *et al.*, 2001). Of these results, the faunal abundance record of Black *et al.* (1999) resolves annual variability of the past century. Based on the abundance of the planktonic foraminifer *G. bulloides* with respect to sediment mass, the authors observed an anti-correlation (*ca.* r=-0.8) with North Atlantic sea surface temperature anomalies at approximately 50°N, 35°W. This result suggests a linear, coupled response between subtropical-subpolar sea surface temperatures, northeasterly trade wind intensity, and coastal upwelling. To address this hypothesis, this study has three objectives: (1) to demonstrate decadal- to centennial-scale surface coral trace element variability in the Cariaco Basin; (2) to correlate this variability with a unique geochemical process; and (3) to link this mechanism with tropical or extratropical forcing. The surface coral results from Isla Tortuga, Venezuela demonstrate the potential importance of centennial-scale variability in this region.

The utility of surface coral trace element proxies is supported by multiple calibration studies, and a brief synopsis is provided. First, Shen and Boyle (1987) and Lea *et al.* (1989) demonstrated Cd/Ca, Ba/Ca, and Pb/Ca variability consistent with anthropogenic emissions and equatorial Pacific SST variability, suggesting elemental ratios qualitatively reflect past surface ocean chemistry. Several additional trace elements, including manganese (Shen *et al.*, 1991, 1992b), uranium (Min *et al.*, 1995; Shen and Dunbar, 1995) and the rare earth elements (Sholkovitz and Shen, 1995), have also been calibrated for surface corals.

These calibrations are supported by surface coral Cd/Ca results and mean annual surface ocean phosphate estimates, observing positive correlation (r=0.83) among ten sites and eight coral species (see Chapter 1). Down-core trace element correlations are also observed on seasonal to centennial time scales (Shen *et al.*, 1992a; Delaney *et al.*, 1993).

Trace element variability in surface corals also includes significant kinetic artifacts to be considered when interpreting these records (see Section 5.3.1), similar to the growth rate dependence reported by de Villiers *et al.* (1994, 1995) for Sr/Ca ratios. One example of trace element kinetic artifacts is shown in Chapter 3, where systematic Pb/Ca offsets were observed within and among *Diploria* records. Trace element records cannot be completely interpreted without considering these possible kinetic effects, and a universal calibration cannot be applied to individual coral records.

Given this proxy system, what elemental variability is expected in the Cariaco Basin region, particularly for the trace elements cadmium and barium? Coastal upwelling represents one significant mechanism, resulting from upper ocean Ekman transport in boreal winter (see Section 5.2.2 for details). To evaluate the response of cadmium and barium to upwelling, the dissolved cadmium (Jacobs *et al.*, 1987) and barium (Falkner *et al.*, 1993) profiles must be considered (Figure 5-1). The greater cadmium concentration gradient (0.383 pM m^{-1}) relative to barium (0.007 nM m^{-1}) is evident within the upper 150 meters, resulting from the established shallower regeneration of labile phytodetritus (Boyle *et al.*, 1976, 1981) relative to biogenic barite (*e.g.*, Chan *et al.*, 1977; Dehairs *et al.*, 1980; Bishop, 1988). Assuming upwelling extends to the base of the seasonal pycnocline (*ca.* 150 meters, Müller-Karger *et al.*, 2001), a greater change in cadmium concentrations would be expected relative to barium. This response, however, is likely non-conservative and complex, including biological uptake of upwelled cadmium, the admixture of upper thermocline water with other surface water masses, and possible island effect upwelling near reef sites. The quantitative merit of the trace element proxies is limited by their unknown modern response within the Cariaco Basin and adjacent reef sites. A key assumption of this study is elevated mixed layer cadmium concentrations reflects intensified upwelling.

A second primary trace element source is regional fluvial inputs. The Orinoco River is the greatest expected input to this region, with greatest discharge in late boreal fall corre-

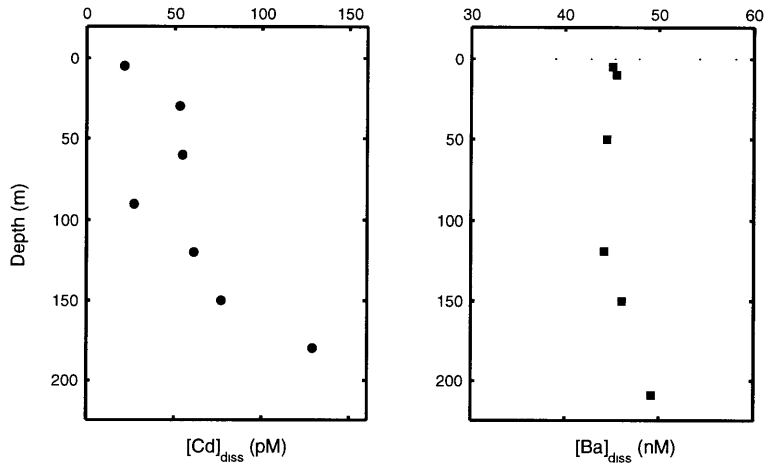

Figure 5-1: Dissolved cadmium and barium profiles from the Cariaco Basin: Jacobs *et al.* (1987) and Falkner *et al.* (1993), respectively. Between 5 and 150 meters, the linear concentration gradients are 0.383 pM m^{-1} for d[Cd]/dz and 0.007 nM m^{-1} for d[Ba]/dz. The greater cadmium concentration gradient supports its possible sensitivity to upwelling variability.

ponding to the precipitation maximum associated with the ITCZ. Seasonal fluvial inputs are best demonstrated by satellite ocean color observations, where Orinoco and Amazon River nutrient fluxes increase pigment and colored dissolved organic matter concentrations in areally-extensive plumes to the southern Caribbean (>3x10^5 km^2, Müller-Karger *et al.*, 1988; Müller-Karger, 1989; Hochman *et al.*, 1994). Given elevated cadmium and barium concentrations measured from the Orinoco and Changjiang Rivers (Cd≈700 pM, Ba≈225 nM, Edmond *et al.*, 1985) and their subsequent particulate desorption in estuaries, a fluvial input is hypothesized. Like upwelling variability, any resulting change in trace element concentrations is complex, dependent upon seawater dilution of the river plume, its advection into the Cariaco Basin, and possible biological removal.

5.2 Methods

The methods utilized for this study include several established techniques (Shen and Boyle, 1988a) updated for current quadrupole ICP-MS instrumentation. Complete details regarding the collection, sampling, and analysis of the coral cores are given in Appendix A. First,

the collection and analysis of the cores is described, followed by a brief discussion of the Cariaco Basin physiography, hydrography, and climatology.

5.2.1 Analytical Methodology

Surface coral cores were collected from two sites along the southern coast of Isla Tortuga, Venezuela, in 1996 and 1998 (Figure 5-3). Water depths ranged from approximately 2 to 3 meters, and characteristic sections of *Montastrea annularis* and *Siderastrea siderea* are shown in Figure 5-2. Following core collection and sectioning, the dissepiment[1] orientation was determined by X-radiography, measuring annual extension rates, growth axis position, and any section breaks. Chronologies were based on the annual density couplet common to these species (see Hudson *et al.*, 1976) and seasonal $\delta^{13}C$ cycles. Samples were collected along the primary growth axis with a diamond-coated steel wire (130.2x0.08 mm, Crystalite), and the coral slab only contacted polycarbonate surfaces during sampling. Coarse sampling resolution is required for adequate sample masses (*ca.* 250 mg), resulting in five to six samples per year for *M. annularis* and two samples per year for *S. siderea.* This coarse resolution will alias the seasonal cycle (Leder *et al.*, 1996; Quinn *et al.*, 1996), and new trace element sampling methods would be required for quantitative seasonal estimates. Prior to analysis, the surface corals were cleaned following a modified method of Shen and Boyle (1988a) described in Appendix A, including two primary cleaning sequences of both coarse aragonite fragments and a 280-700 μm size fraction.

The analytical methods used in this study include graphite furnace AAS (GFAAS) and isotope dilution ICP-MS (ID-ICP-MS), and all analyses were completed on homogenized splits of individual samples. First, cadmium concentrations were determined via GFAAS, preconcentrating cadmium from the $CaCO_3$ matrix with the Co-APDC coprecipitation method (Boyle and Edmond, 1975; Shen and Boyle, 1988a). The reaction was completed at pH 10.7 via distilled NH_3 additions, observing elevated and consistent recoveries (95.2±3.0, n=16) relative to pH 0.8 (77.3, n=4). This result likely reflects diminished H^+ competition for the APDC complex, consistent with the Zn^{2+} and Fe^{2+} observations of Boyle and

[1]Defined by Wells (1956) as the 'thin, curved, or tabular sheets in the spaces between septa or costae that support the lower surface...', corresponding to the laminated, planar unit of the colony 'stratigraphy'.

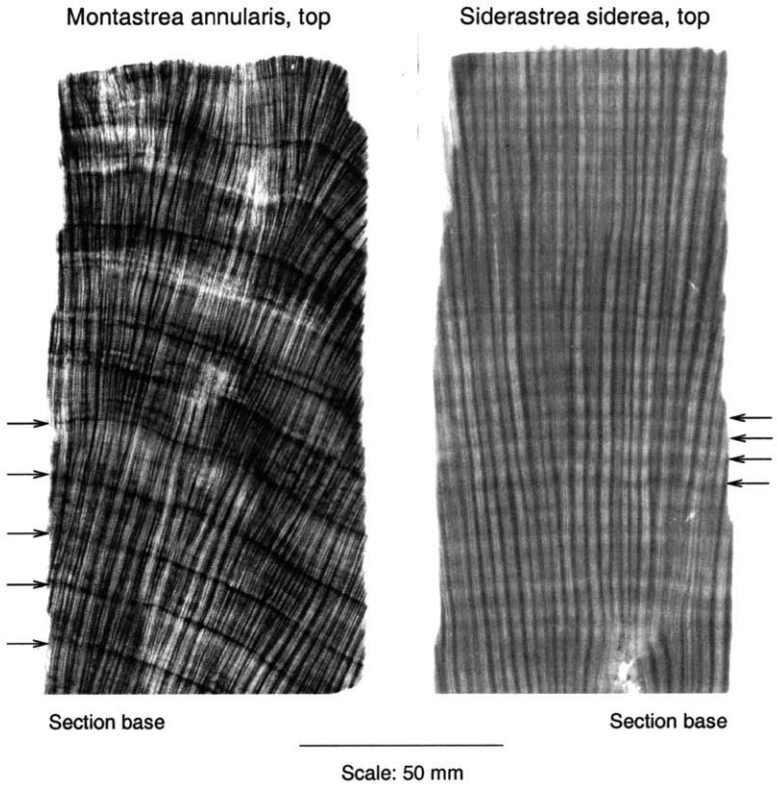

Figure 5-2: Surface coral X-radiograph positives, *M. annularis* (left) and *S. siderea* (right). Realistic sections are shown here, including typical variations in dissepiment orientation, micro-banding, and calix structure. The sections are vertically-oriented, and a 50 mm scale bar is shown. Arrows mark annual low-density bands, and the striped pattern of the dissepiments is most apparent for *M. annularis*. Note the annual extension rates between the two species and the faint horizontal dissepiments of *S. siderea* relative to the vertical calices.

Edmond (1975). Lead and barium concentrations were determined by ID-ICP-MS (VG PlasmaQuad 2^+), spiking sample solutions with well-characterized ^{135}Ba and ^{204}Pb spike standards (Klinkhammer and Chan, 1990; Wu and Boyle, 1997b). All spikes were continuously calibrated with gravimetric ICP-MS standards (J. T. Baker) prior to use. Standard corrections for instrumental backgrounds, isobaric interferences (^{204}Hg), and procedural blanks were utilized. Please see Appendix A for additional analytical details.

5.2.2 Cariaco Basin Hydrography

Before presenting the trace element results, the regional hydrography and climatology must be considered. The Cariaco Basin represents two extensional sub-basins bounded to the south by the South American continent and to the north by the Tortuga Bank (Richards and Vaccaro, 1956). The high-resolution (Smith and Sandwell, 1997) bathymetry is shown in Figure 5-3. The shallow Tortuga Bank is transected by the Canal Centinela to the northwest (116 meters) and the Canal de la Tortuga to the northeast (195 meters) (Müller-Karger *et al.*, 2001), restricting intermediate water flow above 200 meters. This bathymetry results in uniform temperature (16.9°C) and salinity (36.2‰) from 300 to 1390 meters (Richards and Vaccaro, 1956). Low intermediate water ventilation, high integrated primary production (540 to 690 gC m^{-2} yr^{-1}, Müller-Karger *et al.*, 2001), and subsequent organic matter degradation (Scranton *et al.*, 1987) creates the well-known water column anoxia.

The shallow mixed layer and upper thermocline of the Cariaco Basin are affected by boreal winter coastal upwelling (Figure 5-3) resulting from Ekman divergence forced by the northeasterly trade winds. South American coastal upwelling, the associated surface currents, and their temperature-salinity characteristics are complex (see Hernández-Guerra and Joyce, 2000, and refs. therein). This system includes two distinct upwelling centers near northern Venezuela and Colombia, westerly countercurrents south of Caribbean Current, and salinity minima associated with fall freshwater influxes from the Orinoco and Amazon Rivers (*ibid.*).

5.2.3 Tropical North Atlantic Climatology

The climate of the tropical North Atlantic is governed by the seasonal position of the Intertropical Convergence Zone (ITCZ, see Hastenrath and Lamb, 1977; Li and Philander, 1997). During late boreal winter (March to April), the ITCZ reaches its southernmost extreme, associated with SST and precipitation maxima in the tropical South Atlantic and a hemispheric SST gradient of -4 to -5°C (N-S domains, Curtis and Hastenrath, 1995). EOF analysis by Nobre and Shukla (1996) have demonstrated SST anomalies in this region are preceded by wind stress anomalies two months in advance, suggesting a SST response to the coupled interactions. In boreal summer, the ITCZ shifts to the north, reversing the SST

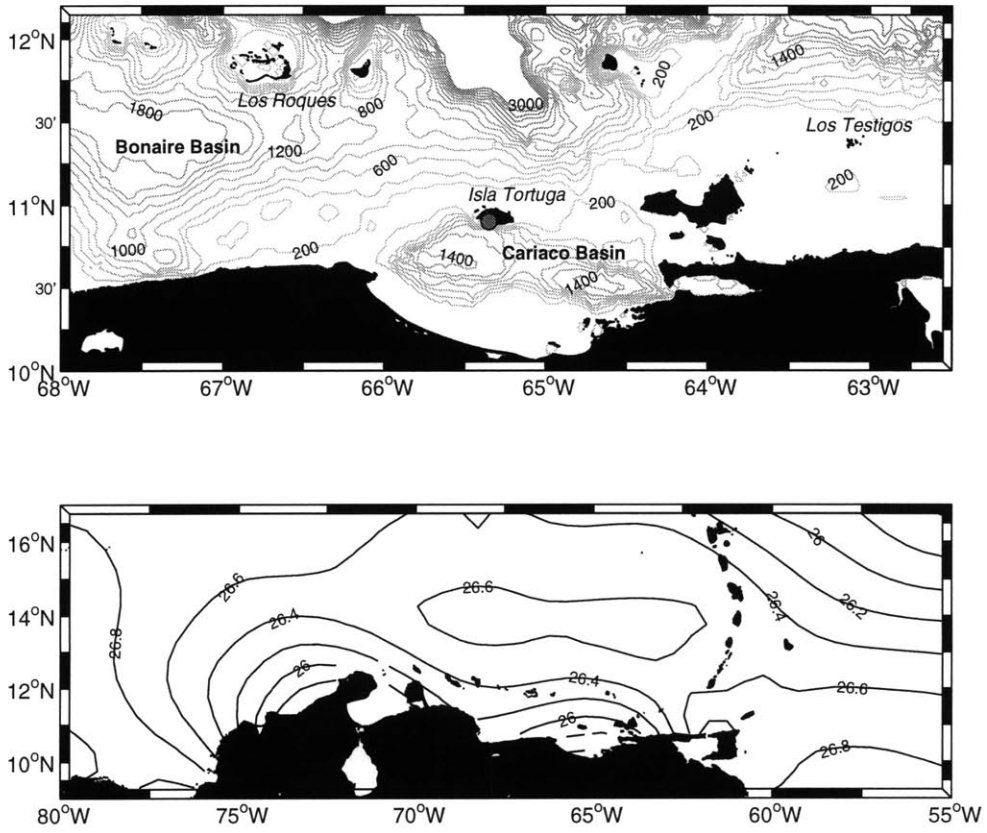

Figure 5-3: Cariaco Basin site location map and winter SST distribution. The upper panel shows the Isla Tortuga site location, regional bathymetry, and additional sampled coral reef sites. The bathymetry data are taken from the Smith and Sandwell (1997) two minute grid, using a 200 meter contour interval. The lower panel includes the mean January-February-March sea surface temperature distribution of the southern Caribbean. Note the reduced SSTs near the South American continent, including the two upwelling zones near Venezuela and Colombia. The SST data are taken from the Da Silva *et al.* (1994) 0.5x0.5° climatology, and a 0.2°C contour interval is utilized.

gradient, increasing tropical North Atlantic precipitation, and reducing the cross-equatorial wind velocities. The mean position and dynamics of the ITCZ are thus governed by coupled ocean-atmosphere variability (Philander, 1996), affecting SST distributions in the tropical Atlantic and precipitation variability in the African Sahel and Brazilian Nordeste (*e.g.*,

Folland *et al.*, 1986; Hastenrath and Greischar, 1993; Moura and Shukla, 1981; Nobre and Shukla, 1996).

Multiple climate forcing mechanisms have been developed to explain tropical North Atlantic variability. Coupled air-sea interactions are an important mechanism in this region, associated with a SST 'dipole' between the northern and southern tropical Atlantic (see Servain, 1991; Chang *et al.*, 1997). The persistence of this feature is currently debated (Houghton and Tourre, 1992; Chang *et al.*, 1997; Enfield and Mayer, 1997), however, northern and southern tropical Atlantic SSTs are significantly anti-correlated. For example, Carton *et al.* (1996) noted nine positive sea surface temperature anomaly (SSTA) events (>0.5°C) in the northeast tropical Atlantic correlated with five negative South Atlantic SSTA events. Chang *et al.* (1997) also observed a significant dipole SST pattern in the first leading mode of a joint (surface wind and SST) singular value decomposition analysis. Coupled equatorial interactions similar to the Pacific ENSO phenomena have been reported (Covey and Hastenrath, 1978; Zebiak, 1993; Carton and Huang, 1994), although its recurrence and magnitude are less than its Pacific counterpart. Finally, extra- and intra-tropical forcing, including NAO (Kawamura, 1994) and ENSO (Hameed *et al.*, 1993; Nobre and Shukla, 1996; Enfield and Mayer, 1997) coupling have been demonstrated, modulating the 'dipole' dynamics via atmospheric forcing.

5.3 Results and Discussion

The principal trace element records from Isla Tortuga, Venezuela are shown in Figure 5-4 and Table 5.1. The Cd/Ca and Ba/Ca data are also presented in Figure 5-5 as mean annual anomalies[2], and Figure 5-6 shows the annual amplitude of the elemental records. A two-fold Cd/Ca reduction is observed between 1920-1950 (3.48 nmol/mol) and 1950-1995 (1.73 nmol/mol), occurring between 1946 and 1952. The Ba/Ca ratio does not show a comparable transition across this interval, with the Ba/Ca standard deviation equal to 0.35 μmol/mol (2σ). The Cd/Ca reduction is synchronous with a decreased annual amplitude, whereas no comparable Ba/Ca modulation is observed. The difference between the Cd/Ca and Ba/Ca

[2]All anomalies in this study were calculated with respect to the entire record (1920-1995), given simply at time i as $X_i = X_i - \overline{X}_{1920-1995}$.

results and the modern hydrographic distribution supports a possible mid-century reduction in coastal upwelling.

5.3.1 Surface Coral Trace Element Artifacts

Before interpreting these results, the known artifacts influencing surface coral trace element ratios must be addressed. The first consideration is the coral cleaning technique, isolating seawater-derived trace elements associated with the aragonite lattice (Shen and Boyle, 1988a). One useful test is the signal-to-noise ratio, assuming contaminated replicates will not be equal. With a maximum Cd/Ca range of 5.07 nmol/mol and a mean replicate 2σ of 0.20 nmol/mol, the resulting S:N is 25, suggesting the observed signal is not a contamination artifact. The Pb/Ca record (Figure 5-8) supports this argument with no observed Pb/Ca transition and the established Pb/Ca response to sample contamination (Shen and Boyle, 1988a). The mean Cariaco Basin Cd/Ca ratio (2.37 nmol/mol) can also be compared with previous analyses from Bermuda (0.44 nmol/mol, Shen, 1986)[3] and the Galápagos (5.30 nmol/mol, Shen *et al.*, 1992a). Because these ratios are consistent with the mean annual mixed layer phosphate concentrations at each site (0.321, 0.088, and 0.608 μM, Conkright *et al.*, 1994), the mean Cariaco Basin Cd/Ca ratio is consistent with previous, independent trace element analyses.

Kinetic Artifacts

A second known artifact is kinetic trace element fractionation, best demonstrated by the Sr/Ca calibration of de Villiers *et al.* (1994, 1995). Reduced coral extension rates[4] (14 to 6 mm yr^{-1}) resulted in elevated Sr/Ca ratios (*ca.* 9.08 to 9.22 mmol/mol at 1980) for the species *Pavona clavus*. To address this issue for cadmium and barium, we have analyzed two coral species with different extension rates, ranging from 7 mm yr^{-1} for *Siderastrea siderea* to 13 mm yr^{-1} for *Montastrea annularis*. The results are shown in Figure 5-7,

[3]This estimate was determined from the 1867-1899 Cd/Ca mean to minimize potential anthropogenic cadmium contributions to North Rock, Bermuda. See Shen (1986) for details.

[4]Extension rate is used here as a proxy for coral growth rate, which includes extension and thickening of the coral calices (Barnes and Lough, 1993). An exact determination of growth rate (as g cm^{-2} yr^{-1}) requires density measurements.

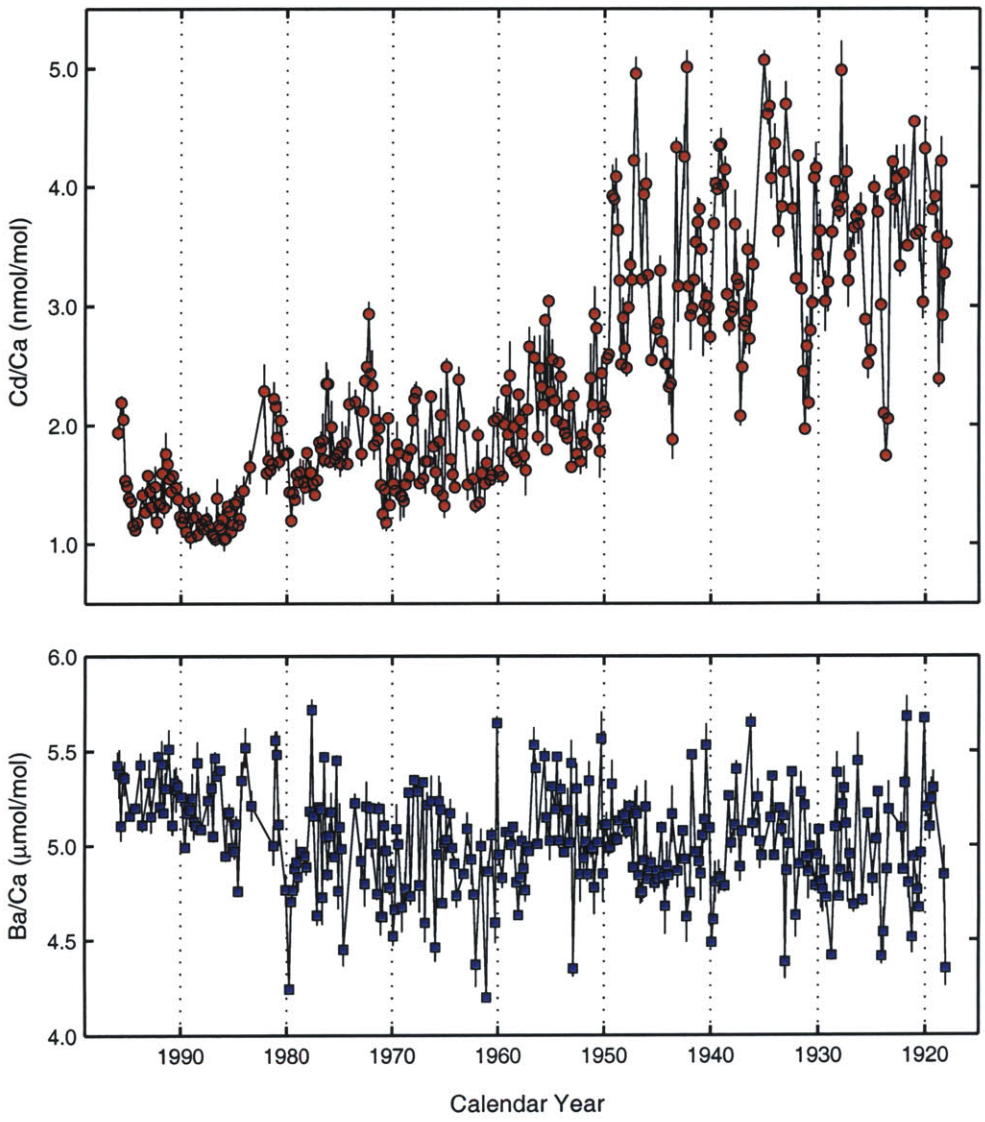

Figure 5-4: Isla Tortuga raw Cd/Ca and Ba/Ca records. These results reflect replicate analyses of a single *M. annularis* colony. The upper panel shows the replicate Cd/Ca ratios (nmol/mol), whereas the lower panel includes the Ba/Ca record (μmol/mol). Error bars are 2σ. Note the Cd/Ca transition at 1950 and no corresponding shift in Ba/Ca. A systematic increase in Ba/Ca is also observed at 1981.

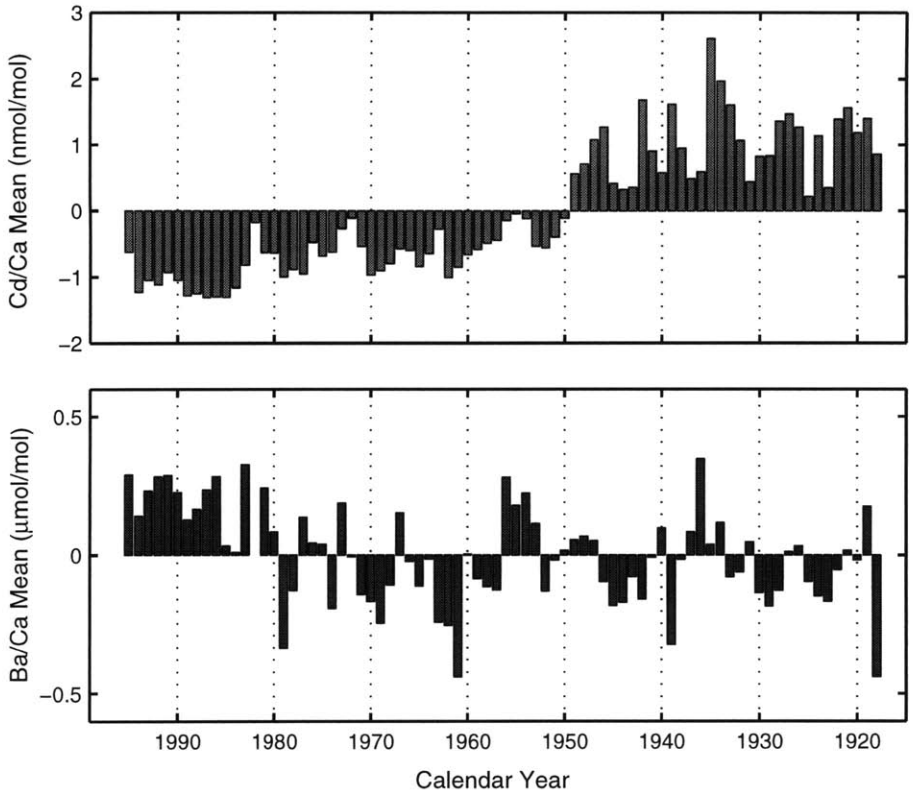

Figure 5-5: Isla Tortuga Cd/Ca and Ba/Ca annual mean anomalies. The anomalies are calculated with respect to the entire mean annual trace element records (1918-1996). Note the predominant Cd/Ca transition at 1950 and the diminished mean annual Ba/Ca variability.

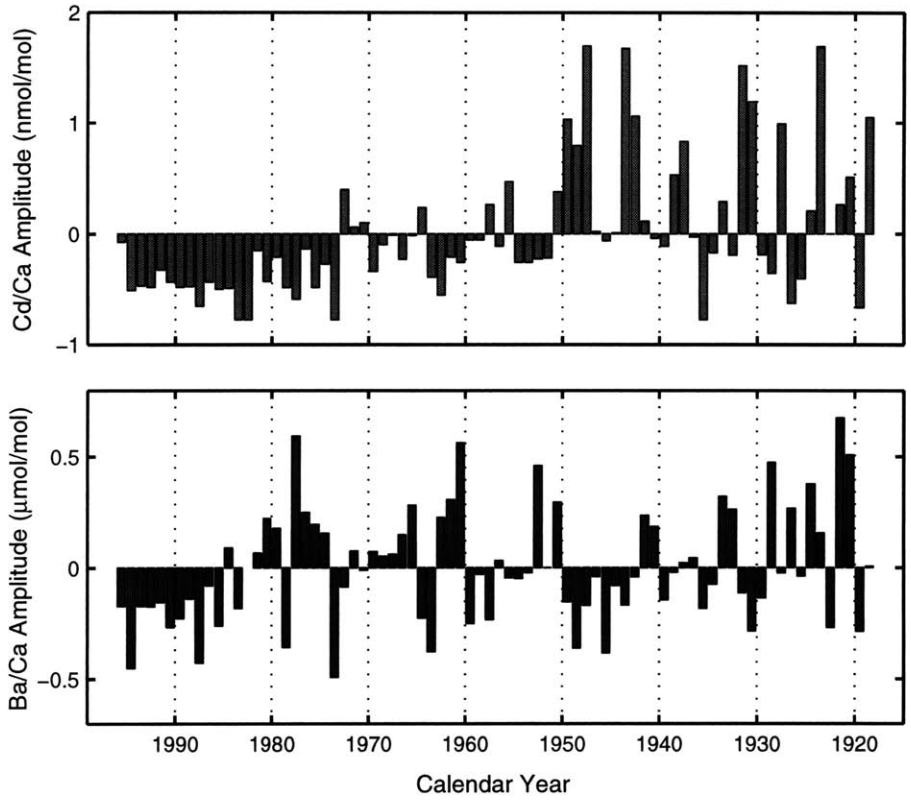

Figure 5-6: Isla Tortuga Cd/Ca (nmol/mol) and Ba/Ca (μmol/mol) annual amplitude anomalies. The amplitude anomalies are calculated following Figure 5-5. Note the dampened Cd/Ca amplitude after 1950 and no comparable shift in Ba/Ca.

observing consistently higher and variable trace element ratios for *S. siderea*. Interspecies differences for Ba/Ca (6.0 μmol/mol) and Cd/Ca (2.3 nmol/mol) are greater than or equal to the observed range from the Cariaco Basin.

The results shown in Figure 5-7 suggest kinetic artifacts will affect both the absolute elemental ratio and the relative variability. For example, the Ba/Ca range (1976-1994) is from 0.66 μmol/mol for *M. annularis* to 4.10 μmol/mol for *S. siderea*. Because the *S. siderea* colony was not located at the exact same site, some of the elemental differences might reflect local variability. High-resolution seawater cadmium and barium measurements at these reef sites, however, presently do not exist. Elemental contamination from the dense trabeculae of *S. siderea* might also contribute to the elevated noise observed in this record. To eliminate these uncertainties, the *M. annularis* record will be the focus of this study.

Can the Isla Tortuga Cd/Ca transition be explained by this significant kinetic artifact? Two observations oppose this hypothesis. First, no corresponding Ba/Ca reduction is observed as expected from the Cd/Ca and Ba/Ca kinetic effect (Figure 5-7). Second, no significant difference in extension rate was observed across this interval: the 1920-1950 (13.3$\pm$4.0 mm yr^{-1}) and 1950-1995 (13.3$\pm$4.3 mm yr^{-1}) averages are equal within the 95% confidence interval. Kinetic effects are significant determinants of surface coral trace element ratios, but they cannot completely explain the mid-century Cd/Ca reduction.

Anthropogenic Artifacts

Finally, anthropogenic cadmium influxes represent another possible artifact given possible emissions from metal smelting, chemical processing, or municipal wastes (*e.g.*, Nriagu, 1979b; Nriagu and Pacyna, 1988). This hypothesis is supported by known anthropogenic contributions to coastal northern Venezuela, including municipal and industrial wastes at reef sites (Weiss and Goddard, 1977) and elevated mollusc (Jaffé *et al.*, 1995) and sedimentary (Bastidas *et al.*, 1999) heavy metal concentrations near the Tuy, Tocuyo, and Aroa Rivers. To test this hypothesis, Pb/Ca ratios were measured from the *M. annularis* core, observing two significant Pb/Ca maxima at 1937 and 1968. The second maxima is correlated with a 1969 Pb/Ca maximum observed from the Galápagos (Shen and Boyle,

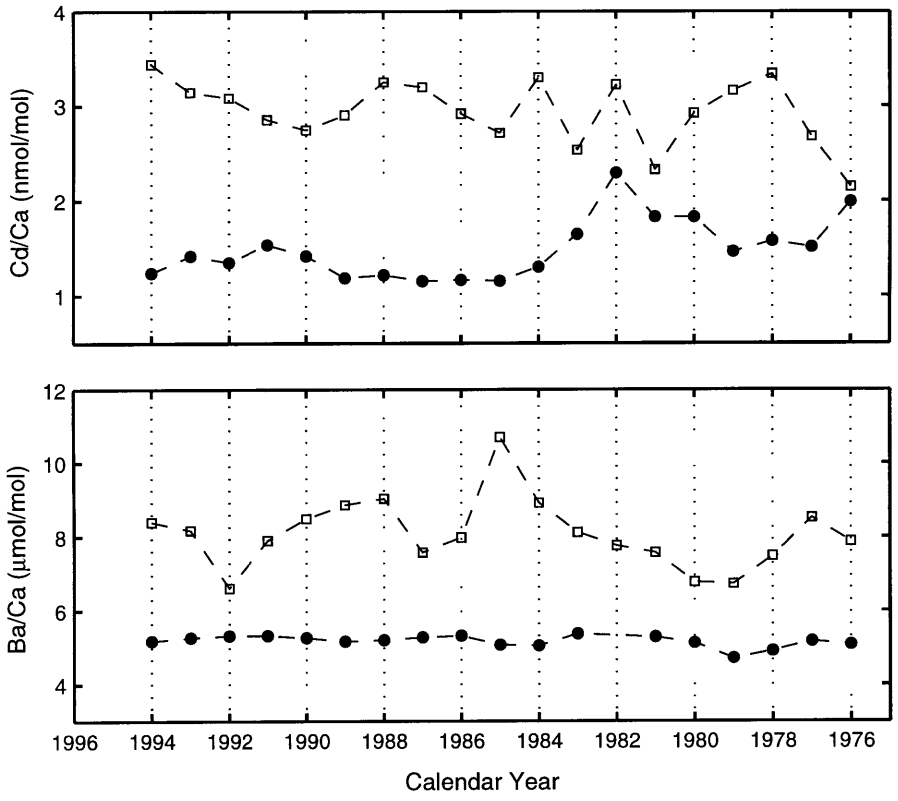

Figure 5-7: Trace element interspecies comparison, *Siderastrea siderea* and *Montastrea annularis*. The *S. siderea* data are shown as open squares, and the *M. annularis* results are given as closed circles for Cd/Ca (upper panel) and Ba/Ca (lower panel). The time interval is from 1976 to 1994.

1988a), suggesting this result might be regionally significant[5]. Most importantly, the Pb/Ca results show no comparable mid-century reduction. Because anthropogenic cadmium and lead can be derived from separate sources, this observation cannot completely eliminate an anthropogenic cadmium artifact. The Pb/Ca observations, however, are consistent with the upwelling hypothesis.

[5]The Galápagos maximum was interpreted by Shen (1986) to reflect sample contamination; reanalysis of both records will address this issue.

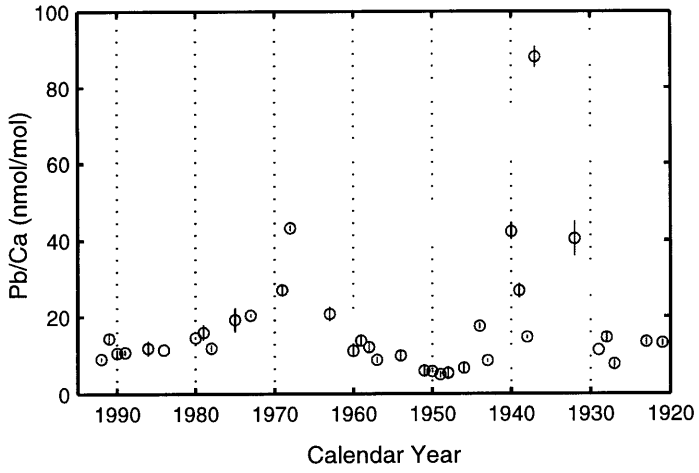

Figure 5-8: Cariaco Basin Pb/Ca record: Isla Tortuga. Note the Pb/Ca maxima at 1968 and 1937 and the good agreement among sample replicates. No systematic Pb/Ca reduction is observed at 1950. Error bars are $\pm 2\sigma$.

5.3.2 Seasonal Trace Element Variability

If upwelling variability offers the best explanation of these observations, one useful validation is the expected geochemical seasonality. As previously stated, the coarse sampling resolution (n=5-6 yr^{-1}) precludes a quantitative estimate of the seasonal cycle. Assessment of the attenuated cycle, however, is still warranted. To evaluate the seasonal variability, both data sets were resampled at the coarsest resolution (n=5 yr^{-1}), calculating the mean of each annual 'quintile' for a given time interval. The results are shown in Figure 5-9. The mean Cd/Ca and Ba/Ca results are anti-correlated, following the generalized seasonal cycle of sea surface temperature and precipitation. From the Da Silva *et al.* (1994) climatology, the annual SST minimum is observed from January to April in this region, associated with the southerly ITCZ position, enhanced North Atlantic wind stress, and intensified upwelling. A seasonal Cd/Ca-SST anti-correlation is observed (r=-0.89), suggesting mixed layer cadmium might have a residence time shorter than the annual cycle. The seasonal hydrological cycle also follows the ITCZ position, with greatest precipitation in this region occurring in boreal fall. Comparison between an Orinoco River hydrograph (Puente Angostura, t=1923-1989,

Fekete *et al.*, 2000) and the Ba/Ca variability yields r=0.81. This station was selected based on its location on the main channel, the duration of the record, and the large Orinoco freshwater fluxes to the southern Caribbean (see above). Quantitative agreement between climatological parameters from a single site and the surface coral trace element records should not necessarily be expected; complications include the earlier and larger discharge from the Amazon River (see Figure 2 of Müller-Karger, 1989), the uncertain residence time of cadmium and barium in reef environments, and possible local-scale influxes of these elements. Most importantly, the significance of small Cd/Ca and Ba/Ca differences must be questioned: the uncertainty for the 1919-1996 interval (as $\sigma_{\mu}^2 = \sigma^2/n$), equals 0.115 nmol/mol (Cd/Ca) and 0.026 μmol/mol (Ba/Ca). From this simplified analysis of the attenuated seasonal variability, the surface coral results are consistent with the expected SST and precipitation patterns in this region.

5.3.3 Decadal-Scale Trace Element Variability

To quantify the decadal-scale component, the Cd/Ca record was analyzed using established power spectral techniques (see discussion in Riedel *et al.*, 1994; Dettinger *et al.*, 1995). The multi-taper method is suitable for short, low signal-to-noise time series, and the original cadmium data were resampled at a period of 0.2 years prior to analysis. The results, shown in Figure 5-10, indicate the greatest decadal-scale power at 6.8 years (99% confidence interval), with significant power also observed at 2.4 and 2.0 years. The reconstructed 6.8 year period shows the largest amplitude prior to 1950, indicating both the timing and magnitude of upwelling in this region has varied throughout the twentieth century. A comparable period (6.2 yr.) is also observed in the faunal abundance record of Black *et al.* (1999), although an equivalent modulation is not apparent from 1920 to 1990. This 6- to 7-year period observed in both records is less than the 12- to 13-year period determined by Chang *et al.* (1997) from the tropical North Atlantic dipole reconstruction. This period broadly agrees with the three to seven year period of multiple ENSO indices, although the sharpness of both spectral peaks is unexpected relative to the historical analysis (see Figure 5 of Trenberth and Hoar, 1996). This result from the Cd/Ca record, however, is greatly limited by the record length and resolution; it should be interpreted with caution.

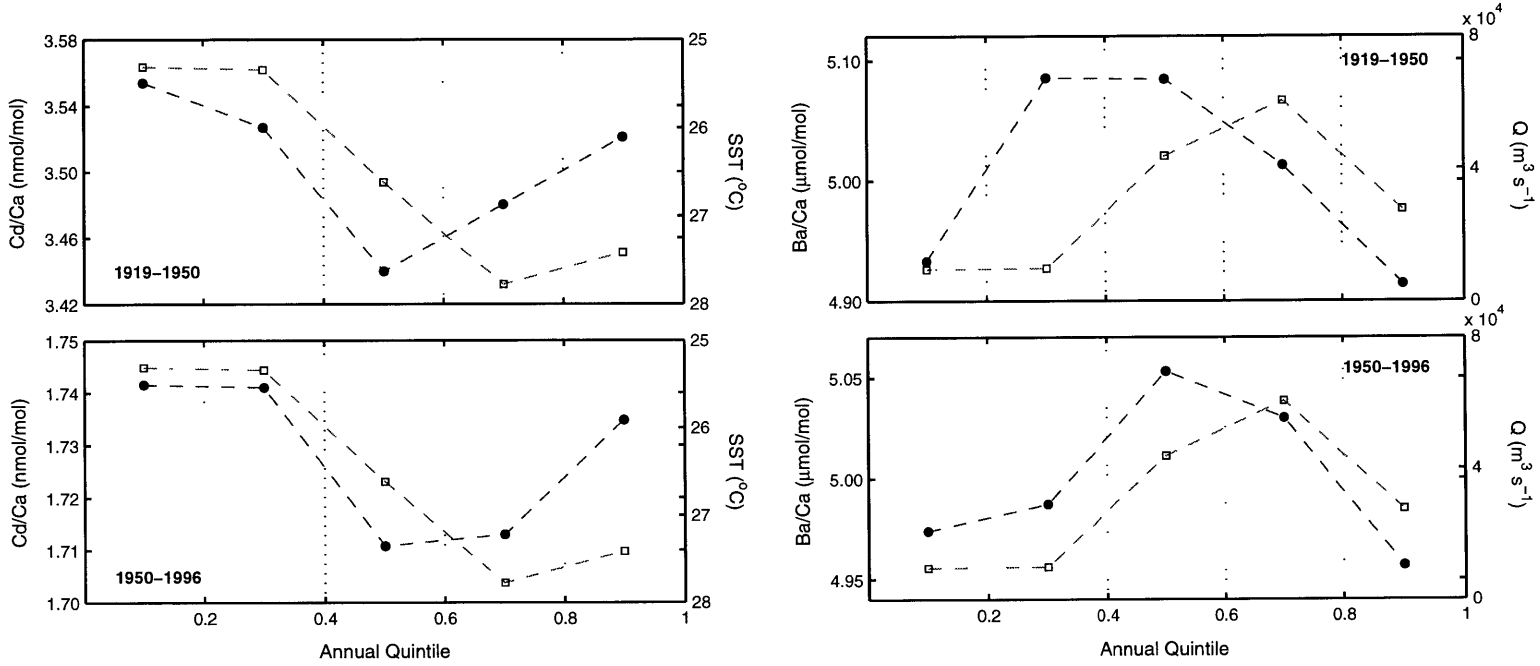

Figure 5-9: Trace element seasonality, Cariaco Basin. The Cd/Ca and Ba/Ca results are shown as annual 'quintiles', and a complete description of this method is provided in the text. The left panels shows the mean Cd/Ca results (nmol/mol, closed circles) and the degraded SST climatology from Da Silva *et al.* (1994, 0.5x0.5° at 65.25°W, 10.25°N, open squares). The upper panel reflects the 1919-1950 interval, and the lower panel includes the 1950-1996 interval. The SST ordinate is reversed for comparison. The right panel includes the mean Ba/Ca results (μmol/mol, closed squares) and the degraded discharge climatology from an Orinoco River station (Puente Angostura, Fekete *et al.*, 2000, open squares). Note the Cd/Ca maximum present in the first and second quintile, whereas the Ba/Ca maximum occurs in the third quintile. The two time intervals exhibit the same general pattern.

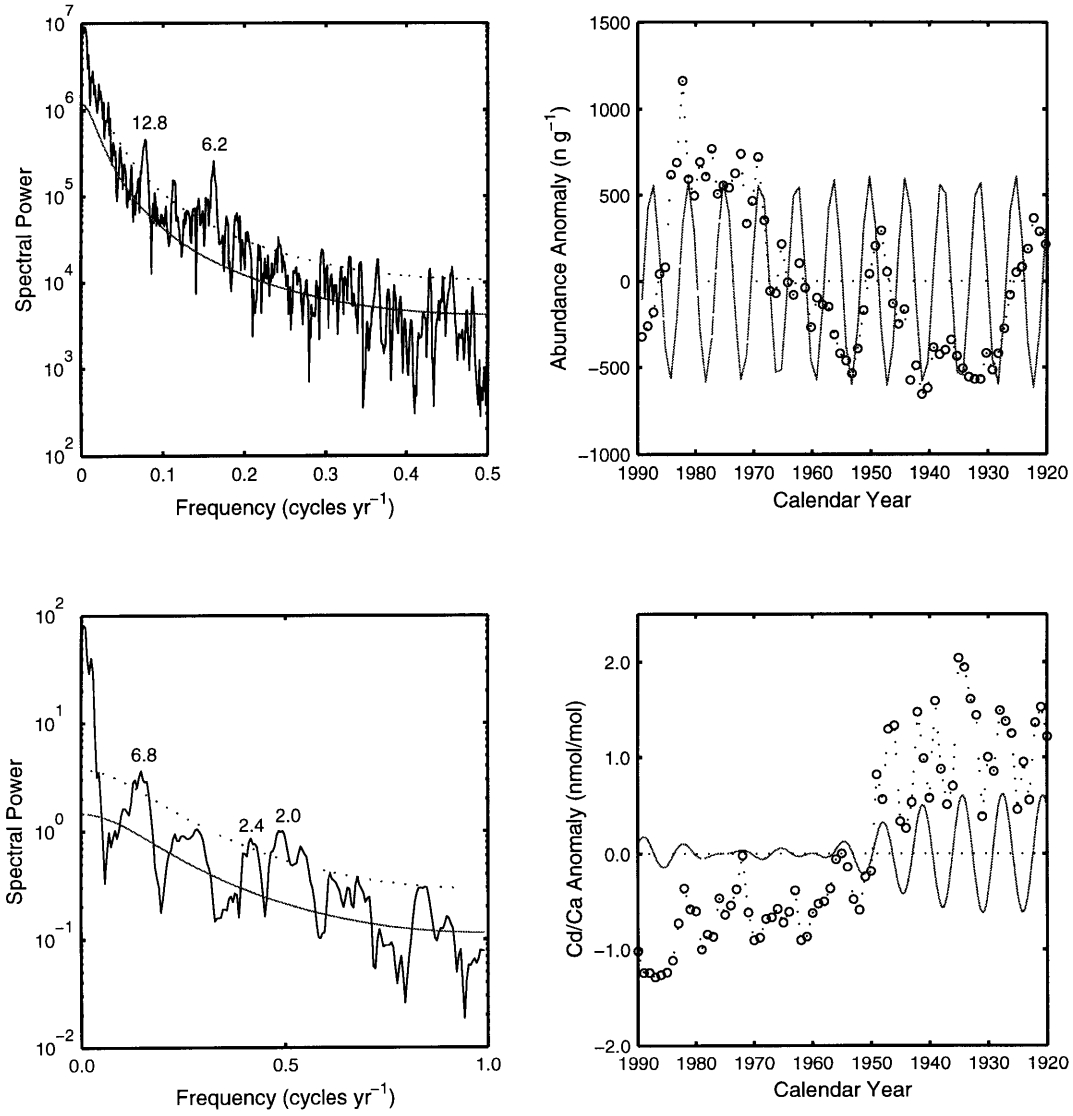

Figure 5-10: Spectral analyses, Cd/Ca and faunal abundance records. The left panels show the log periodograms (multi-taper method, 3 tapers) of the faunal abundance (upper) and Cd/Ca (lower) data, including the median (solid line) and 99% confidence interval (dashed line). The right panels show the filtered reconstructions for the 6.2 and 6.8 year periods, respectively. The faunal abundance reconstruction includes a gain factor of 10 for comparison, and note the amplitude modulation observed for the Cd/Ca record.

5.3.4 Interdecadal Trace Element Variability

Upwelling variability provides the best explanation for the trace element results given the limited Ba/Ca variability associated with the Cd/Ca reduction. This hypothesis can be tested with historical climate observations from the Cariaco Basin, including marine air temperature (MAT) and sea surface temperature (SST) observations from the COADS data set (Woodruff *et al.*, 1987). This data set was selected for its 2x2° observations extending to 1859 (centered on 65°W, 11°N); 5x5° grids or above do not adequately resolve Cariaco Basin upwelling. Historical climate records include two well-known artifacts: bias resulting from discrepant measurement techiques and aliasing due to inadequate annual observations. Multiple techniques were utilized to address these artifacts, shown in Figure 5-11. First, the measured SST variability was compared with the maximum estimated bias ($\overline{x}$ =0.49°C from 1903 to 1941, Jones *et al.*, 1986), neglecting interannual variability below this limit. Second, temperature differences were calculated between the Cariaco Basin and a Caribbean, non-upwelling domain (65°W, 13°N), reducing the expected bias. The utility of the difference calculation is supported by the mean annual temperature difference between the 11°N and 13°N domains (-0.877°C) resulting from persistent coastal upwelling throughout the annual cycle. The MAT data are also included for completeness, based on their lower estimated measurement bias ($\overline{x}$ =0.23°C from 1903 to 1941, Jones *et al.*, 1986).

All three historical climate records show negative temperature anomalies from approximately 1920 to 1943, followed by positive temperature anomalies from 1943 to 1988 (Figure 5-11). These observations are in general agreement with the 1950 Cd/Ca reduction. Anomalously cool winter SSTs (-3.2°C) were observed at 1946, suggesting the inferred timing of the final 1946 Cd/Ca maximum is reasonable despite the apparent disagreement with the mean annual data. Winter SST anomalies less than -3°C were also observed in seven years from 1920 to 1950 (1922, 1923, 1926, 1936, 1937, 1939, 1946), whereas only two winters from 1950 to 1995 (1957, 1992) were of equivalent magnitude. The potentially complex response of mixed layer cadmium concentrations to upwelling at the site is largely unknown, thus the trace element proxy records might not necessarily reflect a linear response to Cariaco Basin upwelling. A mid-century reduction in upwelling intensity, however, provides a consistent explanation for the trace element (Cd/Ca, Ba/Ca, and Pb/Ca) and historical

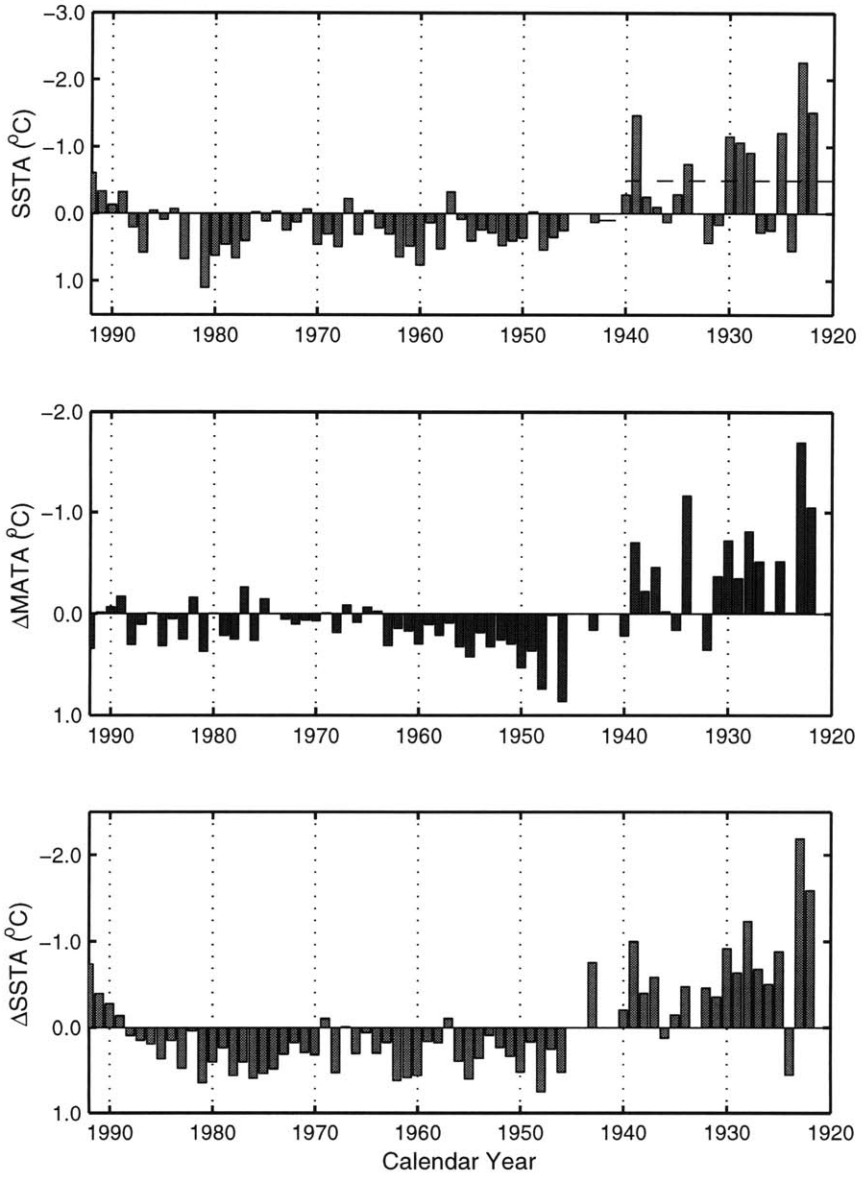

Figure 5-11: Historical climate records from the Cariaco Basin, COADS data series. The top panel shows the sea surface temperature anomaly (SSTA) record from the 65°W, 11°N grid, including the bias limits given by Jones *et al.* (1986). Anomalies were calculated with respect to the 1920-1992 interval. The middle and lower panels denote the marine air temperature and sea surface temperature difference anomalies between the 13°N and 11°N grids. Correlation (r=0.846) between the SSTA and ΔSSTA results suggests the Cariaco grid determines the temperature difference.

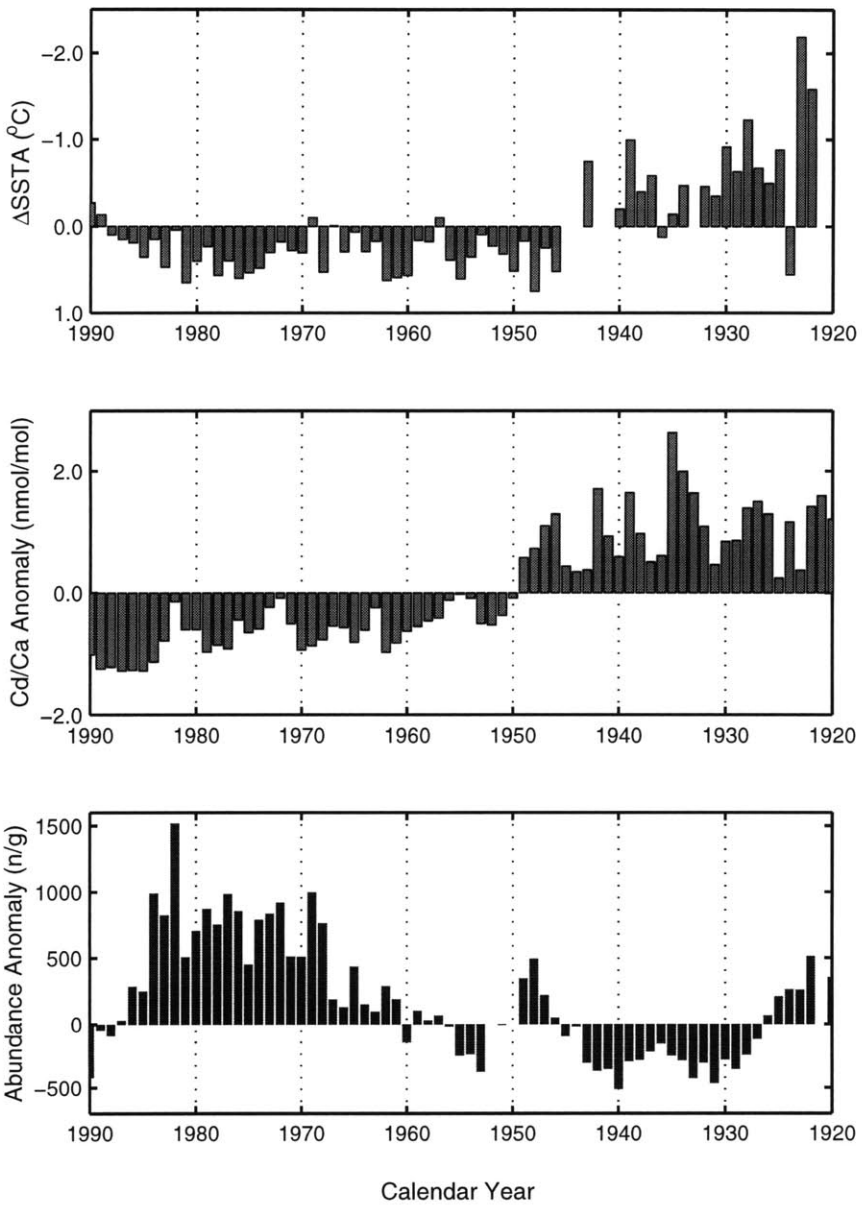

Figure 5-12: Cariaco Basin proxy records and historical climate comparison. The upper two panels show the previously-described mean annual ΔSSTA and Cd/Ca records from this site. The lower panel shows the *G. bulloides* faunal abundance data of Black *et al.* (1999), core PL07-71BC.

climate records.

Considering this apparent shift in Cariaco Basin upwelling, to what extent does this interpretation agree with the sedimentary proxy records? The best comparison can be made with the annually-resolved *G. bulloides* abundance record of Black *et al.* (1999), where the relative and absolute abundance of this planktonic foraminfera from February to June has been correlated with upwelling intensity at this site (Peterson *et al.*, 1991, and refs. therein). As shown in Figure 5-12, from 1920 to 1990 the trace element and faunal abundance records are inconsistent, with a greater correlation between Cd/Ca and mean annual SST relative to *G. bulloides* abundance. This observation does not necessarily refute the interpretation of (Black *et al.*, 1999) given the significant correlation (r=0.87) between *G. bulloides* abundance and the tropical Atlantic SST gradient, but it suggests the nature of both geochemical and micropalentological upwelling proxies might be more complicated than generally assumed.

Despite the agreement between the historical climate records and the Cd/Ca results, these observations cannot provide a simple interpretation of upwelling variations in this region. The Cd/Ca variability might be of local significance, resulting from island upwelling effects or local-scale cadmium sources, either natural or anthropogenic. This interpretation is supported by the tropical North Atlantic observations, including the zonal wind speed, interhemispheric SST anomalies, and North Atlantic SST anomalies (see Figure 3 of Black *et al.*, 1999). This negative interpretation, however, ignores multiple historical climate observations from this site, and a historical SST bias greater than 1°C is unlikely. Coastal upwelling in the Cariaco Basin region might also not reflect a linear response to extratropical North Atlantic forcing. This is supported by a simple correlation map of the COADS SST data set (1854-1992) shown in Figure 5-13: greatest correlation is observed within the southern Caribbean and tropical North Atlantic, whereas reduced correlation exists within the subtropical North Atlantic (compare with Figure 1 of Black *et al.*, 1999). Most importantly, false correlations result from comparing low frequency signals within short time series records; the limited trace element observations presented here must be extended for a quantitative assessment. Systematic interpretation of the trace element records requires longer, multiple, and calibrated records from several upwelling sites in this region.

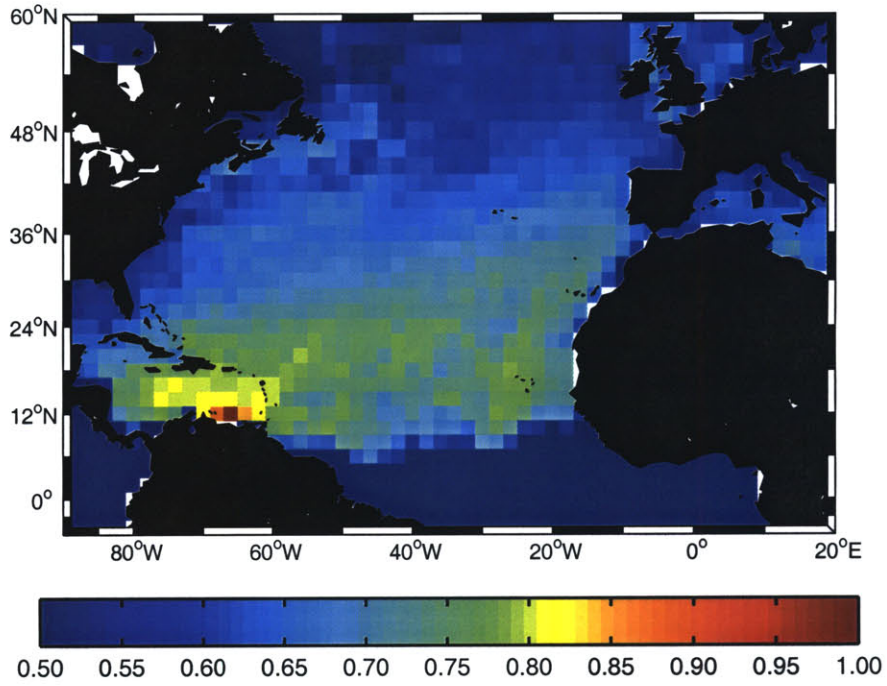

Figure 5-13: Correlation map of Cariaco Basin SST. Historical SST data from 1854 to 1992 were taken from the COADS data set (Woodruff *et al.*, 1987). Correlations were determined with respect to the 11°N 65°W grid point, and the colormap is scaled to include only r>0.5. Note the greatest correlation with the southern Caribbean and the tropical North Atlantic relative to the extratropical North Atlantic. Please see the text for discussion.

5.4 Conclusions

In conclusion, the surface coral Cd/Ca and Ba/Ca records have raised several new questions regarding Cariaco Basin upwelling and its response to tropical Atlantic forcing. Three conclusions are obtained from these observations:

1. A two-fold reduction in the Cd/Ca ratio of *Montastrea annularis* is observed from 1946 to 1952. No associated shift in the Ba/Ca ratio is apparent across this interval. This variability is consistent with the hydrographic distribution of cadmium and barium in the Cariaco Basin, suggesting a two-fold reduction in upwelling intensity at this site.

2. Trace element artifacts are significant for surface coral records. Both Cd/Ca and Ba/Ca ratios exhibit a kinetic dependence between *Montastrea annularis* and *Siderastrea siderea*, with an approximate two-fold increase in elemental ratios associated with an equivalent reduction in annual extension rate. Anthropogenic variability at this site, inferred from Pb/Ca ratios, is also significant, with two maxima observed at 1937 and 1968. These artifacts do not explain the mid-century Cd/Ca reduction.

3. The trace element variability agrees with the historical climate observations from the Cariaco Basin, including absolute and relative historical records. The inferred upwelling intensity does not corroborate the faunal abundance records from this region or the inferred North Atlantic extratropical forcing.

These results demonstrate the potential utility of combined geochemical and micropaleontological proxies from separate, annually-resolved systems. The discrepant results between faunal abundance records, geochemical proxies, and the historical climate records suggests the response of these proxy systems to tropical upwelling is more complicated than generally assumed, requiring systematic modern calibrations. From these results, past upwelling within the Cariaco Basin might therefore reflect a complex, non-linear system exhibiting centennial-scale variability.

Table 5.1: Cd/Ca and Ba/Ca results, Isla Tortuga, Cariaco Basin. The Cd/Ca (nmol/mol) and Ba/Ca (μmol/mol) records are given as two separate chronologies (see Methods), and replicate standard deviation reflects 2σ.

Year 1	**Cd/Ca**	2σ	**Year 2**	**Ba/Ca**	2σ
1995.9	1.94	0.10	1995.9	5.42	0.14
1995.6	2.19	0.10	1995.8	5.38	0.26
1995.4	2.05	0.24	1995.6	5.10	0.14
1995.3	1.53	0.06	1995.4	5.36	0.12
1995.1	1.49	0.02	1995.3	5.36	0.18
1994.9	1.39	0.16	1994.8	5.16	0.02
1994.7	1.36	0.34	1994.3	5.20	0.02
1994.5	1.16	0.14	1993.8	5.43	0.12
1994.3	1.12	0.06	1993.6	5.11	0.06
1994.1	1.18	0.06	1992.9	5.33	0.24
1993.6	1.41	0.14	1992.8	5.15	0.16
1993.4	1.27	0.02	1992.1	5.47	0.06
1993.1	1.57	0.04	1991.9	5.21	0.08
1992.9	1.44	0.14	1991.8	5.43	0.24
1992.8	1.31	0.22	1991.6	5.17	0.04
1992.4	1.48	0.34	1991.4	5.30	0.16
1992.3	1.19	0.18	1991.1	5.51	0.20
1992.1	1.33	0.08	1990.8	5.11	0.10
1991.9	1.34	0.12	1990.6	5.33	0.14
1991.8	1.59	0.42	1990.4	5.30	0.24
1991.6	1.31	0.16	1990.3	5.31	0.10
1991.4	1.76	0.36	1989.9	5.26	0.06
1991.3	1.67	0.24	1989.6	4.99	0.02
1991.1	1.55	0.02	1989.4	5.17	0.12
1990.9	1.44	0.28	1989.3	5.21	0.06
1990.8	1.57	0.10	1989.1	5.19	0.10
1990.4	1.47	0.10	1988.9	5.25	0.26
1990.3	1.38	0.10	1988.8	5.13	0.18
1990.1	1.23	0.18	1988.6	5.11	0.08
1989.9	1.18	0.24	1988.4	5.44	0.22
1989.7	1.22	0.14	1988.1	5.09	0.02
1989.5	1.10	0.14	1987.4	5.24	0.26
1989.3	1.36	0.24	1987.1	5.30	0.26
1989.1	1.06	0.18	1986.9	5.05	0.06
1988.9	1.22	0.14	1986.8	5.46	0.06
1988.8	1.38	0.06	1986.6	5.37	0.04
1988.6	1.23	0.42	1986.3	5.40	0.04
1988.4	1.08	0.01	1985.8	4.95	0.04
1988.1	1.17	0.14	1985.6	5.17	0.01
1987.9	1.13	0.12	1985.4	5.18	0.08
1987.8	1.20	0.01	1985.1	4.99	0.01
1987.6	1.21	0.20	1984.9	4.97	0.08

Data continued on next page

Table 5.1: *Data continued from previous page*

Year 1	**Cd/Ca**	2σ	**Year 2**	**Ba/Ca**	2σ
1987.4	1.15	0.22	1984.8	5.11	0.08
1987.1	1.09	0.01	1984.6	4.76	0.04
1986.9	1.06	0.06	1984.3	5.34	0.20
1986.8	1.04	0.10	1983.9	5.52	0.20
1986.6	1.38	0.32	1983.3	5.21	0.16
1986.4	1.16	0.22	1981.3	5.00	0.20
1986.3	1.13	0.14	1981.1	5.56	0.10
1986.1	1.21	0.16	1980.9	5.48	0.24
1985.9	1.04	0.18	1980.8	5.11	0.22
1985.8	1.05	0.08	1980.1	4.77	0.16
1985.6	1.31	0.08	1979.8	4.24	0.02
1985.4	1.27	0.20	1979.6	4.70	0.04
1985.3	1.10	0.02	1979.4	4.77	0.04
1985.1	1.16	0.06	1979.3	4.88	0.02
1984.9	1.33	0.22	1979.1	4.91	0.24
1984.8	1.36	0.26	1978.9	4.83	0.14
1984.6	1.16	0.08	1978.6	4.97	0.01
1984.4	1.21	0.02	1978.3	4.95	0.06
1984.1	1.45	0.24	1978.1	4.89	0.08
1983.5	1.65	0.28	1977.8	5.18	0.02
1982.2	2.29	0.44	1977.6	5.72	0.10
1981.9	1.59	0.34	1977.4	5.16	0.10
1981.8	1.70	0.16	1977.1	4.63	0.10
1981.6	1.62	0.14	1976.9	5.20	0.04
1981.4	1.67	0.12	1976.8	5.19	0.04
1981.3	2.22	0.28	1976.6	4.73	0.28
1981.1	2.16	0.02	1976.4	5.47	0.04
1980.9	1.89	0.22	1976.3	5.04	0.06
1980.8	1.69	0.14	1976.1	4.85	0.06
1980.6	2.04	0.32	1975.9	5.05	0.12
1980.3	1.75	0.10	1975.8	5.18	0.20
1980.1	1.76	0.02	1975.4	4.94	0.04
1979.9	1.77	0.06	1975.3	5.45	0.06
1979.8	1.43	0.08	1975.1	4.76	0.18
1979.6	1.20	0.10	1974.9	5.10	0.24
1979.4	1.43	0.12	1974.8	4.98	0.04
1979.3	1.37	0.08	1974.6	4.45	0.16
1979.1	1.58	0.08	1973.5	5.22	0.10
1978.9	1.52	0.06	1972.9	4.92	0.18
1978.8	1.60	0.22	1972.6	4.80	0.24
1978.4	1.52	0.36	1972.4	5.21	0.26
1978.3	1.48	0.06	1972.1	5.20	0.06
1978.1	1.77	0.08	1971.9	5.01	0.14
1977.7	1.60	0.20	1971.4	4.75	0.06
1977.5	1.51	0.14	1971.3	5.19	0.06
1977.3	1.41	0.01	1971.1	4.63	0.20

Data continued on next page

Table 5.1: *Data continued from previous page*

Year 1	**Cd/Ca**	2σ	**Year 2**	**Ba/Ca**	2σ
1977.1	1.53	0.24	1970.9	4.62	0.04
1976.9	1.86	0.02	1970.8	5.11	0.22
1976.8	1.80	0.28	1970.6	4.97	0.04
1976.6	1.87	0.44	1970.3	4.78	0.08
1976.4	1.71	0.10	1970.1	4.86	0.12
1976.3	2.35	0.36	1969.9	4.52	0.10
1976.1	2.35	0.24	1969.8	4.66	0.01
1975.9	1.69	0.01	1969.6	5.09	0.26
1975.8	1.98	0.44	1969.4	5.01	0.04
1975.4	1.72	0.18	1969.1	4.67	0.26
1975.3	1.75	0.02	1968.8	4.77	0.18
1975.1	1.77	0.12	1968.4	5.28	0.04
1974.9	1.68	0.22	1968.3	4.73	0.08
1974.8	1.83	0.40	1967.9	5.35	0.06
1974.4	1.85	0.28	1967.6	5.28	0.08
1974.3	1.67	0.04	1967.4	4.79	0.28
1974.1	2.18	0.36	1967.1	5.33	0.01
1973.5	2.20	0.20	1966.9	4.59	0.20
1972.9	1.76	0.20	1966.7	5.22	0.12
1972.8	2.12	0.14	1966.3	5.24	0.26
1972.6	2.37	0.01	1965.9	4.46	0.14
1972.4	2.49	0.18	1965.8	4.95	0.14
1972.3	2.94	0.20	1965.6	5.24	0.26
1972.1	2.43	0.02	1965.4	5.19	0.28
1971.9	2.33	0.58	1965.3	4.70	0.04
1971.8	1.83	0.24	1965.1	5.01	0.04
1971.6	2.04	0.04	1964.9	5.03	0.22
1971.4	1.87	0.12	1964.5	5.17	0.14
1971.3	1.98	0.36	1964.3	4.99	0.08
1971.1	1.49	0.12	1964.1	4.90	0.06
1970.9	1.25	0.24	1963.9	4.74	0.12
1970.8	1.46	0.08	1963.3	4.85	0.02
1970.6	1.18	0.14	1962.9	5.09	0.16
1970.4	2.06	0.06	1962.5	4.93	0.26
1970.3	1.33	0.02	1962.3	4.74	0.06
1970.1	1.70	0.06	1962.1	4.37	0.22
1969.9	1.51	0.06	1961.6	5.00	0.18
1969.8	1.45	0.10	1961.1	4.20	0.04
1969.6	1.84	0.38	1960.9	4.86	0.10
1969.4	1.77	0.14	1960.6	5.06	0.06
1969.3	1.41	0.42	1960.3	4.59	0.22
1969.1	1.40	0.16	1960.1	5.65	0.06
1968.9	1.36	0.26	1959.9	4.95	0.10
1968.8	1.50	0.04	1959.6	4.83	0.10
1968.6	1.73	0.10	1959.3	5.07	0.02
1968.4	1.57	0.14	1958.9	5.07	0.02

Data continued on next page

Table 5.1: *Data continued from previous page*

Year 1	**Cd/Ca**	2σ	**Year 2**	**Ba/Ca**	2σ
1968.3	1.80	0.22	1958.8	5.00	0.14
1968.1	2.04	0.24	1958.6	5.10	0.01
1967.9	2.22	0.24	1958.3	4.81	0.04
1967.8	2.28	0.16	1958.1	4.63	0.01
1967.4	1.51	0.08	1957.9	4.83	0.10
1967.1	1.55	0.12	1957.8	5.02	0.10
1966.9	1.69	0.54	1957.6	4.88	0.04
1966.6	1.69	0.06	1957.4	4.77	0.12
1966.4	2.24	0.10	1957.3	5.00	0.02
1966.1	1.82	0.08	1957.1	4.97	0.02
1965.9	1.60	0.28	1956.6	5.53	0.18
1965.8	1.45	0.04	1956.4	5.41	0.08
1965.6	1.86	0.22	1956.3	5.01	0.04
1965.4	2.09	0.44	1955.6	5.47	0.08
1965.3	1.40	0.08	1955.4	5.15	0.18
1965.1	1.32	0.20	1955.1	5.03	0.20
1964.9	2.49	0.14	1954.9	5.31	0.02
1964.5	1.71	0.06	1954.6	5.19	0.02
1964.3	1.58	0.26	1954.4	5.47	0.04
1964.1	1.48	0.08	1954.3	5.03	0.06
1963.8	2.38	0.20	1954.1	5.30	0.10
1963.3	2.00	0.30	1953.8	4.96	0.01
1962.9	1.50	0.26	1953.4	5.18	0.24
1962.4	1.54	0.20	1953.3	5.01	0.06
1962.1	1.32	0.12	1953.1	5.44	0.24
1961.9	1.92	0.12	1952.9	4.35	0.08
1961.8	1.35	0.10	1952.6	5.30	0.26
1961.6	1.60	0.10	1952.3	4.85	0.28
1961.3	1.50	0.30	1952.1	5.13	0.08
1961.1	1.68	0.30	1951.9	4.93	0.10
1960.8	1.54	0.02	1951.8	5.02	0.04
1960.6	1.58	0.14	1951.6	4.85	0.08
1960.4	2.04	0.22	1951.4	5.34	0.20
1960.1	2.06	0.32	1951.3	4.98	0.08
1959.9	1.61	0.08	1951.1	4.99	0.08
1959.6	1.57	0.16	1950.9	4.78	0.28
1959.4	2.01	0.16	1950.6	5.02	0.14
1959.3	2.29	0.08	1950.3	5.57	0.28
1959.1	1.92	0.06	1950.1	4.85	0.30
1958.9	2.42	0.56	1949.9	5.11	0.06
1958.8	1.77	0.04	1949.8	5.11	0.12
1958.6	1.98	0.32	1949.6	4.99	0.08
1958.4	1.73	0.06	1949.4	4.99	0.06
1958.3	1.69	0.12	1949.3	5.32	0.24
1958.1	2.26	0.04	1949.1	5.03	0.02
1957.9	2.05	0.18	1948.9	5.04	0.06

Data continued on next page

Table 5.1: *Data continued from previous page*

Year 1	**Cd/Ca**	2σ	**Year 2**	**Ba/Ca**	2σ
1957.8	1.93	0.04	1948.8	5.03	0.02
1957.6	1.74	0.06	1948.6	5.13	0.08
1957.4	1.62	0.42	1948.3	5.16	0.06
1957.3	2.13	0.06	1948.1	5.16	0.16
1957.1	2.66	0.32	1947.9	5.10	0.12
1956.6	2.57	0.36	1947.8	5.07	0.06
1956.3	1.90	0.14	1947.6	5.21	0.06
1956.1	2.48	0.54	1947.3	4.88	0.04
1955.9	2.32	0.02	1947.1	5.18	0.20
1955.8	2.17	0.18	1946.9	5.17	0.28
1955.6	2.88	0.10	1946.8	4.84	0.20
1955.4	1.79	0.08	1946.6	4.75	0.10
1955.3	3.04	0.10	1946.4	4.76	0.10
1955.1	2.28	0.24	1946.3	4.92	0.14
1954.9	2.55	0.34	1946.1	5.20	0.28
1954.7	2.21	0.26	1945.9	4.82	0.01
1954.5	2.03	0.08	1945.8	4.87	0.01
1954.3	2.53	0.01	1945.6	4.91	0.10
1954.1	2.41	0.10	1945.3	4.80	0.08
1953.9	2.00	0.10	1945.1	4.87	0.02
1953.7	1.93	0.14	1944.9	4.83	0.10
1953.5	1.89	0.10	1944.6	5.09	0.06
1953.3	2.17	0.24	1944.4	4.84	0.08
1953.1	1.65	0.01	1944.3	4.68	0.30
1952.9	2.25	0.14	1944.1	4.89	0.24
1952.6	1.76	0.06	1943.9	4.84	0.10
1952.3	1.69	0.20	1943.6	5.17	0.30
1952.1	1.92	0.22	1943.1	4.87	0.18
1951.9	1.86	0.10	1942.6	5.08	0.04
1951.7	1.83	0.40	1942.4	4.93	0.06
1951.3	2.40	0.58	1942.3	4.63	0.26
1951.1	2.17	0.24	1941.9	4.75	0.01
1950.9	2.94	0.46	1941.8	5.48	0.04
1950.8	2.81	0.02	1941.4	4.97	0.06
1950.6	1.97	0.16	1941.1	4.92	0.06
1950.4	1.78	0.44	1940.9	4.85	0.28
1950.3	2.44	0.26	1940.8	5.05	0.20
1950.1	2.16	0.16	1940.6	5.14	0.24
1949.9	2.11	0.16	1940.4	5.53	0.22
1949.8	2.56	0.10	1940.1	5.09	0.28
1949.6	2.59	0.02	1939.9	4.49	0.04
1949.3	3.93	0.52	1939.8	4.61	0.06
1949.1	3.90	0.22	1939.6	4.81	0.20
1948.9	4.09	0.30	1939.3	4.83	0.18
1948.8	3.64	0.36	1939.1	4.83	0.10
1948.6	3.22	0.10	1938.7	4.79	0.06

Data continued on next page

Table 5.1: *Data continued from previous page*

Year 1	**Cd/Ca**	2σ	**Year 2**	**Ba/Ca**	2σ
1948.4	2.51	0.02	1938.3	5.26	0.04
1948.3	2.90	0.34	1938.1	5.01	0.10
1948.1	2.64	0.04	1937.8	5.11	0.12
1947.9	2.48	0.14	1937.6	5.40	0.08
1947.8	2.99	0.22	1937.3	4.89	0.16
1947.6	3.35	0.22	1937.1	5.07	0.01
1947.4	3.22	0.36	1936.3	5.65	0.08
1947.3	4.22	0.46	1936.1	5.12	0.14
1947.1	4.96	0.28	1935.6	5.26	0.18
1946.5	3.23	0.14	1935.4	5.02	0.28
1946.3	3.94	0.24	1935.3	4.95	0.04
1946.1	4.03	0.50	1934.4	5.15	0.01
1945.9	3.26	0.20	1934.3	5.37	0.02
1945.6	2.55	0.06	1934.1	4.95	0.01
1945.1	2.81	0.08	1933.6	5.20	0.04
1944.9	2.86	0.18	1933.4	5.09	0.08
1944.8	3.30	0.24	1933.3	5.16	0.10
1944.6	2.70	0.01	1933.1	4.38	0.18
1944.3	2.52	0.16	1932.9	4.87	0.18
1944.1	2.51	0.34	1932.8	5.01	0.02
1943.9	2.32	0.30	1932.4	5.39	0.03
1943.8	2.35	0.14	1932.1	4.63	0.22
1943.6	1.88	0.32	1931.8	4.90	0.14
1943.3	4.33	0.16	1931.6	5.28	0.22
1943.1	3.17	0.60	1931.3	5.21	0.18
1942.5	4.25	0.54	1931.1	4.94	0.14
1942.3	5.01	0.28	1930.9	4.86	0.28
1942.1	3.17	0.02	1930.8	5.00	0.24
1941.9	2.92	0.58	1930.3	4.79	0.06
1941.8	2.98	0.18	1930.1	4.95	0.22
1941.6	3.22	0.14	1929.9	5.08	0.06
1941.4	3.54	0.22	1929.8	4.81	0.28
1941.3	3.70	0.40	1929.6	4.77	0.24
1941.1	3.82	0.16	1929.4	4.87	0.16
1940.9	3.48	0.02	1929.3	4.73	0.10
1940.8	2.88	0.60	1928.8	4.42	0.04
1940.6	3.01	0.36	1928.4	5.10	0.18
1940.4	3.08	0.16	1928.3	5.39	0.22
1940.3	2.99	0.06	1928.1	4.73	0.02
1940.1	2.74	0.12	1927.9	4.87	0.06
1939.8	3.69	0.03	1927.8	5.22	0.12
1939.6	4.03	0.02	1927.6	5.30	0.22
1939.4	3.98	0.10	1927.4	5.12	0.16
1939.3	4.34	0.06	1927.3	4.83	0.26
1939.1	4.36	0.26	1927.1	4.95	0.16
1938.9	4.01	0.36	1926.7	4.69	0.08

Data continued on next page

Table 5.1: *Data continued from previous page*

Year 1	**Cd/Ca**	2σ	**Year 2**	**Ba/Ca**	2σ
1938.7	4.15	0.20	1926.3	5.45	0.30
1938.5	3.10	0.10	1925.9	4.71	0.06
1938.3	2.83	0.16	1925.4	5.17	0.01
1938.1	2.95	0.18	1924.9	4.82	0.18
1937.9	3.00	0.36	1924.6	5.03	0.02
1937.8	3.69	0.56	1924.4	5.28	0.02
1937.6	3.23	0.28	1924.1	4.41	0.08
1937.4	3.18	0.14	1923.9	4.54	0.26
1937.3	2.08	0.16	1923.6	4.88	0.08
1937.1	2.49	0.14	1923.4	5.19	0.30
1936.9	2.84	0.46	1922.3	5.09	0.14
1936.8	2.88	0.44	1922.1	4.87	0.02
1936.6	3.48	0.32	1921.9	5.33	0.10
1936.4	2.73	0.24	1921.8	5.68	0.20
1936.3	3.00	0.28	1921.6	4.80	0.16
1936.1	3.35	0.30	1921.3	4.51	0.16
1935.1	5.07	0.16	1921.1	4.94	0.06
1934.8	4.61	0.16	1920.8	4.77	0.14
1934.6	4.68	0.42	1920.6	4.67	0.04
1934.4	4.07	0.32	1920.4	4.96	0.06
1934.1	4.36	0.32	1920.1	5.67	0.02
1933.8	3.63	0.26	1919.9	5.20	0.10
1933.4	3.83	0.02	1919.6	5.10	0.12
1933.3	4.13	0.42	1919.4	5.24	0.22
1933.1	4.70	0.38	1919.3	5.30	0.18
1932.4	3.82	0.32	1918.3	4.85	0.30
1932.1	3.23	0.08	1918.1	4.35	0.18
1931.9	4.26	0.02	-	-	-
1931.6	3.15	0.56	-	-	-
1931.4	2.45	0.50	-	-	-
1931.3	1.97	0.02	-	-	-
1931.1	2.66	0.48	-	-	-
1930.9	2.18	0.10	-	-	-
1930.8	2.80	0.58	-	-	-
1930.6	3.03	0.42	-	-	-
1930.4	4.08	0.32	-	-	-
1930.3	4.16	0.42	-	-	-
1930.1	3.43	0.36	-	-	-
1929.9	3.63	0.34	-	-	-
1929.4	3.04	0.50	-	-	-
1929.1	3.20	0.50	-	-	-
1928.8	3.62	0.06	-	-	-
1928.4	4.04	0.08	-	-	-
1928.3	3.84	0.22	-	-	-
1928.1	3.79	0.16	-	-	-
1927.9	4.99	0.48	-	-	-

Data continued on next page

Table 5.1: *Data continued from previous page*

Year 1	**Cd/Ca**	2σ	**Year 2**	**Ba/Ca**	2σ
1927.8	3.91	0.12	-	-	-
1927.4	4.13	0.44	-	-	-
1927.3	3.21	0.44	-	-	-
1927.1	3.43	0.28	-	-	-
1926.7	3.66	0.32	-	-	-
1926.5	3.75	0.08	-	-	-
1926.3	3.69	0.32	-	-	-
1926.1	3.81	0.28	-	-	-
1925.6	2.89	0.10	-	-	-
1925.4	2.52	0.24	-	-	-
1925.1	2.63	0.18	-	-	-
1924.8	3.99	0.20	-	-	-
1924.5	3.79	0.26	-	-	-
1924.2	3.01	0.04	-	-	-
1923.9	2.10	0.16	-	-	-
1923.7	1.74	0.10	-	-	-
1923.5	2.05	0.08	-	-	-
1923.3	3.94	0.54	-	-	-
1923.1	4.21	0.02	-	-	-
1922.9	3.89	0.48	-	-	-
1922.8	4.07	0.56	-	-	-
1922.4	3.34	0.16	-	-	-
1922.1	4.12	0.46	-	-	-
1921.7	3.51	0.04	-	-	-
1921.1	4.55	0.08	-	-	-
1920.9	3.61	0.08	-	-	-
1920.6	3.63	0.50	-	-	-
1920.3	3.03	0.26	-	-	-
1920.1	4.32	0.54	-	-	-
1919.4	3.81	0.08	-	-	-
1919.1	3.92	0.52	-	-	-
1918.9	3.58	0.28	-	-	-
1918.8	2.39	0.14	-	-	-
1918.6	4.22	0.40	-	-	-
1918.4	2.92	0.46	-	-	-
1918.3	3.28	0.20	-	-	-
1918.1	3.53	0.20	-	-	-

Appendix A

Surface Coral Preparation and Elemental Analysis

Low elemental ratios in coral aragonite (<10 nmol/mol) relative to organic or oxide contaminants requires their quantitative removal from an acid-soluble mineral lattice, first developed for Cd/Ca ratio analysis of benthic foraminifera (see Boyle and Keigwin, 1982). The surface coral method of Shen and Boyle (1988a) has been modified for this study, shown schematically in Figure A-1. Here a description of the analytical method is provided, including several modifications for rapid analyses of elemental and isotopic ratios.

A.1 Acquisition and Sampling

First, continuous surface coral cores must be obtained from a well-surveyed location. The three primary sampling prerequisites include: (1) massive colonies of a suitable coral species and morphotype; (2) a reef location within the water mass of interest; and (3) a proper drilling environment, including adequate anchor points and water depth. Core samples were taken by SCUBA, utilizing a hydraulic drill (Tech 2000) equipped with a water pump and a wet-drilling steel carbide core bit. The short (<5 m) cores were taken manually, coring orthogonal to the coral growth surface. Following the first recovery, extension rods were employed for deeper sections. All cores were labeled and oriented at the drilling site.

The cores were then sectioned with a water-lubricated, diamond bit tile saw and placed in

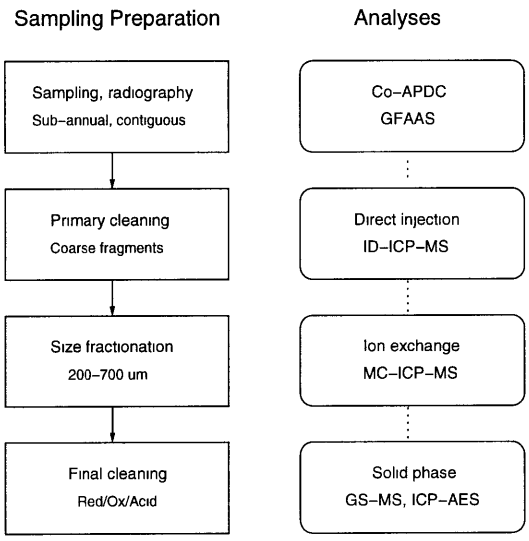

Figure A-1: Protocol for surface coral sample preparation and analyses, modified from Shen and Boyle (1988a). The left side shows the sequential cleaning procedure, including coral sampling with X-radiography, initial cleaning of large fragments, size fractionation to 200-700 μm, and final cleaning with oxidants, reductants, and weak acids. The right side shows the independent analytical protocols, including GFAAS and ICP techniques. See text for definitions.

an ultrasonic bath for thirty minutes, removing drilling contaminants from the cut sections. X-radiographs of the dried sections were taken on a Hewlett-Packard 43905N Faxitron X-ray system, using a tube voltage of 50 kV and an exposure of 30 seconds. Negatives were created with Kodak diagnostic film (Type X-OMAT, TL-2) and Kodak GBX developer and fixer. A continuous sampling template was then generated from each radiograph, noting the orientation of the growth axis, the dissepments, and any occlusions present.

Coral sections were sampled from the X-ray template with a variable-speed scroll saw (Dewalt), using a thin-kerf, diamond-coated wire (130.2x0.08 mm, Crystalite). Dissepiment orientation was followed from the template, cutting the samples perpendicular to the calices. Including preparative losses, at least 200 mg is required for triplicate analysis of 30 mg samples, resulting in coarse sampling resolution relative to standard drilling techniques. With extension rates reaching 12 to 14 mm yr^{-1} for *Montastrea annularis*, typically five to six samples per year are collected. As noted by Quinn *et al.* (1996), sampling resolution below 12 samples per year will alias the seasonal cycle, and Leder *et al.* (1996) suggested

up to 20 samples per year are required for *Montastrea annularis*. Thus additional trace element methods will be required to accurately quantify the seasonal cycle.

A.2 Sample Cleaning

Prior to sample cleaning, all reagents must be prepared for trace element analysis, completing all work in a laminar flow bench (EACI). Solutions were prepared from trace-element grade water ($d\mathrm{H_2O}$), generated from distilled, deionized water in a Corning MegaPure Vycor-borosilicate still. High-density polyethylene plasticware was cleaned in 1N HCl at 55°C for 48 hours, then rinsed three times in $d\mathrm{H_2O}$. All HDPE plastics were then leached in 0.1N triple-distilled HCl, followed by a single rinse with the solution of interest. Teflon plasticware (PFA and PFTE) was first cleaned in concentrated aqua regia at 70°C for 48 hours, followed by the standard leaching procedure.

Reagent preparation utilized several techniques, including coprecipitation, vapor-phase or sub-boiling distillation, ion exchange chromatography, and solvent extraction. First, the 0.2N NaOH solution (Mallinckrodt) is prepared by coprecipitation with 1.0N LaOH (Reacton), removing the precipitate by centrifugation. Ammonia is prepared by vapor-phase distillation of concentrated ammonia (J.T. Baker) to $d\mathrm{H_2O}$, and nitric and hydrochloric acids were triple-distilled in a Vycor distillation column. Citric acid was prepared by batch extraction with purified Chelex 100 for twenty four hours, and the 2.5 mM $\mathrm{CoCl_2}$ solution (Mallinckrodt) was prepared with a BioRad AG-1X8 anion exchange column (chloride form, 200-400 mesh). Finally, solvent extraction of 2% ammonium pyrrolidine dithiocarbamate (APDC, Kodak) with distilled carbon tetrachloride (Mallinckrodt) ensured quantitative trace element removal, utilizing five extractions. Note that $\mathrm{H_2O_2}$ and hydrazine (EM Science) consistently exhibit low trace element blanks; no additional preparation is required.

Following reagent preparation, the coral samples follow a primary cleaning procedure. The cut sections were crushed to a small diameter (2-4 mm) in an acid-leached agate mortar and pestle. The fragments were placed into clean 1.5 mL polyethylene vials, setting the vials into hand-made Lexan polycarbonate racks. The coarse fragments were then cleaned with the following sequence, using 500 to 700 μL reagent volumes for each step:

1. 3x dH$_2$O with ultrasonic cleaning for ten minutes
2. 2x 0.1N HNO_3 with brief ultrasonic cleaning for two minutes
3. 1x 15% H_2O_2 - 0.1N NaOH for 30 minutes in a 90°C water bath, including one minute intervals in the ultrasonic bath every five minutes
4. 1x 0.1N HNO_3 with brief ultrasonic cleaning for two minutes
5. 1x 15% H_2O_2 - 0.1N NaOH for 30 minutes in a 90°C water bath

The precleaned fragments were dried overnight in a laminar flow bench, crushed with an agate mortar and pestle, and separated with two 280 and 700 μm polyethylene sieves. The fine fractions were retained for minor element or isotopic analyses. Then 30.0±0.5 mg of the 280-700 μm fraction is weighed into clean 1.5 mL vials, three-fold less than the 100 mg utilized by Shen and Boyle (1988a). Two replicates are initially analyzed, leaving 40 to 60 mg for the sample archive. The purpose of the precleaning step is to remove most of the accessory phases before the final cleaning. Crushing the fragments to a smaller size fraction opens the coral septa and trabeculae, exposing organic and oxide phases contained within the skeletal framework.

A secondary cleaning process then ensures complete removal of contaminants, including oxidative, reductive, and weak acid cleaning:

1. 3x dH$_2$O with ultrasonic cleaning for ten minutes
2. 1x 0.1N HNO_3 with brief (30 seconds) ultrasonic cleaning for two minutes, ensuring mixture of fragments
3. 1x 15% H_2O_2 - 0.1N NaOH for 30 minutes in a 90°C water bath, including one minute intervals in the ultrasonic bath every five minutes
4. 2x dH$_2$O with ultrasonic cleaning for ten minutes
5. 1x reducing cleaner in a 90°C water bath, including 1 part concentrated hydrazine, 6 parts distilled NH_3, and 3 parts citric acid
6. 1x 0.1N HNO_3 with brief ultrasonic cleaning for two minutes
7. 1x 15% H_2O_2 - 0.1N NaOH, following the previous step
8. 3x 0.1N HNO_3 with brief ultrasonic cleaning for two minutes

Analysis Stage	Start (°C)	End (°C)	Time (s)	Flow (mL/min)
Dry	50	60	40	200
Ash	85	350	15	200
Ash	350	350	6	200
Ash	350	350	4	10
Atomize	2600	2600	4	10
Clean	2700	2700	5	200

Table A.1: GFAAS temperature program for cadmium. Initial and final temperatures are given for each interval. Reduced gas flows during the final ashing stage and atomization diminishes sample loss.

Adequate ultrasonic cleaning and acid leaching are required for complete removal of fine, contaminant-laden particles, and close attention must be given to removal of fines. The cleaned coral fragments were then transferred via pipette to clean 1.5 mL vials, rinsed 3x with 0.1N HNO_3, and dissolved in 75 μL 8.0N HNO_3, added dropwise. Following the required dilutions, all samples are ready for elemental and isotopic analysis.

A.3 GFAAS Analysis

Cadmium concentrations were determined for this study by graphite furnance atomic absorption spectrophometry (GFAAS). All solutions were analyzed on a Hitachi Z-8100 graphite furnace atomic absorption spectrophometer with Zeeman background correction. Standard analytical conditions were utilized, including a 7.5 mA lamp current, a 12.5 mA boost current, and a 20 μL sample injection volume. Duplicate injections were completed for each sample, and a representative temperature program is given in Table A.1. A long drying interval (35 to 40 seconds) is required to minimize sample loss due to elevated cobalt concentrations, and a high atomization temperature provides narrow peak widths. The resulting replicate precision on matrix standards is 1.2% (n=5), although the true replicate precision is limited by complete removal of contaminant phases.

Given the significant calcium interference for cadmium, a Co-APDC coprecipitation was required prior to analysis. Calcium concentrations were first determined by flame atomic absorption, diluting all samples in a La/HCl matrix. The Co-APDC reaction was completed with 250 μL 2.5 mM $CoCl_2$, 100 μL vapor-distilled NH_3, and 250 μL 1% APDC. To eliminate

calcium from the samples, the precipitate is washed with 1 mL dH$_2$O, centrifuged, and dried overnight in a laminar flow bench. The dried precipitate is then digested with 25 μL 8.0N HNO_3 and diluted to 125 mL with dH$_2$O. Matrix standards were prepared from dilute cadmium standards, following the exact coprecipitation reaction.

The reaction pH for the Co-APDC coprecipitation warrants consideration, and we have observed improved and consistent cadmium recoveries at elevated pH. At pH 10.7, cadmium recovery was 95.2±3.0% (2σ, n=16), whereas recovery was reduced to 77.3% at pH 0.8 (n=4). Intermediate recoveries at pH 6.0 (82.7%, n=4) and 8.0 (84.5, n=4) were similarly observed. This result does not agree with Boyle and Edmond (1975), who observed reduced cadmium recovery at elevated pH using a ^{110}Cd radiotracer experiment. The reduction in cadmium recovery at low pH is a possible consequence of hydrogen ion competition for APDC, in agreement with the observed pK_a of 3.0 for pyrrolidine dithiocarbamate (Hulanicki, 1967). Similar behavior has also been noted for Fe^{2+} and Zn^{2+} for the coprecipitation reaction (Boyle and Edmond, 1975). GFAAS and Co-APDC coprecipiation therefore provides a rapid, quantitative method for elemental ratio analysis.

A.4 Isotope Dilution ICP-MS

The concentration of lead and barium were determined in surface corals and seawater with isotope dilution ICP-MS (ID-ICP-MS), following the standard analytical protocol (see Fassett and Paulsen, 1989). Isotope ratio measurements were completed on a VG Plasmaquad 2^+ at MIT, and analytical conditions are given in Table A.4. Sample analyte intensities were corrected for instrumental backgrounds, isobaric interferences, and procedural blanks. The ^{204}Hg isobaric interference on ^{204}Pb was detemined via ^{202}Hg measurements and an assumed ^{204}Hg/^{202}Hg ratio of 0.2299, accounting for less than 0.5% of the total mass 204 intensity. The mean blank contribution for lead was 0.33% (n=214), ranging from 0.01% to 1.28% for all surface coral analyses. Barium procedural blanks were slightly higher; the mean upper limit observed, however, was 3.44% (n=37), ranging from 3.08% to 4.02%. Final concentrations were determined from the isotopic ratio and concentration of well-characterized spikes, including the GEOSECS S-6 ^{135}Ba spike (Klinkhammer and Chan,

1990) and the Oak Ridge National Laboratory ^{204}Pb spike (Wu and Boyle, 1997a). The external precision (2σ) determined from gravimetric standards is consistently less than 2% for both Ba (1.62%, n=5), and Pb (1.52%, n=7) concentrations.

Isotope dilution represents a useful technique for surface coral Pb/Ca analysis, and this study includes a direct measurement technique. Given the relatively low Pb/Ca ratios in corals (*e.g.*, 6 nmol/mol for North Rock, Bermuda), one must first consider the relative importance of matrix suppression. Aliquots of known Pb/Ca ratios were diluted to determine the instrumental response to increasing calcium concentrations, shown in Figure A-2. Above approximately 500 μM [Ca], the ^{208}Pb intensity is constant, resulting from ionization suppression in the plasma, an established phenomenon for acid and cation matrices (Montaser, 1998). A second consideration is long-term signal stability resulting from sample deposition on the nebulizer orifice, sampling cone, and skimmer cone. Signal loss can be minimized by compromising signal intensity (lowering total dissolved solids), replacing the cone and skimmer, or refocusing the attenuated ion beam. Any signal loss with ID-ICP-MS does not affect data quality beyond the counting statistic, and replicate precision is consistently better than 1%. Similar experiments were attempted for direct Cd/Ca analysis, although inadequate signals were observed due to its reduced first ionization potential (7.4V) and Cd/Ca ratios (2 to 10 nmol/mol). Thus direct analysis by isotope dilution represents a rapid, quantitative method for surface coral Pb/Ca determinations.

A.5 Method Validation

Given the cleaning and analytical protocols, what observations can validate their effectiveness? Agreement among sample replicates is one criterion, assuming equal sample masses will not retain equal amounts of accessory phases following sample cleaning. The North Rock Pb/Ca record offers one useful comparison between this method and the Shen and Boyle (1988a) technique. With the described cleaning method and ID-ICP-MS analysis, the mean replicate 2σ standard deviation is 1.3 nmol/mol, significantly less than the standard deviation of 3.6 nmol/mol reported by Shen (1986) for a comparable North Rock Pb/Ca record. For the observed Pb/Ca range at North Rock (69.8 nmol/mol), the resulting signal-

Instrumental Parameter	Set Point	Unit
Nebulizer gas	0.940	L min^{-1}
Auxiliary gas	0.711	L min^{-1}
Cool gas	14.02	L min^{-1}
Forward power	1350	W
Reflected power	0	W
Interface pressure	2.5	mbar
Intermediate pressure	$1.0x10^{-5}$	mbar
Analyzer pressure	$1.4x10^{-6}$	mbar
Acquistion time	120	seconds
Uptake rate	1100	μL min^{-1}
Sensitivity	400,000	cps ppb^{-1}

Table A.2: VG PlasmaQuad 2^{+} quadrupole ICP-MS instrumental conditions. Gas flows were stablized via a 20 psi back-pressure on the mass flow controller. The higher interface pressure results from a larger sampling aperature utilized for the Pb/Ca analyses. Sensitivity was determined for each session with a ^{209}Bi standard.

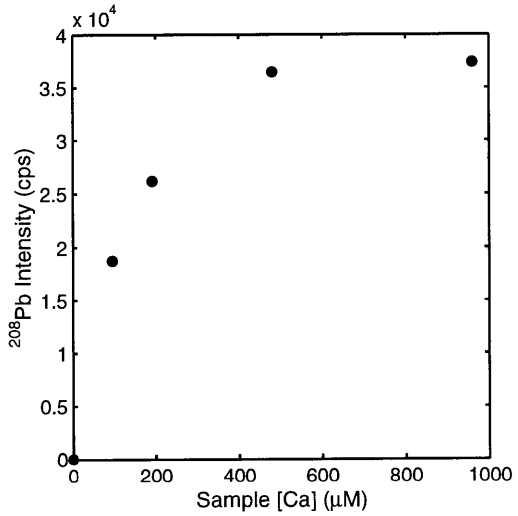

Figure A-2: ^{208}Pb suppression by concomitant calcium. The abscissa reflects the ^{208}Pb intensity given in counts per second, and the ordinate denotes the sample calcium concentration. Ionization suppression is observed at less than 400 μM [Ca].

to-noise ratio for this method is 55.0. More importantly, the results must be consistent with other sites, best tested with respect to previous analyses. As shown in Chapter 1, the correlation between the Cd/Ca ratios and mixed layer [PO_4] is 0.83, and the Cariaco Basin results agree with the general trend, with the mean Cd/Ca ratio (2.20 nmol/mol) in-

termediate between the Bermuda (0.44 nmol/mol) and Galápagos (5.30 nmol/mol) results. The surface coral cleaning and analytical protocols thus provide consistent results among sample replicates and previous observations.

Appendix B

North Rock Surface Coral Pb/Ca and Lead Isotope Results

These tabulated results include Pb/Ca ratios and stable lead isotope results from North Rock, Bermuda, including the surface corals *Diploria strigosa* and *Diploria labyrinthiformis*. The lead isotope data also include seawater analyses from Station S, Bermuda. A complete description of the analytical protocols is given in Chapter 2 and Appendix A, whereas description of the data is provided in Chapter 3.

B.1 North Rock Pb/Ca Results

Table B.1: Pb/Ca results: North Rock, Bermuda. The Pb/Ca ratio is given in units of nmol/mol, including the replicate 2σ standard deviation. Species (1) corresponds to *Diploria labyrinthiformis*, and species (2) reflects *Diploria strigosa*. The 1976 and 1979 values are suspect due to possible tissue layer contamination.

Year	Pb/Ca	2σ	Spec.	n/4	Comments
1884	6.40	0.04	1	2	
1885	6.10	0.56	1	2	
1886	6.21	0.68	1	2	
1887	6.44	0.74	1	2	
1888	6.60	0.68	1	2	
1889	7.16	0.18	1	2	
1890	7.39	0.10	1	2	
1891	7.84	0.94	1	2	
1892	8.02	0.02	1	2	
1893	8.32	1.24	1	2	
1894	8.56	0.30	1	2	
1895	9.68	0.90	1	2	
1896	9.18	0.44	1	2	
1897	9.01	0.02	1	2	
1898	9.71	0.58	1	2	
1899	9.33	0.12	1	2	
1900	9.58	0.02	1	2	
1901	11.75	0.04	1	2	
1902	11.05	0.02	1	2	
1903	11.25	3.60	1	2	
1904	12.65	0.74	1	2	
1905	13.85	0.48	1	2	
1906	15.47	0.50	1	2	
1907	15.76	0.06	1	2	
1908	14.54	1.14	1	2	
1909	15.94	0.52	1	2	
1910	16.11	0.16	1	2	
1911	17.00	0.76	1	2	
1912	19.75	1.52	1	4	
1913	17.24	0.76	1	4	
1914	16.19	0.26	1	2	
1915	16.93	0.40	1	2	
1916	18.29	0.78	1	2	
1917	18.31	2.38	1	2	
1918	17.40	1.12	1	2	
1919	18.14	0.18	1	2	

Data continued on next page

Table B.1: *Data continued from previous page*

Year	Pb/Ca	2σ	Spec.	n/4	Comments
1920	19.98	3.34	1	2	
1921	27.11	3.54	1	2	
1922	26.32	0.58	1	2	
1923	21.54	2.38	1	2	
1924	23.21	0.30	1	2	
1925	23.87	1.12	1	2	
1926	25.01	0.76	1	2	
1927	23.68	0.26	1	2	
1928	23.95	0.98	1	2	
1929	23.38	0.70	1	2	
1930	25.52	3.98	1	2	
1931	25.56	3.56	1	2	
1932	26.74	3.40	1	2	
1933	24.26	1.10	1	2	
1934	24.04	0.56	1	2	
1935	25.12	0.76	1	2	
1936	23.83	3.70	1	2	
1937	24.79	0.52	1	2	
1938	24.87	2.08	1	2	
1938	31.91	0.12	2	2	
1939	22.10	0.38	1	2	
1939	29.65	3.62	2	2	
1940	32.92	1.52	2	2	
1941	31.45	0.52	1	2	
1942	30.49	2.98	1	2	
1942	36.64	2.32	2	2	
1943	27.91	1.82	1	2	
1943	36.56	4.00	2	2	
1944	27.28	2.34	1	2	
1944	35.51	1.40	2	2	
1945	32.30	0.06	2	2	
1946	25.48	0.38	1	2	
1946	33.60	3.40	2	2	
1947	25.05	0.50	1	2	
1947	33.21	1.78	2	2	
1948	40.00	0.32	2	2	
1949	39.09	2.36	2	2	
1950	47.51	0.78	2	2	
1952	54.83	3.68	2	2	
1953	61.13	2.50	2	3	
1954	61.21	2.56	2	3	
1955	65.89	0.30	2	3	
1956	64.47	3.08	2	3	
1957	59.22	0.08	2	3	
1958	55.21	0.68	2	3	
1959	60.87	0.14	2	3	

Data continued on next page

Table B.1: *Data continued from previous page*

Year	Pb/Ca	2σ	Spec.	n/4	Comments
1960	64.89	1.06	2	3	
1961	63.08	0.58	2	3	
1962	65.12	1.22	2	3	
1963	66.74	1.92	2	2	
1965	67.06	2.12	2	2	
1967	58.65	3.10	2	2	
1969	66.43	1.38	2	2	
1971	75.87	2.62	2	2	
1972	72.55	1.16	2	2	
1973	75.17	2.68	2	2	
1974	70.61	0.24	2	2	
1976	78.25	3.50	2	2	Tissue layer?
1979	72.37	3.42	2	2	Tissue layer?

B.2 North Rock and Station S Stable Lead Isotope Results

Table B.2: Lead isotope results: North Rock, Bermuda. Type reflects either North Rock surface coral (1) or Station S seawater (2) stable lead isotope analysis. The 2σ standard deviation represents internal statistics for 30, ten second integrations via MC-ICP-MS.

Year	206/207	2σ	208/207	2σ	206/204	2σ	Type
1886	1.2106	0.0026	2.4867	0.0028	18.4850	0.3660	1
1887	1.2109	0.0056	2.4881	0.0038	19.3970	0.9780	1
1888	1.2102	0.0016	2.4840	0.0040	18.8610	0.3140	1
1893	1.2114	0.0024	2.4844	0.0038	19.0310	0.4220	1
1898	1.2076	0.0016	2.4816	0.0028	19.2750	0.2480	1
1901	1.1998	0.0016	2.4786	0.0026	18.9670	0.7680	1
1903	1.1986	0.0018	2.4773	0.0162	18.5450	0.2180	1
1904	1.1976	0.0018	2.4774	0.0058	19.2190	0.3820	1
1905	1.1976	0.0014	2.4781	0.0036	18.5400	0.4320	1
1907	1.1944	0.0020	2.4735	0.0038	19.3120	0.2660	1
1908	1.1920	0.0016	2.4730	0.0038	19.0060	0.2780	1
1910	1.1887	0.0016	2.4692	0.0036	17.4760	0.7100	1
1911	1.1885	0.0044	2.4679	0.0032	18.9510	0.8020	1
1913	1.1896	0.0018	2.4677	0.0022	18.6010	0.2660	1
1914	1.1885	0.0026	2.4670	0.0026	19.9360	0.4460	1
1915	1.1871	0.0010	2.4622	0.0040	21.1650	0.2140	1
1916	1.1879	0.0022	2.4654	0.0026	18.5780	0.2780	1
1917	1.1876	0.0016	2.4644	0.0030	19.3550	0.2920	1
1919	1.1875	0.0018	2.4646	0.0022	19.6150	0.2460	1
1920	1.1834	0.0012	2.4601	0.0044	18.6830	0.2340	1
1921	1.1830	0.0018	2.4603	0.0038	18.4570	0.2640	1
1922	1.1795	0.0018	2.4573	0.0048	19.3290	0.2480	1
1923	1.1825	0.0014	2.4596	0.0038	18.4440	0.2440	1
1924	1.1821	0.0014	2.4577	0.0042	18.4740	0.1480	1
1925	1.1820	0.0014	2.4581	0.0064	20.9680	0.2760	1
1926	1.1837	0.0012	2.4598	0.0096	18.5910	0.1980	1
1927	1.1848	0.0018	2.4611	0.0040	18.4430	0.2520	1
1928	1.1853	0.0032	2.4611	0.0108	18.8420	0.3880	1
1929	1.1860	0.0024	2.4603	0.0046	18.6540	0.3900	1
1932	1.1852	0.0026	2.4600	0.0040	18.9240	0.3600	1
1935	1.1827	0.0018	2.4563	0.0044	21.2720	0.2840	1
1936	1.1828	0.0022	2.4563	0.0048	18.5010	0.2080	1
1937	1.1852	0.0014	2.4514	0.0044	18.7630	0.2460	1
1940	1.1855	0.0016	2.4528	0.0040	18.6350	0.2700	1
1941	1.1853	0.0016	2.4537	0.0052	18.9140	0.2200	1
1942	1.1863	0.0014	2.4536	0.0048	19.4420	0.3800	1
1943	1.1864	0.0014	2.4532	0.0078	18.7210	0.1660	1

Data continued on next page

Table B.2: *Data continued from previous page*

Year	**206/207**	2σ	**208/207**	2σ	**206/204**	2σ	**Type**
1944	1.1849	0.0022	2.4527	0.0074	19.4390	0.2880	1
1945	1.1866	0.0014	2.4554	0.0102	19.7380	0.2560	1
1946	1.1864	0.0020	2.4550	0.0048	19.0020	0.2880	1
1947	1.1866	0.0018	2.4551	0.0074	19.1420	0.3060	1
1948	1.1872	0.0032	2.4560	0.0072	20.0410	0.4340	1
1949	1.1856	0.0026	2.4546	0.0066	18.8070	0.2420	1
1950	1.1879	0.0014	2.4545	0.0068	17.8290	0.2900	1
1951	1.1900	0.0016	2.4550	0.0044	18.6490	0.2100	1
1952	1.1884	0.0012	2.4546	0.0052	17.3290	0.3060	1
1953	1.1843	0.0010	2.4522	0.0054	18.5550	0.2080	1
1954	1.1842	0.0010	2.4510	0.0044	17.4750	0.2320	1
1956	1.1812	0.0018	2.4496	0.0042	18.8110	0.2860	1
1957	1.1790	0.0010	2.4475	0.0048	17.3620	0.2740	1
1958	1.1816	0.0018	2.4500	0.0034	18.4940	0.3680	1
1959	1.1793	0.0018	2.4483	0.0040	18.4270	0.4260	1
1960	1.1809	0.0008	2.4467	0.0104	20.0650	0.2000	1
1961	1.1841	0.0020	2.4504	0.0044	18.6890	0.2280	1
1962	1.1830	0.0012	2.4491	0.0048	18.7050	0.1960	1
1964	1.1826	0.0010	2.4477	0.0042	19.2330	0.2100	1
1968	1.1801	0.0016	2.4455	0.0096	18.5290	0.2360	1
1970	1.1905	0.0038	2.4487	0.0048	20.6260	0.2620	1
1972	1.1977	0.0016	2.4528	0.0042	18.8620	0.2360	1
1973	1.1971	0.0016	2.4507	0.0034	18.8630	0.2580	1
1974	1.1976	0.0010	2.4518	0.0046	18.8380	0.1760	1
1975	1.2008	0.0018	2.4532	0.0062	21.6840	0.2800	1
1976	1.2033	0.0014	2.4566	0.0032	18.8270	0.1820	1
1977	1.2053	0.0050	2.4574	0.0062	18.9090	2.3580	1
1978	1.2010	0.0014	2.4543	0.0040	18.8410	0.2180	1
1981	1.1994	0.0006	2.4545	0.0032	18.3180	0.1380	1
1982	1.1993	0.0010	2.4510	0.0024	18.8090	0.1100	2
1984	1.1976	0.0006	2.4505	0.0028	18.7720	0.0780	2
1985	1.1958	0.0012	2.4496	0.0048	18.7260	0.1300	2
1987	1.1937	0.0016	2.4494	0.0040	18.7150	0.1760	2
1988	1.1844	0.0012	2.4457	0.0052	18.4990	0.1940	2
1989	1.1852	0.0016	2.4461	0.0060	18.5750	0.2220	2
1990	1.1797	0.0010	2.4432	0.0030	18.4920	0.1840	2
1994	1.1784	0.0022	2.4442	0.0050	18.2600	0.4780	2
1995	1.1740	0.0024	2.4404	0.0030	18.3960	0.5000	2
1996	1.1749	0.0020	2.4430	0.0032	18.3190	0.3380	2
1997	1.1747	0.0022	2.4437	0.0056	18.4130	0.2680	2
1999	1.1766	0.0022	2.4443	0.0072	18.5010	0.3320	2
2000	1.1743	0.0020	2.4432	0.0050	18.4470	0.3420	2

Bibliography

Alibert, C. and M. T. McCulloch, 1997: Strontium/calcium ratios in modern *Porites* corals from the Great Barrier Reef as a proxy for sea surface temperature: Calibration of the thermometer and monitoring of ENSO. *Paleoceanography*, **12**(3), 345–363.

Alleman, L. Y., A. J. Véron, T. M. Church, A. R. Flegal, and B. Hamelin, 1999: Invasion of the abyssal North Atlantic by modern anthropogenic lead. *Geophysical Research Letters*, **26**(10), 1477–1480.

Allen, L. A., J. L. Leach, and R. S. Houk, 1997: Spatial location of the space charge effect in individual ion clouds using monodisperse dried microparticulate injection with a twin quadrupole inductively coupled plasma mass spectrometer. *Analytical Chemistry*, **69**, 2384–2391.

Amiel, A. J., G. M. Friedman, and D. S. Miller, 1973: Distribution and nature of incorporation of trace elements in modern aragonitic corals. *Sedimentology*, **20**, 47–64.

Bacon, M. P., D. W. Spencer, and P. G. Brewer, 1976: $^{210}Pb/^{226}Ra$ and $^{210}Pb/^{210}Po$ disequilibrium in seawater and suspended particulate matter. *Earth and Planetary Science Letters*, **32**, 277–296.

Bainbridge, A. E., 1987: *GEOSECS Atlantic Ocean Expedition, Sections and Profiles*, vol. 2 of *GEOSECS Atlantic, Pacific, and Indian Ocean Expeditions*. National Science Foundation, Washington.

Barnes, D. J., 1970: Coral skeletons: an explanation of their growth and structure. *Science*, **170**, 1305–1308.

Barnes, D. J. and B. E. Chalker, 1990: Calcification and photosynthesis in reef-building corals and algae. In Z. Dubinsky, editor, *Coral Reefs*, Elsevier, Amsterdam. pp. 109–131.

Barnes, D. J. and J. M. Lough, 1993: On the nature and causes of density banding in massive coral skeletons. *Journal of Experimental Marine Biology and Ecology*, **167**, 91–108.

Bastidas, C., D. Bone, and E. M. Garcia, 1999: Sedimentation rates and metal content of sediments in a Venezuelan coral reef. *Marine Pollution Bulletin*, **38**(1), 16–24.

Beck, J. W., R. L. Edwards, E. Ito, F. W. Taylor, J. Recy, F. Rougerie, P. Joannot, and C. Henin, 1992: Sea-surface temperature from coral skeleton strontium/calcium ratios. *Science*, **257**, 644–647.

Belshaw, N. S., P. A. Freedman, R. K. O'Nions, M. Frank, and Y. Guo, 1998: A new variable dispersion double-focusing plasma mass spectrometer with performance illustrated for Pb isotopes. *International Journal of Mass Spectrometry*, **181**, 51–58.

Biggins, P. D. E. and R. M. Harrison, 1979: Atmospheric chemistry of automotive lead. *Environmental Science and Technology*, **13**, 558–565.

Bishop, J. K. B., 1988: The barite-opal-organic carbon association in oceanic particulate matter. *Nature*, **332**, 341–343.

Black, D. E., L. C. Peterson, J. T. Overpeck, A. Kaplan, M. N. Evans, and M. Kashgarian, 1999: Eight centuries of North Atlantic ocean atmosphere variability. *Science*, **286**, 1709–1713.

Bollhöfer, A. and K. J. R. Rosman, 2000: Isotopic source signatures for atmospheric lead: the Southern Hemisphere. *Geochimica et Cosmochimica Acta*, **64**(19), 3251–3262.

Bollhöfer, A. and K. J. R. Rosman, 2001: Isotopic source signatures for atmospheric lead: the Northern Hemisphere. *Geochimica et Cosmochimica Acta*, **65**(11), 1727–1740.

Boutron, C. F., U. Görlach, J.-P. Candelone, M. A. Bolshov, and R. J. Delmas, 1991: Decrease in anthropogenic lead, cadmium, and zinc in Greenland snows since the late 1960s. *Nature*, **353**, 153–156.

Boyle, E. A., 1988: Cadmium: Chemical tracer of deepwater paleoceanography. *Paleoceanography*, **3**, 471–489.

Boyle, E. A., S. D. Chapnick, G. T. Shen, and M. P. Bacon, 1986: Temporal variability of lead in the western North Atlantic. *Journal of Geophysical Research*, **91**(C7), 8573–8593.

Boyle, E. A. and J. M. Edmond, 1975: Determination of trace metals in aqueous solution by APDC chelate co-precipitation. In T. R. P. Gibb, editor, *Analytical Methods in Oceanography*, American Chemical Society, New York, vol. 147. pp. 44–55.

Boyle, E. A. and J. M. Edmond, 1976: Copper in surface waters south of New Zealand. *Nature*, **253**, 107–109.

Boyle, E. A., J. M. Edmond, and F. Sclater, 1976: On the marine geochemistry of cadmium. *Nature*, **263**, 42–44.

Boyle, E. A. and S. Huested, 1983: Aspects of the surface distributions of copper, nickel, cadmium, and lead in the North Atlantic and North Pacific. In C. S. Wong, E. A. Boyle, K. W. Bruland, and J. D. Burton, editors, *Trace Metals in Seawater*, Plenum, New York. pp. 379–395.

Boyle, E. A., S. S. Huested, and S. P. Jones, 1981: On the distribution of copper, nickel, and cadmium in the surface waters of the North Atlantic and North Pacific Ocean. *Journal of Geophysical Research*, **86**(C9), 8048–8066.

Boyle, E. A. and L. D. Keigwin, 1982: Deep circulation of the north Atlantic over the last 200,000 years: geochemical evidence. *Science*, **218**, 784–787.

Boyle, E. A. and L. D. Keigwin, 1987: North Atlantic thermohaline circulation during the past 20,000 years linked to high-latitude surface temperatures. *Nature*, **330**, 35–40.

Broecker, W. S., M. Andree, G. Bonani, W. Wolfli, H. Oeschger, M. Klas, A. Mix, and W. Curry, 1988: Preliminary estimates for the radiocarbon age of deep water in the glacial ocean. *Paleoceanography*, **3**(6), 659–669.

Broecker, W. S. and T.-H. Peng, 1982: *Tracers in the Sea*. Eldigio Press, Palisades, N.Y.

Brown, J. S., 1967: Isotopic zoning of lead and sulfur in southeast Missouri. In *Genesis of stratiform lead-zinc-fluorite deposits (Mississippi Valley type deposits)*. Economic Geology, New York, vol. 3, pp. 410–425.

Bruland, K. W., 1980: Oceanographic distributions of cadmium, zinc, nickel, and copper in the North Pacific. *Earth and Planetary Science Letters*, **47**, 176–198.

Bruland, K. W., 1992: Complexation of cadmium by natural organic ligands in the central North Pacific. *Limnology and Oceanography*, **37**(5), 1008–1017.

Bruland, K. W. and R. P. Franks, 1983: Mn, Ni, Cu, Zn, and Cd in the western North Atlantic. In C. S. Wong, E. A. Boyle, K. W. Bruland, and J. D. Burton, editors, *Trace Metals in Seawater*, Plenum, New York. pp. 395–414.

Bruland, K. W., G. Knauer, and J. Martin, 1978: Cadmium in northeast Pacific waters. *Limnology and Oceanography*, **23**, 618–625.

Burgoyne, T. W., G. M. Hieftje, and R. A. Hites, 1997: Space charge evaluation in a plasma-source mass spectrograph. *Analytical Chemistry*, **69**, 485–489.

Byrne, R. H., L. R. Kump, and K. J. Cantrell, 1988: The influence of temperature and pH on trace metal speciation in seawater. *Marine Chemistry*, **25**, 163–181.

Candelone, J.-P., S. Hong, C. Pellone, and C. F. Boutron, 1995: Post-Industrial Revolution changes in large-scale atmospheric pollution of the Northern Hemisphere by heavy metals as documented in central Greenland snow and ice. *Journal of Geophysical Research*, **100**(D8), 16,605–16,616.

Capodaglio, G., K. H. Coale, and K. W. Bruland, 1990: Lead speciation in surface waters of the eastern North Pacific. *Marine Chemistry*, **29**, 221–233.

Carton, J. A., X. Cao, B. S. Giese, and A. M. Da Silva, 1996: Decadal and interannual SST variability in the tropical Atlantic Ocean. *Journal of Physical Oceanography*, **26**, 1165–1175.

Carton, J. A. and B. H. Huang, 1994: Warm events in the tropical Atlantic. *Journal of Physical Oceanography*, **24**(5), 888–903.

Chan, L. H., D. Drummond, J. M. Edmond, and B. Grant, 1977: On the barium data from the Atlantic GEOSECS Expedition. *Deep Sea Research*, **24**, 613–649.

Chang, P., L. Ji, and H. Li, 1997: A decadal climate variation in the tropical Atlantic Ocean from thermodynamic air-sea interactions. *Nature*, **385**, 516–518.

Chen, X. S. and R. S. Houk, 1996: Spatially resolved measurements of ion density behind the skimmer of an inductively coupled plasma mass spectrometer. *Spectrochimica Acta*, **51B**(1), 41–54.

Chow, T. J. and J. L. Earl, 1970: Lead aerosols in the atmosphere: increasing concentrations. *Science*, **176**, 510–513.

Chow, T. J. and J. L. Earl, 1972: Lead isotopes in North American coals. *Science*, **176**, 510–511.

Chow, T. J. and M. S. Johnstone, 1965: Lead isotopes in gasoline and aerosols of Los Angeles Basin, California. *Science*, **147**, 502–503.

Chow, T. J. and C. C. Patterson, 1962: The occurrence and significance of lead isotopes in pelagic sediments. *Geochimica et Cosmochimica Acta*, **26**, 263–308.

Chow, T. J., C. B. Snyder, and J. L. Earl, 1975: Isotope ratios of lead as pollutant source indicators. In *Proceedings of the International Atomic Energy Agency*, Vienna, vol. IAEA-SM-191/4. pp. 95–108.

Church, T. M., A. Véron, C. C. Patterson, D. Settle, Y. Erel, H. R. Maring, and A. R. Flegal, 1990: Trace elements in the North Atlantic troposphere: shipboard results of precipitation and aerosols. *Global Biogeochemical Cycles*, **4**(4), 431–443.

Cole, J. E., R. G. Fairbanks, and G. T. Shen, 1993: Recent variability in the Southern Oscillation: isotopic results from a Tarawa Atoll coral. *Science*, **260**, 1790–1793.

Collier, R. and J. Edmond, 1984: The trace element geochemistry of marine biogenic particulate matter. *Progress in Oceanography*, **13**, 113–199.

Conkright, M., S. Levitus, and T. Boyer, 1994: *World Ocean Atlas 1994 Volume 1: Nutrients*. No. 1 in NOAA Atlas NESDIS. U. S. Department of Commerce, Washington, D. C.

Covey, D. and S. Hastenrath, 1978: The Pacific El Niño phenomenon and the Atlantic circulation. *Monthly Weather Review*, **106**, 1280–1287.

Craig, H., S. Krishnaswami, and B. L. K. Somayajulu, 1973: ^{210}Pb - ^{226}Ra: radioactive disequilibrium in the deep sea. *Earth and Planetary Science Letters*, **17**, 295–305.

Cullen, J. T., T. W. Lane, F. M. M. Morel, and R. M. Sherrell, 1999: Modulation of cadmium uptake in phytoplankton by seawater CO_2 concentration. *Nature*, **402**, 165–167.

Cumming, G. L., S. E. Kesler, and D. Krstic, 1979: Isotopic composition of lead in Mexican mineral deposits. *Economic Geology*, **74**, 1395–1402.

Curtis, S. and S. Hastenrath, 1995: Forcing of anomalous sea surface temperature evolution in the tropical Atlantic during Pacific warm events. *Journal of Geophysical Research*, **100**(C8), 15,835–15,847.

Da Silva, A., A. C. Young, and S. Levitus, 1994: *Atlas of Surface Marine Data*. NOAA Atlas NESDIS 6. U.S. Department of Commerce, Washington D.C.

de Villiers, S., B. K. Nelson, and A. R. Chivas, 1995: Biological controls on coral Sr/Ca and δ^{18}O reconstructions of sea surface temperature. *Science*, **269**, 1247–1249.

de Villiers, S., G. T. Shen, and B. K. Nelson, 1994: The Sr/Ca-temperature relationship in coralline aragonite: Influence of variability in $(Sr/Ca)_{seawater}$ and skeletal growth parameters. *Geochimica et Cosmochimica Acta*, **58**, 197–208.

Dehairs, F., R. Chesselet, and J. Jedwab, 1980: Discrete suspended particles of barite and the barium cycle in the open ocean. *Earth and Planetary Science Letters*, **49**, 529–550.

Delaney, M. L., L. J. Linn, and E. R. M. Druffel, 1993: Seasonal cycles of manganese and cadmium in coral from the Galapagos Islands. *Geochimica et Cosmochimica Acta*, **57**, 347–354.

Delevaux, M. H., A. P. Pierce, and J. C. Antweiler, 1966: New isotopic measurements of Colorado ore leads. *USGS Professional Paper*, **550C**, 178–186.

Dettinger, M. D., M. Ghil, C. M. Strong, W. Weibel, , and P. Yiou, 1995: Software expedites singular-spectrum analysis of noisy time series. *Eos, Transactions, American Geophysical Union*, **76**(2), 12–21.

Dickey, T., D. Frye, H. Jannasch, E. Boyle, D. Manov, D. Sigurdson, J. McNeil, M. Stramska, A. Michaels, N. Nelson, D. Siegel, G. Chang, J. Wu, and A. Knap, 1998: Initial results from the Bermuda Testbed Mooring program. *Deep-Sea Research*, **I**(45), 771–794.

Dodge, R. E., R. C. Aller, and J. Thomson, 1974: Coral growth related to resuspension of bottom sediments. *Nature*, **247**, 574–577.

Dodge, R. E. and T. R. Gilbert, 1984: Chronology of lead pollution contained in banded coral skeletons. *Marine Biology*, **82**(1), 9–13.

Doe, B. R., 1970: *Lead Isotopes*. Springer-Verlag, New York.

Doney, S. C. and J. L. Bullister, 1992: A chlorofluorocarbon section in the eastern North Atlantic. *Deep-Sea Research*, **11-12A**, 1857–1883.

Druffel, E. R. M., 1989: Decade time scale variability of ventilation in the North Atlantic: high-precision measurements of bomb radiocarbon in banded corals. *Journal of Geophysical Research*, **94**(C3), 3271–3285.

Druffel, E. R. M., 1997: Geochemistry of corals: proxies of past ocean chemistry, ocean circulation, and climate. *Proceedings of the National Academy of Sciences, USA*, **94**, 8354–8361.

Duce, R. A., P. S. Liss, J. T. Merrill, E. L. Atlas, P. Buat-Ménard, B. B. Hicks, J. M. Miller, J. M. Prospero, R. Arimoto, T. M. Church, W. Ellis, J. N. Galloway, L. Hansen, T. D. Jickells, A. H. Knap, K. H. Reinhardt, B. Schneider, A. Soudine, J. J. Tokos, S. Tsunogai, R. Wollast, and M. Zhou, 1991: The atmospheric input of trace species to the world ocean. *Global Biogeochemical Cycles*, **5**(3), 193–259.

Dunbar, R. B. and J. E. Cole, editors, 1993: *Coral records of ocean-atmosphere variability*, vol. 10 of *NOAA Climate and Global Change Program*. University Corporation for Atmospheric Research, Boulder, Colorado.

Dunbar, R. B. and G. M. Wellington, 1981: Stable isotopes in a branching coral monitor seasonal temperature variations. *Nature*, **293**, 453–455.

Dunbar, R. B., G. M. Wellington, M. W. Colgan, and P. W. Glynn, 1994: Eastern Pacific sea surface temperature since 1600 A. D.: The δ^{18}O record of climate variability in Galapagos corals. *Paleoceanography*, **9**(2), 291–315.

Dunstan, L. P., J. W. Gramlich, I. L. Barnes, and W. C. Purdy, 1980: Absolute isotopic abundance and the atomic weight of a reference sample of thallium. *Journal of Research of the National Bureau of Standards*, **85**, 1–10.

Edmond, J. M., A. Spivack, B. C. Grant, H. Ming-Hui, C. Zexiam, C. Sung, and Z. Xiushau, 1985: Chemical dynamics of the Changjiang estuary. *Continental Shelf Research*, **4**(1/2), 17–36.

Edwards, R. L., J. H. Chen, and G. J. Wasserburg, 1987: U-238 U-234-Th-230-Th-232 systematics and the precise measurement of time over the past 500,000 years. *Earth and Planetary Science Letters*, **81**(2-3), 175–192.

Elderfield, H. and R. E. M. Rickaby, 2000: Oceanic Cd/P ratio and nutrient utilization in the glacial Southern Ocean. *Nature*, **405**, 305–310.

Enfield, D. B. and D. A. Mayer, 1997: Tropical Atlantic sea surface temperature variability and its relation to El Niño–Southern Oscillation. *Journal of Geophysical Research*, **102**(C1), 929–945.

England, M. H. and S. Rahmstorf, 1999: Sensitivity of ventilation rates and radiocarbon uptake to subgrid-scale mixing in ocean models. *Journal of Physical Oceanography*, **29**(11), 2802–2827.

Facchetti, S. and F. Giess, 1982: Isotopic lead experiment. Tech. Rep. EUR 8352 EN, Commission of the European Communities, Joint Research Center.

Fairbanks, R. G. and R. E. Dodge, 1979: Annual periodicity of the ^{18}O/^{16}O and ^{13}C/^{12}C ratios in the coral *Montastrea annularis*. *Geochimica et Cosmochimica Acta*, **43**, 1009–1020.

Fairbanks, R. G. and R. K. Matthews, 1978: The marine oxygen isotope record in Pleistocene coral, Barbados, West Indies. *Quaternary Research*, **10**, 181–196.

Falkner, K. K., G. P. Klinkhammer, T. S. Bowers, J. F. Todd, B. L. Lewis, W. M. Landing, and J. M. Edmond, 1993: The behavior of barium in anoxic marine waters. *Geochimica et Cosmochimica Acta*, **57**, 537–554.

Fassett, J. D. and P. J. Paulsen, 1989: Isotope dilution mass spectrometry for accurate elemental analysis. *Analytical Chemistry*, **61**(10), 643A–649A.

Fekete, B. M., C. J. Vörösmarty, and W. Grabs, 2000: Global, composite runoff fields based on observed river discharge and simulated water balanaces. Tech. rep., Complex Systems Research Center, University of New Hampshire.

Flegal, A. R., T. F. Duda, and S. Niemeyer, 1989: High gradients of lead isotopic composition in north-east Pacific upwelling filaments. *Nature*, **339**, 458–460.

Flegal, A. R., K. Itoh, C. C. Patterson, and C. S. Wong, 1986: Vertical profile of lead isotopic compositions in the north-east Pacific. *Nature*, **321**, 689–690.

Folland, C. K., T. N. Palmer, and D. E. Parker, 1986: Sahel rainfall and worldwide sea surface temperatures, 1901-85. *Nature*, **320**, 602–606.

Francis, C. W., G. Chesters, and L. A. Haskin, 1970: Determination of ^{210}Pb mean residence time in the atmosphere. *Environmental Science and Technology*, **4**, 586–589.

Fratantoni, D. M., 2001: North Atlantic surface circulation during the 1990's observed with satellite-tracked drifters. *Journal of Geophysical Research*, **106**(C10), 22,067–22,093.

Gagan, M. K., L. K. Ayliffe, J. W. Beck, J. E. Cole, E. R. M. Druffel, R. B. Dunbar, and D. P. Schrag, 2000: New views of tropical paleoclimates from corals. *Quaternary Science Reviews*, **19**, 45–64.

Galer, S. J. G. and W. Abouchami, 1998: Practical application of lead triple spiking for correction of instrumental mass discrimination. *Mineralogical Magazine*, **62A**, 491–492.

Gill, A. E., 1982: *Atmosphere-Ocean Dynamics*, vol. 30 of *International Geophysics Series*. Academic Press, New York.

Gillson, G. R., D. J. Douglas, J. E. Fulford, K. W. Halligan, and S. D. Tanner, 1988: Nonspectroscopic interelement interferences in inductively coupled plasma mass spectrometry. *Analytical Chemistry*, **60**, 1472–1474.

Goreau, T. F., 1963: Calcium carbonate deposition by coralline algae and corals in relation to their role as reef-builders. *Annals of the New York Academy of Science*, **109**, 127–167.

Goreau, T. F. and N. I. Goreau, 1959: The physiology of skeleton formation in corals. II. Calcium deposition by hermatypic corals under various conditions in the reef. *Biological Bulletin*, **117**, 239–250.

Goreau, T. F., N. I. Goreau, R. K. Trench, and R. L. Hayes, 1996: Calcification rates in corals. *Science*, **274**, 117.

Graney, J. R., A. N. Halliday, G. J. Keeler, J. O. Nriagu, J. A. Robbins, and S. A. Norton, 1995: Isotopic record of lead pollution in lake sediments from the northeastern United States. *Geochimica et Cosmochimica Acta*, **59**(9), 1715–1728.

Greegor, R. B., N. E. P. Jr., and F. W. Lytle, 1997: Strontianite in coral skeletal aragonite. *Science*, **275**, 1452–1454.

Grousset, F. E., C. R. Quétel, B. Thomas, P. Buat-Ménard, O. F. X. Donard, and A. Bucher, 1994: Transient Pb isotopic signatures in the western European atmosphere. *Environmental Science and Technology*, **28**, 1605–1608.

Gunnesch, K. A., A. Baumann, and M. Gunnesch, 1990: Lead isotope variations across the central Peruvian Andes. *Economic Geology*, **85**, 1384–1401.

Halliday, A. N., J. N. Christensen, D.-C. Lee, C. M. Hall, X. Luo, and M. Rehkämper, 2000: Multiple-collector inductively coupled plasma mass spectrometry. In C. M. Barshick, D. C. Duckworth, and D. H. Smith, editors, *Inorganic Mass Spectrometry: Fundamentals and Applications*, Marcel Dekker, New York. pp. 291–328.

Hameed, S., K. R. Sperber, and A. Meinster, 1993: Teleconnections of the Southern Oscillation in the tropical North Atlantic sector in the OSU coupled upper ocean atmosphere GCM. *Journal of Climate*, **6**(3), 487–498.

Hamelin, B., J. L. Ferrand, L. Alleman, E. Nicholas, and A. J. Véron, 1997: Isotopic evidence of pollutant lead transport from North America to the subtropical North Atlantic gyre. *Geochimica et Cosmochimica Acta*, **61**, 4423–4428.

Hamelin, B., F. E. Grousset, P. E. Biscaye, A. Zindler, and J. M. Prospero, 1989: Lead isotopes in trade wind aerosols at Barbados: the influence of European emissions over the North Atlantic. *Journal of Geophysical Research*, **94**(C11), 16,243–16,250.

Hamelin, B., G. Manhes, F. Albaréde, and C. J. Allégre, 1985: Precise lead isotope measurements by the double spike technique: a reconsideration. *Geochimica et Cosmochimica Acta*, **49**, 173–182.

Hastenrath, S., 1990: Decadal-scale changes of the circulation in the tropical Atlantic sector associated with Sahel drought. *International Journal of Climatology*, **10**, 459–472.

Hastenrath, S. and L. Greischar, 1993: Circulation mechanisms related to northeast Brazil rainfall anomalies. *Journal of Geophysical Research*, **98**(D3), 5093–5102.

Hastenrath, S. and P. J. Lamb, 1977: *Climatic Atlas of the Tropical Atlantic and Eastern Pacific Oceans*. University of Wisconsin Press, Madison.

Haug, G. H., K. A. Hughen, D. M. Sigman, L. C. Peterson, and U. Röhl, 2001: Southward migration of the Intertropical Convergence Zone through the Holocene. *Science*, **293**, 1304–1308.

Helmers, E. and M. M. Rutgers van der Loeff, 1993: Lead and aluminum in Atlantic surface waters (50°N to 50°S) reflecting anthropogenic and natural sources in the eolian transport. *Journal of Geophysical Research*, **98**(C11), 20,261–20,273.

Henderson, L. M. and F. C. Kracek, 1927: The fractional precipitation of barium and radium chromates. *Journal of the American Chemical Society*, **49**, 739–749.

Hernández-Guerra, A. and T. M. Joyce, 2000: Water masses and circulation in the surface layers of the Caribbean at 66°W. *Geophysical Research Letters*, **27**(21), 3497–3500.

Hirata, T., 1996: Lead isotopic analysis of NIST standard reference materials using multiple collector-inductively coupled plasma mass spectrometry coupled with modified external correction method for mass discrimination effect. *The Analyst*, **121**, 1407–1411.

Hochman, H. T., F. E. Müller-Karger, and J. J. Walsh, 1994: Interpretation of the coastal zone color scanner signature of the Orinoco River plume. *Journal of Geophysical Research*, **99**(C4), 7443–7455.

Hodge, V., S. R. Johnson, and E. D. Goldberg, 1978: Influence of atmospherically transported aerosols on surface ocean water composition. *Geochemical Journal*, **12**(1), 7–20.

Horlick, G. and A. Montaser, 1998: Analytical characteristics of ICP-MS. In A. Montaser, editor, *Inductively Coupled Plasma Mass Spectrometry*, Wiley-VCH, New York. pp. 503–588.

Houghton, R. W. and Y. M. Tourre, 1992: Characteristics of low-frequency sea surface temperature. *Journal of Climate*, **5**(765-771).

Hudson, J. H., E. A. Shinn, R. B. Halley, and B. Lidz, 1976: Sclerochronology: a tool for interpreting past environments. *Geology*, **4**, 361–364.

Hughen, K. A., J. T. Overpeck, S. J. Lehman, M. Kashgarian, J. Southon, L. C. Peterson, R. Alley, and D. M. Sigman, 1998: Deglacial changes in ocean circulation from an extended radiocarbon calibration. *Nature*, **391**, 65–68.

Hughen, K. A., J. T. Overpeck, L. C. Peterson, and R. F. Anderson, 1996a: The nature of varved sedimentation in the Cariaco Basin, Venezuela, and its paleoclimatic significance. In A. E. S. Kemp, editor, *Paleoclimatology and Paleoceanography from Laminated Sediments*, The Geological Society, London.

Hughen, K. A., J. T. Overpeck, L. C. Peterson, and S. Trumbore, 1996b: Rapid climate changes in the tropical Atlantic region during the last deglaciation. *Nature*, **380**, 51–54.

Hughen, K. A., J. R. Southon, S. J. Lehman, and J. T. Overpeck, 2000: Synchronous radiocarbon and climate shifts during the last deglaciation. *Science*, **290**, 1951–1954.

Huizenga, D. L. and D. R. Kester, 1982: The distribution of vanadium in the northwestern Atlantic Ocean. *Eos, Transactions, American Geophysical Union*, **63**, 990.

Hulanicki, A., 1967: Complexation reactions of dithiocarbamates. *Talanta*, **14**, 1371–1390.

International Lead and Zinc Study Group, 1992: *Principle Uses of Lead and Zinc, 1960-1990*. The Group, London.

Iselin, C. O., 1936: A study of the circulation of the western North Atlantic. *Papers in Physical Oceanography and Meterology*, **4**, 101.

Jacobs, L., S. Emerson, and S. S. Huested, 1987: Trace metal geochemistry in the Cariaco Trench. *Deep Sea Research*, **34**(5/6), 965–981.

Jaffé, R., I. Leal, J. Alvarado, P. Gardinali, and J. Sericano, 1995: Pollution effects of the Tuy River on the central Venezuelan coast: anthropogenic organic compounds and heavy metals in *Tivela mactroidea*. *Marine Pollution Bulletin*, **30**(12), 820–825.

Jenkins, W. J., 1980: Tritrium and ^{3}He in the Sargasso Sea. *Journal of Marine Research*, **38**, 533–569.

Jickells, T. D., A. H. Knap, and T. M. Church, 1984: Trace metals in Bermuda rainwater. *Journal of Geophysical Research*, **89**, 1423–1428.

Johnson, K. S., R. M. Gordon, and K. H. Coale, 1997: What controls dissolved iron concentrations in the world ocean? *Marine Chemistry*, **57**(3-4), 137–161.

Jones, P. D., T. M. L. Wigley, and P. B. Wright, 1986: Global temperature variations between 1861 and 1984. *Nature*, **322**, 430–434.

Kawamura, R., 1994: A rotated EOF analysis of global sea surface temperature variability with interannual and interdecadal scales. *Journal of Physical Oceanography*, **24**(3), 707–715.

Klinkhammer, G. P. and L. H. Chan, 1990: Determination of barium in marine waters by isotope dilution inductively coupled plasma mass spectrometry. *Analytica Chimica Acta*, **232**, 323–329.

Knutson, D. K., R. W. Buddemeier, and S. V. Smith, 1972: Coral chronometers: seasonal growth bands in reef corals. *Science*, **177**, 270–272.

Kraus, K. A. and G. E. Moore, 1953: Anion exchange studies. VI. The divalent transition elements manganese to zinc in hydrochloric acid. *Journal of the American Chemical Society*, **75**, 1460–1462.

Lea, D. W. and E. A. Boyle, 1989: Barium content of benthic foraminifera controlled by bottom water composition. *Nature*, **338**, 751–753.

Lea, D. W., G. T. Shen, and E. A. Boyle, 1989: Coralline barium records temporal variability in equatorial Pacific upwelling. *Nature*, **340**, 373–375.

Leder, J. J., P. K. Swart, A. M. Szmant, and R. E. Dodge, 1996: The origin of variations in the isotopic record of scleractinian corals: I. Oxygen. *Geochimica et Cosmochimica Acta*, **60**(15), 2857–2870.

Lee, D. G. and F. M. M. Morel, 1995: Replacement of zinc by cadmium in marine phytoplankton. *Marine Ecology - Progress Series*, **127**(1-3), 305–309.

Levitus, S. R., R. Burgett, and T. P. Boyer, 1994: *World Ocean Atlas 1994 Volume 3: Salinity*, vol. NOAA Atlas NESDIS 3. U.S. Department of Commerce, Washington.

Li, T. and S. G. H. Philander, 1997: On the seasonal cycle of the equatorial Atlantic Ocean. *Journal of Climate*, **10**(4), 813–817.

Lin, H. L., L. C. Peterson, J. T. Overpeck, S. E. Trumbore, and D. W. Murray, 1997: Late Quaternary climate change from $\delta^{18}O$ records of multiple species of planktonic foraminifera: High-resolution records from the anoxic Cariaco Basin, Venezuela. *Paleoceanography*, **12**(3), 415–427.

Linn, L. J., M. L. Delaney, and E. R. M. Druffel, 1990: Trace metals in contemporary and seventeenth-century Galapagos coral: records of seasonal and annual variations. *Geochimica et Cosmochimica Acta*, **54**, 387–394.

Logan, A. and T. Tomascik, 1991: Extension growth-rates in two coral species from high-latitude reefs of Bermuda. *Coral Reefs*, **10**(3), 155–160.

Longerich, H. P., B. J. Fryer, and D. F. Strong, 1987: Determination of lead isotope ratios by inductively couple plasma-mass spectrometry (ICP-MS). *Spectrochimica Acta*, **42B**(1-2), 39–48.

Lorens, R. B., 1981: Sr, Cd, Mn, and Co distribution coefficients in calcite as a function of calcite precipitation rate. *Geochimica et Cosmochimica Acta*, **45**, 553–561.

Ma, T. Y. H., 1934: On the season change of growth in a reef coral: *Favia speciosa* (Dana) and the temperature of the Japanese seas during the latest geological times. *Proceedings of the Imperial Academy (Tokyo)*, **10**, 353–356.

Maréchal, C., P. Télouk, and F. Albarède, 1999: Precise analysis of Cu and Zn isotopic compositions by plasma-source mass spectrometry. *Chemical Geology*, **156**, 251–273.

Maring, H., D. M. Settle, P. Buat-Ménard, F. Dulac, and C. C. Patterson, 1987: Stable lead isotope tracers of air-mass trajectories in the Mediterranean region. *Nature*, **330**, 154–156.

Maring, H. B. and R. A. Duce, 1990: The impact of atmospheric aerosols on trace-metal chemistry in open ocean surface seawater. 3. Lead. *Journal of Geophysical Research*, **95**(C4), 5341–5347.

Martin, J. H., K. W. Bruland, and W. W. Broenkow, 1976: Cadmium transport in the California Current. In H. Windom and R. Duce, editors, *Marine Pollutant Transfer*, Lexington Books. pp. 159–184.

McConnaughey, T., 1989a: ^{13}C and ^{18}O isotopic disequilibrium in biological carbonates: I. Patterns. *Geochimica et Cosmochimica Acta*, **53**, 151–162.

McConnaughey, T., 1989b: ^{13}C and ^{18}O isotopic disequilibrium in biological carbonates: II. In vitro simulation of kinetic isotope effects. *Geochimica et Cosmochimica Acta*, **53**, 163–171.

McConnaughey, T. A., J. Burdett, J. F. Whelan, and C. K. Paull, 1997: Carbon isotopes in biological carbonates: Respiration and photosynthesis. *Geochimica et Cosmochimica Acta*, **61**(3), 611–622.

McManus, J., W. M. Berelson, G. P. Klinkhammer, T. E. Kilgore, and D. E. Hammond, 1994: Remobilization of barium in continental margin sediments. *Geochimica et Cosmochimica Acta*, **58**(22), 4899–4907.

Min, G. R., R. L. Edwards, F. R. Taylor, J. Recy, C. D. Gallup, and J. W. Beck, 1995: Annual cycles of U/Ca in coral skeletons and U/Ca thermometry. *Geochimica et Cosmochimica Acta*, **59**(10), 2025–2042.

Mitsuguchi, T., E. Matsumoto, O. Abe, T. Uchida, and P. J. Isdale, 1996: Mg/Ca thermometry in coral skeletons. *Science*, **274**, 961–963.

Montaser, A., 1998: *Inductively Coupled Plasma Mass Spectrometry*. J. Wiley, New York.

Morse, J. W. and M. L. Bender, 1990: Partition coefficients in calcite: examination of factors influencing the validity of experimental results and their application to natural systems. *Chemical Geology*, **82**, 265–277.

Moura, A. D. and J. Shukla, 1981: On the dynamics of droughts in northeast Brazil: Observations, theory, and numerical experiments with a general circulation model. *Journal of Atmospheric Science*, **38**, 2657–2675.

Müller-Karger, F., R. Varela, R. Thunell, M. Scranton, R. Bohrer, G. Taylor, J. Capelo, Y. Astor, E. Tappa, T.-Y. Ho, and J. J. Walsh, 2001: Annual cycle of primary production in the Cariaco Basin: response to upwelling and implications for vertical export. *Journal of Geophysical Research*, **106**(C3), 4527–4542.

Müller-Karger, F. E., 1989: Pigment distribution in the Caribbean Sea: Observations from space. *Progress in Oceanography*, **23**, 23–64.

Müller-Karger, F. E., C. R. McClain, and P. L. Richardson, 1988: The dispersal of the Amazon's water. *Nature*, **333**, 56–59.

Murozumi, M., T. J. Chow, and C. C. Patterson, 1969: Chemical concentrations of pollutant lead aerosols, terrestrial dusts and sea salts in Greenland and Antarctic snow strata. *Geochimica et Cosmochimica Acta*, **33**, 1247–1294.

National Geophysical Data Center, 1988: Data Announcement 88-MGG-02: Digital relief of the surface of the Earth. Tech. rep., NOAA.

Ng, A. and C. C. Patteron, 1982: Changes of lead and barium with time in California off-shore basin sediments. *Geochimica et Cosmochimica Acta*, **46**, 2307–2321.

Ng, A. and C. C. Patterson, 1981: Natural concentrations of lead in ancient Arctic and Antarctic ice. *Geochimica et Cosmochimica Acta*, **45**, 2109–2121.

Niu, H. and R. S. Houk, 1996: Fundamental aspects of ion extraction in inductively coupled plasma mass spectrometry. *Spectrochimica Acta*, **51B**, 779–815.

Nobre, P. and J. Shukla, 1996: Variations of sea surface temperature, wind stress, and rainfall over the tropical Atlantic and South America. *Journal of Climate*, **9**(10), 2464–2479.

Nozaki, Y., J. Thomson, and K. K. Turekian, 1976: The distribution of Pb-210 and Po-210 in the surface waters of the Pacific Ocean. *Earth and Planetary Science Letters*, **32**, 304–312.

Nozaki, Y. and S. Tsunogai, 1976: ^{226}Ra, ^{210}Pb, ^{210}Po disequilibria in the western North Pacific. *Earth and Planetary Science Letters*, **32**, 313–321.

Nriagu, J. O., 1979a: Global inventory of natural and anthropogenic emissions of trace metals to the atmosphere. *Nature*, **279**, 409–411.

Nriagu, J. O., 1979b: Production, uses, and properties of cadmium. In J. O. Nriagu, editor, *Cadmium in the Environment, Part I: Ecological Cycling*, John Wiley and Sons, New York. p. 682.

Nriagu, J. O., 1985: Cupellation: the oldest quantitative chemical process. *J. Chem. Ed.*, **62**(8), 668–674.

Nriagu, J. O., 1989: A global assessment of natural sources of atmospheric trace metals. *Nature*, **338**, 47–49.

Nriagu, J. O. and J. M. Pacyna, 1988: Quantitative assessment of worldwide contamination of air, water, and soils by trace metals. *Nature*, **333**, 134–139.

Östlund, H. G. and C. Grall, 1987: Transient Tracers in the Ocean, North and Tropical Atlantic Tritium and Radiocarbon. Tech. Rep. 16, University of Miami, Rosenstiel School of Marine and Atmospheric Science.

Patterson, C. C. and D. M. Settle, 1976: The reduction of order of magnitude errors in lead analyses of biological materials and natural waters by evaluating and controlling the extent and sources of industrial lead contamination introduced during sample collection, handling, and analysis. In P. D. La Fleur, editor, *Accuracy in Trace Analysis: Sampling, Sample Handling, and Analysis*. National Bureau of Standards Special Publication, Gaithersburg, Maryland, pp. 321–351.

Patterson, C. C. and D. M. Settle, 1981: Enewetak: Pb/Si-dust ratios are greater in precipitation than in air. *SEAREX Newsletter*, **1**(4), 10–12.

Patterson, C. C. and D. M. Settle, 1987: Review of data on eolian fluxes of industrial and natural lead to the land and seas in remote regions on a global scale. *Mar. Chem.*, **22**, 137–162.

Peterson, L. C., J. T. Overpeck, N. G. Kipp, and J. Imbrie, 1991: A high-resolution late Quaternary upwelling record from the anoxic Cariaco Basin, Venezuela. *Paleoceanography*, **6**(1), 99–119.

Philander, S. G. H., 1996: Why the ITCZ is mostly north of the equator. *Journal of Climate*, **9**(12), 2958–2972.

Quinn, T. M., F. W. Taylor, T. J. Crowley, and S. M. Link, 1996: Evaluation of sampling resolution in coral stable isotope records: a case study using records from New Caledonia and Tarawa. *Paleoceanography*, **11**(5), 529–542.

Rehkämper, M. and A. Halliday, 1998: Accuracy and long-term reproducibility of lead isotopic measurements by multiple-collector inductively coupled plasma mass spectrometry using an external method for correction of mass discrimination. *International Journal of Mass Spectrometry*, **181**, 123–133.

Rehkämper, M. and K. Mezger, 2000: Investigation of matrix effects for Pb isotope ratio measurements by multiple collector ICP-MS: verification and application of optimized analytical protocols. *Journal of Analytical Atomic Spectrometry*, **15**, 1451–1460.

Richards, F. A. and R. F. Vaccaro, 1956: The Cariaco Trench, an anaerobic basin in the Caribbean Sea. *Deep Sea Research*, **3**, 214–228.

Riedel, K. S., A. Sidorenko, and D. Thomson, 1994: Spectral estimation of plasma fluctuations 1. Comparison of methods. *Physics of Plasmas*, **1**(3), 485–500.

Ritson, P. I., B. K. Esser, S. Niemeyer, and A. R. Flegal, 1994: Lead isotopic determination of historical sources of lead to Lake Erie, North America. *Geochimica et Cosmochimica Acta*, **58**(15), 3297–3305.

Rosman, K. J. R., W. Chisholm, C. F. Boutron, J.-P. Candelone, and U. Görlach, 1993: Isotopic evidence for the source of lead in Greenland snows since the late 1960s. *Nature*, **362**, 333–335.

Rosman, K. J. R., W. Chisholm, C. F. Boutron, J.-P. Candelone, and S. Hong, 1994: Isotopic evidence to account for changes in the concentration of lead in Greenland snow between 1960 and 1988. *Geochimica et Cosmochimica Acta*, **58**(15), 3265–3269.

Rosman, K. J. R., C. Ly, K. Van de Velde, and C. F. Boutron, 2000: A two century record of lead isotopes in high altitude Alpine snow and ice. *Earth and Planetary Science Letters*, **176**, 413–424.

Rosman, K. J. R., C. C. Patterson, and D. M. Settle, 1990: The distribution of lead between sea salt, dust, and lead-rich aerosols in the mid-South Pacific easterlies at American Samoa. *Journal of Geophysical Research*, **95**(D4), 3687–3691.

Russell, W. A., D. A. Papanastassiou, and T. A. Tombrello, 1978: Ca isotope fractionation on the Earth and other solar system materials. *Geochimica et Cosmochimica Acta*, **42**, 1075–1090.

Schaule, B. K. and C. C. Patterson, 1981: Lead concentrations in the northeast Pacific: evidence for global anthropogenic perturbations. *Earth and Planetary Science Letters*, **54**, 97–116.

Schaule, B. K. and C. C. Patterson, 1983: Perturbations of the natural lead depth profile in the Sargasso Sea by industrial lead. In C. S. Wong, E. Boyle, K. W. Bruland, and J. D. Burton, editors, *Trace Metals in Seawater*, Plenum, New York. pp. 487–502.

Schmitz, W. J. and M. S. McCartney, 1993: On the North Atlantic circulation. *Reviews of Geophysics*, **31**(1), 29–49.

Schuhmacher, H. and H. Zibrowius, 1985: What is hermatypic? A redefinition of ecological groups in corals and other organisms. *Coral Reefs*, **4**, 1–9.

Scranton, M. I., F. L. Sayles, M. P. Bacon, and P. G. Brewer, 1987: Temporal changes in the hydrography and chemistry of the Cariaco Trench. *Deep-Sea Research*, **34**(5/6), 945–963.

Servain, J., 1991: Simple climate indices for the tropical Atlantic Ocean and some applications. *Journal of Geophysical Research*, **96**(C8), 15,137–15,146.

Settle, D. M. and C. C. Patterson, 1980: Lead in albacore: guide to lead pollution in Americans. *Science*, **207**, 1167–1176.

Shannon, R. D., 1976: Revised effective ionic radii and systematic studies of interatomic distances in Halides and Chalcogenides. *Acta Crystallogr.*, **A32**, 751–767.

Shen, G. T., 1986: *Lead and cadmium geochemistry of corals: Reconstruction of historic perturbations in the upper ocean*. Ph.D. thesis, Massachusetts Institute of Technology.

Shen, G. T., 1996: Rapid change in the tropical ocean and the use of corals as monitoring systems. In A. R. Berger and W. J. Iams, editors, *Geoindicators: Assessing Rapid Environmental Changes in Earth Systems*, Balkema Press, Rotterdam. pp. 155–169.

Shen, G. T. and E. A. Boyle, 1987: Lead in corals: reconstruction of historical industrial fluxes to the surface ocean. *Earth and Planetary Science Letters*, **82**, 289–304.

Shen, G. T. and E. A. Boyle, 1988a: Determination of lead, cadmium, and other trace metals in annually-banded corals. *Chemical Geology*, **97**, 47–62.

Shen, G. T. and E. A. Boyle, 1988b: Thermocline ventilation of anthropogenic lead in the western North Atlantic. *Journal of Geophysical Research*, **93**(C12), 15,715–15,732.

Shen, G. T., E. A. Boyle, and D. W. Lea, 1987: Cadmium in corals as a tracer of historical upwelling and industrial fallout. *Nature*, **328**, 794–796.

Shen, G. T., T. M. Campbell, R. B. Dunbar, G. M. Wellington, M. W. Colgan, and P. W. Glynn, 1991: Paleochemistry of manganese in corals from the Galapagos Islands. *Coral Reefs*, **10**, 91–100.

Shen, G. T., J. E. Cole, D. W. Lea, L. J. Linn, T. A. McConnaughey, and R. G. Fairbanks, 1992a: Surface ocean variability at Galapagos from 1936-1982: Calibration of geochemical tracers in corals. *Paleoceanography*, **7**(563-588).

Shen, G. T. and R. B. Dunbar, 1995: Environmental controls on uranium in reef corals. *Geochimica et Cosmochimica Acta*, **59**(10), 2009–2024.

Shen, G. T., L. J. Linn, and T. M. Campbell, 1992b: A chemical indicator of trade wind reversal in corals from the western tropical Pacific. *Journal of Geophysical Research*, **97**(C8), 12,689–12,697.

Sherrell, R. M., E. A. Boyle, and B. Hamelin, 1992: Isotopic equilibration between dissolved and suspended particulate lead in the Atlantic Ocean: Evidence from ^{210}Pb and stable Pb isotopes. *Journal of Geophysical Research*, **97**(7), 11,257–11,268.

Shirahata, H., R. W. Elias, C. C. Patterson, and M. Koide, 1980: Chronological variations in concentrations and isotopic compositions of anthropogenic atmospheric lead in sediments of a remote subalpine pond. *Geochimica et Cosmochimica Acta*, **44**, 149–162.

Sholkovitz, E. R. and D. L. Schneider, 1991: Cerium redox cycles and rare earth elements in the Sargasso Sea. *Geochimica et Cosmochimica Acta*, **55**, 2737–2743.

Sholkovitz, E. R. and G. T. Shen, 1995: The incorporation of rare earth elements in modern coral. *Geochimica et Cosmochimica Acta*, **59**(13), 2749–2756.

Shotyk, W., D. Weiss, P. G. Appleby, A. K. Cheburkin, R. Frei, M. Gloor, J. D. Kramers, S. Reese, and W. O. Van Der Knaap, 1998: History of atmospheric lead deposition since 12,370 ^{14}C yr BP from a peat bog, Jura Mountains, Switzerland. *Science*, **281**, 1635–1640.

Simonetti, A., C. Gariépy, and J. Carignan, 2000: Pb and Sr isotopic evidence for sources of atmospheric heavy metals and their deposition budgets in northeastern North America. *Geochimica et Cosmochimica Acta*, **64**(20), 3439–3452.

Sinnott, R. W., 1984: Virtues of the Haversine. *Sky and Telescope*, **68**(2), 159.

Smith, W. H. F. and D. T. Sandwell, 1997: Global seafloor topography from satellite altimetry and ship depth soundings. *Science*, **277**, 1957–1962.

Stacey, J. S., R. E. Zartman, and I. T. NKomo, 1968: A lead isotope study of galenas and selected feldspars from mining districts in Utah. *Economic Geology*, **63**, 796–814.

Steiger, R. H. and E. Jäger, 1977: Subcommission on geochronology: convention on the use of decay constants in geo- and cosmochronology. *Earth and Planetary Science Letters*, **36**, 1213–1232.

Strelow, F. W. E., 1978: Distribution coefficients and anion exchange behavior of some elements in hydrobromic-nitric acid mixtures. *Analytical Chemistry*, **50**(9), 1359–1361.

Sturges, W. T. and L. A. Barrie, 1987: Lead 206/207 isotope ratios in the atmosphere of North America as tracers of US and Canadian emissions. *Nature*, **329**, 144–146.

Swart, P. K., 1981: The strontium, magnesium, and sodium composition of recent scleractinian coral skeletons as standards for paleoenvironmental analysis. *Palaeogeography, Palaeoclimatology, Palaeoecology*, **34**, 115–136.

Thirlwall, M. F., 2000: Inter-laboratory and other errors in Pb isotope analysis investigated using a $^{207}Pb/^{204}Pb$ double spike. *Chemical Geology*, **163**, 299–322.

Thirlwall, M. F., 2001: Inappropriate tail corrections can cause large inaccuracy in isotope ratio determination by MC-ICP-MS. *Journal of Analytical Atomic Spectrometry*, **16**, 1121–1125.

Todt, W., R. A. Cliff, A. Hanser, and A. W. Hofmann, 1996: Evaluation of a ^{202}Pb-^{205}Pb double spike for high-precision lead isotope analysis. *Geophysical Monographs*, **95**, 429–437.

Trenberth, K. E. and T. J. Hoar, 1996: The 1990-1995 El Niño-Southern Oscillation event: Longest on record. *Geophysical Research Letters*, **23**(1), 57–60.

Turner, P. J., T. O. Merren, J. Speakman, R. C. Haines, Z. Palacz, and S. Meffan-Main, 2000: Ion optics of multi-collector ICP-MS systems for precise and accurate isotope ratio measurements. Tech. rep., Micromass UK Ltd.

Véron, A. J., T. M. Church, and A. R. Flegal, 1998: Lead isotopes in the western North Atlantic: Transient tracers of pollutant lead inputs. *Environmental Research, Section A*, **78**, 104–111.

Véron, A. J., T. M. Church, A. R. Flegal, C. C. Patterson, and Y. Erel, 1993: Response of lead cycling in the surface Sargasso Sea to changes in tropospheric input. *Journal of Geophysical Research*, **98**, 18,269–18,276.

Véron, A. J., T. M. Church, C. C. Patterson, and A. R. Flegal, 1994: Use of stable lead isotopes to characterize the sources of anthropogenic lead in North Atlantic surface waters. *Geochimica et Cosmochimica Acta*, **58**(15), 3199–3206.

Véron, A. J., T. M. Church, I. Rivera-Duarte, and A. R. Flegal, 1999: Stable lead isotopic ratios trace thermohaline circulation in the subarctic North Atlantic. *Deep-Sea Research*, **46**, 919–935.

Véron, A. J., C. E. Lambert, A. Isley, P. Linet, and F. Grousset, 1987: Evidence of recent lead pollution in deep north-east Atlantic sediments. *Nature*, **326**, 278–281.

Vink, S., E. A. Boyle, C. I. Measures, and J. Yuan, 2000: Automated high resolution determination of the trace elements iron and aluminum in the surface ocean using a towed Fish coupled to flow injection analysis. *Deep-Sea Research*, **47**, 1141–1156.

Walder, A. J., 1997: Advanced isotope ratio mass spectrometry II: Isotope ratio measurements by multiple collector inductively coupled plasma mass spectrometry. In I. T. Platzner, K. Habfast, A. J. Walder, and A. Goetz, editors, *Modern Isotope Ratio Mass Spectrometry*, Wiley, New York. pp. 83–108.

Walder, A. J. and P. A. Freedman, 1992: Isotopic ratio measurement using a double focusing magnetic sector mass analyzer with an inductively coupled plasma as an ion source. *Journal of Analytical Atomic Spectrometry*, **7**, 571–575.

Webster, P. J. and T. N. Palmer, 1997: The past and the future of El Niño. *Nature*, **390**, 562–564.

Weiss, D., E. A. Boyle, V. Chavagnac, M. Herwegh, and J. Wu, 2000: Determination of lead isotope ratios in seawater by quadrupole inductively couple plasma mass spectrometry after $Mg(OH)_2$ co-precipitation. *Spectrochim. Acta*, **55B**, 363–374.

Weiss, D., W. Shotyk, P. G. Appleby, J. D. Kramers, and A. K. Cheburkin, 1999: Atmospheric Pb deposition since the Industrial Revolution recorded by five Swiss peat profiles: enrichment factors, fluxes, isotopic composition, and sources. *Environmental Science and Technology*, **33**(9), 1340–1352.

Weiss, M. P. and D. A. Goddard, 1977: Man's impact on coastal reefs - an example from Venezuela. In M. P. Weiss and J. B. Saunders, editors, *Reefs and Related Carbonates - Ecology and Sedimentology*, AAPG, Tulsa. pp. 171–179.

Wellington, G. M. and P. W. Glynn, 1983: Environmental influences on skeletal banding in eastern Pacific (Panama) corals. *Coral Reefs*, **1**, 215–222.

Wells, J. W., 1956: Scleractinia. In R. C. Moore, editor, *Treatise on Invertebrate Paleontology*, Geological Society of America and University of Kansas Press, Lawrence, Kansas. pp. F328–F444.

White, W. M., F. Albarède, and P. Télouk, 2000: High-precision analysis of Pb isotope ratios by multiple collector ICP-MS. *Chemical Geology*, **167**, 257–270.

Whitfield, M. and D. R. Turner, 1980: The theoretical studies of the chemical speciation of lead in seawater. In M. Branica and Z. Konrad, editors, *Lead in the Marine Environment*, Pergamon, New York. p. 353.

Wolgemuth, K. and W. S. Broecker, 1970: Barium in sea water. *Earth and Planetary Science Letters*, **8**, 372–378.

Woodhead, J. D., F. Volker, and M. T. McCulloch, 1995: Routine lead isotope determinations using a lead-207-lead-204 double spike: a long-term assessment of analytical precision and accuracy. *Analyst*, **120**, 35–39.

Woodruff, S. D., R. J. Slutz, R. L. Jenne, and P. M. Steurer, 1987: A comprehensive ocean-atmosphere data set. *Bulletin of the American Meterological Society of America*, **68**, 1239–1250.

Wu, J. and E. A. Boyle, 1997a: Lead in the western North Atlantic Ocean: Completed response to leaded gasoline phaseout. *Geochimica et Cosmochimica Acta*, **61**(15), 3279–3283.

Wu, J. and E. A. Boyle, 1997b: Low blank preconcentration technique for the determination of lead, copper, and cadmium in small-volume seawater samples by isotope dilution ICP-MS. *Analytical Chemistry*, **69**(13), 2464–2470.

York, D., 1966: Least-squares fitting of a straight line. *Canadian Journal of Physics*, **44**, 1079–1086.

Zartman, R. E. and J. S. Stacey, 1971: Lead isotopes and mineralization ages in belt supergroup rocks, northwestern Montana and northern Idaho. *Economic Geology*, **66**(6), 849–857.

Zebiak, S. E., 1993: Air-sea interaction in the equatorial Atlantic region. *Journal of Climate*, **6**, 1567–1586.

Zirino, A. and S. Yamamoto, 1972: A pH-dependent model for the chemical speciation of copper, zinc, cadmium, and lead in seawater. *Limnology and Oceanography*, **17**(5), 661–671.